

# **Age-dependent hippocampal network dysfunction in a mouse model of alpha-synucleinopathy**

**Clare Tweedy**

Thesis submitted for the degree of Doctor of Philosophy at Newcastle University

*September 2018*

Supervisors:

*Dr Fiona LeBeau, Dr Gavin Clowry,*

*Dr Amy Reeve, Dr John-Paul Taylor*

Industrial Supervisors:

*Dr Fiona Randall and Dr Peter Atkinson*





## Abstract

Aggregation of the protein alpha-synuclein (ASYN) is a key pathological feature of the alpha-synucleinopathies, a group of diseases including Lewy body dementia and Parkinson's disease. A common symptom of alpha-synucleinopathy is cognitive dysfunction, and impairment in hippocampal gamma-frequency oscillations may underlie some of the cognitive deficits associated with ASYN pathology. The *Thy-1* A30P mouse model overexpresses human mutant ASYN, with mice developing hippocampal spatial memory impairment by 12 months (Freichel *et al.* 2007). The aim of this thesis was to explore age-related hippocampal network changes in 2-4 month (A30P2+) mice and 10-13 month (A30P10+) mice to assess the effect of overexpression of mutant ASYN on hippocampal network activity *in vitro*. Using acute brain slice preparations of isolated hippocampi, A30P2+ mouse slices were found to exhibit excitatory/inhibitory network changes in region CA3 in the form of increased spontaneous sharp wave amplitude, increased frequency and amplitude of inhibitory postsynaptic potentials, and increased power of kainate-induced gamma-frequency oscillations. Immunohistochemistry revealed an increase in the density of parvalbumin-positive interneurons alongside a decrease in calbindin-positive interneurons. This change was accompanied by a more depolarised resting membrane potential in A30P2+ mouse CA3 pyramidal cells, and a sensitivity to interictal discharges in response to either kainate receptor agonism or GABA<sub>A</sub> receptor antagonism. With ageing, levels of excitability in A30P10+ mice were comparable to WT10+ mice. A30P10+ mice instead exhibited an impairment in cholinergic-induced, but not kainate-induced or spontaneous, gamma-frequency network oscillations. While mitochondrial dysfunction was not detectable with COX/SDH histochemistry until 15+ months in A30P mice, A30P10+ mice did show increased immunoreactivity for Iba1+ microglia. An environment of inflammation and excitotoxicity may be present in older A30P mice as a result of early network hyperexcitability, and this thesis explores early network changes in A30P mice and the wider dysfunction that follows.



## Acknowledgements

I would like to start by extending my gratitude to my supervisory team at Newcastle University for all their support and guidance over the years: Dr Fiona LeBeau, Dr Gavin Clowry, Dr Amy Reeve, and Dr John-Paul Taylor. A particular thank you must go to Fiona for being so supportive of me and for the good company during my time here. I have developed both as a person and as a scientist over the past four years, and to all of you I am grateful. Thank you to Gavin for all your help with immunohistochemistry, Amy for your help with the mitochondrial experiments, and John-Paul for your help with understanding DLB!

A huge thank you to my industrial supervisors Dr Fiona Randall and Dr Peter Atkinson, for making an industrial placement as part of my PhD a successful venture! I also extend my gratitude to Eisai and the Medical Research Council for funding the MRC Industrial CASE Studentship. Without the funding and support this research really would not have been possible. I learned so much during my time in the US, and thank you in particular to Fiona for taking me under your wing while I was there! I learned some amazing scientific techniques, and also made some lasting friendships. Thank you to everyone at Eisai's AiM Institute and the other interns including Iain for making my experience a memorable one.

I would also like to acknowledge the guidance and contributions of the members of my progress panel for keeping me on track: Prof. Mark Cunningham, Dr Elizabeta Mukaetova-Ladinska, and Dr Sasha Gartside. Getting some perspective and learning how to defend my experimental choices was incredibly helpful!

All the work presented in this thesis is my own, with the exception of assistance from undergraduate and Masters students that I have supervised and worked with over the years. Megan Ingham, Keir Cox, Elizaveta Olkhova, and Joshua Curry assisted with data collection for a number of electrophysiological experiments detailed throughout this thesis. Nathan Kindred and Christopher Williams assisted with data collection for electrophysiological experiments detailed in Chapter 4 of this thesis, as well as assisting in the immunohistochemical experiments detailed throughout. Pippa Gleave assisted with immunohistochemical data collection for Chapter 3. I am grateful to the assistance you all provided in the data collection process. I must also extend my gratitude to Karen, for keeping our labs running from the technical side, and always being happy to help me out when I needed it!

A PhD can be an incredibly stressful experience, and so I would like to acknowledge the friendship and support provided by the members of the office and lab over the years who I have come to call good friends. A particular thank you must go to Felix Chan, for being the greatest friend one could wish for, even though you're now across the pond! Myrto: for your constant support, friendship, and supply of baklava. Jean, Anderson, Tamara, Ashan, Beth, Mark, Nelson: I will miss lunch club. Thank you for many laughs and making the office a fun place to work in. Even when you all judge me for my unhealthy consumption of a certain carbonated beverage, you've all been amazing in keeping me sane and motivated and I can't thank you all enough! To Grace for the endless support and friendship, and to those who were once a part of the office and lab but are now spread across the country (and even the world): Yingdi, John, Gemma, Joe, Chris T, Claire. To Abby, my Boston tour guide and now long-distance friend – thank you for all your support during the writing process.

My family have been incredibly supportive of me during the PhD process: from dealing with my mood swings after a long day of experimenting or thesis writing, to being unsure why I am so excited about finding statistical significance but being excited for me all the same! Mum and Dad: I did it! I am indebted to you for your constant support, love, and advice. As much as I know you've been counting down the years (!) till I finally get a job, hearing how proud you are of me certainly kept me going.

Thank you for also taking me back in home to write my thesis after my trip to Boston when I returned homeless and disorientated! Having my cat Pebbles to assist me with the writing process really brightened my days. A special thank you also to my sister Carol, Rob, Faye, and my niece Charlotte: I think I had more fun playing with your toys to destress from thesis writing than you did! And I can't wait to do the same with my future nephew to destress from whichever jobs I end up in! To my Grandma for all your support, and also my late Nana and Grandad who I know would have loved to hear all about my research and be at my graduation. Thank you all.

The only person that remains left to thank is Adam, for your endless support and reassurance. I couldn't have done this without you. Thank you.

## Conference Presentations

Work from this thesis was presented at the following conferences:

### **British Neuroscience Association**

**(Edinburgh, UK) April 2015**

Poster: *“The role of NMDA receptors and synaptic plasticity in the induction and build-up of hippocampal gamma-frequency oscillations in vitro”.*

### **Federation of European Neuroscience Societies**

**(Copenhagen, Denmark) July 2016**

Poster: *“Hippocampal gamma-frequency oscillations and hyperexcitability in a mouse model of alpha-synucleinopathy”*

### **North East Postgraduate Conference**

**(Newcastle, UK) November 2016**

Poster and Oral Presentation: *“Hippocampal gamma-frequency oscillations and hyperexcitability in a mouse model of alpha-synucleinopathy”*

### **13<sup>th</sup> International Conference on Alzheimer’s & Parkinson’s Diseases**

**(Vienna, Austria) March 2017**

Poster: *“Impaired hippocampal gamma-frequency oscillations and hyperexcitability in a mouse model of alpha-synucleinopathy”*

### **Society for Neuroscience**

**(Washington D.C., USA) November 2017**

Posters: *“Early hippocampal network excitability in a mouse model of alpha-synucleinopathy”* and *“Impaired hippocampal gamma-frequency oscillations and mitochondrial dysfunction in a mouse model of alpha-synucleinopathy”*

### **Federation of European Neuroscience Societies**

**(Berlin, Germany) July 2018**

Poster: *“Hippocampal hyperexcitability precedes gamma-frequency oscillation impairment in a mouse model of alpha-synucleinopathy”.*

## Publications

Work expanded on in Chapter 5 has been published with shared first authorship:

Robson E, **Tweedy C**, Manzanza N, Taylor JP, Atkinson P, Randall F, Reeve A, Clowry GJ, LeBeau FEN. *Impaired Fast Network Oscillations and Mitochondrial Dysfunction in a Mouse Model of Alpha-synucleinopathy (A30P)*. *Neuroscience* (2018) 377: 161-173. DOI: 10.1016/j.neuroscience.2018.02.032.



## Table of Contents

Abstract.....	iii
Acknowledgements.....	v
Conference Presentations.....	vii
Publications.....	viii
Table of Contents.....	ix
List of Figures.....	xii
List of Tables.....	xiv
List of Abbreviations.....	xv
<b>Chapter 1. Introduction .....</b>	<b>1</b>
1.1 Alpha-synucleinopathy.....	3
1.1.1 <i>Thy-1 A30P mouse model</i> .....	6
1.2 The hippocampus.....	9
1.2.1 <i>Hippocampal structure and function</i> .....	9
1.2.2 <i>Inhibitory interneurons</i> .....	11
1.2.3 <i>Excitatory/inhibitory neurotransmission</i> .....	12
1.3 Neuroglia.....	15
1.3.1 <i>Astrocytes</i> .....	16
1.3.2 <i>Microglia</i> .....	17
1.4 Oxidative Stress.....	19
1.4.1 <i>Mitochondria</i> .....	19
1.4.2 <i>Mechanisms of oxidative stress</i> .....	20
1.4.3 <i>Perineuronal nets</i> .....	21
1.5 Hippocampal network activity.....	23
1.5.1 <i>The electroencephalogram (EEG)</i> .....	23
1.5.2 <i>Generation of in vitro network oscillations</i> .....	24
1.5.3 <i>Spontaneous sharp waves</i> .....	26
1.6 Neurodegeneration in alpha-synucleinopathy.....	28
1.7 Aims of thesis.....	30
<b>Chapter 2. General Methods .....</b>	<b>31</b>
2.1 Animal provision.....	33
2.2 Preparation of acute brain slices.....	34
2.3 Slice maintenance.....	36
2.4 Pharmacological compounds.....	37
2.5 Data Acquisition.....	38
2.6 Data Analysis.....	39

2.7	Free-floating immunohistochemistry .....	40
2.7.1	<i>DAB Immunoperoxidase</i> .....	41
2.7.2	<i>Immunofluorescence</i> .....	43
2.8	Open field test for locomotor activity .....	44
2.9	COX/SDH histochemistry.....	45
2.10	Statistical Analysis .....	47

### **Chapter 3. Spontaneous Hippocampal Network Activity..... 49**

3.1	Introduction.....	51
3.2	Aims.....	53
3.3	Methods.....	54
3.4	Results.....	55
3.4.1	<i>Expression of human ASYN within the A30P mouse hippocampus</i> .....	55
3.4.2	<i>No change in spontaneous network oscillations in A30P2+ mice</i> .....	59
3.4.3	<i>Presence of spontaneous SPWs in hippocampal slice preparations</i> .....	63
3.4.4	<i>Increased SPW amplitude but not frequency in A30P2+ mice</i> .....	65
3.4.5	<i>IPSPs correlate with SPWs in A30P2+ mice</i> .....	70
3.4.6	<i>Pharmacological manipulation of spontaneous SPWs</i> .....	72
3.4.6.1	<i>SPW amplitude is reduced by GABA<sub>A</sub> receptor antagonism</i> .....	74
3.4.6.2	<i>SPWs are not sensitive to NMDA receptor antagonism</i> .....	76
3.4.6.3	<i>Cholinergic receptor agonism</i> .....	78
3.4.7	<i>Increase in PV+ interneurons in the CA3 region of A30P2+ mice</i> .....	80
3.4.8	<i>Increase in PNN+ cells in the CA3 region of A30P2+ mice</i> .....	83
3.4.9	<i>Decrease in CB+ interneurons in the CA3 region of A30P2+ mice</i> .....	85
3.5	Discussion .....	87
3.5.1	<i>Differential vulnerability of CA3 interneurons in A30P mice</i> .....	87
3.5.2	<i>Spontaneous network oscillations are intact in A30P mice</i> .....	92
3.5.3	<i>Altered spontaneous hippocampal SPWs in young A30P mice</i> .....	93
3.5.4	<i>Perineuronal net changes may be a neuroprotective adaptation</i> .....	95
3.6	Conclusion.....	97

### **Chapter 4. Early Hippocampal Hyperexcitability in A30P mice ..... 99**

4.1	Introduction.....	101
4.2	Aims.....	103
4.3	Methods.....	104
4.4	Results.....	105
4.4.1	<i>Increased power of KA-induced oscillations in A30P2+ mice</i> .....	105
4.4.2	<i>Interictal discharges in A30P2+ mice at low concentrations of KA</i> .....	109
4.4.3	<i>Concentration-dependent changes in KA-induced oscillations</i> .....	113
4.4.4	<i>Increased sensitivity to GABA<sub>A</sub> receptor antagonism in A30P2+ mice</i> ..	116
4.4.5	<i>CA3 pyramidal cells intrinsically more excitable in A30P2+ mice</i> .....	119
4.4.6	<i>Hyperlocomotion in A30P mice</i> .....	122

4.4.7	<i>Decrease in GFAP+ astrocytes in the A30P2+ mouse CA3 region</i> .....	124
4.5	Discussion.....	126
4.5.1	<i>Hyperexcitability in young A30P mice normalises with ageing</i> .....	126
4.5.2	<i>Increased sensitivity to GABA<sub>A</sub> receptor antagonism in A30P2+ mice</i> ..	129
4.5.3	<i>Functional output of cortical hyperexcitability in vivo</i> .....	131
4.6	Conclusion .....	134
<b>Chapter 5. Age-Dependent Network Deficits in A30P mice</b> .....		<b>135</b>
5.1	Introduction .....	137
5.2	Aims.....	139
5.3	Methods .....	140
5.4	Results.....	141
5.4.1	<i>Build-up of hippocampal CCH-induced oscillations</i> .....	141
5.4.2	<i>The time-dependent build-up of CCH-induced gamma-frequency oscillations is an NMDA-receptor dependent process</i> .....	144
5.4.3	<i>Reduced power stable CCH gamma oscillations in A30P10+ mice</i> .....	147
5.4.4	<i>No difference in CCH oscillation rhythmicity in A30P mice</i> .....	152
5.4.5	<i>Propagation from CA3 to CA1 is intact in A30P mice</i> .....	154
5.4.6	<i>Mitochondrial dysfunction in A30P15+ mice</i> .....	157
5.4.7	<i>Increase in Iba1+ microglia in A30P10+ mice</i> .....	159
5.5	Discussion.....	161
5.5.1	<i>Cholinergic-induced network oscillation deficit in A30P10+ mice</i> .....	161
5.5.2	<i>Changes in microglia in both young and ageing A30P mice</i> .....	164
5.6	Conclusion .....	166
<b>Chapter 6. General Discussion</b> .....		<b>167</b>
6.1	Summary of changes in A30P mice .....	169
6.2	Early hyperexcitability affects the E/I network in A30P mice .....	170
6.3	Age-dependent network deficits in A30P mice .....	175
6.4	Therapeutic implications .....	178
6.5	Future Work .....	179
<b>References</b> .....		<b>180</b>

## List of Figures

### Chapter 1

Figure 1.1 <b>Alpha-synuclein protein domain structure</b> .....	5
Figure 1.2 <b>Cytoarchitecture of mouse hippocampus</b> .....	9
Figure 1.3 <b>Neuroprotective and neurotoxic states of microglia and astrocytes</b> . ....	15
Figure 1.4 <b>The process of oxidative phosphorylation</b> .....	19
Figure 1.5 <b>Pyramidal cell-interneuron circuitry in the hippocampal CA3 region</b> . ....	25

### Chapter 2

Figure 2.1 <b>Classification of mouse dorsal and ventral slices</b> .....	35
Figure 2.2 <b>Schematic of DAB peroxidase immunohistochemistry</b> .....	42
Figure 2.3 <b>Summary of COX/SDH histochemistry</b> . ....	46

### Chapter 3

Figure 3.1 <b>Expression of human ASYN in the A30P mouse hippocampus</b> .....	56
Figure 3.2 <b>Differential expression of human ASYN in CA3 interneurons</b> . ....	58
Figure 3.3 <b>No difference in spontaneous 15 – 45 Hz oscillations in A30P mice</b> .....	61
Figure 3.4 <b>No difference in rhythmicity of spontaneous oscillations in A30P mice</b> . ....	62
Figure 3.5 <b>Proportion of slices with SPWs upon immediate recording</b> . ....	64
Figure 3.6 <b>No difference in SPW frequency in A30P mice</b> . ....	66
Figure 3.7 <b>Increased amplitude of SPWs in the A30P2+ mouse CA3 region</b> .....	67
Figure 3.8 <b>No difference in SPWs between dorsal/ventral slices</b> .....	69
Figure 3.9 <b>SPWs in the field correlate to the arrival of IPSPs in pyramidal cells</b> . ....	71
Figure 3.10 <b>SPWs remain stable for 1 hour in control conditions once established</b> . ....	73
Figure 3.11 <b>GABA<sub>A</sub> receptor antagonism significantly decreases SPW amplitude</b> . ....	75
Figure 3.12 <b>No effect of NMDA receptor antagonism on SPWs</b> .....	77
Figure 3.13 <b>Induction of fast network oscillations with CCH abolishes SPWs</b> . ....	79
Figure 3.14 <b>Increase in PV+ cells in the A30P2+ mouse CA3 region</b> . ....	81

Figure 3.15 <b>No change in optical density of PV+ slices in A30P mice.</b> .....	82
Figure 3.16 <b>Increased PNN+ cells in the A30P2+ mouse CA3 region.</b> .....	84
Figure 3.17 <b>Decreased CB+ cells in the A30P2+ mouse CA3 region.</b> .....	86

## **Chapter 4**

Figure 4.1 <b>Increased power of KA-induced oscillations in A30P2+ mice.</b> .....	106
Figure 4.2 <b>No change in rhythmicity of KA-induced oscillations in A30P mice.</b> .....	108
Figure 4.3 <b>A30P2+ mouse slices exhibit IIDs in low concentrations of KA.</b> .....	110
Figure 4.4 <b>KA-induced interictal discharges in A30P2+ mice.</b> .....	112
Figure 4.5 <b>Increased KA power over increasing concentrations in A30P mice.</b> .....	115
Figure 4.6 <b>A30P2+ mice more sensitive to GABA<sub>A</sub>-R antagonism.</b> .....	117
Figure 4.7 <b>More depolarised RMP of CA3 pyramidal cells of A30P2+ mice.</b> .....	120
Figure 4.8 <b>No difference in spiking parameters at firing threshold in A30P mice.</b> .....	121
Figure 4.9 <b>Hyperlocomotion in A30P mice.</b> .....	123
Figure 4.10 <b>Decreased GFAP+ astrocytes in the A30P2+ mouse CA3 region.</b> .....	125

## **Chapter 5**

Figure 5.1 <b>Time-dependent changes in CCH-induced oscillations.</b> .....	143
Figure 5.2 <b>NMDA-R antagonism accelerates CCH oscillation build-up in WT mice.</b> ....	145
Figure 5.3 <b>No difference in CCH-induced oscillations in A30P2+ mice.</b> .....	148
Figure 5.4 <b>Reduced power of CCH-induced oscillations in A30P10+ mice.</b> .....	151
Figure 5.5 <b>No difference in rhythmicity of CCH-induced oscillations in A30P mice.</b> ....	153
Figure 5.6 <b>CA3 to CA1 propagation time of CCH oscillations.</b> .....	155
Figure 5.7 <b>CCH-induced oscillations propagate from CA3 to CA1 in A30P mice.</b> .....	156
Figure 5.8 <b>Increased mitochondrial dysfunction in A30P15+ mice.</b> .....	158
Figure 5.9 <b>Decreased Iba1+ cells in A30P2+ mice increased in A30P10+ mice.</b> .....	160

## List of Tables

### Chapter 1

Table 1.1 Summary of literature surrounding <i>Thy-1</i> A30P mice. ....	8
Table 1.2 Summary of ionotropic glutamate receptor properties and pharmacology. .	13
Table 1.3 Patterns of activity between 0.5 and 80 Hz. ....	23
Table 1.4. Effect of antagonists on sharp waves and gamma-frequency oscillations. .	27

### Chapter 2

Table 2.1 List of chemicals used in preparation of artificial CSF solutions. ....	34
Table 2.2 List of drugs used in this thesis. ....	37
Table 2.3 List of primary antibodies and lectin used in this thesis. ....	40
Table 2.4 List of biotinylated secondary antibodies used in this thesis. ....	41
Table 2.5 List of fluorescent secondary antibodies used in this thesis. ....	43

### Chapter 6

Table 6.1. Summary of changes in A30P mice. ....	169
--	-----

## List of Abbreviations

A30P	Alanine to proline exchange in position 30
A53E	Alanine to glutamic acid exchange at position 53
A53T	Alanine to threonine exchange in position 53
aCSF	Artificial cerebrospinal fluid
AD	Alzheimer's disease
AMPA	$\alpha$ -amino-3-hydroxy-5-methyl-4-isoxazolepropionic acid
ANOVA	Analysis of variance
APP	Amyloid precursor protein
ASYN	Alpha-synuclein
ATP/DP	Adenosine triphosphate/diphosphate
Ca <sup>2+</sup>	Calcium ion
CA3/1	Cornus ammonis region 3/1
CaMKII	Calcium/calmodulin-dependent protein kinase II
CB	Calbindin
CCH	Carbachol
COX	Cytochrome c oxidase
CR	Calretinin
DAB	Diaminobenzidine
D-AP5	D-(-)-2-Amino-5-phosphonopentanoic acid
DAPI	4',6-diamidino-2-phenylindole
DF	Degrees of freedom
DG	Dentate gyrus
DLB	Dementia with Lewy bodies
DMSO	Dimethyl sulfoxide
DNA	Deoxyribonucleic acid
E/I	Excitatory/Inhibitory
E46K	Glutamic acid to tyrosine exchange at position 46
EC	Entorhinal Cortex
EEG	Electroencephalogram
EPSP	Excitatory postsynaptic potential
ER	Endoplasmic reticulum
ETC	Electron transport chain
FADH <sub>2</sub>	Flavin adenine dinucleotide

G51D	Glycine to aspartic acid exchange at position 51
GABA	$\gamma$ -aminobutyric acid
GAD65/67	Glutamate decarboxylase 65/67
GFAP	Glial fibrillary acidic protein
H <sub>2</sub> O	Water
H50Q	Histidine to glutamine exchange at position 50
Iba1	Ionised calcium-binding adapter molecule 1
IC	Intracellular
IgG	Immunoglobulin G
IID	Interictal discharge
ING	Interneuron network gamma
IPSP	Inhibitory postsynaptic potential
K <sup>+</sup>	Potassium ion
KA	Kainate
K <sub>v</sub>	Voltage-gated potassium channel
LBD	Lewy body dementia
LFP	Local field potential
LTP/D	Long term potentiation/depression
mGluR	Metabotropic glutamate receptor
MPTP	1-methyl-4-phenyl-1,2,3,6-tetrahydropyridine
MRI	Magnetic resonance imaging
MSA	Multiple system atrophy
Na <sup>+</sup>	Sodium ion
NADH	Nicotinamide adenine dinucleotide
NMDA	N-Methyl-D-aspartic acid
OD	Optical density
PBS	Phosphate buffered saline
PD	Parkinson's disease
PDD	Parkinson's disease dementia
PDGF	Platelet derived growth factor
PFA	Paraformaldehyde
P <sub>i</sub>	Inorganic phosphate
PING	Pyramidal-interneuron network gamma
PKA/C	Protein kinase A/C
PMS	Phenazine methosulfate



PNN	Perineuronal net
PP1/2	Protein phosphatase 1/2
PS1	Presenilin 1
PV	Parvalbumin
RGB	Red, green, blue
RI	Rhythmicity index
RMP	Resting membrane potential
ROS	Reactive oxygen species
SDH	Succinate dehydrogenase
SEM	Standard error of mean
SER129	Phosphorylation of serine at position 129
SNARE	Soluble NSF (N-ethylmaleimide-sensitive factor) attachment protein receptor
SPW	Sharp wave
<i>St.</i>	Stratum
TPBS	Triton phosphate buffered saline
WFA/WFL	Wisteria floribunda lectin
WT	Wild type



## **Chapter 1. Introduction**



## 1.1 Alpha-synucleinopathy

The Lewy body dementias (LBD) are the second most common neurodegenerative dementia, making up 15-20% of neuropathologically defined cases (Savica *et al.*, 2013). The LBDs consist of dementia with Lewy bodies (DLB) and Parkinson's disease dementia (PDD), diseases which show considerable overlap. A diagnosis of PDD may be made if dementia occurs in a patient with well-established Parkinson's disease (PD) of at least one year (McKeith *et al.*, 2017). Recent criteria highlights progressive cognitive decline as an essential feature for DLB diagnosis, occurring before or concurrently with Parkinsonism, though not all DLB patients develop Parkinsonism (McKeith *et al.*, 2017). Fluctuating cognition, visual hallucinations, and sleep disorder are also core features of DLB but many patients may only exhibit one or two core symptoms (Marui *et al.*, 2004; McKeith *et al.*, 2017).

LBD is marked by deficits in dopaminergic and cholinergic neurotransmitter systems (Perry *et al.*, 1990). This is reminiscent of the neurotransmitter deficits observed in PD and Alzheimer's disease (AD), respectively. The cholinergic deficits in DLB were, however, found to be greater than in AD, and directly correlate to the degree of cognitive impairment (Duda, 2004). Currently, no effective treatments exist to alleviate or reverse the cognitive deficits of LBD, though modest success has been achieved with the use of the acetylcholinesterase inhibitors donepezil or rivastigmine, or the NMDA-receptor antagonist memantine in some patients (Stinton *et al.*, 2015).

LBD is more common in males and sporadic forms occur on average between the ages of 50 to 83 (McKeith, 2004). A number of family studies have revealed rare familial forms associated with specific mutations in the SNCA gene (Rossor *et al.*, 2010). Diagnosis is typically confirmed post-mortem by appearance of Lewy bodies, which are intracellular, cytoplasmic inclusions containing the protein alpha-synuclein (ASYN) (Spillantini *et al.*, 1997). Pathology is proposed to first appear in PD within the lower brainstem and olfactory bulb, before progressing further through the brainstem to reach the substantia nigra and later reaching cortical areas (Braak *et al.*, 2003).

While patients with PDD and DLB exhibit similar pathology, it has been proposed that patients with DLB exhibit a higher burden of cortical Lewy body pathology than in PDD (Ruffmann *et al.*, 2016). Furthermore, PDD and DLB may both involve amyloid and tau co-pathology, proteins that misfold and form plaques and tangles respectively in AD (McKeith *et al.*, 2017). Amyloid plaque deposition has been linked to an accelerated progression to dementia in LBD (Ruffmann *et al.*, 2016), and

mice exhibiting both AD and DLB pathology showed an accelerated cognitive decline and spread of neuropathology (Clinton *et al.*, 2010).

ASYN is a small, soluble 140 amino acid protein (Figure 1.1) encoded by the SNCA gene and present throughout the brain (Norris *et al.*, 2004). At the presynaptic terminal, ASYN is proposed to play a role in regulating neurotransmitter release by facilitating SNARE complex assembly (Chandra *et al.*, 2005; Bendor *et al.*, 2013) and in the process of synaptic plasticity through modulation of neurotransmitter release (Liu *et al.*, 2004). Within dopaminergic neurons, ASYN is involved in the regulation of neurotransmission (Butler *et al.*, 2017) and has been shown to reduce the recycling rate of vesicles (Jenco *et al.*, 1998). Furthermore, ASYN has been shown to negatively modulate neurotransmitter release in cultured glutamatergic hippocampal neurons through inhibition of synaptic vesicle clustering following exocytosis (Nemani *et al.*, 2010). ASYN has also been reported to be involved in neurotransmitter reuptake in cultured dopaminergic neurons through interaction with the dopamine transporter (Lee *et al.*, 2001), and a similar mechanism is proposed in both serotonergic and noradrenergic neurons (Wersinger *et al.*, 2006a; Wersinger *et al.*, 2006b).

ASYN is a natively unstructured protein with no stable secondary structure until bound to a phospholipid membrane (Davidson *et al.*, 1998; Sahay *et al.*, 2015). ASYN monomers are capable of dynamic transition to form oligomers, which may then aggregate to form insoluble fibrils (El-Agnaf *et al.*, 1998). Post-translational modifications of ASYN further enrich the diversity of functions that ASYN carries out but may also promote or prevent ASYN aggregation (Beyer, 2006).

A pathological accumulation of aggregated ASYN is referred to as alpha-synucleinopathy, a group of diseases encompassing PD, LBD, and multiple system atrophy (MSA). Multiple system atrophy is a sporadic and rare form of alpha-synucleinopathy, marked by Parkinsonism, cerebellar ataxia, and autonomic failure (for review see Krismer and Wenning, 2017). Unlike the primarily intraneuronal ASYN+ inclusions of LBD, ASYN+ inclusions in MSA are frequently found in glia (for review see Savica *et al.*, 2018). The ASYN found in glial cytoplasmic inclusions in MSA has recently been shown to be structurally and biochemically distinct from the ASYN found in Lewy bodies, and is more potent at seeding ASYN aggregation (Peng *et al.*, 2018). Interestingly, MSA does not typically present with dementia (Wenning *et al.*, 1997), and so this makes it distinct from LBD despite the presence of ASYN+ inclusions.

Much remains to be understood about the complex interactions and mechanisms of ASYN pathology though studies involving familial forms of alpha-synucleinopathy have helped develop our understanding. To explore the role of ASYN in the pathogenesis of alpha-synucleinopathy, and its ultimate contribution to cognitive deficits, a number of rodent models are frequently used. Models most commonly consist of a human gene insert into the rodent genome, either in wild type (WT) form, or with various mutations isolated from patients with familial alpha-synucleinopathy (Figure 1.1; including A30P and A53T). Rodent models may also involve the viral expression of human ASYN, injection of preformed ASYN fibrils to targeted regions, or toxin-induced neurodegeneration (Sommer *et al.*, 2000).

A variety of promoters can be used to control the expression of the human ASYN gene insert in mice, including the *Thy-1* promoter. The *Thy-1* promoter is commonly used in mice to optogenetically control populations of *Thy-1* expressing neurons. An early study of mice expressing a fluorescent protein under the *Thy-1* promoter demonstrated fluorescence in hippocampal pyramidal neurons (Feng *et al.*, 2000). The *Thy-1* promoter reaches the highest expression levels within the hippocampus and striatum (Kemshead *et al.*, 1982), and low levels within the substantia nigra (Neumann *et al.*, 2002). This allows examination of some of the cognitive and motor deficits associated with alpha-synucleinopathy.

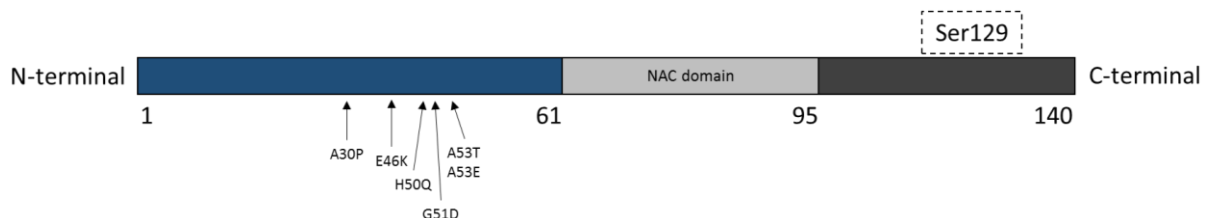


**Figure 1.1 Alpha-synuclein protein domain structure.** Location of common mutations including A30P marked on the 140 amino acid sequence, in addition to the location of the Ser129 phosphorylation site. Adapted from: Interaction between Neuronmelanin and Alpha-Synuclein in Parkinson’s Disease (Xu and Chan, 2015).

Overexpression of A30P or A53T mutant ASYN lead to a more severe neurodegenerative phenotype than overexpression of WT ASYN (Chandra *et al.*, 2005). This may be due to A30P and A53T ASYN forming oligomers at accelerated rates compared to WT ASYN (Sommer *et al.*, 2000). On the other hand, A30P ASYN forms fibrils more slowly than WT ASYN while A53T ASYN forms fibrils more quickly than WT ASYN (Sommer *et al.*, 2000). All mutated forms of ASYN are capable of self-aggregation into structures sharing a number of ultrastructural properties with human

Lewy bodies (Sommer *et al.*, 2000). ASYN+ inclusions in transgenic mice have been noted to appear as fine granular deposits, as opposed to the fibrillar structure of ASYN within human Lewy bodies (for review see Sommer *et al.*, 2000).

Interestingly, structures sharing more similarities with human Lewy bodies can be formed in mice lacking endogenous murine ASYN but overexpressing human WT ASYN (Fares *et al.*, 2016). The authors describe the ASYN+ inclusions to be similar to Lewy bodies in their solubility, immunoreactivity, fibrillisation process, and sensitivity to pharmacological inhibitors of aggregation (Fares *et al.*, 2016). Despite the possible advantages of human ASYN expression on a rodent ASYN null background, most models used to study alpha-synucleinopathy also express endogenous murine ASYN.

### 1.1.1 *Thy-1* A30P mouse model

First reported in a patient with familial PD (Kruger *et al.*, 1998), the autosomal dominant A30P missense mutation in the SNCA gene constitutes a G → C substitution at nucleotide position 88. This, in turn, leads to an alanine → proline exchange at amino acid position 30. Under control of the *Thy-1* promoter, an A30P mouse model was first used to investigate the transport of mutant ASYN to synapses. While A30P ASYN was present in the synapse at normal levels, the protein was found accumulated in neuronal cell bodies upon overexpression (Kahle *et al.*, 2000) and appeared to show a reduced tendency to bind to vesicles (Jensen *et al.*, 1998).

The *Thy-1* A30P mouse model was further employed to study alpha-synucleinopathy across several systems, and a summary of the existing literature can be found in *Table 1.1*. A30P mice exhibit up to 3 fold higher expression of human ASYN than endogenous murine ASYN (Kahle *et al.*, 2001). The same group found that endogenous murine ASYN does not aggregate like human ASYN, and maintains normal staining patterns when human ASYN is over-expressed (Kahle *et al.*, 2001).

Many of the physiological functions of ASYN are reduced or altered by the A30P mutation both *in vitro* and *in vivo*, including decreased interactions with the cytoskeleton (Esposito *et al.*, 2007; Sousa *et al.*, 2009), reduced or absent membrane binding (for review see Snead and Eliezer, 2014), and abnormal interactions with proteins regulating synaptic vesicle trafficking (Dalfo *et al.*, 2004). The A30P mutation leads to a reduced capacity of the dopaminergic storage pool (Yavich *et al.*, 2004). While this does not impact basal neurotransmission, the authors predicted an impairment in prolonged bursting of dopaminergic neurons (Yavich *et al.*, 2004).



Phenotypically, A30P mice exhibit fine motor impairment from the first few months of life (Ekmark-Lewen *et al.*, 2018), with hippocampal spatial memory performance in the Morris water maze declining by 12 months (Freichel *et al.*, 2007). More recently, work from our lab has highlighted a reduction in the power of *in vitro* carbachol-induced gamma-frequency oscillations and mitochondrial dysfunction by 9+ months of age (Robson *et al.*, 2018) in A30P mice. Severe motor dysfunction has been reported in A30P mice from around 16 months of age (Freichel *et al.*, 2007). Prior to this, A30P mice have been reported to exhibit unsteady gait, a weakening of the extremities, and abnormal tail posture and movement (Neumann *et al.*, 2002). Mice then develop paralysis and die prematurely at 17-18 months (Freichel *et al.*, 2007).

The motor deficits exhibited by A30P mice are not strictly Parkinsonian in nature, which is defined by bradykinesia, rigidity, rest tremor, and postural instability (for review see Keener and Bordelon, 2016). Interestingly, when human ASYN is virally expressed within the rat substantia nigra, WT ASYN results in Parkinsonian impairment whilst A30P ASYN expression does not (Gaugler *et al.*, 2012). The authors proposed that this may be due to impaired binding of A30P ASYN to the presynaptic membrane in dopaminergic neurons (Gaugler *et al.*, 2012). As a result, the *Thy-1* A30P mouse model appears more useful for investigation in to cortical-hippocampal network changes associated with the overexpression of human A30P ASYN.

The exact time course of neuronal dysfunction has not yet been elucidated in A30P mice, nor have the underlying cellular causes leading to the reported cognitive dysfunction. This thesis will focus particularly on hippocampal function, especially given evidence of hippocampal spatial memory impairment on the Morris water maze in ageing A30P mice (Freichel *et al.*, 2007). Whilst alpha-synucleinopathy in patients tends to present with cognitive deficits associated with prefrontal rather than hippocampal dysfunction, hippocampal pathology has indeed been shown to contribute to cognitive impairment in DLB (Adamowicz *et al.*, 2017).

<b>Months</b>	<b>Pathology</b>	<b>Motor</b>	<b>Cognition</b>
1-4 months	<ul style="list-style-type: none"> <li>• Insoluble ASYN in whole brain extracts, swollen ASYN+ neurites (Kahle <i>et al.</i>, 2001)</li> <li>• No loss of septal cholinergic neurons until mice were treated with mitochondrial Complex I toxin MPTP (Szego <i>et al.</i>, 2013).</li> </ul>	<ul style="list-style-type: none"> <li>• Fine motor impairment on beam test (Ekmark-Lewen <i>et al.</i>, 2018)</li> </ul>	
6-8 months	<ul style="list-style-type: none"> <li>• Loss of serotonin in striatum of males, increase in females. Increase in serotonin in frontal cortex (Neumann <i>et al.</i>, 2002).</li> <li>• Accumulation of oligomers in neuronal cell bodies (Ekmark-Lewen <i>et al.</i>, 2018).</li> </ul>	<ul style="list-style-type: none"> <li>• Decreased locomotor activity on open field test over 20 minutes and fine motor impairment on beam test (Ekmark-Lewen <i>et al.</i>, 2018).</li> </ul>	
10-14 months	<ul style="list-style-type: none"> <li>• Biochemically defined ASYN aggregates in the subthalamus, midbrain, and other regions. Histochemically defined ASYN aggregates in the brainstem (Neumann <i>et al.</i>, 2002).</li> <li>• Somal and neuritic ASYN pathology in the amygdala (Freichel <i>et al.</i>, 2007).</li> <li>• Modest reduction of GABA in the caudate putamen and forebrain (Keane, 2013).</li> <li>• Accumulation of oligomers in the brainstem, midbrain, and hippocampus. Increased GFAP+ astrocytes in areas with high ASYN e.g. the brainstem. No evidence of microglial activation and no change in cytokines (Ekmark-Lewen <i>et al.</i>, 2018).</li> </ul>	<ul style="list-style-type: none"> <li>• No change on rotarod, stride length gait, or grip strength. Exploratory behaviour was reduced (Keane, 2013)</li> <li>• Fine motor impairment on beam test (Ekmark-Lewen <i>et al.</i>, 2018)</li> <li>• Hyperlocomotion on open field test over 120 minutes (Freichel <i>et al.</i>, 2007), conflicting no change in distance travelled in open field test over 20 minutes (Ekmark-Lewen <i>et al.</i>, 2018)</li> </ul>	<ul style="list-style-type: none"> <li>• Hippocampal spatial memory impairment on the Morris water maze (Freichel <i>et al.</i>, 2007) but no Barnes maze impairment (Keane, 2013)</li> </ul>
16-18 months	<ul style="list-style-type: none"> <li>• Accumulation of ASYN in the cytoplasm of neurons. CA3/1 hippocampal regions positive for ASYN in dot-like structures (Schell <i>et al.</i>, 2012).</li> </ul>	<ul style="list-style-type: none"> <li>• Severe motor dysfunction on rotarod, paralysis (Freichel <i>et al.</i>, 2007)</li> </ul>	<ul style="list-style-type: none"> <li>• Impaired fear conditioning (Schell <i>et al.</i>, 2012).</li> </ul>

Table 1.1 **Summary of literature surrounding *Thy-1 A30P* mice.** Sub-divided by age groups and nature of deficits: pathology, motor dysfunction, and cognitive dysfunction.

## 1.2 The hippocampus

### 1.2.1 Hippocampal structure and function

When a bilateral temporal lobe resection left patient H.M. with anterograde amnesia, declarative memory was first attributed to the temporal lobe, in particular the hippocampal formation (for review see Augustinack *et al.*, 2014). To explore the cellular mechanisms underpinning memory, studies were moved to rodents where hippocampal structure and function are relatively conserved. In the years that followed, the hippocampus was implicated in spatial memory and navigation through place cells (O'Keefe and Dostrovsky, 1971), and sequencing the past, present, and future events of episodic memory (Suzuki and Eichenbaum, 2000). This association is supported by hippocampal atrophy visualised with magnetic resonance imaging (MRI) in pathological states associated with episodic and spatial memory impairment, including AD and post-traumatic stress disorder (McEwen and Magarinos, 1997).

Existing as a bilateral structure in the temporal lobe of the human and rodent brain, the hippocampal formation is composed of the dentate gyrus (DG) and cornu ammonis (CA) regions (Figure 1.2). From the DG, the hippocampus proceeds through CA3 to CA1, before reaching the subiculum and extending to the cortex.

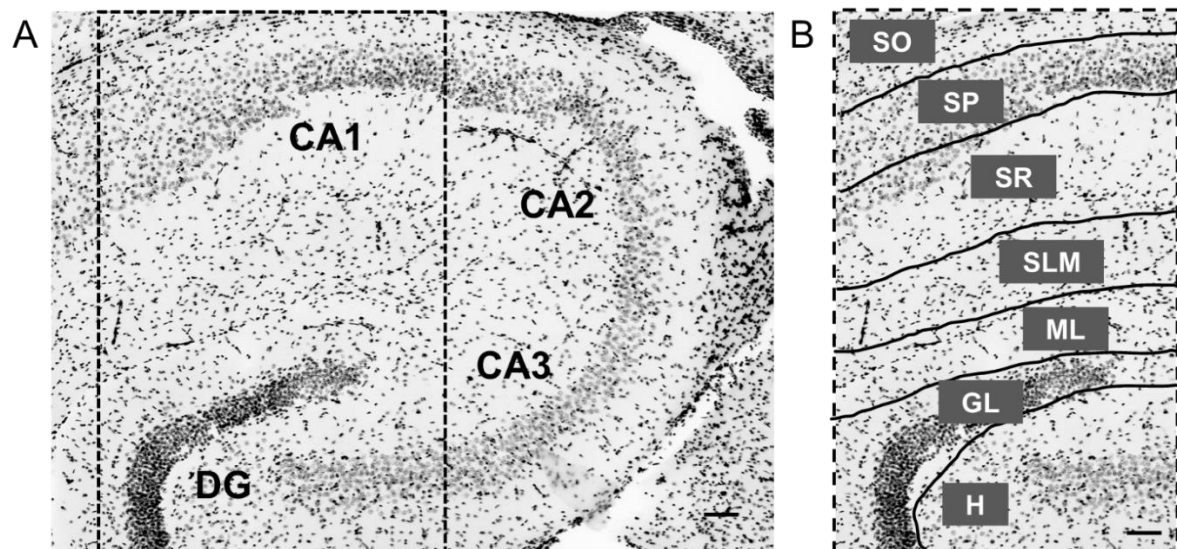


Figure 1.2 **Cytoarchitecture of mouse hippocampus.** Nuclear (DAPI) stained mouse hippocampal slice at x4 magnification showing the dentate gyrus (DG) and cornu ammonis (CA) regions CA3, CA2, and CA1 (A) and the defined layers across the hippocampus within the highlighted box (B): *stratum oriens* (SO), *stratum pyramidale* (SP), *stratum radiatum* (SR), *stratum lacunosum-moleculare* (SLM), molecular layer (ML), granule cell layer (GL), and the dentate gyrus hilus (H). Image inverted and presented in greyscale. Scale bar 100  $\mu$ m.

Pathways within the hippocampus were once believed to flow unilaterally from the entorhinal cortex (EC) to the DG and through regions CA3 and CA1 then back to the EC. However, it is now accepted that the EC is capable of projecting to both CA3 and CA1 (Witter *et al.*, 2000). The hippocampus is further divided along the anterior and posterior axis (the ventral and dorsal axis in rodents, respectively), with differentiation in connectivity and cognitive functions along the hippocampal axis (Moser and Moser, 1998; Fanselow and Dong, 2010).

Two main populations of neurons exist within the hippocampus. The principal cells of the CA regions are the glutamatergic pyramidal cells which provide excitation to the network. GABAergic interneurons make up ~10% of the network and provide effective inhibition due to their extensive arbors (for review see Freund and Buzsaki, 1996). Both pyramidal cells and interneurons are further innervated and modulated by a variety of cholinergic, dopaminergic, serotonergic and noradrenergic inputs (for review see Avery and Krichmar, 2017).

Pyramidal cells, so named for the shape of their somata, are concentrated in the eponymous *stratum pyramidale*. They possess both apical and basal dendrites and receive on average 30,000 excitatory inputs and 1700 inhibitory inputs per cell (Megias *et al.*, 2001). Basal dendrites extend from *stratum pyramidale* into the *stratum oriens*, while apical dendrites extend through *stratum radiatum* and *stratum lacunosum-moleculare*. Schaffer collateral fibres project from CA3 to CA1, and a cell-free sulcus divides the DG and CA1 (for review see Miles *et al.*, 1996).

The cell bodies of interneurons are typically present in or near *stratum pyramidale*, though some are found in *stratum oriens* or *stratum radiatum* (Kosaka *et al.*, 1987). Whilst interneurons primarily innervate pyramidal cells, it is estimated that 5-15% of synaptic contacts from interneurons are to other GABAergic cells (Cobb *et al.*, 1997). Following the first reports of electrical coupling between cells by gap junctions (Brightman and Reese, 1969), their presence between inhibitory interneurons of the same type was reported and proposed to function independently from chemical transmission (Gibson *et al.*, 1999). A complex network of excitatory and inhibitory connectivity is further enriched by a subset of interneurons known to specifically target other interneurons within the hippocampus (Urban *et al.*, 2002).

## 1.2.2 Inhibitory interneurons

Hippocampal interneurons can be characterised by a number of methods including cellular morphology, innervation of pyramidal cells, expression of calcium ( $\text{Ca}^{2+}$ ) binding proteins, expression of neuropeptides, receptor subtype expression, and electrophysiology (for review see Freund and Buzsaki, 1996). This section will briefly cover characterisation by expression of the  $\text{Ca}^{2+}$  binding proteins parvalbumin (PV), calbindin (CB), and calretinin (CR) as this method has been shown to largely differentiate GABAergic interneurons without overlap (for review see Freund and Buzsaki, 1996).  $\text{Ca}^{2+}$  plays a critical role in cellular signalling and associated aspects of neurotransmitter release and plasticity (for review see Clapham, 2007). While all three  $\text{Ca}^{2+}$  binding proteins have been found in the hippocampus, their expression varies between regions and cell types.

PV expression is restricted to a subpopulation of GABAergic interneurons within the hippocampus and constitute approximately 20-24% of hippocampal GABAergic interneurons (Celio, 1986; Kosaka *et al.*, 1987). Over 50% of PV+ cell bodies are located in or near *stratum pyramidale*, with 30-40% in *stratum oriens* and a small proportion in *stratum radiatum* (Kosaka *et al.*, 1987). All PV+ interneurons can be classified as either basket cells or chandelier cells (also known as axo-axonic cells) within the hippocampus, though not all basket cells and chandelier cells express PV (Ribak *et al.*, 1990). A single basket cell innervates the somata and proximal dendrites of 1500-2500 pyramidal cells (Kosaka *et al.*, 1987), whilst a single chandelier cell innervates the axon initial segment of at least 1200 pyramidal cells (Li *et al.*, 1992; Somogyi and Klausberger, 2005). Both cell types also innervate other interneurons.

PV+ interneurons are noted to show weak GABA immunoreactivity compared to other interneurons, and this is proposed to be a result of the high firing rate of PV+ interneurons meaning a fast turnover and release of GABA (Kosaka *et al.*, 1987). The majority of PV+ interneurons are fast-spiking, which is defined by a short action potential duration and a high frequency of firing without adaptation (Povysheva *et al.*, 2013). The fast-spiking property is proposed to be conveyed by expression of the voltage-gated potassium  $\text{K}_v3.1$  channel (Du *et al.*, 1996), and the majority of PV+ cells express  $\text{K}_v3.1$  (Chow *et al.*, 1999). However, a proportion of PV+ interneurons express channels such as  $\text{K}_v3.2$ , which possess a slower deactivation time than  $\text{K}_v3.1$  channels (Hernandez-Pineda *et al.*, 1999). It can therefore be inferred that while the majority of PV+ cells are also fast-spiking, this is not always the case.

Unlike PV, CB+ and CR+ cells show a more varied pattern of expression and are not specific to GABAergic interneurons (Sloviter *et al.*, 1991). Expression is found in granule cells of the DG and in pyramidal cells of the CA1 region, in addition to inhibitory interneurons throughout the hippocampus (Freund and Buzsaki, 1996). CR+ interneurons are capable of innervating pyramidal cells, though preferentially target other interneurons, particularly CB+ or other CR+ cells (Yamaguchi *et al.*, 1991). CR+ cells are present throughout all layers and subfields of the hippocampus and can be further classified by the presence or absence of spines (Yamaguchi *et al.*, 1991).

CB+ interneurons constitute only around 10-12% of GABAergic interneurons within the hippocampus and many CB+ cell bodies are located within *stratum radiatum* (Toth and Freund, 1992). CB+ interneurons tend to innervate pyramidal cell dendrites and are often classified as *oriens-lacunosum moleculare* (O-LM) cells, bistratified cells, or radial trilaminar cells. CR+ and CB+ interneurons do not possess the fast-spiking property that the majority of PV+ interneurons possess but are crucial for providing inhibition and maintaining the balance of excitation and inhibition within the hippocampal network (Puig *et al.*, 2008).

### **1.2.3 Excitatory/inhibitory neurotransmission**

The most abundant excitatory neurotransmitter in the mammalian brain is glutamate (for review see Petroff, 2002). There are two types of glutamate receptors: ionotropic (ligand-gated ion channels) and metabotropic (G-protein coupled receptors). Ionotropic receptors act directly to open an ion channel in the cell membrane, while metabotropic receptors act indirectly through an intracellular signalling mechanism (for review see Willard and Koochekpour, 2013). Subsets of ionotropic glutamate receptors are named after compounds that selectively bind to each: AMPA, Kainate, and NMDA (Table 1.2). Metabotropic glutamate receptors are subdivided into three groups: Group I (mGluR1, mGluR5), Group II (mGluR2, mGluR3), and Group III (mGluR4, mGluR6, mGluR7, mGluR8). Each receptor subtype is further modulated by differential subunit expression. The diversity of glutamate receptors allows a diversity of responses to one abundantly used neurotransmitter (for review see Willard and Koochekpour, 2013).

The AMPA receptor is crucially involved in the process of synaptic plasticity, a process which is important for the formation of memories and the process of learning (Morris *et al.*, 1986; Whitlock *et al.*, 2006). Synaptic plasticity can be either short-term (milliseconds to minutes) or long-term (minutes to hours), with the latter including long-term potentiation (LTP) and long-term depression (LTD) (for review see Bear *et al.*,

2015). Synaptic plasticity can be dependent on, or independent of, the NMDA receptor though both mechanisms require an influx of  $\text{Ca}^{2+}$  and pathways leading to AMPA-receptor insertion (Wang *et al.*, 1997). NMDA-independent plasticity may involve kainate receptors (Lauri *et al.*, 2001) or mGluRs (Hunt and Castillo, 2012), for example.

	<b>NMDA-R</b>	<b>AMPA-R</b>	<b>KA-R</b>
Properties	Voltage-dependent, depolarisation to remove $\text{Mg}^{2+}$ block. Requires co-agonist glycine. Permeable to $\text{Na}^+$ , $\text{Ca}^{2+}$ , and $\text{K}^+$ .	Fast synaptic transmission. Permeable to $\text{Na}^+$ and $\text{K}^+$ , can be either $\text{Ca}^{2+}$ impermeable or permeable.	Transmission slower than AMPA-R. Permeable to $\text{Na}^+$ and $\text{K}^+$ , sometimes $\text{Ca}^{2+}$ permeable depending on subunits.
Key Agonists	Glutamate or NMDA and glycine and depolarisation	Glutamate or AMPA	Glutamate or kainate
Key Antagonists	D-AP5, MK-801, Ketamine, PCP, Memantine	CNQX, NBQX, DCPG, GYKI53655, Perampanel	CNQX, NBQX, UBP-310, NS102 (many also target AMPA-R)
Most common clinical relevance	Anaesthetics, schizophrenia, dementia.	Seizures	Seizures

Table 1.2 **Summary of ionotropic glutamate receptor properties and pharmacology.** NMDA-R, AMPA-R, KA-R properties, key agonists and antagonists, and clinical relevance. Adapted from (Golan *et al.*, 2011) and (Bear *et al.*, 2015).

NMDA-dependent LTP can occur due to the removal of the voltage-dependent magnesium block of the NMDA-receptor upon high-frequency stimulation. The influx of  $\text{Ca}^{2+}$  into the cell acts upon  $\text{Ca}^{2+}$ /calmodulin-dependent protein kinase II (CaMKII) and protein kinase A/C (PKA/C). This leads to the insertion of fast-acting AMPA receptors into the synaptic membrane and potentiation of excitatory postsynaptic potentials (EPSPs). Changes in membrane AMPA-receptor composition are short-lived, and maintenance requires protein synthesis and gene expression (Taube and Schwartzkroin, 1988). LTD occurs following low frequency stimulation whereby protein phosphatase 1/2A (PP1/2) leads to removal of AMPA-receptors from the synaptic membrane. As a result, EPSPs are depressed (Mauna *et al.*, 2011). Interestingly, it has also been suggested that ASYN may play a complex role in synaptic plasticity

(Marxreiter *et al.*, 2013). ASYN oligomers applied to rat hippocampal slices oppose LTP by increasing basal synaptic transmission through NMDA receptor activation, thus preventing EPSP potentiation by high-frequency stimuli (Diogenes *et al.*, 2012).

The main inhibitory neurotransmitter in the mammalian brain is GABA (Roberts and Frankel, 1950; for review see Petroff, 2002). The role of GABAergic neurotransmission in synaptic plasticity should not be overlooked. High frequency stimulation of excitatory neurons in the hippocampus induces both LTP in other excitatory neurons, and LTD in inhibitory neurons (McMahon and Kauer, 1997). Connectivity of excitatory and inhibitory neurons is therefore crucial. GABA is synthesised from glutamate (Golan *et al.*, 2011), and acts on two types of GABA receptors: the ligand-gated ion channel ionotropic GABA receptors (GABA<sub>A</sub> and GABA<sub>C</sub>) and a G-protein coupled metabotropic GABA receptor (GABA<sub>B</sub>). As with glutamatergic receptors, further diversity occurs with differential subunit expression. By far the most abundant GABAergic receptor in the mammalian brain is the GABA<sub>A</sub> receptor (Golan *et al.*, 2011). Agonists of the GABA<sub>A</sub> receptor include muscimol, while antagonists include gabazine, bicuculline, and picrotoxin.

Dysfunction in excitatory/inhibitory neurotransmission is implicated in a number of diseases and disorders. Excess glutamatergic activity is involved in the process of excitotoxicity, which can lead to cell death due to high levels of intracellular Ca<sup>2+</sup> (Manev *et al.*, 1989). This mechanism is proposed to occur in AD and PD (Hynd *et al.*, 2004; Dong *et al.*, 2009), as well as in epilepsy (for review see Barker-Haliski and White, 2015). Excitotoxicity is the targeted mechanism of the NMDA-receptor antagonist memantine, which shows some effectiveness in treating cognitive deficits in LBD (Aarsland *et al.*, 2009). Conversely, NMDA receptor hypofunction has been proposed to underpin schizophrenia (Olney *et al.*, 1999), implicating a glutamatergic deficit (Bitanhirwe *et al.*, 2009).

Changes in GABAergic neurotransmission have long been explored in psychiatric disorders and epilepsy, the latter of which can involve a marked reduction in GABAergic inhibition leading to seizure activity (Wong *et al.*, 2003). However, it is only in more recent years that evidence of a GABAergic deficit in AD has been explored following earlier studies of post-mortem tissue showing a loss of GABA within the hippocampus (Rossor *et al.*, 1984) whilst other studies found a less significant reduction (Ellison *et al.*, 1986). Conversely, excess GABA can cause sleep disturbances and even lead to absence seizures (Arnulf *et al.*, 2005; Cope *et al.*, 2009).



### 1.3 Neuroglia

Neuroglia were first named in 1859 by Rudolf Virchow, and so named for their supposed function as the “glue” of the brain holding neurons in place (for reviews see Hof *et al.*, 2009; Bear *et al.*, 2015). Knowledge of glia has advanced greatly since then, and their active role and importance in brain functions is now known to be just as important as that of neurons. Glia express ion channels and receptors for neurotransmitters, cytokines, and chemokines, though expression of each varies at different stages of development and in different regions of the brain (Verkhratsky and Butt, 2007). Astrocytes and microglia may be pro-inflammatory or anti-inflammatory (Figure 1.3), which has important implications for disease pathology and therapeutics (Crotti and Ransohoff, 2016; Liddelow *et al.*, 2017).

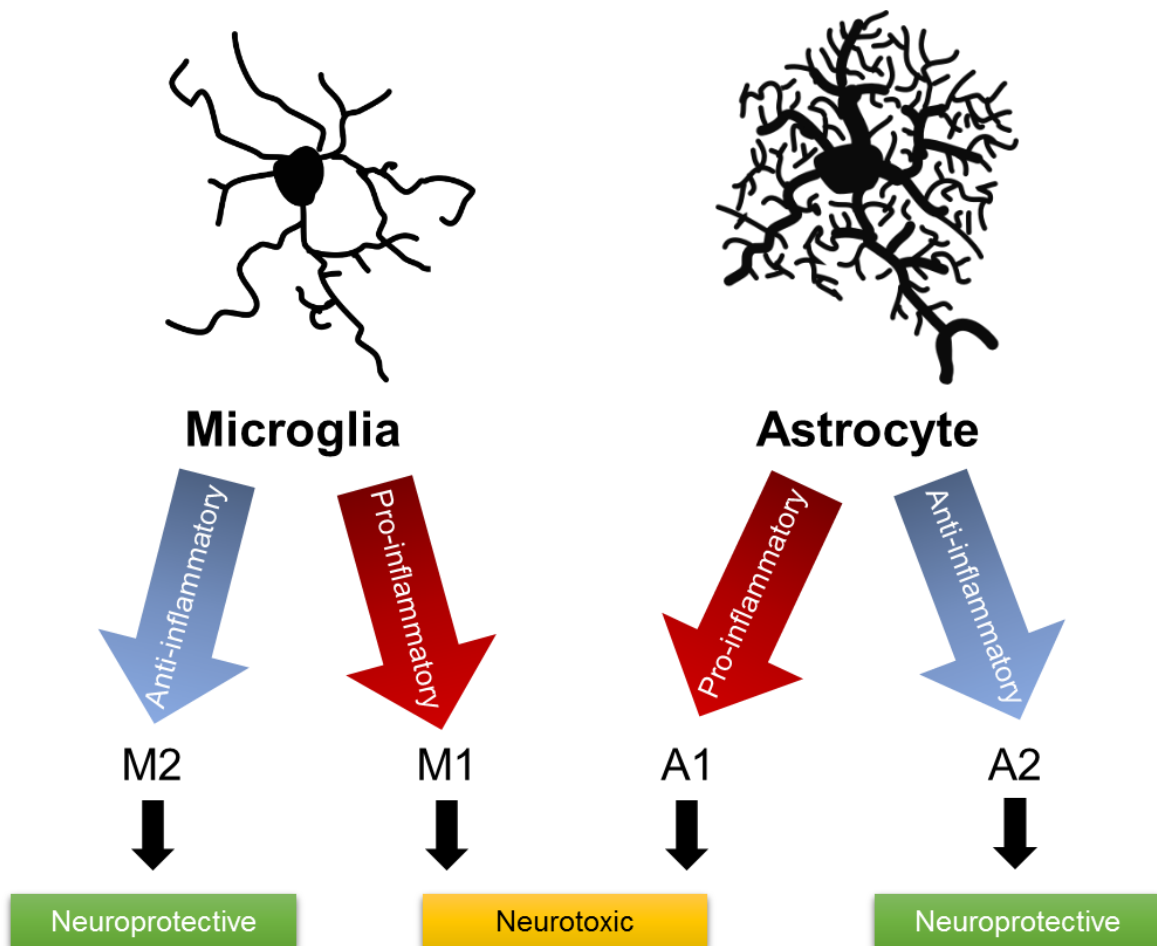


Figure 1.3 **Neuroprotective and neurotoxic states of microglia and astrocytes.** Adapted from (Jha *et al.*, 2015) with microglia/astrocyte outlines taken with permission with Riken Center for Brain Science: Laboratory for Neuron-Glia Circuitry: Creative Commons Public Domain [accessed July 2018].

### 1.3.1 Astrocytes

Astrocytes are star-shaped glia making up anywhere from 20 to 50% of brain volume and surrounding neuronal synapses, dendrites, and somata with their processes (for review see Hof *et al.*, 2009). Astrocytes can be broadly subdivided into protoplasmic astrocytes of the grey matter, and fibrous astrocytes of the white matter. Protoplasmic and fibrous astrocytes both make contact with blood vessels, but differ in where they contact neurons (Verkhratsky and Butt, 2007).

The role that astrocytes play is diverse and includes the control of neuronal migration during development and functional modulation of mature synapses (for review see Vesce *et al.*, 1999). Astrocytes form a tripartite synapse with the presynaptic and postsynaptic terminal of a neuron (Sofroniew and Vinters, 2010). The electrical connection between astrocytes through gap junctions allows coordination of responses and aids in the spread of calcium waves throughout the astrocytic network (Bennett *et al.*, 2003). Astrocytes respond to most neurotransmitters, which evoke an increase in astrocytic intracellular calcium levels and modulation of synaptic transmission within the tripartite synapse (Vesce *et al.*, 1999). Furthermore, astrocytes can synchronously activate groups of pyramidal cells (Haydon and Carmignoto, 2006), thus allowing wider control of network activity.

Astrocytes have further been shown to release neurotransmitters such as glutamate and GABA to modulate both excitatory and inhibitory neuronal activity (for review see Verkhratsky and Butt, 2007), and are also closely associated with memory formation due to their role in synaptic remodelling and plasticity (Zorec *et al.*, 2015). Neuronal excitability is regulated by the astrocytic network through its critical role in maintaining the concentration of extracellular glutamate at physiologically low levels by clearance of synaptically released glutamate (for review see Vesce *et al.*, 1999), in addition to buffering extracellular potassium to control neuronal excitability (Wallraff *et al.*, 2006). Furthermore, astrocytes provide metabolic support to neurons through neurovascular coupling (Viswanathan and Freeman, 2007).

In response to injury, infection or disease, a reactive change occurs in astrocyte number, morphology, or molecular expression pattern to protect or repair nearby neurons (for review see Sofroniew and Vinters, 2010). While astrogliosis typically ends in scar formation, a cascade of changes occur before this point which are often reversible, including upregulation of glial fibrillary acid protein (GFAP) and vimentin, both intermediate filaments forming the astrocytic cytoskeleton (for review see

Verkhatsky and Butt, 2007; Anderson *et al.*, 2014). GFAP upregulation has been reported in a number of pathological conditions, including an increase following seizures in rats to support increased neuronal activity (Steward *et al.*, 1992) and post-mortem in AD patients (Bignami *et al.*, 1972; Kamphuis *et al.*, 2014).

Activated astrocytes have more recently been classified as two distinct forms: A1 and A2 astrocytes. A1 astrocytes are pro-inflammatory, lose their ability to perform normal physiological functions, and secrete neurotoxic factors to remove neurons and synapses (Liddelow *et al.*, 2017). Conversely, A2 astrocytes are anti-inflammatory and participate in the process of neuroprotection and repair (for review see Sofroniew and Vinters, 2010). The number of A1 astrocytes are increased in physiological ageing and may therefore infer a vulnerability to neurodegeneration (Clarke *et al.*, 2018).

### **1.3.2 Microglia**

Due to the role of the blood-brain barrier in excluding immune cells from the brain, the brain's native microglial cells act as immune regulators (for review see Hof *et al.*, 2009) and make up around 10–15% of cells within the brain (Lawson *et al.*, 1992). The so-called “resting” microglia are incorrectly named, given their active role in surveillance of their microenvironment and maintaining homeostasis (Davis *et al.*, 1994). Instead, resting microglia are preferentially referred to as ramified microglia due to their small somata and long processes (for review see Hof *et al.*, 2009).

Potassium (K<sup>+</sup>) channels on microglia respond to small disturbances in extracellular K<sup>+</sup>, often caused by damaged or ruptured cells (Gehrmann *et al.*, 1995). Microglia also recognise and respond to immune threats and misfolded proteins (for review see Verkhatsky and Butt, 2007). The response of microglia is to become activated or “reactive” (Davis *et al.*, 1994), and upregulation of the ionised calcium-binding adapter molecule 1 (Iba1) can be used to detect this change (Ito *et al.*, 1998). Reactive microglia are marked by a change in morphology, with a larger somata and shorter processes (for review see Verkhatsky and Butt, 2007). Reactive microglia carry out a number of roles including the release of mediators (for review see Hof *et al.*, 2009) and activation of astrocytes (Liddelow *et al.*, 2017).

Microglia also play a role in synaptic pruning in network development (Paolicelli *et al.*, 2011) through phagocytosis (for review see Miyamoto *et al.*, 2013). Consequently, microglia are implicated in synaptic plasticity through phagocytosis of weaker synapses and maturation of postsynaptic responses (for review see Miyamoto

*et al.*, 2013). Microglia make brief connections with neurons and astrocytes, and it has been shown that following contact neuronal activity is reduced (for review see Miyamoto *et al.*, 2013). Microglia may also indirectly modulate neuronal excitability through activation of astrocytes (for review see Miyamoto *et al.*, 2013). It is unsurprising therefore that like astrocytes, microglia are implicated in the pathogenesis of epilepsy (Devinsky *et al.*, 2013). There is also growing evidence of neuroinflammation in AD and PD, which may be a result of misfolded proteins inducing microglial reactivity (Mrak and Griffin, 2005; Barnum and Tansey, 2012; Meraz-Rios *et al.*, 2013).

Similarly to the A1/A2 phenotype of reactive astrocytes, reactive microglia have also been proposed to occupy two distinct states of neurotoxicity (M1) and neuroprotection (M2), marked by the differential release of pro-inflammatory or anti-inflammatory factors, respectively (for review see Bolos *et al.*, 2017). While both phenotypes of microglia are marked by Iba1 upregulation, specific markers can be used to differentiate between each state (for review see Bolos *et al.*, 2017). Conversion of microglia from M2 to M1 can occur as a result of physiological ageing or in neurodegenerative disease (Tang and Le, 2016). Conversion back to the neuroprotective M2 form has been shown to be promoted by non-steroidal anti-inflammatory drugs (Moehle and West, 2015).

## 1.4 Oxidative Stress

### 1.4.1 Mitochondria

The brain is a highly energy-demanding organ and must replenish levels of adenosine triphosphate (ATP) through oxidative phosphorylation in mitochondria or glycolysis in the cytosol (Erecinska and Silver, 2001; Distelmaier *et al.*, 2009). The importance of mitochondria in the brain cannot be understated, for in addition to their role in energy production they have also been linked to metabolism, cell death through apoptosis, cell signalling pathways, control of the cell cycle, and calcium signalling (Green, 1998; McBride *et al.*, 2006).

Mitochondria consist of highly folded inner membranes known as cristae, and within these spaces is the matrix (for review see Bear *et al.*, 2015). It is within the matrix that the Krebs cycle occurs, where acetyl coenzyme A derived from pyruvate enters a series of redox reactions and ultimately produces ATP, NADH, and FADH<sub>2</sub> (for review see Bear *et al.*, 2015). NADH and FADH<sub>2</sub> then participate in a series of redox reactions along a series of protein complexes imbedded in the inner membrane of the mitochondria (Figure 1.4). Briefly, NADH and FADH<sub>2</sub> enter the electron transport chain at Complex I (NADH dehydrogenase) or II (succinate dehydrogenase, SDH), respectively, and donate electrons. As a result, protons are pumped across the membrane from the matrix to the intermembrane space at Complex I (for reviews see Lodish *et al.*, 2000; Berg *et al.*, 2002). This establishes a proton gradient, further contributed to as electrons pass through Complex III (cytochrome C reductase).

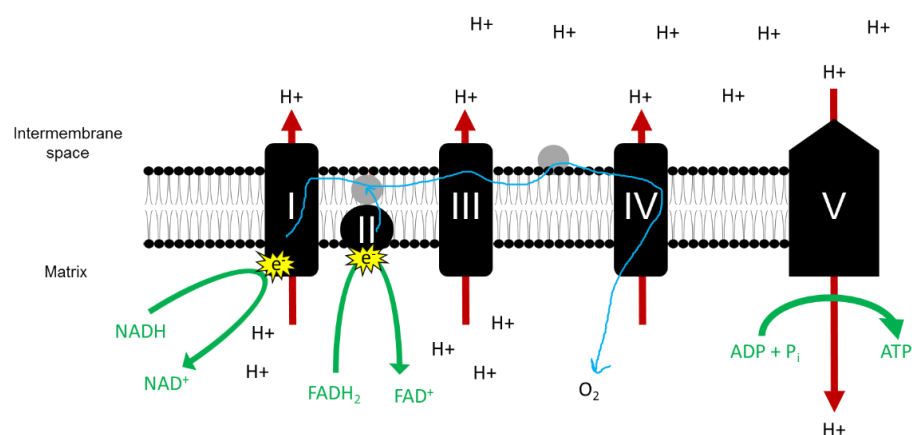


Figure 1.4 **The process of oxidative phosphorylation.** Movement of electrons (e-) in blue and protons (H<sup>+</sup>) in red through Complexes I to V. NADH/NAD<sup>+</sup> nicotinamide adenine dinucleotide. FADH<sub>2</sub>/FAD<sup>+</sup> flavin adenine dinucleotide. ADP adenosine diphosphate. P<sub>i</sub> inorganic phosphate. ATP adenosine triphosphate. Adapted from OpenStax CNX, Rice University [Accessed July 2018] [https://cnx.org/contents/GFy\\_h8cu@10.87:7oTVAgrZ@7/Oxidative-Phosphorylation](https://cnx.org/contents/GFy_h8cu@10.87:7oTVAgrZ@7/Oxidative-Phosphorylation).

When electrons reach Complex IV (cytochrome C oxidase, COX), they are transferred to oxygen and reduced to form water (H<sub>2</sub>O). As a result of the established proton gradient, protons flow through Complex V (ATP synthase) down their concentration gradient and this movement is coupled with the formation of ATP and H<sub>2</sub>O from ADP and phosphate (Boyer, 1997; Lodish *et al.*, 2000).

The majority of ATP production within a cell comes from oxidative phosphorylation (Rich, 2003) and it is estimated that around 28-30 ATP molecules are produced from one molecule of glucose. This number takes into account the leak of electrons from Complex I and Complex III (Cadenas *et al.*, 1977), a physiological occurrence leading to the production of reactive oxygen species (ROS). ROS can act as signalling molecules, but their excess production can occur as a result of dysfunction of the electron transport chain (ETC), as demonstrated by Complex I inhibition with rotenone increasing ROS production (Turrens and Boveris, 1980).

Beyond their crucial role in energy production, mitochondria also play important roles as calcium buffers to maintain homeostasis (Pozzan *et al.*, 1994; Berridge *et al.*, 2000) and as a result can regulate the excitability of cells. Reciprocal interplay between ROS and calcium also means that excess calcium can increase ROS levels, whilst excess ROS production can affect calcium influx (for review see Görlach *et al.*, 2015).

#### **1.4.2 Mechanisms of oxidative stress**

The process of oxidative stress describes excess production of ROS such as superoxide and hydroxyl radicals, and the associated damage they cause. ROS are primarily produced by the ETC in mitochondria and excess ROS can lead to the damage of lipids, proteins, and DNA (Frisard and Ravussin, 2006). Mitochondria are protected under physiological conditions from oxidative damage by antioxidants such as superoxide dismutase, but an increase in ROS production or a reduction in antioxidant defences can lead to oxidative stress (Ceriello, 2000).

Oxidative stress is associated with the mechanisms of physiological ageing (Harman, 1956). A decline in the activity of mitochondrial ETC Complexes I, III and IV has been reported in aged mice (Desai *et al.*, 1996) and is proposed to lead to increased ROS production. Interestingly, the overexpression of antioxidant genes in *Drosophila* reduce oxidative damage and increase lifespan (Orr and Sohal, 1994).

Oxidative stress has further been reported in pathological states including inflammation (Furukawa *et al.*, 2004; Sofroniew and Vinters, 2010), Alzheimer's

disease (Mecocci *et al.*, 1994; Milton, 2004), and schizophrenia (Nishioka and Arnold, 2004). A deficiency in mitochondrial Complex I has also been reported in PD (Schapira *et al.*, 1990), and the import of over-expressed or aggregated ASYN into mitochondria has been suggested as a mechanism for Complex I inhibition (Devi *et al.*, 2008; Reeve *et al.*, 2015). Whilst mitochondrial dysfunction may in itself lead to the production of ROS through the leak of electrons, this may generate a cycle whereby ROS causes further mitochondrial dysfunction (Lee and Wei, 2005).

Interestingly, *Thy-1* A30P mice have shown a possible increased sensitivity to mitochondrial Complex I toxin MPTP, indicating a deficiency in Complex I function (Nieto *et al.*, 2006). Furthermore, mitochondrial proteins have been reported to be oxidised in A30P mice (Poon *et al.*, 2005), suggesting an interaction between oxidative stress and ASYN. Physiologically, ASYN has been shown to play a role in the modulation of mitochondrial morphology and function under conditions of stress by colocalising with mitochondria (Li *et al.*, 2007; Guardia-Laguarta *et al.*, 2014). As a result, the protective role of ASYN may be altered by the presence of the A30P mutation and may lead to inhibition of ETC complexes.

The interneuron energy hypothesis proposes that due to the high metabolic demands of fast-spiking PV+ interneurons, they are more vulnerable to dysfunction due to metabolic or oxidative stress (Kann, 2016). PV+ interneurons have been shown to be highly enriched with mitochondria and express high levels of cytochrome c (Inan *et al.*, 2016; Kann, 2016), a mitochondrial protein that transfers electrons between Complex III and Complex IV. Conversely, CB+ interneurons express a moderate amount of cytochrome c, and CR+ interneurons express very little (Gulyas *et al.*, 2006). Due to the fast-spiking property of the majority of PV+ interneurons, they are selectively vulnerable to oxidative stress whilst CB+ and CR+ interneurons are not (Cabungcal *et al.*, 2013b). This highlights the importance of mitochondrial function to fast-spiking interneurons, in addition to their enhanced vulnerability to mitochondrial dysfunction.

### **1.4.3 Perineuronal nets**

Vulnerable subpopulations of neurons with high energy demands are afforded some protection against oxidative stress and excitotoxicity in the form of perineuronal nets (PNNs) (Morawski *et al.*, 2004; Suttkus *et al.*, 2012). The PNN is a highly specialised extracellular matrix of proteins surrounding neurons, of which the primary components are hyaluronan, chondroitin sulfate proteoglycans, tenascins, and link proteins (Zimmermann and Dours-Zimmermann, 2008; Lau *et al.*, 2013). Highly

metabolically active neurons are preferentially surrounded by PNNs, and they are therefore proposed to play a role in ion homeostasis by buffering ions including excess  $K^+$ ,  $Na^+$ , and  $Ca^{2+}$  (Bruckner *et al.*, 1993; Hartig *et al.*, 1999; Morawski *et al.*, 2004). In addition, PNNs chelate iron and transition metals involved in ROS formation (Cabungcal *et al.*, 2013b). The relationship between PNNs and oxidative stress is complex; while PNNs can induce the expression of anti-oxidants (Canas *et al.*, 2007), ROS degrade hyaluronan and chondroitin sulfates in PNNs (Rees *et al.*, 2004).

PNNs surround the majority of fast-spiking PV+ interneurons and a small number of PV- interneurons (Hartig *et al.*, 1992; Lensjo *et al.*, 2017). The majority of PV+ interneurons with a PNN also express  $Kv3.1$ , associated with the fast-spiking property of PV+ interneurons (Hartig *et al.*, 1999). Interestingly, the presence of the PNN has been shown to enhance the excitability of fast-spiking interneurons (Balmer, 2016). A subpopulation of hippocampal PV+ interneurons lack a PNN (Yamada and Jinno, 2015), and it can be inferred that this may be the non-fast spiking population.

Beyond their role in neuroprotection and enhancing excitability, PNNs also play a role in the closure of the critical period in development and synaptic plasticity (Bruckner *et al.*, 2000; Friauf, 2000; Bukalo *et al.*, 2001). It is unsurprising therefore that PNN changes have been reported in various pathological states associated with memory deficits, though the exact nature of the change varies depending on the region studied and the specific marker measured. While one study found a loss of the N-acetylgalactosamine sugar in AD post-mortem tissue (Baig *et al.*, 2005), another study using a mouse model of AD with early life memory deficits found an increase in hyaluronan, neurocan, brevican, and tenascin-R (Vegh *et al.*, 2014). The authors also found that memory deficits could be reversed by PNN degradation (Vegh *et al.*, 2014).

Interestingly, the PNN component aggrecan was found to be increased following a single seizure early in life in rats (McRae *et al.*, 2010). The authors propose that this occurs directly due to increased neuronal activity and highlights the plastic nature of PNN expression (McRae *et al.*, 2010). It could be inferred that the increase in PNN expression may be a compensatory attempt to control seizure activity by increasing the excitability of fast-spiking interneurons (Balmer, 2016). Conversely, prolonged seizure activity in the adult rat hippocampus led to a decrease in aggrecan expression for at least 2 months (McRae *et al.*, 2012). It is suggested that this leaves inhibitory interneurons capable of synaptic reorganisation and plasticity.



## 1.5 Hippocampal network activity

### 1.5.1 The electroencephalogram (EEG)

First described by Hans Berger in 1929, the mammalian electroencephalogram (EEG) is a well-established, non-invasive method of recording electrical activity. Recordings can be taken in humans via electrodes on the surface of the scalp during various states of rest, sleep, and activity. The measurable activity on EEG is generated by synchronous firing of populations of neurons, with precise timing of activity important for information processing across brain regions. For the purpose of this thesis, frequencies up to 80 Hz are briefly summarised in Table 1.3.

Abnormal EEG burst-pattern activity has been reported in the frontal region of patients with DLB (Crystal *et al.*, 1990), which could well underpin fluctuating cognition. Whilst the cognitive dysfunction associated with LBD is more prefrontal than hippocampal in nature, a general slowing of EEG activity to lower frequency bands has been observed in DLB patients (Bonanni *et al.*, 2008; Andersson *et al.*, 2010; Morris *et al.*, 2015; Stylianou *et al.*, 2018). A precise interplay between prefrontal and hippocampal activity orchestrates complex cognitive processes such as memory (Preston and Eichenbaum, 2013; Sigurdsson and Duvarci, 2015), and therefore the effect of ASYN expression on hippocampal function should not be understated.

Pattern	Frequency	Associated states
Delta	0.5 – 4 Hz	Slow-wave sleep and periods of unconsciousness (Bonanni <i>et al.</i> , 2012).
Theta	4 – 12 Hz	Active exploration (Buzsaki, 2005), and REM sleep (Grosmark <i>et al.</i> , 2012). Often seen with superimposed gamma activity in the hippocampus.
Alpha	8 - 10 Hz	Relaxed wakefulness with closed eyes (Niedermeyer, 1997).
Beta	I: 15 – 20 Hz II: 20 – 30 Hz	Relaxed wakefulness with open eyes (Niedermeyer, 1997). Role in motor control, e.g. planning and suppression of movement (Zhang <i>et al.</i> , 2008).
Gamma	30 – 80 Hz	Exploration, navigation, conscious perception, cognitive processing, learning and memory (Lu <i>et al.</i> 2012).

Table 1.3 **Patterns of activity between 0.5 and 80 Hz.** The frequency ranges and associated states of activity bands from delta to gamma frequency.

Suggested to be a potential solution to the binding problem, gamma activity is theorised to play a role in segregating and combining sensory inputs to allow the brain to process multimodal stimuli (Uhlhaas and Singer, 2006). It is proposed that high frequency oscillations allow the rapid and precise transfer of information across regions of the brain. In addition to their role in navigation (likely due to superimposition on theta activity), gamma waves are frequently implicated in cognitive processing, learning and memory (Lu *et al.*, 2012b). Furthermore, gamma activity has been observed in the temporal lobe of rodents both *in vivo* (Bragin *et al.*, 1995) and *in vitro* (Fisahn *et al.*, 1998), allowing for exploration of the mechanisms of network activity over the years.

Since the first recordings of electrical activity in an acute brain slice preparation using a chemically defined artificial media (Yamamoto and McIlwain, 1966), a wealth of work has been performed within the hippocampus to understand the physiology and pharmacology of the region. It is widely understood that a single neuron is not capable of orchestrating higher cognitive functions alone, and instead acts in synchrony with other neurons (Quiroga, 2013) to produce detectable fluctuations in the local field potential (LFP) which can be recorded from a brain slice.

### **1.5.2 Generation of *in vitro* network oscillations**

As gamma-frequency oscillations occur above the frequency of pyramidal cell firing (1 – 3 Hz), their generation *in vitro* was not fully understood until GABAergic interneurons were implicated, which fire at up to 40 Hz (Whittington *et al.*, 1995). Indeed, the frequency of network oscillations is dependent on the decay kinetics of GABA (Otis and Mody, 1992; Heistek *et al.*, 2010; Lee and Jones, 2013). As inhibitory GABAergic interneurons project to both excitatory pyramidal cells and other inhibitory cells, two models incorporating these cell types have been proposed.

The interneuron network gamma (ING) model was first elucidated *in vitro* in the rat hippocampus (Whittington *et al.*, 1995). Upon application of antagonists for the ionotropic glutamate receptors NMDA, AMPA and kainate, a metabotropic glutamate agonist was added to a slice and induced gamma activity. With only inhibitory circuits intact, it was suggested that gamma-frequency activity can be generated locally by interneurons, with gap junctions proposed to form an axonal plexus and help stabilise the oscillatory cycle through fast, electrical transmission (Traub *et al.*, 1999). The ING model, however, did not explain the projection of gamma-frequency activity over large distances both within the hippocampus and beyond. The principal-cell interneuron

network gamma model (PING) (Borgers and Kopell, 2005) compensates for this distance by the incorporation of excitatory principal cell transmission (Figure 1.5).

A network of connected interneurons and pyramidal cells are proposed to exist in the PING model, with pyramidal cells firing earlier than interneurons in a cycle (for review see Hajos and Paulsen, 2009). The resultant EPSPs generated in interneurons generate an inhibitory feedback mechanism upon excitatory cells. Rhythmic trains of inhibitory postsynaptic potentials (IPSPs) occur in excitatory cells and end the cycle. Once the IPSP has dissipated, pyramidal cells are able to fire again and start the next cycle. Thus, interneurons are required for precise spike timing in pyramidal cells.

Interest in fast-spiking PV+ interneurons has grown due to their involvement in gamma-frequency network oscillations in rodents *in vivo*, as demonstrated in mice by optogenetically silencing or driving fast-spiking PV+ interneurons (Sohal *et al.*, 2009). CA3 region gamma-frequency oscillations in slices from rodents *in vitro* are also dependent upon functional fast-spiking PV+ interneurons (Traub *et al.*, 2000; Fuchs *et al.*, 2007; Ferando and Mody, 2015). In turn, this has led to PV+ interneuron dysfunction serving as a possible explanation for cognitive deficits (Fuchs *et al.*, 2007) and lost network connectivity in a number of disorders, including schizophrenia (Nakazawa *et al.*, 2012) and AD (Brady and Mufson, 1997)

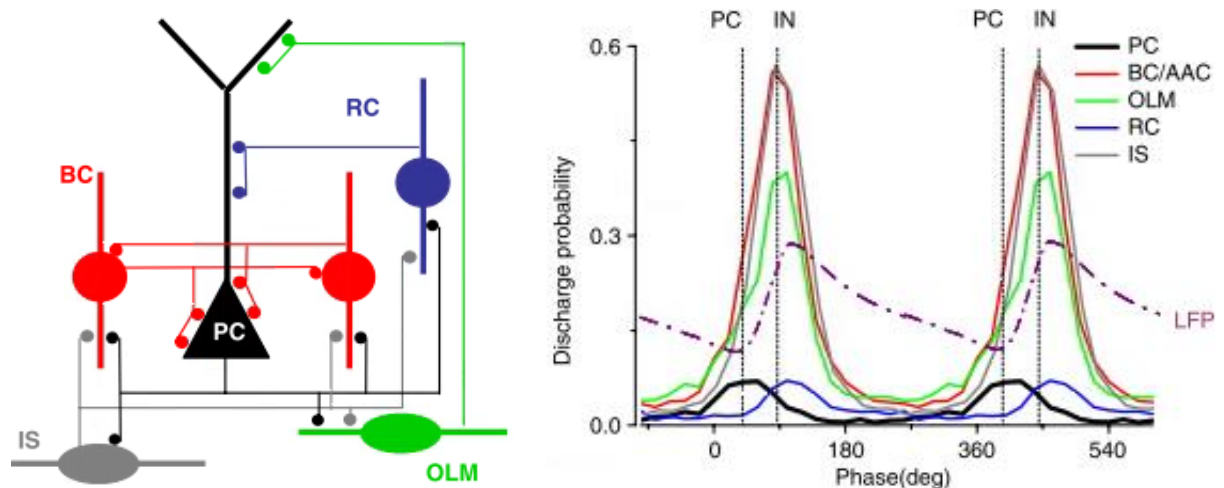


Figure 1.5 **Pyramidal cell-interneuron circuitry in the hippocampal CA3 region.** PC pyramidal cell. BC basket cell. AAC axo-axonic cell. OLM oriens lacunosum moleculare cell. RC *stratum radiatum* cell. IS interneuron-selective interneurons. LFP local field potential. IN inhibitory neuron. Modified and used with permission from Network mechanisms of gamma oscillations in the CA3 region of the hippocampus (Hajos and Paulsen, 2009) *Neural Networks*, 22 (8), pp. 1113-9.

The generation and investigation of oscillations *in vitro* allows investigation of the association between network oscillations and underlying cellular activity in an isolated region of the brain. While in some rodent hippocampal slice preparations spontaneous gamma-frequency activity can be observed, this activity relies on increased preservation of cell viability during the preparation of slices (Skrobot, 2008; Pietersen *et al.*, 2009; Modebadze, 2014). Therefore, methods to more reliably induce persistent hippocampal gamma-frequency oscillations using interface chamber recordings can be achieved pharmacologically by providing excitation to the network through use of carbachol (Traub *et al.*, 1992; Fisahn *et al.*, 1998) or kainate (Hajos *et al.*, 2000; Hormuzdi *et al.*, 2001). Carbachol (CCH) is a cholinergic agonist that activates both muscarinic and nicotinic acetylcholine receptors, whilst kainate (KA) is an agonist for the ionotropic glutamatergic kainate receptor.

The three models of hippocampal gamma-frequency oscillations in rodents (spontaneous, CCH, and KA) can possess different peak frequencies and maximal powers depending on the region and layer of the hippocampus investigated (Palhalmi *et al.*, 2004; Vreugdenhil and Toescu, 2005; Modebadze, 2014), as well as recruiting distinct interneuron types as a result of differential expression of receptors.

### **1.5.3 Spontaneous sharp waves**

Another form of hippocampal activity detectable through LFP recordings are slow shifts (2-4 Hz) in the field potential known as sharp waves, which are often associated with fast (200 Hz) ripple oscillations (Buzsaki, 1986; Buzsaki *et al.*, 1992). The presence of fast ripple oscillations has long been investigated due to their association with epilepsy (Bragin *et al.*, 1999) as they represent a hyper-synchronous state of excitatory cell firing. As the work in this thesis focuses on LFP recordings from the *stratum radiatum*, and ripples are mostly found within *stratum pyramidale* (Ylinen *et al.*, 1995), the sharp wave component of sharp wave-ripples will be discussed in more detail in the context of rodent *in vitro* hippocampal slice preparations.

Sharp waves (SPWs) have been shown to be generated within the hippocampus and are involved in memory consolidation, particularly during slow wave sleep (Ego-Stengel and Wilson, 2010). As a result, their disruption can lead to deficits in forming new spatial memories within the hippocampus (Girardeau *et al.*, 2009). Spontaneous SPWs have been detected in rodent hippocampal slices (Schneiderman, 1986; Papatheodoropoulos and Kostopoulos, 2002b; Wu *et al.*, 2002; Kubota *et al.*,

2003) but were also reported in non-human primate tissue, where they were described to be physiological and non-epileptic in nature (Schwartzkroin and Haglund, 1986).

A specific model of spontaneous SPWs has been elucidated by Wu *et al.* (2002) in mouse hippocampal slices and were noted to comprise the summation of GABA<sub>A</sub> receptor-dependent IPSPs from a population of pyramidal cells. Synchronised EPSPs were also observed in interneurons within the same region, whilst no rhythmicity occurred in presumed glial cells during the recording period, indicating that SPWs are synaptic in origin. Like gamma-frequency oscillations, spontaneous SPWs depend on both excitation and inhibition. The authors found that the CA3 region was capable of generating spontaneous SPWs that propagate to CA1, whilst the isolated CA1 region only generated SPWs when stimulated. Since the initial study, further mechanisms of spontaneous SPWs have been explored in rodent hippocampal slices and indicate that SPWs are dependent on the thickness of the slice (Wu *et al.*, 2005b) and the temperature of the recording chamber (Maier *et al.*, 2009).

For the purpose of this thesis, persistent *in vitro* gamma-frequency oscillations and spontaneous SPWs are summarised in Table 1.4.

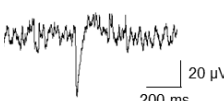
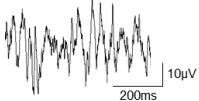
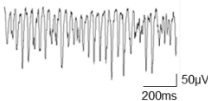
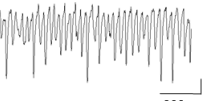
Effect of antagonist	Spontaneous sharp waves	Gamma-frequency oscillations		
		Spontaneous	Carbachol	Kainate
<b>LFP</b>				
<b>GABA<sub>A</sub>-R</b>	Abolished	Abolished	Abolished	Abolished
<b>NMDA-R</b>	↑ or no effect	No effect	↑ power or no effect	↑ power or no effect
<b>KA/AMPA-R (CNQX)</b>	Abolished	↓ power or no effect	↓ power	↓ power
<b>Cholinergic (atropine)</b>	↑ or no effect	↓ power or no effect	Abolished	No effect
<b>Gap junctions</b>	↓ or no effect	↓ power	↓ power	↓ power
<b>mGluR5</b>	Unknown	↑ power	↑ power or no effect	↑ power or no effect
<b>mGluR2/3</b>	↓ or no effect	No effect	No effect	No effect

Table 1.4. **Effect of antagonists on sharp waves and gamma-frequency oscillations.** Example LFP with scale bar presented under each activity. Information assembled from (Fisahn *et al.*, 1998; Maier *et al.*, 2003; Colgin *et al.*, 2005; Wu *et al.*, 2005a; Skrobot, 2008; Pietersen *et al.*, 2009; Modebadze, 2014; Hofer *et al.*, 2015).

## 1.6 Neurodegeneration in alpha-synucleinopathy

The process of neurodegeneration encompasses both neuronal loss and neuronal dysfunction, and can impair molecules, synapses, neurons, local circuits and even entire networks (Palop *et al.*, 2006). Whilst the traditional view of alpha-synucleinopathy encompassed a focus on ASYN aggregates with age, in recent years it is the oligomeric and sometimes protofibril form of ASYN that has been implicated in cytotoxicity and mechanisms of neurodegeneration (Lindstrom *et al.*, 2014). It is even proposed that the aggregation of ASYN may be a protective mechanism to sequester oligomers (Wan and Chung, 2012). *In vitro*, oxidative stress, nitrative stress and acidity induce oligomerisation of ASYN (Unal-Cevik *et al.*, 2011). A contributing factor to the accumulation of oligomers, fibrils, and aggregates may also be failure of the proteasome to degrade misfolded ASYN (Song *et al.*, 2009).

A prion-like spread has been suggested to underlie the progressive spread of alpha-synucleinopathy through the brain to higher cortical areas (Masuda-Suzukake *et al.*, 2014). ASYN monomers can pass through the cell membrane by diffusion, whereas oligomers and aggregates can be secreted by exocytosis (Grozdanov and Danzer, 2018). Once in the extracellular space, ASYN can be taken up by either by diffusion if in the monomeric form, or by a type of endocytosis called pinocytosis if not monomeric (Grozdanov and Danzer, 2018). ASYN may also be taken up by reactive astrocytes and microglia through phagocytosis (Zhang *et al.*, 2005).

If the cell fails to degrade ASYN, ASYN is released into the cytoplasm and can induce natively folded ASYN to misfold and become phosphorylated at residue Serine 129 (Foulds *et al.*, 2013; Lee *et al.*, 2014a). Phosphorylated ASYN has been shown to misfold and form fibrils at accelerated rates (Samuel *et al.*, 2016). Whilst WT ASYN binding to presynaptic membranes was unaffected by phosphorylation, A30P ASYN binding was increased when phosphorylated, and this was proposed by the authors to contribute to intracellular accumulation of A30P ASYN following increased internalisation of membrane bound A30P ASYN (Samuel *et al.*, 2016).

It has been suggested that ASYN may induce cell death by a number of mechanisms, including the formation of pores to disrupt ion homeostasis (Danzer *et al.*, 2007; Ying *et al.*, 2011), endoplasmic reticulum stress (Smith *et al.*, 2005), induction of mitochondrial dysfunction (Braidy *et al.*, 2013), excess influx of calcium (Adamczyk and Strosznajder, 2006; Hettiarachchi *et al.*, 2009), and excitotoxicity (Huls *et al.*, 2011). Interestingly, the aforementioned mechanisms may lead to further ASYN

aggregation due to the production of ROS and the activity-dependent release of ASYN from dysfunctional neurons (Yamada and Iwatsubo, 2018).

Deficits within a mitochondrion's ETC can occur in both normal ageing (Lenaz *et al.*, 1997) and PD (Schapira *et al.*, 1990). Chronic treatment with Complex I toxin MPTP causes aggregation of ASYN in dopaminergic neurons of the substantia nigra in mice (Vila *et al.*, 2000). High-frequency oscillations are heavily dependent upon mitochondria, particularly within fast-spiking PV+ interneurons, due to the metabolic demands of sustained high-frequency firing (Kann *et al.*, 2011; Kann, 2016). This is highlighted by a blockade of Complex I leading to impaired hippocampal gamma-frequency oscillations via fast-spiking interneuron dysfunction (Whittaker *et al.*, 2011).

Fast-spiking PV+ interneurons, are particularly vulnerable to oxidative stress (Cabungcal *et al.*, 2013b) and indeed are noted post-mortem to be reduced in the dentate gyrus and hippocampal region CA1 of LBD patients (Bernstein *et al.*, 2011). Interestingly, interneurons expressing PV have been reported to either be free from Lewy bodies (Gomez-Tortosa *et al.*, 2001), or possessing abnormal ASYN accumulation in only 2% of hippocampal PV+ interneurons (Bernstein *et al.*, 2011). Recently, a loss of excitatory CB+ cells in the dentate gyrus was found in post-mortem tissue from DLB patients, and in mice overexpressing human WT ASYN under the *Thy-1* promoter (Morris *et al.*, 2015). However, changes in CB+ interneurons specifically have not been extensively examined in mouse models of alpha-synucleinopathy.

The fact that one interneuron can innervate thousands of pyramidal cells could explain why small changes can affect an entire network (Kosaka *et al.*, 1987; Li *et al.*, 1992; Somogyi and Klausberger, 2005). While the existing literature often only accounts for interneuron cell loss and does not take interneuron function into account, this thesis aims to explore cellular dysfunction and hippocampal network changes in a mouse model of alpha-synucleinopathy.

## 1.7 Aims of thesis

The aims of this thesis are briefly summarised below:

- Elucidate the time-course of changes in A30P mice leading to later life hippocampal network dysfunction
  - Utilising *in vitro* electrophysiology and immunohistochemistry, with particular focus on changes in excitatory/inhibitory balance
- Explore evidence of early changes preceding later life hippocampal network dysfunction that could be used as potential biomarkers or therapeutic targets



## **Chapter 2. General Methods**



## 2.1 Animal provision

The following procedures were performed in accordance with the UK Animals (Scientific Procedures) Act 1986, and the European Union Directive 2010/63/EU under the provision of appropriate personal and project licenses. All animals were maintained on a 12 hour light/dark cycle with access to food and water *ad libitum* and environmental enrichment in same-sex groups no larger than 6 mice. Wherever possible, animals were not housed alone for longer than 24 hours.

(*Thy-1*)-h[A30P] $\alpha$ SYN mice on a C57BL/6 background (henceforth referred to as A30P mice) were kindly provided by Prof. Philipp Kahle (University of Tübingen, Germany) and a colony was established at internal animal facilities in Newcastle University. Homozygous mice were crossed with C57BL/6 mice to produce the F1 generation. Mice were ear notched following weaning (~21 days) and samples were genotyped externally (Transnetyx Inc., Tennessee, USA) before two separate lines were generated for wild type and homozygous A30P mice. Heterozygous mice were used for preliminary electrophysiological recordings. Lines were maintained separately, with the potential to cross again as needed.

A30P mice present with severe motor deficits from ~16 months onwards, with premature death occurring in homozygous mice from around 17-18 months (Freichel *et al.*, 2007). Therefore, all mice used in this thesis were between the ages of 2 months and 17 months and separated into four distinct groups: 2-4 months (WT/A30P2+), 6-8 months (WT/A30P6+), 10-13 months (WT/A30P10+), and 15-17 months (WT/A30P15+). It was decided to compare data within each age group as the same mice were not used longitudinally. Some C57BL/6 mice were purchased from external sources within the 15+ month age group when availability of WT mice was low.

(*PDGF*)-h[WT] $\alpha$ SYN mice on a C57BL/6 background (Masliah *et al.*, 2000), and corresponding wild type littermates previously genotyped, were kindly provided by Dr Chris Morris from internal animal facilities in Newcastle University. Mice were used at 2-6 months of age only, due to an insufficient number available to age.

## 2.2 Preparation of acute brain slices

Animals were anaesthetised with inhaled isoflurane (IsoFlo 100% w/w; Zoetis, UK) prior to an intramuscular injection of ketamine (Narketan-10 100 mg/ml; Vetoquinol, UK; used at 0.25 ml >100 mg/kg) and xylazine (Xylacare 20 mg/ml; AnimalCare, UK; used at 0.25 ml >10 mg/kg). Reflexes were checked via pedal withdrawal and eye blink. Once all reflexes ceased, the abdominal cavity and ribcage were opened to expose the heart and the left ventricle of the heart was pierced with a needle. An incision was made in the right atrium and a transcardial perfusion of chilled, carbogenated (95% O<sub>2</sub> / 5% CO<sub>2</sub>) sucrose artificial cerebrospinal fluid (sucrose aCSF) was performed with 30 ml solution at an approximate rate of 0.5 ml/sec.

Sucrose aCSF was prepared using distilled water by dilution of: 252 mM sucrose, 3 mM KCl, 1.25 mM NaH<sub>2</sub>PO<sub>4</sub>, 24 mM NaHCO<sub>3</sub>, 2 mM MgSO<sub>4</sub>, 2 mM CaCl<sub>2</sub> and 10 mM glucose. Regular aCSF was prepared by use of 126 mM NaCl instead of 252 mM sucrose. Chemicals were stored according to supplier recommendations, with full details of each chemical provided in Table 2.1. Stock solutions were maintained for 2 weeks to allow daily preparation of regular or sucrose aCSF. aCSF was prepared fresh daily, whilst sucrose aCSF was kept refrigerated for no longer than 48 hours.

Perfusion of animals with high sucrose aCSF prior to acute brain slice preparation has been shown to preserve the cytoarchitecture of the brain, particularly the viability of fast-spiking interneurons (Aghajanian and Rasmussen, 1989).

Chemical name	Formula	Vendor
Sucrose	C <sub>12</sub> H <sub>22</sub> O <sub>11</sub>	Sigma-Aldrich (16104)
Potassium chloride	KCl	VWR International (101985M)
Sodium dihydrogen orthophosphate	NaH <sub>2</sub> PO <sub>4</sub>	VWR International (307164T)
Sodium bicarbonate	NaHCO <sub>3</sub>	Tocris (3152)
Magnesium sulphate	MgSO <sub>4</sub>	Sigma-Aldrich (M7506-M)
Calcium chloride	CaCl <sub>2</sub>	VWR International (275844L)
Glucose	C <sub>6</sub> H <sub>12</sub> O <sub>6</sub>	VWR International (101176K)
Sodium chloride	NaCl	Sigma-Aldrich (S7653)

Table 2.1 **List of chemicals used in preparation of artificial CSF solutions.** Note that sucrose is used only in sucrose artificial CSF, and sodium chloride used only in regular artificial CSF. Chemical name, formula, and vendor with stock number.

Following perfusion, the animal's spinal cord was cut and the skull was exposed by incision. Further dissection of the skull revealed the brain, which was excised into a petri dish of chilled, carbogenated sucrose aCSF. The brain was trimmed with a razor blade to remove the brainstem and prefrontal area. The dorsal portion of the brain was then glued to the chuck of a Leica VT1000 microtome (Leica Microsystems, Germany) and the entire brain covered in chilled, carbogenated sucrose aCSF. After sectioning the most ventral region of the brain until the hippocampus was visible, 450  $\mu\text{m}$  transverse slices were collected in a petri dish of chilled, carbogenated sucrose aCSF then the hippocampus was trimmed away from the rest of the slice.

Slices were noted for being either dorsal or ventral for further analysis (Figure 2.1). The dorsal portion of the mouse hippocampus is marked by an elongated structure and the "V" shape of the dentate gyrus, while ventral hippocampal slices are defined by a more rounded structure and the "C" shape of the dentate gyrus (Peng and Houser, 2005; Amaral *et al.*, 2007).

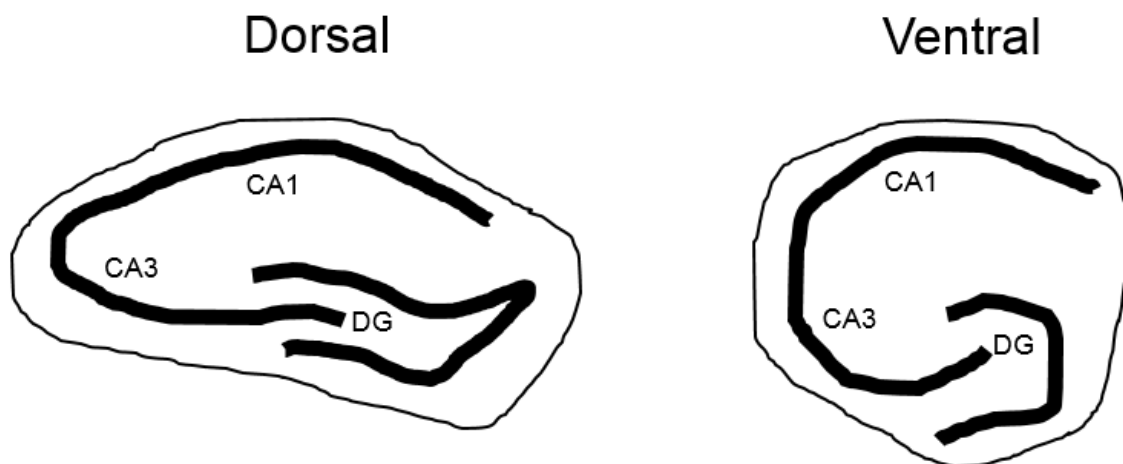


Figure 2.1 **Classification of mouse dorsal and ventral slices.** Note the elongated structure of the mouse dorsal hippocampus (including cornu ammonis regions CA3 and CA1) and the distinctive "V" shape of the dentate gyrus (DG), compared to the rounded structure of ventral slices with a "C" shaped DG.

### 2.3 Slice maintenance

Immediately following slice preparation, hippocampal slices were transferred to an interface holding chamber maintained at room temperature in carbogenated aCSF (126 mM NaCl instead of sucrose). The chamber was covered with parafilm and left for 1 hour for slices to recover and allow sufficient time for water soluble anaesthetics (isoflurane, ketamine, and xylazine) to wash away (Dickinson *et al.*, 2003).

Following this, 2 slices were transferred to an interface recording chamber, supplied with a continuous flow (~ 1.2 ml/min) of carbogenated aCSF through a Gilson Minipuls3 pump. The chamber was maintained at a temperature of 30 – 31 °C using a heater (FH16-D; Grant Instruments Ltd, UK), with temperature measurements taken by infrared thermometer throughout the experimental day.

Wherever possible to maximise slice use, multiple rigs with one recording chamber and two electrodes on each were used simultaneously. It has previously been reported that thin (150 – 180 µm) hippocampal slices prepared without sucrose aCSF perfusion remained viable in a submerged holding chamber for at least 4 hours before significant cell loss occurred (Fukuda *et al.*, 1995). As transcordial perfusion with sucrose aCSF is neuroprotective (Aghajanian and Rasmussen, 1989), the experimental design within this thesis is proposed to extend the viability of acute brain slices though all experiments were performed within 6 hours of slice preparation.

## 2.4 Pharmacological compounds

All compounds were stored according to manufacturer's recommendations. Water soluble compounds were constituted in distilled water, and water insoluble drugs prepared in dimethylsulfoxide (DMSO; Sigma-Aldrich, UK). Stock solutions were kept frozen (-20°C) or refrigerated (4°C), depending on manufacturer instructions and frequency of use. All drugs (Table 2.2) were bath applied by addition to circulating carbogenated aCSF to reach slices in the chamber within minutes.

Name	Chemical name	Action	Supplier
Carbachol	<i>Carbamylcholine chloride</i>	Cholinergic agonist	Sigma-Aldrich (C4382)
D-AP5	<i>D-(-)-2-Amino-5-phosphonopentanoic acid</i>	Selective, competitive NMDA receptor antagonist	HelloBio (HB0225)
Gabazine (SR95531)	<i>2-(3-carboxypropyl)-6-(4-methoxyphenyl)-2,3-dihydropyridazin-3-iminium bromide</i>	Selective, competitive GABA <sub>A</sub> receptor antagonist	Abcam (ab120042)
Kainic acid (referred to as <i>kainate</i> )	<i>(2S,3S,4S)-3-(Carboxymethyl)-4-prop-1-en-2-ylpyrrolidine-2-carboxylic acid</i>	Kainate receptor agonist, partial AMPA receptor agonist	Sigma-Aldrich (K0250)

Table 2.2 **List of drugs used in this thesis.** Each drug name is expanded by chemical name, intended action, and supplier with product code.

## 2.5 Data Acquisition

For local field potential recordings, glass microelectrodes (1.2 mm OD, 0.94 mm ID, 100 mm L; 30-0050 G120TF-10, Harvard Apparatus Ltd., UK) were pulled using a P-97 Flaming/Brown puller (Sutter Instrument Co., USA). This produced electrodes with a resistance of approximately 2 - 5 m $\Omega$ . For sharp intracellular recordings, sharper glass microelectrodes (1.2 mm OD, 0.69 mm ID, 100 mm L; 30-0044 GC120F, Harvard Apparatus Ltd., UK) were prepared to a resistance of 70 - 140 m $\Omega$ .

Field electrodes were filled with aCSF. Intracellular electrodes were filled with 2M chilled potassium acetate. All electrodes were placed in a holder attached to a headstage preamplifier held in place by a micromanipulator. Each rig contained 2 micromanipulators, and therefore 2 channels. Microelectrodes were positioned using the micromanipulator and inserted into the desired region of the hippocampus – CA3 or CA1, *stratum radiatum* (*st. radiatum*) or *stratum pyramidale* (*st. pyramidale*). Each of the two electrodes could be placed either in separate slices or the same slice.

Data were recorded with an Axoclamp-2B amplifier (Axon Instruments Inc., UK) and activity was band-pass filtered with Neurolog external filters at 0.001 kHz high pass and 0.4 kHz low pass. Intracellular signals were low-pass filtered at 2 kHz. Data were re-digitised at 10 kHz using an ITC-16 interface (Digitimer, UK). A HumBug (Digitimer, UK) was used to remove 50 Hz electrical mains noise. Recordings were made using AxoGraph software (Version X, Axon Instruments Inc., USA) and analysed offline.



## 2.6 Data Analysis

Power spectral density analysis was undertaken using AxoGraph's Fast Fourier Transform algorithms. Using 8192 frequency bins, data were represented by frequency (Hz) and power ( $\mu\text{V}^2 / \text{Hz}$ ). For each trace, the area under the curve (area power;  $\mu\text{V}^2$ ) and peak frequency (Hz) were measured between 15 and 45 Hz. Area power represents the strength of the oscillation within the 15 – 45 Hz frequency band.

Gamma-frequency oscillations in mouse hippocampal slices are often classified in the literature as occurring between 20 - 80 Hz and at a slower frequency than oscillations in rat slices (Vreugdenhil and Toescu, 2005). Furthermore, gamma-frequency oscillations in acute hippocampal slice preparations are temperature-dependent, and recordings in this thesis are performed at a relatively low 30 – 31 °C (Dickinson *et al.*, 2003). As a result, a 15 – 45 Hz gamma-frequency band was selected for recordings in this thesis to accurately detect all gamma-frequency activity.

Auto-correlation analysis of a 1 second epoch of data was performed to compute a rhythmicity index (RI) value. The original signal is shifted in time to compare how similar the signal is to the time shifted version. The amplitude of the first side peak gives a normalised RI value with a maximum of 1. Cross-correlation analysis of a 1 second epoch of data was performed to compute the time delay in milliseconds between regions CA3 and CA1. The time delay of the maximum peak amplitude (the central peak) represents the time delay between the two signals.

Measurements of resting membrane potential (RMP) and firing threshold were made at the time of intracellular recordings by comparing the voltage when the electrode was inside the cell to when the electrode was outside the cell. Intracellular spikes recorded at firing threshold were defined as a positive deflection in voltage greater than 5 \* the standard deviation of baseline. Measurements of spike frequency and amplitude were performed using MATLAB (MathWorks, USA) peak detect functions and results were visually confirmed to correlate with spiking events.

IPSPs were recorded at –30 mV in current-clamp conditions and defined as a negative deflection in voltage larger than 1 mV. IPSP frequency was calculated in MATLAB using a peak detect function. IPSP amplitude was computed by the difference between the trough and the average peak amplitude on either side of the trough.

## 2.7 Free-floating immunohistochemistry

Hippocampal sections (450  $\mu\text{m}$ ) used in electrophysiology were stored in buffered (4%) paraformaldehyde (PFA powder; Sigma-Aldrich P-6148) for at least 2 days before being transferred to a solution of 30% sucrose phosphate buffered saline (PBS tablets; Sigma-Aldrich P4417) for 2-3 days. Slices were then re-sectioned to 40  $\mu\text{m}$  using a freezing stage microtome and collected in a well plate containing 0.3% Triton–PBS (TPBS; Triton X-100 from Sigma-Aldrich T-8787).

To each well, a solution containing TPBS, 3% serum (species depending on which species the secondary antibody is raised in), and the appropriate concentration of biotinylated lectin or primary antibody was added (Table 2.3).

Target	Host	Concentration	Vendor	Serum used
Biotinylated Wisteria Floribunda Lectin; N-acetylgalactosamine sugar (PNNs)	N/A	1:500 for IP	Vector Labs (B1355)	N/A
Calbindin D-28k (CB)	Rabbit	1:10,000 for IP 1:10,000 for IF	SWANT (CB38)	Goat (S-1000, Vector Laboratories)
GFAP (astrocytes)	Mouse	1:1000 for IP	Abcam (ab10062)	Horse (S-2000, Vector Laboratories)
Human ASYN (15G7)	Rat	1:1000 for IP 1:500 for IF	Abcam (ab195561)	Goat (S-1000, Vector Laboratories)
Iba1 (microglia)	Goat	1:500 for IP	Abcam (ab5076)	Horse (S-2000, Vector Laboratories)
Parvalbumin (PV)	Mouse	1:5000 for IP 1:2000 for IF	Sigma-Aldrich (P3088)	Horse (S-2000, Vector Laboratories)

Table 2.3 **List of primary antibodies and lectin used in this thesis.** Detailed by the intended target, host species, concentration used for immunoperoxidase (IP) and immunofluorescence (IF), vendor, and blocking serum used.

Slices were incubated in primary antibody or lectin overnight (18-20 hours) on a rotating platform with gentle agitation in a cold room (4°C). The following day, slices were removed from the cold room and the primary antibody solution was carefully removed from the wells and replaced with TPBS. The well plates were placed on a rotating platform with gentle agitation for 10 minutes. This wash step was then repeated two more times for 5 minutes each time. At this point, slices were processed with either DAB immunoperoxidase or immunofluorescence staining techniques.

### 2.7.1 DAB Immunoperoxidase

A solution containing the secondary antibody was assembled according to the primary antibody host species, with the exception of lectin which is already biotinylated (Table 2.4). The solution was added to the appropriate wells and left on a rotating platform with gentle agitation for 2 hours at room temperature. The solution was then removed carefully, and 3 x 5 minute washes with TPBS were carried out.

Target	Concentration	Vendor
Anti-goat biotinylated IgG secondary antibody, raised in horse	1:200	Vector Laboratories (BA9500)
Anti-mouse biotinylated IgG secondary antibody, raised in horse	1:200	Vector Laboratories (BA2000)
Anti-rabbit biotinylated IgG secondary antibody, raised in goat	1:200	Vector Laboratories (BA1000)
Anti-rat biotinylated IgG secondary antibody, raised in goat	1:200	Vector Laboratories (BA9400)

Table 2.4 **List of biotinylated secondary antibodies used in this thesis.** Detailed by the intended target and host species, concentration used, and vendor.

Each well was filled with horseradish peroxidase (HRP) conjugated streptavidin (1:200; Vector Laboratories, SA5004) and incubated for 1 hour at room temperature on a rotating platform. Following this, 3 x 5 minute washes were carried out with TPBS. To prepare the Diaminobenzidine (DAB) substrate, a DAB peroxidase substrate kit (Vector Laboratories, SK4100) was used and made up in distilled water. The solution

was added to wells after the final wash and left for 3 minutes. The reaction was stopped by removal of the solution. Slices were then washed for 2 x 5 minutes with TPBS.

Slices were mounted on to gelatin-subbed microscope slides (Fisher Scientific, SuperFrost slides 26 x 76 x 1 mm) and left to dry. Once completely dried, slides were washed with distilled water for 30 seconds before being moved through an ethanol dehydration series (70%, 95%, 100%, 100%) with 5 minutes in each concentration. Slides were then cleared for 10 minutes in HistoChoice Clearing Agent (National Diagnostics, HS200) and left in this solution while slides were coverslipped (VWR coverglass 22 x 50 mm, 631-0137) using ImmunoHistoMount (AgarSci, HS103) mounting solution. Slides were left to dry for at least 2 days under a fumehood.

A summary of DAB peroxidase techniques for conventional stains and with biotinylated Lectin for perineuronal nets is illustrated in Figure 2.2.

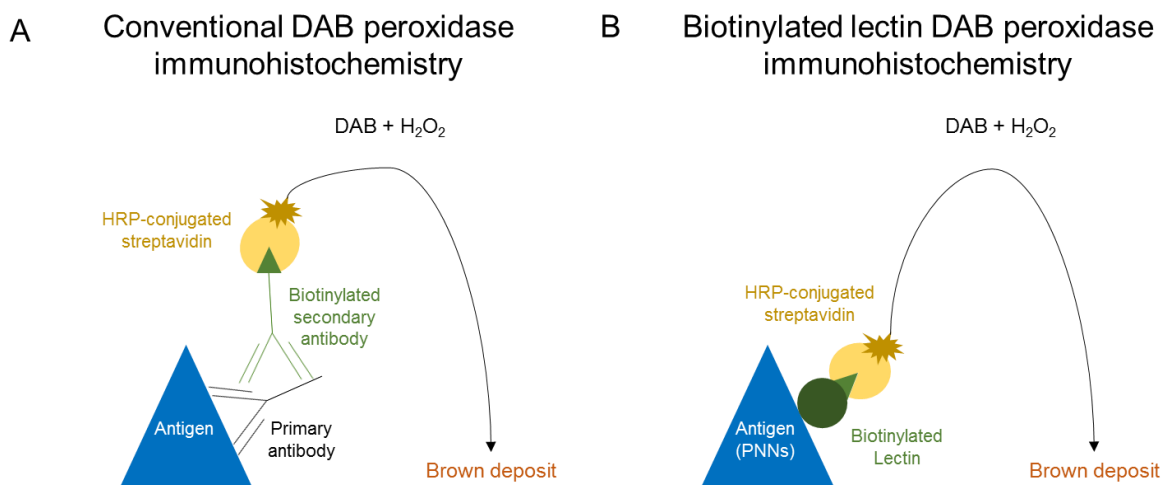


Figure 2.2 **Schematic of DAB peroxidase immunohistochemistry.** Conventional DAB peroxidase stain with biotinylated secondary antibodies (A), and biotinylated lectin stain (B). Both result in formation of a brown deposit at site of detected antigen.

Images were taken on an Olympus BX51 stereology microscope with an Olympus U-TV1X-2 T2 Camera using PictureFrame software (Softonic, Spain). Cells in regions CA3/1 were counted using the meander scan function in StereoInvestigator at x40 magnification (MBF Bioscience, USA), as has previously been described (Pitts *et al.*, 2012; Chan, 2017). The count was then divided by the defined area in mm to give a normalised measure of cell density (cells/mm<sup>2</sup>). Only clearly defined cell bodies of the correct size were counted as a cell, with consistency maintained between slices. Slices were counted with investigator blinded to genotype whenever possible.

Optical density measures were made in regions CA3/1 using ImageJ (NIH). There is a linear relationship between time and optical density for 6 minutes following DAB incubation (H. Benno *et al.*, 1985). All slices used in this thesis were incubated with DAB for 3 minutes. Images were deconvoluted to leave only the brown DAB stain with pixel density measured on a scale from 0 to 255. 255 represents white and the absence of a stain, which when converted to optical density would give a value of 0.

$$\text{Optical Density (OD)} = \log \left( \frac{\text{Maximum pixel density (255)}}{\text{Mean pixel density}} \right)$$

Wherever possible, 2-5 slices from each mouse were averaged to give a value per mouse, then averaged again to give a value for that age/genotype. When hippocampal regions CA3 and CA1 were examined, this was done in the same slice.

### 2.7.2 Immunofluorescence

Following overnight incubation with two primary antibodies, slices were washed for 3 x 5 mins with TPBS. Biotinylated goat anti-rat IgG antibody (Vector Laboratories, BA-9400; 1:200) was added to wells for 2 hours at room temperature to detect the anti-human ASYN rat primary antibody. 3 x 5 min washes with TPBS were performed, before a solution containing two fluorescent secondary antibodies was added (Table 2.5). Slices were left on a rotating platform in the dark for 2 hours at room temperature.

Target	Concentration	Vendor
Texas Red 594 Streptavidin to detect biotinylated goat anti-rat IgG antibody	1:200	Vector Laboratories (SA-5006)
And Chicken anti-mouse IgG (H+L) Cross-Adsorbed Secondary, Alexa Fluor 488	1:200	ThermoFisher Invitrogen (A-21200)
Or Goat anti-rabbit IgG (H+L) Cross-Adsorbed Secondary, Alexa Fluor 488	1:200	ThermoFisher Invitrogen (A-11008)

Table 2.5 **List of fluorescent secondary antibodies used in this thesis.** Detailed by the intended target and host species, concentration used, and vendor.

A solution of DAPI (1:10,000, Sigma-Aldrich, D9542) was added and incubated for 10 minutes in the dark to stain all nuclei. The solution was removed, and 3 x 5 min washes with TPBS carried out. Slices were mounted on to gelatin-subbed microscope slides and left to dry for 5 mins before being coverslipped using Fluoroshield (Sigma-Aldrich, F6182) mounting media. Imaging was performed using the epifluorescence Axio Imager M1 (Zeiss) microscope with an AxioCam MrM camera.

## **2.8 Open field test for locomotor activity**

All behavioural experiments were conducted between the hours of 8am and 12pm, to control for circadian variation throughout the day. In a room with dimmed lights, four locomotor boxes (42 cm x 42 cm) were cleaned and a small amount of sawdust was scattered at the bottom of each locomotor box. A balanced experimental design was achieved by alternating which mouse genotype was placed in which box, and mice of the same sex were tested in a single session to avoid any effect of mixing sexes. A cohort of 2-4 month old mice were tested over a period of 3 days, and a separate cohort of 10-13 month old mice over a period of 2 days.

Mice were placed in the centre of the locomotor box and recordings started immediately. Experimenters then left the room for the duration of the 90 minute recording period to allow mice to explore undisturbed. Locomotor activity was measured by beam breaks using the Auto-Track System for the Opto-Varimex (Columbus Instruments, USA). A measure of distance travelled (cm) was made at each minute and later grouped into 5 minute blocks. At each minute of recording, the number of seconds mice spent ambulatory was measured and averaged over the entire 90 minute recording period to give an average measure of ambulatory time (seconds).

## 2.9 COX/SDH histochemistry

COX/SDH histochemistry is an effective technique to identify mitochondrial dysfunction (Ross, 2011). Mice were anaesthetised with inhaled isoflurane before an intramuscular injection of ketamine and xylazine, as described in *Chapter 2.2*. Once eye blink and pedal withdrawal reflexes ceased, the brain was quickly removed and snap frozen using isopentane immersed in liquid nitrogen. Brains were stored at  $-80^{\circ}\text{C}$  until ready to cryosection. Snap frozen whole brains were sectioned at  $10\ \mu\text{m}$  using a cryostat at  $-20^{\circ}\text{C}$  and collected on to slides (Plus+ Frost positively charged microslides, Fisher Scientific). Three slices were collected per slide, each containing at least one hippocampus, and slides were then stored at  $-80^{\circ}\text{C}$ .

Slides were removed from the freezer and dried at room temperature for 1 hour before histochemistry. Individual slices were highlighted with a hydrophobic marker, and wherever possible slides were processed in large batches to maintain consistency in enzymatic reactions. The first slice of every slide was used as a control to ensure consistency of incubation media. Half of the controls received COX incubation media only, and the other half received SDH incubation media only. All other slices received both media sequentially. Mitochondrial Complex IV (COX) is encoded by mitochondrial DNA, whereas Complex II (SDH) is encoded by nuclear DNA (Ross, 2011).

The COX incubation media was prepared by adding  $100\ \mu\text{M}$  Cytochrome *c* to 1X DAB and mixed with a few crystals of catalase.  $50\ \mu\text{L}$  of COX media was applied to each slice, and all slides were incubated for 40 minutes at  $37^{\circ}\text{C}$ . The brown DAB product saturates cells with functional Complex IV (COX) activity. COX media was then removed carefully from each slide and 2 x 5 min washes with 0.1 M PBS were performed. After the final wash, excess PBS was removed from the slides. Sequential staining with SDH incubation media was then performed.

The SDH incubation media was prepared by mixing together 1.5 mM nitroblue tetrazolium (NBT), 130 mM sodium succinate, 0.2 mM phenazine methosulfate (PMS), and 1.0 mM sodium azide. Care was taken to protect the PMS (and resultant final media) from light.  $50\ \mu\text{L}$  of SDH media was applied to each slice, and all slices were incubated for 40 minutes at  $37^{\circ}\text{C}$ . The blue product formed by NBT visualises Complex II (SDH) activity, and saturates cells not already saturated by the brown DAB product. SDH media was removed and 2 x 5 minute washes with 0.1 M PBS were carried out.

All techniques were carried out as previously described by the Mitochondrial Research Group at Newcastle University and reagents used are identical to those published previously (Betts *et al.*, 2006; Robson *et al.*, 2018).

Slides were dehydrated through an ethanol concentration gradient (70%, 95%, 100%, 100%) with 5 minutes at each concentration and 10 minutes in the final 100% concentration. Slides were then transferred to two consecutive pots of HistoClear for 5 minutes of clearing in each. Slides were left in the final pot of HistoClear until coverslipped. Slides were mounted with DPX (Fisher Scientific, #15538321) and then coverslipped, before being left to dry overnight before imaging took place. A summary of the COX/SDH histochemical technique can be seen in Figure 2.3.

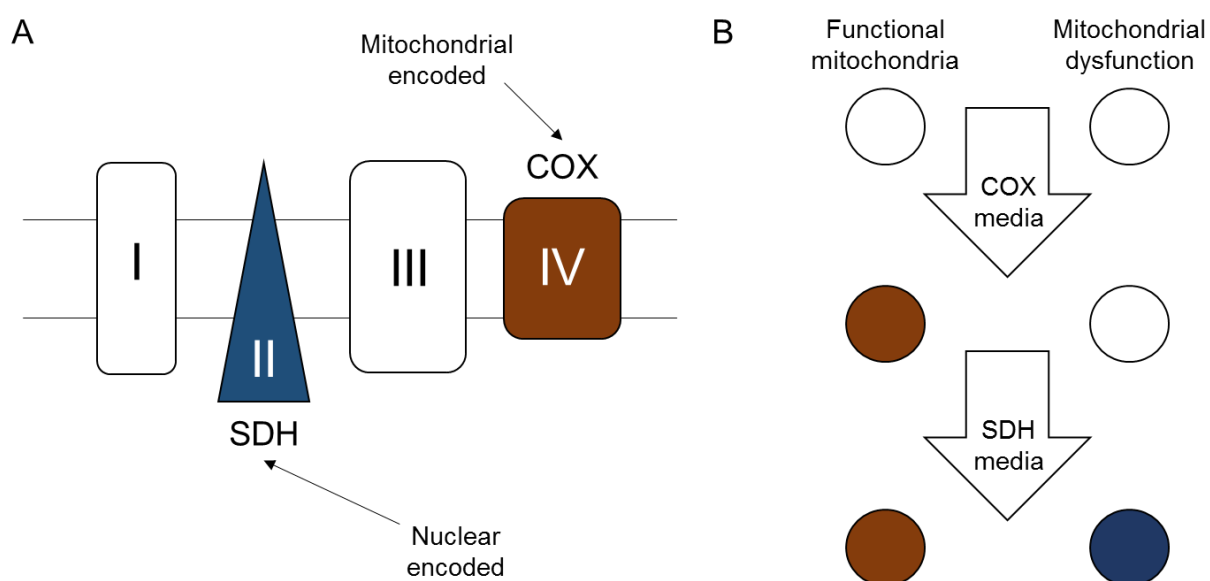


Figure 2.3 **Summary of COX/SDH histochemistry.** A) Schematic of the electron transport chain complexes I to IV, showing Complex II (SDH) and Complex IV (COX). B) Diagram of individual cells staining brown with functional COX, or blue without functional COX in the case of mitochondrial dysfunction.

Using an Olympus BX51 stereology microscope with an Olympus U-TV1X-2 T2 camera, images were taken at x10 magnification of the CA3 region of the hippocampus. All slides were assigned a random numerical value to blind the imaging and quantification processes. Using ImageJ's histogram tool, a freehand selected area of the CA3 pyramidal layer was analysed for mean RGB (red, green, blue) values from 0 to 255. All values were noted, but the mean blue value was compared as a measure of mitochondrial dysfunction. Multiple slices (2-7) per mouse were averaged per animal, and then animals were compared by group.



## 2.10 Statistical Analysis

All statistical analysis was performed using SigmaPlot (Systat Software Inc., USA). Graphs were produced using Prism (GraphPad Software, USA). Significance was defined as  $p < 0.05$ . All sample sizes ( $n$ ) are presented in figure legends.

Data were tested for normality (Shapiro-Wilk test) and equal variance (Brown-Forsythe test). If data were found to follow a normal (Gaussian) distribution then parametric tests were applied. Data were always treated as non-parametric if the group overall did not follow a normal distribution, including the area power of oscillations, the frequency of sharp waves and interictal discharges, and measures of optical density. Parametric data were presented as mean  $\pm$  standard error of the mean (SEM) and plotted as bar charts or line graphs with error bars representing SEM. Non-parametric data were presented as median with interquartile range (IQR, Q1 – Q3) and plotted as boxplots with individual data values marked with “o”.

To compare two independent samples, unpaired  $t$  tests were used if data were parametric or the Mann-Whitney rank sum test was used if data were non-parametric. To compare the effect of two independent variables on one dependent variable, a 2-way ANOVA was used if data were parametric or a 2-way ANOVA on ranks if data were non-parametric. If comparisons were made over the same set of slices, the test incorporated repeated measures (RM). If significance was found, multiple comparisons were performed post-hoc using the Holm-Sidak test. Holm-Sidak allows for multiple comparisons with more power than the Bonferroni or Tukey methods, while not being restricted to use following ANOVA as the Tukey method is (Seaman *et al.*, 1991).

A post-hoc power analysis was performed using G\*Power 3.1.9.2 software (University of Düsseldorf, Germany) to estimate the observed power of each experiment, incorporating both effect size and sample size (Faul *et al.*, 2007). Power is inversely correlated to the obtained  $p$  value, and therefore non-significant effects will always compute a low observed power (Hoenig and Heisey, 2002). As a result, post-hoc power analysis was only carried out when  $p < 0.05$  as a measure of the power to detect a difference as statistically significant when a true difference exists. The probability of making a type I error ( $\alpha$ ) was set at 5%. The probability of making a type II error ( $\beta$ ) was set at 20%. Power is inversely related to  $\beta$  and is defined as  $1 - \beta$ . Adequate statistical power is generally defined as  $\geq 0.8$  (80%).

A chi-square test ( $\chi^2$ ) was used to compare observed proportions against expected proportions, with the assumption that data should be equally distributed between groups. The following equation was used to compute a  $\chi^2$  value, where  $o$  is observed data and  $e$  is expected data. A  $\chi^2$  value of 0 would represent that the observed and expected data were equal.

$$\chi^2 = \sum \frac{(o - e)^2}{e}$$

The null hypothesis of the chi-square test is that there is no significant difference between variables. Hypothesis testing was carried out by examining a  $\chi^2$  distribution table to obtain a  $\chi^2$  value for the level of significance desired ( $p < 0.05$ ) using the degrees of freedom ( $df = \text{groups} - 1$ ). If the computed  $\chi^2$  value is larger than the  $\chi^2$  value for  $p < 0.05$ , then the null hypothesis can be rejected.

## **Chapter 3. Spontaneous Hippocampal Network Activity**



### 3.1 Introduction

ASYN is proposed to play a role in neurotransmitter release and vesicle trafficking. The A30P mutation can alter ASYN's role in neurotransmitter release, with evidence suggesting that the A30P mutation leads to ASYN losing vesicle-binding properties (Jensen *et al.*, 1998). The effect that such factors may have on spontaneous network activity in acute hippocampal slice preparations has not yet been explored in mouse models of alpha-synucleinopathy.

Hippocampal network activity is dependent on contributions from both excitatory pyramidal cells and inhibitory interneurons. Notably, fast-spiking PV+ interneurons play a variety of roles within the hippocampus including synchronising IPSPs in fast network oscillations (Buzsaki *et al.*, 1983) and driving spontaneous sharp waves (SPWs) in rodent slices (Hajos *et al.*, 2013; Schlingloff and Kali, 2014). SPWs are physiological events proposed to play a role in memory consolidation (Buzsaki, 1998; Siapas and Wilson, 1998). The mechanisms of SPWs have been explored over the years, where SPWs have been shown to be inhibitory events correlating with the arrival of IPSPs in pyramidal cells following synchronous activity of interneurons (Maier *et al.*, 2002; Papatheodoropoulos and Kostopoulos, 2002a; Wu *et al.*, 2002; Kubota *et al.*, 2003; Colgin *et al.*, 2004; Wu *et al.*, 2005a; Wu *et al.*, 2006a; Hajos *et al.*, 2013).

More recently, SPWs have been reported at a higher incidence in a double transgenic amyloid precursor protein (APP)/presenilin-1 (PS1) mouse model of AD (Reyes-Marin and Nunez, 2017), though no difference in SPWs was found in mice overexpressing APP alone (Hermann *et al.*, 2009). Reduced inhibitory control of SPWs was observed in a mouse model of tauopathy with no effect on SPW frequency (Witton *et al.*, 2016). To our knowledge, spontaneous SPWs have not yet been examined in acute brain slice preparations in mouse models of alpha-synucleinopathy.

Spontaneous gamma-frequency oscillations have been explored using rodent slices with respect to their mechanisms, where their appearance has been shown to be dependent on the preservation of cell viability and contribution from both excitatory and inhibitory network components (Skrobot, 2008; Pietersen *et al.*, 2009; Modebadze, 2014). Despite this, there has been little progress in exploring changes in spontaneous oscillations in mouse models of neurodegeneration beyond a reduction in the frequency of spontaneous theta oscillations established in a mouse model of AD expressing a double mutant form of human APP (Goutagny *et al.*, 2013).

Given the importance of inhibitory interneurons in the generation of both SPWs and spontaneous oscillations, it is of interest to note that lower expression of ASYN is found in inhibitory interneurons compared to pyramidal cells in a mouse cell culture model expressing human WT ASYN (Taguchi *et al.*, 2014). A similar finding of low expression levels was found post-mortem in DLB patients (Bernstein *et al.*, 2011), where ASYN was found to infrequently colocalise with PV+ interneurons though a partial loss of PV+ cells had occurred. A loss of fast-spiking PV+ interneurons is of particular interest given their role in cognitively relevant gamma-frequency oscillations. Indeed, a leftward shift in spectral power and slowing of EEG rhythms has been noted in both DLB patients (Andersson *et al.*, 2008; Bonanni *et al.*, 2008; Stylianou *et al.*, 2018) and mice over-expressing human WT ASYN (McDowell *et al.*, 2014; Morris *et al.*, 2015), which may be a consequence of altered interneuron function.

Fast-spiking PV+ interneurons are particularly vulnerable to oxidative stress (Steullet *et al.*, 2010; Cabungcal *et al.*, 2013b) and mitochondrial dysfunction (Kann, 2016) as a result of their increased metabolic demands and high density of mitochondria (Inan *et al.*, 2016; Kann, 2016). The presence of PNNs surrounding fast-spiking interneurons afford them with some protection against oxidative stress and excitotoxicity (Morawski *et al.*, 2004). Changes in resistance to oxidative stress and excitotoxicity may therefore underpin PV+ interneuron loss in human post-mortem tissue (Bernstein *et al.*, 2011; Morris *et al.*, 2015), despite low expression of ASYN in vulnerable fast-spiking interneurons (Gomez-Tortosa *et al.*, 2001).

Another consequence of altered inhibition was reported by Morris *et al.* (2015) in the form of epileptiform EEG activity in mice overexpressing human WT ASYN under the Thy-1 promoter. The authors further found that network excitability was associated with a loss of excitatory CB+ granule cells in the dentate gyrus. Recent evidence suggests that a direct epigenetic downregulation of CB expression in dentate gyrus granule cells can occur through proteins activated by increased neuronal activity (You *et al.*, 2017). While CA3 region CB+ interneurons specifically have not yet been examined in A30P mice, CB knockout mice do exhibit a deficit in hippocampal dependent memory processes and so their role should be considered with relevance to cognitive dysfunction (Moreno *et al.*, 2012). The hippocampus is a dynamic network capable of compensatory changes and mechanisms of neurodegeneration can be explored through changes within the excitatory/inhibitory (E/I) network.

### 3.2 Aims

- To assess the incidence and characteristics of spontaneous hippocampal activity *in vitro* in the form of spontaneous oscillations and spontaneous SPWs in A30P and age-matched wild type mice from 2 to 13 months of age.
- Explore changes in GABAergic interneuron populations and associated perineuronal nets through immunohistochemical staining.

### 3.3 Methods

Acute hippocampal slice preparations were made following perfusion of sucrose artificial CSF according to methods described in *Chapter 2.2*. Slices were transferred from a holding chamber after 1 hour and placed into the recording chamber. Field electrodes were immediately inserted into various regions of the hippocampus (CA3 and CA1 *stratum radiatum*) to map spontaneous SPW activity.

Spontaneous SPWs were detected and quantified using AxoGraph's peak detect function following a measure of standard deviation of baseline. Peaks were defined as a negative event 5\* the standard deviation of baseline. Peaks detected were visually confirmed to be spontaneous SPWs rather than electrical mains noise (noise is generally > 1 mV and occurring on both channels at same time). The frequency (Hz) and average amplitude ( $\mu\text{V}$ ) of detected peaks over 60 seconds were measured.

Measurements were repeated after 45 minutes in the CA3 *st. radiatum* to monitor SPWs over time and check for the emergence of spontaneous network oscillations. Spontaneous oscillations were defined by the presence of a discernible peak between 15 and 45 Hz. This was then quantified in AxoGraph to give the peak frequency (Hz) and area power ( $\mu\text{V}^2$ ). Sharp electrode intracellular recordings were carried out in CA3 *st. pyramidale* as outlined in *Chapter 2.5*, with a field electrode placed in the adjacent CA3 *st. radiatum* to confirm the presence of SPWs in a slice.

For pharmacological experiments with spontaneous SPWs, baseline recordings were made 45 minutes after slices were placed in the recording chamber, and D-AP5 (100  $\mu\text{M}$ ), gabazine (100 nM), or CCH (10  $\mu\text{M}$ ) were bath applied. A measure of SPW frequency (Hz) and amplitude ( $\mu\text{V}$ ) was made before and after drug exposure.

Following electrophysiological recordings, slices were fixed in 4% PFA as described in *Chapter 2.7*. No slices used for immunohistochemistry exhibited interictal activity, to control for the effect that this may have on the network. Free-floating immunohistochemistry was carried out using an anti-human ASYN antibody, anti-PV antibody, WFA lectin, or anti-CB antibody as detailed in *Chapter 2.7*. Cells positive for each antigen were counted using StereoInvestigator and normalised to  $\text{mm}^2$ . ImageJ was used for a measure of optical density. Finally, double immunofluorescence was used to examine colocalisation of human ASYN with PV+ or CB+ cells.



### 3.4 Results

#### 3.4.1 Expression of human ASYN within the A30P mouse hippocampus

To justify the study of the hippocampus within the *Thy-1* A30P mouse model it is important to first confirm and quantify the levels of human ASYN within this region. Whilst mice were initially genotyped to establish a homozygous breeding colony, DAB peroxidase staining was utilised to confirm the presence of human ASYN within the mouse hippocampus specifically, given that a number of reports in the literature have implicated region-specific expression of human ASYN according to which promoter and line is used (Kollias *et al.*, 1987; Rockenstein *et al.*, 2002).

Slices from WT mice were not immunoreactive due to a lack of expression of the human ASYN antigen (Figure 3.1A). On the other hand, slices from A30P2+ and A30P10+ mice showed human ASYN expression in hippocampal regions CA3 and CA1 (Figure 3.1B). Immunoreactivity was largely confined to the pyramidal layer and human ASYN appeared to be present in a large number of pyramidal cells (identified by their pyramid shaped soma concentrated in *stratum pyramidale*).

Interestingly, slices from young A30P mice tended to exhibit a pattern of immunoreactivity more confined to deep pyramidal cells than superficial pyramidal cells. There is growing interest in the deep and superficial separation of the hippocampal pyramidal cell layer, though physiological differences in connectivity and expression patterns must be elucidated before investigation in to changes in alpha-synucleinopathy can be fully explored (Slomianka *et al.*, 2011). Deep pyramidal cells are defined by a cell body close to *stratum oriens* and the basal dendrites, whilst superficial pyramidal cells are defined by a cell body close to *stratum radiatum* and the apical dendrites (Slomianka *et al.*, 2011). Ageing A30P mice tended to show immunoreactivity across both deep and superficial pyramidal cells.

CA3 and CA1 region human ASYN+ cells were next quantified, without differentiating between cell types. As age-matched WT mice do not express human ASYN, A30P mice were directly compared between 2+ months and 10+ months of age, and between regions CA3 and CA1. No difference was found in the density of ASYN+ cells between slices from A30P2+ and A30P10+ mice within regions CA3 or CA1 (Figure 3.1C), though there was overall a higher density of human ASYN+ cells within region CA1 compared to region CA3, regardless of the age of A30P mice (A30P2+ CA3 223.8 cells/mm<sup>2</sup> ± 32.0, CA1 414.0 cells/mm<sup>2</sup> ± 43.3; A30P10+ CA3 233.8

cells/mm<sup>2</sup> ± 13.5, CA1 395.7 cells/mm<sup>2</sup> ± 58.0; mouse age p > 0.05, region p < 0.05, interaction p > 0.05; 2-way ANOVA; effect size = 16.94, power (1 - β) = 0.99).

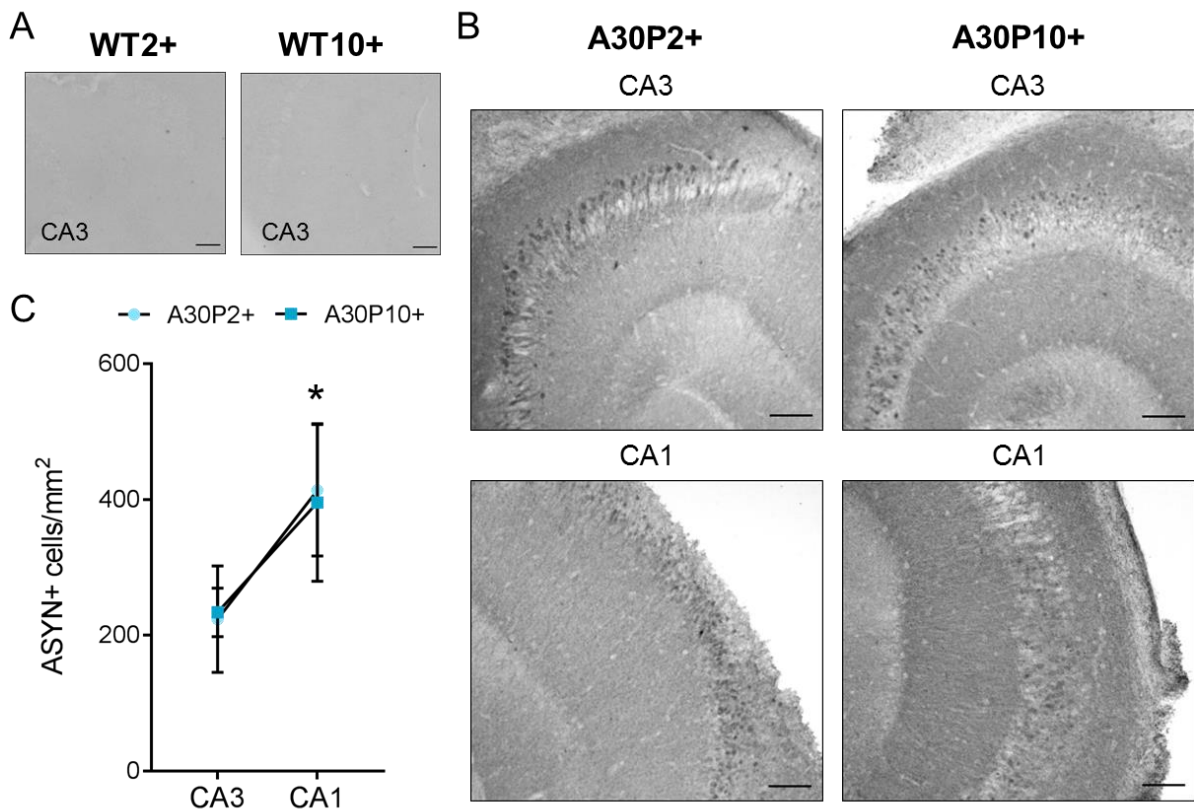


Figure 3.1 **Expression of human ASYN in the A30P mouse hippocampus.** (A) Representative greyscale images at x10 magnification show lack of immunoreactivity in WT mouse slices (n = 6 slices from 3 mice) in region CA3 (A), and predominantly pyramidal layer expression of ASYN in A30P2+ and A30P10+ mouse CA3 and CA1 regions (B). A number of slices from A30P2+ mice showed deep pyramidal cell immunoreactivity, compared to slices from A30P10+ mice which showed immunoreactivity in both deep and superficial pyramidal cells. Scale bars represent 100 μm. (C) Line graph to show ASYN+ cells/mm<sup>2</sup> in slices from A30P2+ (n = 12 slices from 6 mice) and A30P10+ mice (n = 17 slices from 7 mice) in regions CA3 and CA1.

The overall increased density of cells in region CA1 compared to region CA3 has been reported to be a physiological difference in mice (Coulin *et al.*, 2001; Jinno and Kosaka, 2010), rather than regional variation in human ASYN expression. The findings so far are consistent with reports in the literature that human ASYN expression in A30P mice plateaus at 3 - 4 weeks postnatal, and only changes in ASYN aggregation, oligomerisation, and phosphorylation occur with ageing (Neumann *et al.*, 2002; Schell *et al.*, 2009; Ekmark-Lewen *et al.*, 2018). Furthermore, changes in which pyramidal cells express human ASYN may be impacted by the extracellular spread of ASYN (Lee *et al.*, 2014a) and should be examined more closely in future work.

Whilst expression of human ASYN within hippocampal pyramidal cells has been established in this thesis and also previously in A30P mice (Szego *et al.*, 2013), it is a contentious matter in the literature as to how highly ASYN is expressed within inhibitory interneuron populations. Examination of post-mortem DLB tissue has previously reported a loss of PV+ interneurons, particularly within the dentate gyrus and region CA1, as well as a loss of CB+ granule cells from the dentate gyrus (Bernstein *et al.*, 2011; Morris *et al.*, 2015). As this chapter focuses on interneuron changes in alpha-synucleinopathy, I decided to examine human ASYN expression within PV+ and CB+ interneurons in regions CA3 and CA1 of the A30P mouse hippocampus.

Human ASYN was found in hippocampal CA3 and CA1 region PV+ interneurons in A30P2+ mice and A30P10+ mice (Figure 3.2; A30P10+ mouse slices not shown). Conversely, CB+ interneurons in region CA3 did not colocalise with human ASYN in any slice examined at either age. In region CA1, CB is found in both pyramidal cells and interneurons (Freund and Buzsaki, 1996). Evidence of colocalisation with human ASYN was found in a number of what are presumed to be CA1 pyramidal cells.

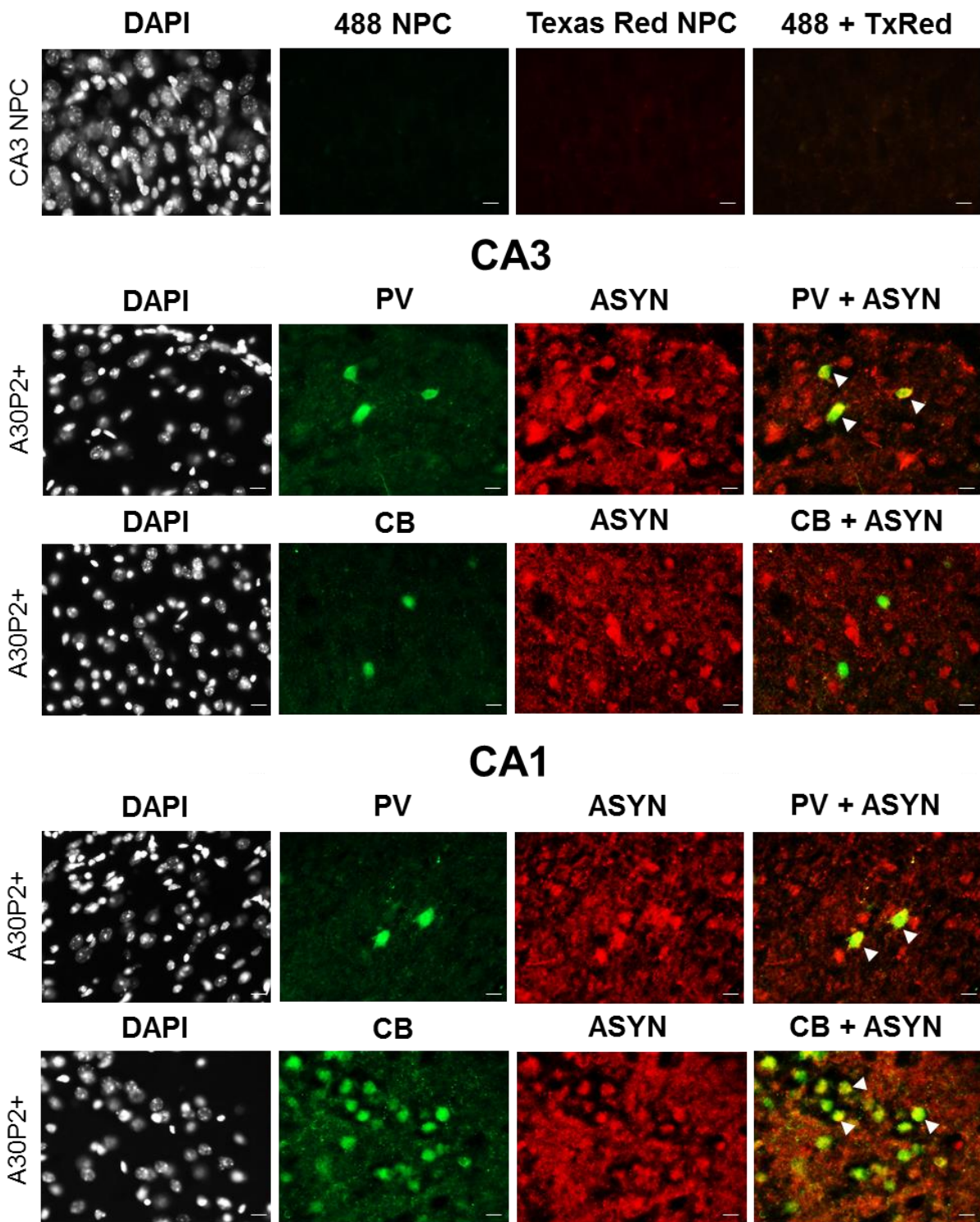


Figure 3.2 **Differential expression of human ASYN in CA3 interneurons.** Double immunofluorescence for DAPI (grey, 405), PV+ interneurons or CB+ cells (green, 488) and human ASYN (red, Texas Red 594) shows colocalisation in A30P2+ mice compared to the lack of immunoreactivity in no primary control sections (NPC). Images taken at x40 magnification in region CA3 or CA1 (note that pyramidal cell expression of CB in region CA1 means that CB is not restricted to interneurons in this region). Scale bar represents 10  $\mu$ m. White arrowheads indicate examples of co-localisation (yellow due to the overlap of red and green). A30P2+ n = 3 slices from 3 mice and A30P10+ n = 3 slices from 3 mice for each antibody and NPC.

### 3.4.2 No change in spontaneous network oscillations in A30P2+ mice

It has been reported that the acute preparation of rodent hippocampal slices can lead to the appearance of spontaneous network oscillations in drug-free conditions of standard artificial CSF (Skrobot, 2008; Pietersen *et al.*, 2009). Spontaneous gamma-frequency oscillations have been shown to occur more frequently in slices from sucrose-perfused animals as this step is neuroprotective (Modebadze, 2014), particularly to inhibitory interneurons (Aghajanian and Rasmussen, 1989). It was therefore interesting to first examine spontaneous oscillations in A30P mice, as an indicator of the state of the hippocampal excitatory/inhibitory network. Extracellular field recordings from *st. radiatum* in the hippocampal CA3 region were classified as either showing a discernible peak within the defined 15 – 45 Hz gamma-frequency range (Figure 3.3A) or showing no discernible peak (Figure 3.3B).

Upon comparing the proportion of spontaneously oscillating slices (Figure 3.3C) in WT2+ mice (20.8%; 5/24 slices) and A30P2+ mice (22.7%; 5/22 slices), no significant difference was found ( $\chi^2$  (df 1) = 0.02,  $p > 0.05$ , chi-square test). Despite a slightly smaller sample size of 6 - 8 month old mice, the same proportion of slices were spontaneously oscillating in WT6+ mice (16.7%; 2/12 slices) and A30P6+ mice (16.7%; 2/12 slices) ( $\chi^2$  (df 1) = 0,  $p > 0.05$ , chi-square test). Likewise, a similar proportion of slices were spontaneously oscillating in WT10+ mice (20.0%; 4/20 slices) and A30P10+ mice (33.3%; 8/24 slices) ( $\chi^2$  (df 1) = 0.98,  $p > 0.05$ , chi-square test). This indicates that sucrose perfusion led to a similar incidence of spontaneous oscillations in all age groups of WT and A30P mice.

Spontaneous gamma-frequency oscillations were of a low amplitude overall, however the area power (Figure 3.3D) was not significantly different in age-matched WT control mice compared to slices from A30P2+ mice (29  $\mu\text{V}^2$  [IQR 11 – 93] versus 23  $\mu\text{V}^2$  [IQR 12 – 83] respectively;  $p > 0.05$ , Mann-Whitney rank sum test), slices from A30P6+ mice (58  $\mu\text{V}^2$  [IQR 53 – 63] versus 28  $\mu\text{V}^2$  [IQR 11 – 44] respectively;  $p > 0.05$ , Mann-Whitney rank sum test), or slices from A30P10+ mice (73  $\mu\text{V}^2$  [IQR 26 – 190] versus 56  $\mu\text{V}^2$  [IQR 16 – 140] respectively;  $p > 0.05$ , Mann-Whitney rank sum test).

The peak frequency of spontaneous oscillations (Figure 3.3E) ranged from 17.8 Hz to 42.1 Hz. Given this level of variability, no significant difference was found in peak frequency in age-matched WT control mice compared to slices from A30P2+ mice (26.4 Hz  $\pm$  2.6 versus 24.4 Hz  $\pm$  2.4 respectively;  $p > 0.05$ , unpaired  $t$  test), slices from

A30P6+ mice (27.2 Hz  $\pm$  8.8 versus 39.1 Hz  $\pm$  3.1 respectively;  $p > 0.05$ , unpaired  $t$  test), or slices from A30P10+ mice (26.6 Hz  $\pm$  1.5 versus 24.4 Hz  $\pm$  1.6 respectively;  $p > 0.05$ , unpaired  $t$  test). Therefore, in addition to a similar rate of occurrence, spontaneous oscillations were also similar in A30P mice in area power and frequency.

Despite no statistically significant difference in spontaneous oscillation occurrence, area power, or frequency, it is possible that changes in the rhythmicity of observed activity had occurred in A30P mice. A value of rhythmicity index (RI) was computed in slices with spontaneous oscillations (Figure 3.4) and it was noted that spontaneous activity was not very rhythmic overall. Regardless, comparisons between WT and A30P mice revealed no significant difference in rhythmicity between age-matched WT control mice and slices from A30P2+ mice (0.12  $\pm$  0.06 versus 0.19  $\pm$  0.11 respectively;  $p > 0.05$ , unpaired  $t$  test), slices from A30P6+ mice (0.10  $\pm$  0.03 versus 0.15  $\pm$  0.05 respectively;  $p > 0.05$ , unpaired  $t$  test), or slices from A30P10+ mice (0.11  $\pm$  0.02 versus 0.11  $\pm$  0.04 respectively;  $p > 0.05$ , unpaired  $t$  test).

This indicates that all parameters of spontaneous gamma-frequency oscillations examined are likely similar in A30P mice. However, due to a low number of slices with spontaneous oscillations in our conditions a difference may not be detectable without a larger sample size. This could be achieved in future by modification of aCSF with neuroprotective compounds to further improve cell viability (Modebadze, 2014).

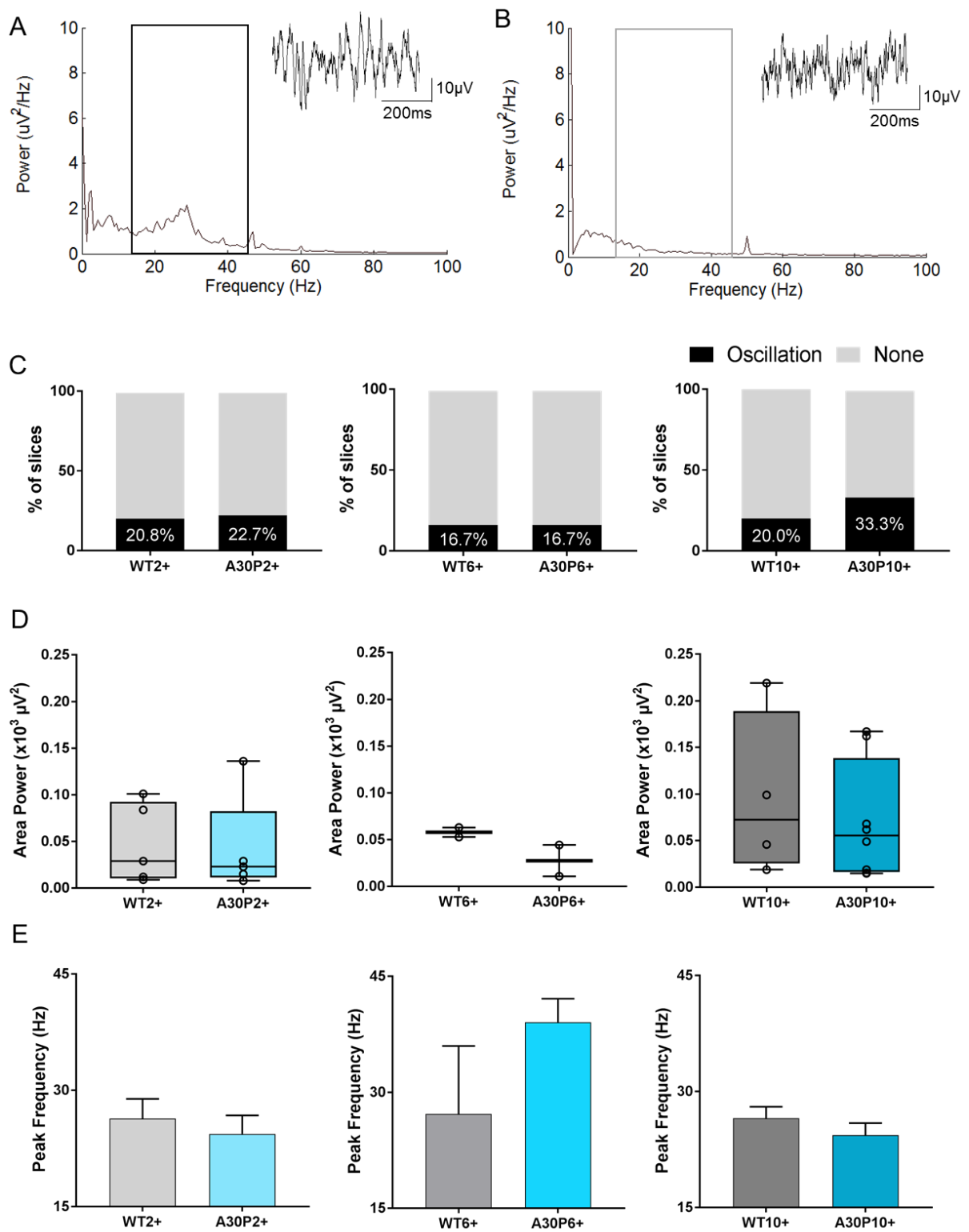


**Figure 3.3 No difference in spontaneous 15 – 45 Hz oscillations in A30P mice.** Representative power spectra and inset LFP traces show baseline activity with (A) and without (B) oscillations; 15 – 45 Hz range indicated. (C) % of slices oscillating in WT2+ (n = 24 slices from 12 mice), A30P2+ (n = 22 slices from 11 mice), WT6+ (n = 12 slices from 6 mice), A30P6+ (n = 12 slices from 6 mice), WT10+ (n = 20 slices from 9 mice), and A30P10+ mice (n = 24 slices from 8 mice). Boxplots showing area power (D) of spontaneous oscillations at each age in subset of slices spontaneously oscillating. Bar charts showing peak frequency (E) of spontaneous oscillations at each age.



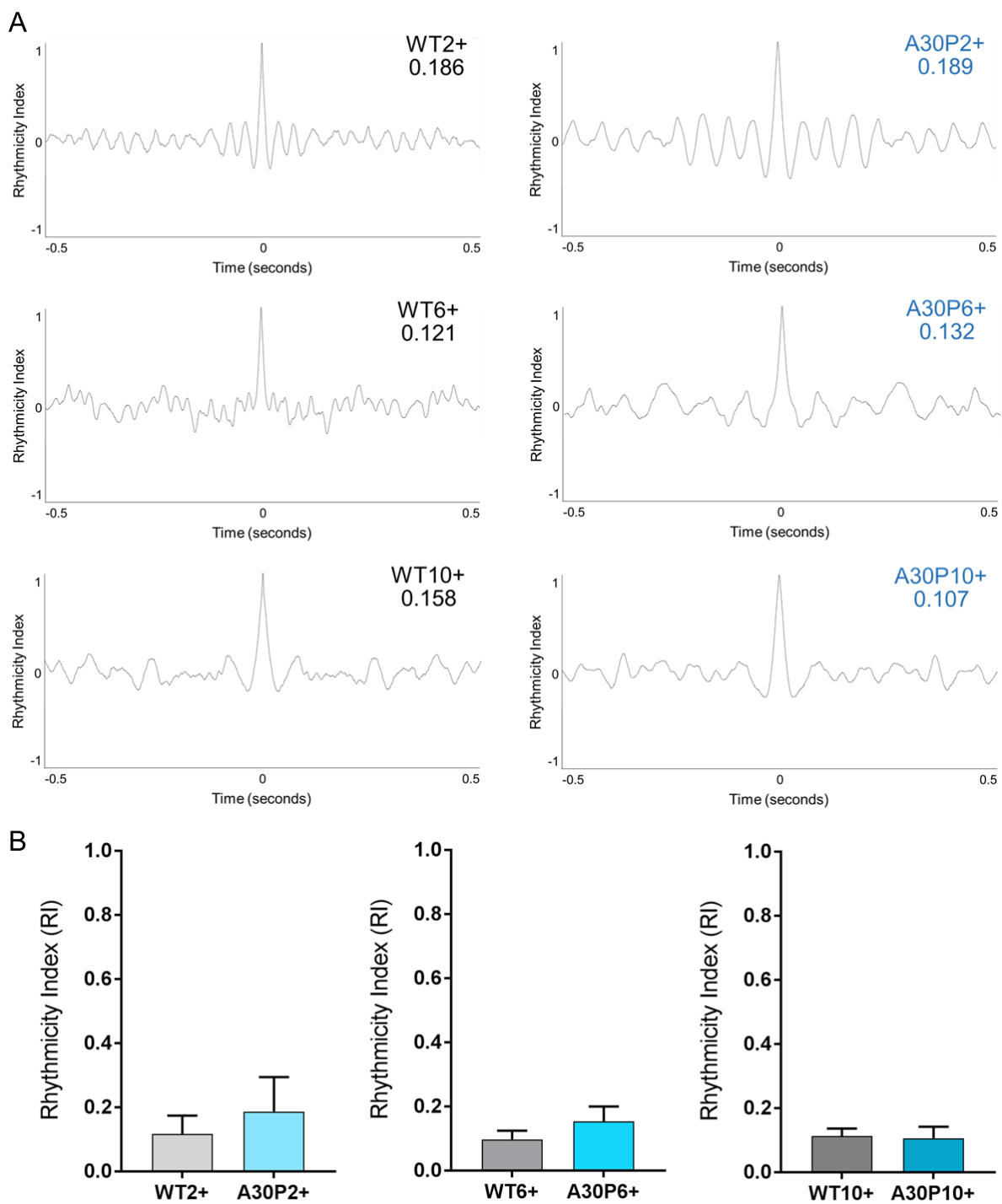


**Figure 3.4 No difference in rhythmicity of spontaneous oscillations in A30P mice.** (A) Representative auto-correlations of spontaneous oscillations with RI values inset. (B) Bar charts to show RI in slices from WT2+ (n = 5 slices from 5 mice), A30P2+ (n = 5 slices from 4 mice), WT6+ (n = 2 slices from 2 mice), A30P6+ (n = 2 slices from 2 mice), WT10+ (n = 4 slices from 3 mice), and A30P10+ mice (n = 8 slices from 5 mice).



### 3.4.3 Presence of spontaneous SPWs in hippocampal slice preparations

Another form of spontaneous network activity reported in rodent acute hippocampal slice preparations are spontaneous sharp waves (SPWs). In slices not spontaneously oscillating within the 15 – 45 Hz range, spontaneous SPWs were observed in a proportion of slices from all genotypes and ages of mice immediately after a slice was placed in the recording chamber (Figure 3.5A).

No significant difference was found in the proportion of slices exhibiting SPWs (Figure 3.5B) between WT2+ mice (35.0%; 7/20 slices) and A30P2+ mice (31.8%; 7/22 slices) ( $\chi^2$  (df 1) = 0.04,  $p > 0.05$ , chi-square test). The same proportion of slices exhibited SPWs in WT6+ mice (22.2%; 2/9 slices) compared to A30P6+ mice (22.2%; 2/9 slices), despite a smaller sample size in this age group ( $\chi^2$  (df 1) = 0,  $p > 0.05$ , chi-square test). Likewise, a similar proportion of slices exhibited SPWs in WT10+ mice (38.5%; 10/26 slices) compared to A30P10+ mice (26.7%; 4/15 slices) ( $\chi^2$  (df 1) = 0.59,  $p > 0.05$ , chi-square test).

SPWs were monitored for a further 45 minutes, at which point all groups showed a greater proportion of slices with SPWs (Figure 3.5C). This is likely due to slices adapting to the recording chamber environment over time. The proportion of slices exhibiting SPWs after 45 minutes was still not significantly different between WT2+ mice (60.0%; 12/20 slices) and A30P2+ mice (72.7%; 16/22 slices) ( $\chi^2$  (df 1) = 0.76,  $p > 0.05$ , chi-square test). Equally, a similar proportion of slices exhibited SPWs in WT10+ mice (65.4%; 17/26 slices) and A30P10+ mice (66.7%; 10/15 slices) ( $\chi^2$  (df 1) = 0.01,  $p > 0.05$ , chi-square test).

Surprisingly, significantly more SPWs were seen in slices from A30P6+ mice (77.8%; 7/9 slices) compared to WT6+ mice (55.6%; 5/9 slices) following 45 minutes in the recording chamber ( $\chi^2$  (df 1) = 3.84,  $p < 0.05$ , chi-square test). It is possible that this result may be due to an inadequate sample size to detect such a small effect, given that the observed power was only 25% (effect size = 0.48, power (1 -  $\beta$ ) = 0.25). Due to the uncertainty about the reliability of this result, I decided to further explore SPW parameters using data recorded immediately after slices were placed in the recording chamber. This would allow a more accurate comparison of SPW parameters given a similar proportion of slices exhibiting SPWs at this immediate time-point.

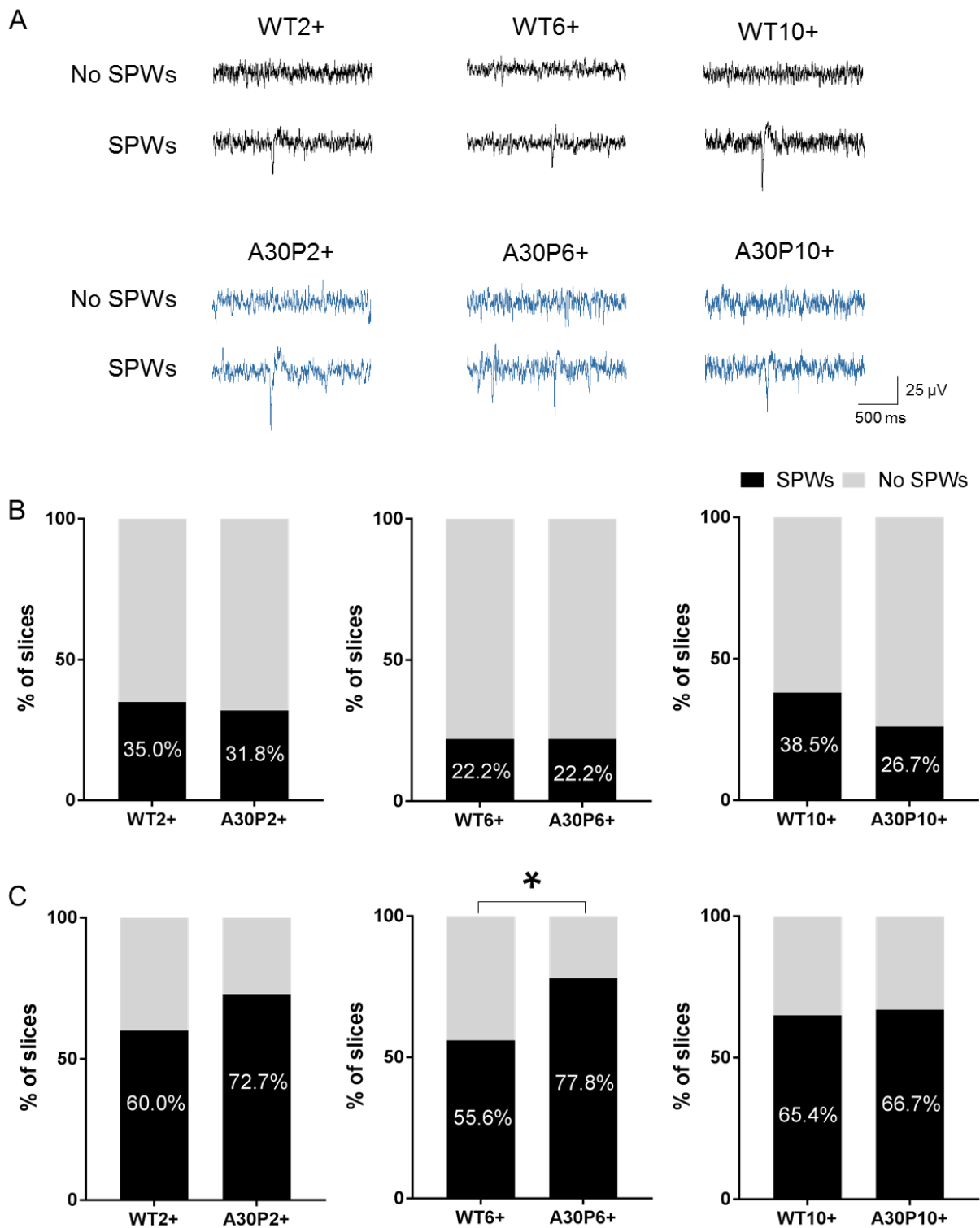


**Figure 3.5 Proportion of slices with SPWs upon immediate recording.** (A) Representative traces showing baseline activity and spontaneous SPW activity in the CA3 *st. radiatum* in A30P and WT mice. % of slices with (black) and without (grey) SPWs immediately after being placed in the recording chamber (B) and following 45 minutes in the recording chamber (C) in WT2+ (n = 20 slices from 10 mice), A30P2+ (n = 22 slices from 15 mice), WT6+ (n = 9 slices from 5 mice), A30P6+ (n = 9 slices from 5 mice), WT10+ (n = 26 slices from 10 mice), and A30P10+ mice (n = 15 slices from 8 mice). \* indicates significance at p < 0.05.

### 3.4.4 Increased SPW amplitude but not frequency in A30P2+ mouse CA3 region

SPW activity is generated in CA3 and propagates to CA1 (Wu *et al.*, 2005a; Bazelot *et al.*, 2016), and so SPW frequency and amplitude in both regions were investigated in slices from WT and A30P mice immediately after slices were placed in the recording chamber. SPW number varied considerably between slices as some slices did not exhibit SPWs. As a result, SPW frequency (Figure 3.6A) was not significantly different in region CA3 between age-matched WT control mice and slices from A30P2+ mice (0 Hz [IQR 0 – 0.02] versus 0 Hz [IQR 0 – 0.02] respectively;  $p > 0.05$ , Mann-Whitney rank sum test), slices from A30P6+ mice (0 Hz [IQR 0 – 0.02] versus 0 Hz [IQR 0 – 0.01] respectively;  $p > 0.05$ , Mann-Whitney rank sum test), or slices from A30P10+ mice (0 Hz [IQR 0 – 0.12] versus 0 Hz [IQR 0 – 0.02] respectively;  $p > 0.05$ , Mann-Whitney rank sum test).

Similarly, no significant difference was found in region CA1 (Figure 3.6B) between age-matched WT control mice and slices from A30P2+ mice (0.02 Hz [IQR 0 – 0.03] versus 0 Hz [IQR 0 – 0.02] respectively;  $p > 0.05$ , Mann-Whitney rank sum test) or slices from A30P10+ mice (0 Hz [IQR 0 – 0.05] versus 0 Hz [IQR 0 – 0.01] respectively;  $p > 0.05$ , Mann-Whitney rank sum test). No data were available for slices from A30P6+ mice within region CA1, though it is reasonable to assume that SPW frequency would not differ in this intermediate age group.

Slices that did exhibit SPWs were next compared by SPW amplitude. Interestingly, SPWs in slices from A30P2+ mice were of a significantly greater amplitude in region CA3 (Figure 3.7A) compared to WT2+ mice ( $-69.49 \mu\text{V} \pm 8.79$  versus  $-28.43 \mu\text{V} \pm 3.92$  respectively;  $p < 0.05$ , unpaired *t* test; effect size = 2.30, power  $(1 - \beta) = 0.98$ ). This finding appeared to persist in slices from A30P6+ mice compared to WT6+ mice though statistical significance was not found ( $-65.98 \mu\text{V} \pm 14.63$  versus  $-23.14 \mu\text{V} \pm 2.36$  respectively;  $p > 0.05$ , unpaired *t* test). By 10+ months, slices from A30P mice showed no significant difference in SPW amplitude compared to WT10+ mice ( $-34.56 \mu\text{V} \pm 2.78$  versus  $-33.52 \mu\text{V} \pm 4.35$  respectively;  $p > 0.05$ , unpaired *t* test).

Conversely, no significant difference in SPW amplitude was found in region CA1 (Figure 3.7B) between WT mice and slices from A30P2+ mice ( $-47.98 \mu\text{V} \pm 9.14$  versus  $-58.52 \mu\text{V} \pm 15.67$  respectively;  $p > 0.05$ , unpaired *t* test) or A30P10+ mice ( $-53.35 \mu\text{V} \pm 12.39$  versus  $-75.79 \mu\text{V} \pm 36.69$  respectively;  $p > 0.05$ , unpaired *t* test). This indicates a CA3-specific increase in spontaneous SPW amplitude in slices from A30P2+ mice.

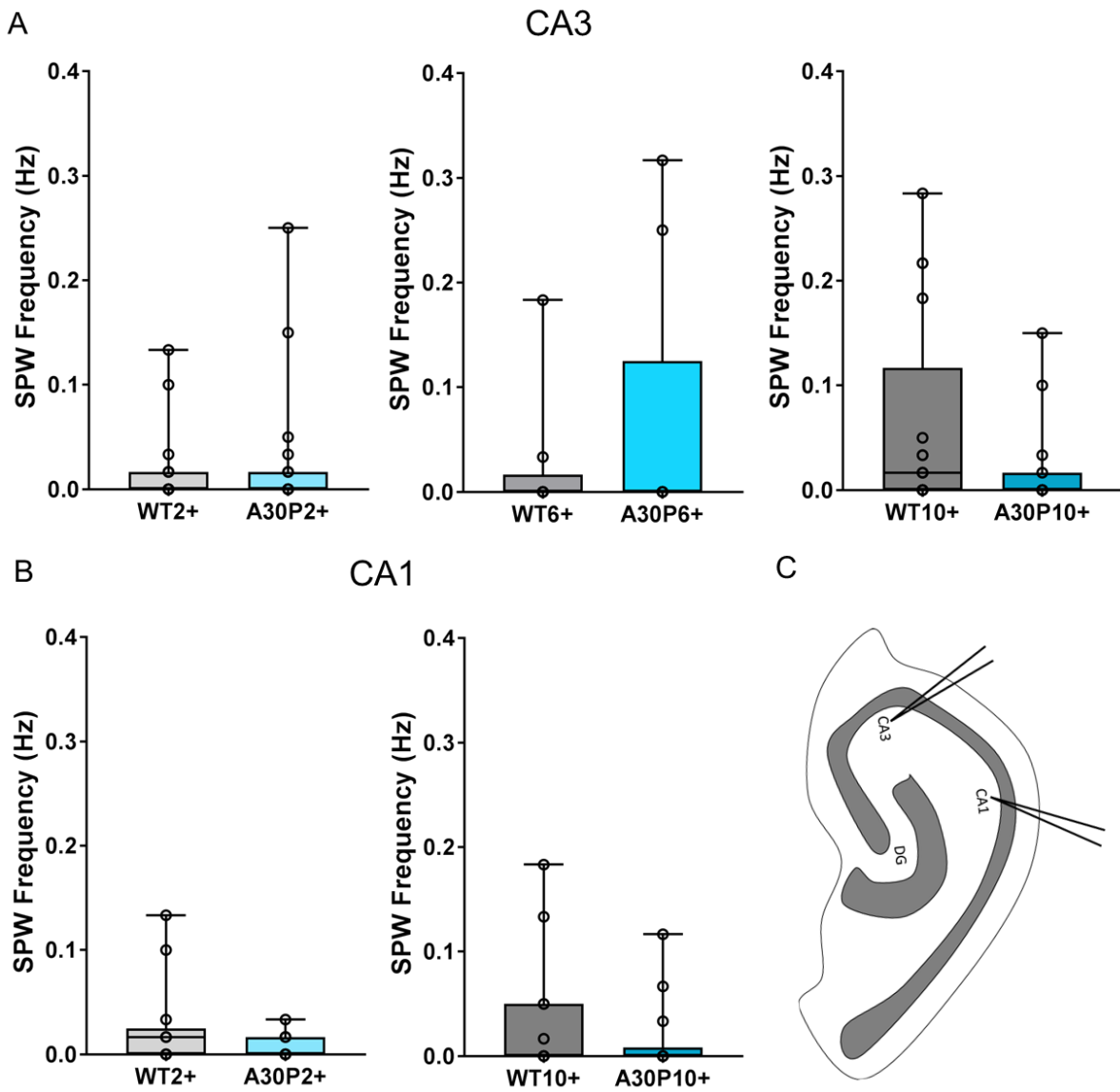
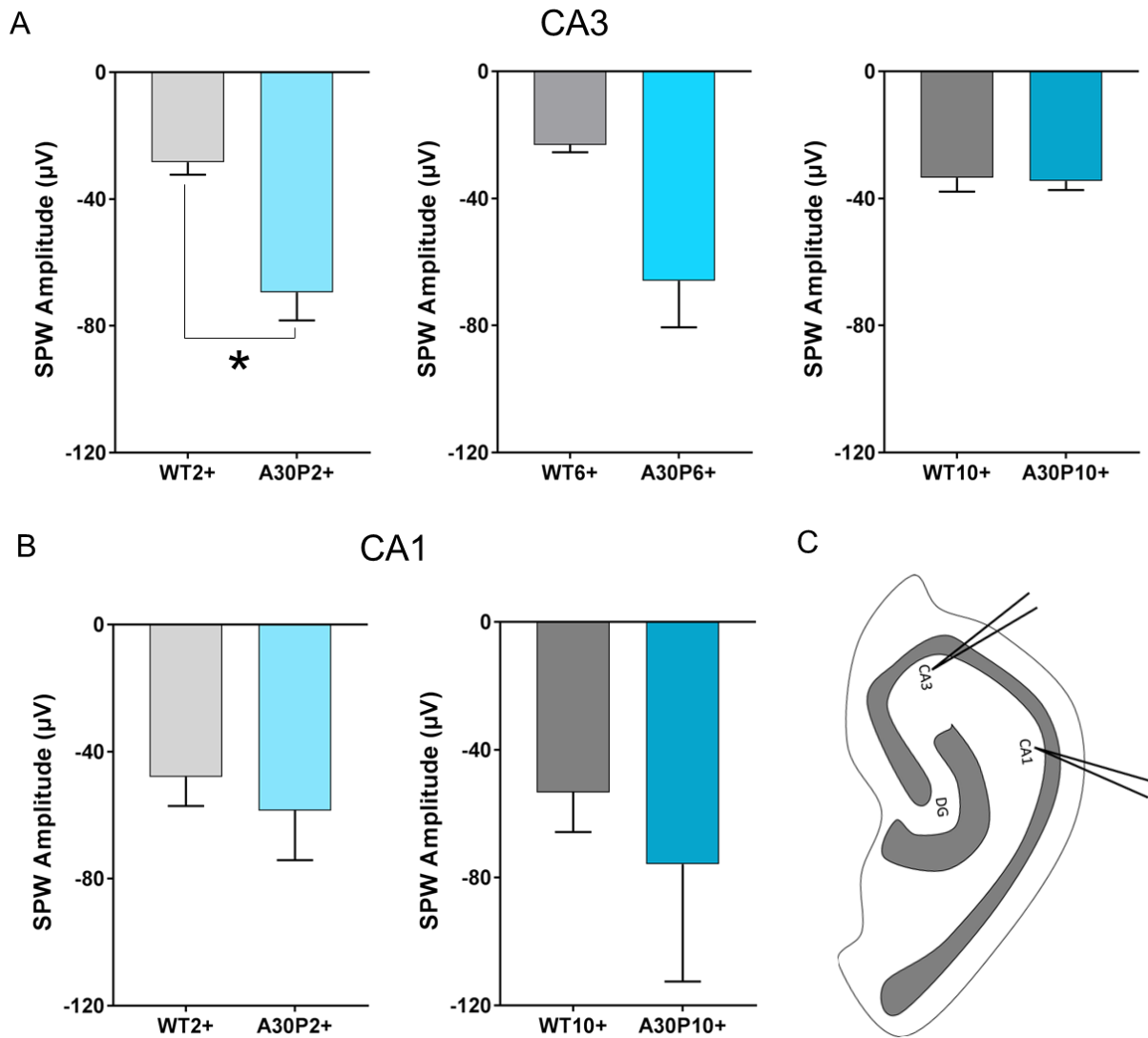


Figure 3.6 **No difference in SPW frequency in A30P mice.** Boxplots to show SPW frequency in region CA3 (A) and CA1 (B) of slices from WT2+ (n = 21 slices from 10 mice), A30P2+ (n = 23 slices from 15 mice), WT6+ (n = 9 slices from 5 mice), A30P6+ (n = 9 slices from 5 mice), WT10+ (n = 17 slices from 7 mice), and A30P10+ mice (n = 15 slices from 8 mice). (C) Schematic of mouse hippocampus showing electrode placement in CA3/1 *st. radiatum*.



**Figure 3.7 Increased amplitude of SPWs in the A30P2+ mouse CA3 region.** Bar charts to show SPW amplitude in region CA3 (A) and CA1 (B) in WT2+ (n = 7 slices from 6 mice), A30P2+ (n = 7 slices from 6 mice), WT6+ (n = 2 slices from 1 mouse), A30P6+ (n = 2 slices from 2 mice), WT10+ (n = 10 slices from 5 mice), and A30P10+ mice (n = 4 slices from 3 mice). \* indicates significance at  $p < 0.05$ . (C) Schematic of mouse hippocampus showing electrode placement in CA3/1 *st. radiatum*.

It has previously been reported that the ventral hippocampus is more likely to exhibit SPWs in mouse hippocampal slices (Papatheodoropoulos and Kostopoulos, 2002b; Papatheodoropoulos and Kostopoulos, 2002a; Wu *et al.*, 2006a). Given the difference along the hippocampal dorsal/ventral axis in functionality and expression of receptors, dorsal/ventral differences in SPWs were next explored.

Surprisingly, SPWs were found at a similar ratio (Figure 3.8A) between the dorsal (37.5%; 3/8 slices) and ventral (33.3%; 4/12 slices) hippocampus in WT2+ mice ( $\chi^2$  (df 1) = 0.04,  $p > 0.05$ ; chi-square test). A similar proportion of SPWs were also exhibited in dorsal (30.8%; 4/13 slices) and ventral (33.3%; 3/9 slices) slices in A30P2+ mice ( $\chi^2$  (df 1) = 0.02,  $p > 0.05$ ; chi-square test). Likewise, SPWs were found at a similar proportion between the dorsal (45.5%; 4/11 slices) and ventral (50.0%; 3/6 slices) hippocampus in WT10+ mice ( $\chi^2$  (df 1) = 0.30,  $p > 0.05$ ; chi-square test), and at a similar proportion between dorsal (25.0%; 3/12 slices) and ventral (33.3%; 1/3 slices) slices in A30P10+ mice ( $\chi^2$  (df 1) = 0.09,  $p > 0.05$ ; chi-square test). Given the smaller number of slices from WT6+ and A30P6+ mice, it was not possible to explore dorsal/ventral differences.

To explore SPW changes in A30P2+ mice further, data were separated by dorsal/ventral location in slices from WT2+ and A30P2+ mice. SPW frequency (Figure 3.8B) was not dependent on dorsal/ventral slice location in WT2+ or A30P2+ mice (WT2+ *dorsal* 0 Hz [IQR 0 – 0.03]; WT2+ *ventral* 0 Hz [IQR 0 – 0.02]; A30P2+ *dorsal* 0 Hz [IQR 0 – 0.02]; A30P2+ *ventral* 0 Hz [IQR 0 – 0.02]; mouse  $p > 0.05$ , location  $p > 0.05$ , interaction  $p > 0.05$ ; 2 way ANOVA on ranks). Similarly, SPW amplitude (Figure 3.8C) was not dependent on dorsal/ventral slice location in WT2+ and A30P2+ mice (WT2+ *dorsal* -34.40  $\mu\text{V} \pm 3.15$ ; WT2+ *ventral* -23.95  $\mu\text{V} \pm 5.76$ ; A30P2+ *dorsal* -70.19  $\mu\text{V} \pm 12.87$ ; A30P2+ *ventral* -68.56  $\mu\text{V} \pm 14.49$ ; genotype  $p < 0.05$ , location  $p > 0.05$ , interaction  $p > 0.05$ ; 2-way ANOVA). This confirms that the increase in SPW amplitude in A30P2+ mice is present throughout the hippocampal axis.

It was finally confirmed that the observed increase in SPW amplitude in slices from A30P2+ mice was likely not dependent on sex, as the increased SPW amplitude in A30P2+ mice persisted when data were separated by sex (WT2+ *male* -21.87  $\mu\text{V} \pm 4.01$  [n = 4 slices]; WT2+ *female* -37.17  $\mu\text{V} \pm 2.93$  [n = 3 slices]; A30P2+ *male* -71.42  $\mu\text{V} \pm 10.30$  [n = 5 slices]; A30P2+ *female* -64.67  $\mu\text{V} \pm 23.07$  [n = 2 slices]; genotype  $p < 0.05$ , sex  $p > 0.05$ , interaction  $p > 0.05$ ; 2-way ANOVA, data not shown).

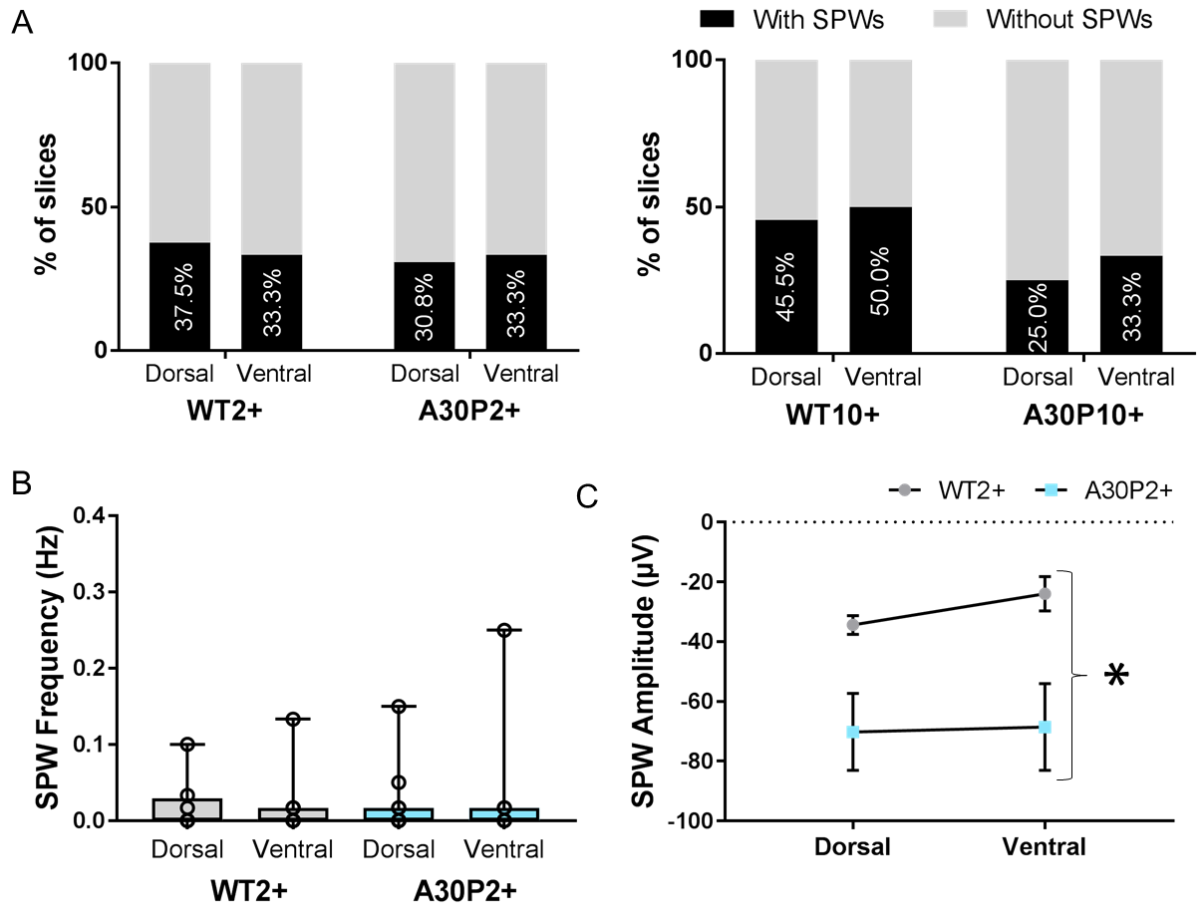


Figure 3.8 **No difference in SPWs between dorsal/ventral slices.** (A) % of dorsal/ventral hippocampal slices with (black) and without (grey) SPWs in WT2+ (dorsal n = 8 slices from 5 mice; ventral n = 12 slices from 8 mice), A30P2+ (dorsal n = 13 slices from 11 mice; ventral n = 9 slices from 8 mice), WT10+ (dorsal n = 11 slices from 8 mice; ventral n = 6 slices from 5 mice), and A30P10+ mice (dorsal n = 12 slices from 7 mice; ventral n = 3 slices from 3 mice). Boxplot to show SPW frequency (B) in dorsal and ventral hippocampal slices. Line graph to show SPW amplitude (C) in dorsal and ventral hippocampal slices. \* indicates significance at  $p < 0.05$ .

### 3.4.5 IPSPs correlate with SPWs in A30P2+ mice

To explore the intracellular correlate of SPWs, sharp intracellular recordings were performed in CA3 pyramidal cells with simultaneous LFP recording in *st. radiatum* in baseline conditions (Figure 3.9A). A subset of slices explored in section 3.4.4 were used for this experiment. SPWs were visually confirmed to correlate with the arrival of IPSPs in pyramidal cells. However, as SPWs are population events, more IPSPs were recorded within pyramidal cells than SPWs in the extracellular field. To achieve an overall comparison of the properties of IPSPs arriving in CA3 pyramidal cells, total IPSPs were compared regardless of whether they correlated to field SPWs.

Slices from A30P2+ mice showed a significant increase in IPSP frequency recorded from CA3 pyramidal cells (Figure 3.9B) compared to slices from WT2+ mice (19.6 Hz  $\pm$  2.0 versus 7.3 Hz  $\pm$  2.0 respectively;  $p < 0.05$ , unpaired  $t$  test; effect size = 4.05, power (1 -  $\beta$ ) = 0.99). IPSP frequency in the absence of any drugs was noted to be significantly faster than the SPW frequency reported in the LFP in section 3.4.4. This is once again explained by the fact that SPWs are population events, and therefore not all IPSPs will contribute to SPW activity within the field.

Spontaneous IPSP amplitude recorded from CA3 pyramidal cells (Figure 3.9C) was also significantly increased in slices from A30P2+ mice compared to slices from WT2+ mice (5.73 mV  $\pm$  0.53 versus 4.27 mV  $\pm$  0.20 respectively,  $p < 0.05$ , unpaired  $t$  test; effect size = 2.34, power (1 -  $\beta$ ) = 0.76). Post-hoc power analysis revealed this experiment to be slightly underpowered at 76% observed power. This is likely due to the detected difference being marginal. Measurements of IPSP amplitude could benefit from a larger sample size in future experiments to detect such small changes. Regardless, this supports an increase in CA3 region IPSP frequency and amplitude at the same age that an increase in field SPW amplitude is observed in A30P2+ mice.



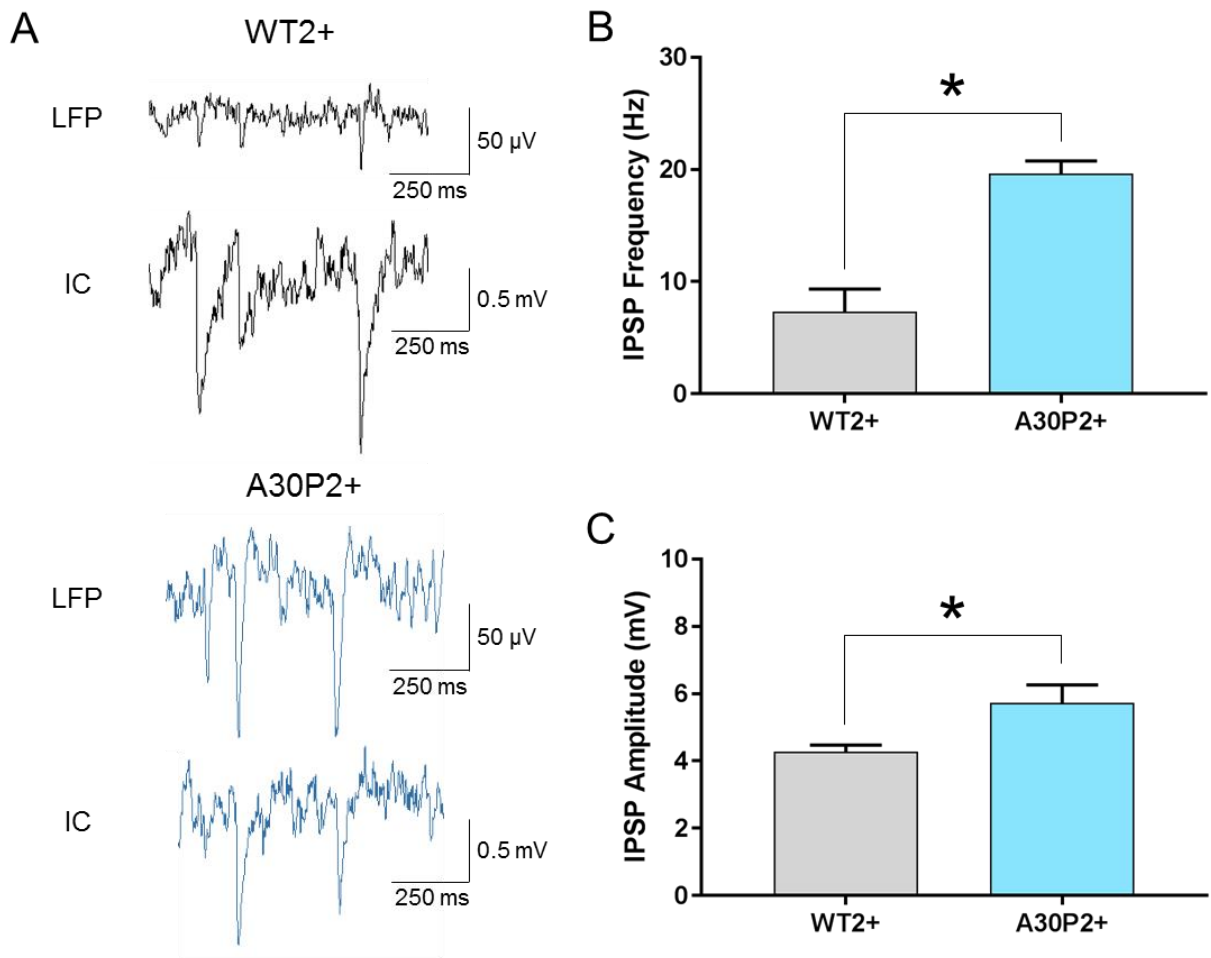


Figure 3.9 **SPWs in the field correlate to the arrival of IPSPs in pyramidal cells.** (A) CA3 region *st. radiatum* LFP and CA3 pyramidal cell intracellular (IC) recordings in slices from WT2+ (n = 4 cells from 3 mice) and A30P2+ mice (n = 3 cells from 3 mice). Bar charts of IPSP frequency (B) and amplitude (C) recorded from CA3 pyramidal cells in WT2+ and A30P2+ mice. \* indicates significance at  $p < 0.05$ .

### 3.4.6 Pharmacological manipulation of spontaneous SPWs

SPWs have been reported to be sensitive to GABA<sub>A</sub> receptor antagonism but not to NMDA receptor antagonism (Wu *et al.*, 2006a). It has also been previously reported that application of choline suppresses SPWs and induces gamma-frequency oscillations in hippocampal slices (Fischer *et al.*, 2014). The effect of each compound on CA3 region SPWs was therefore assessed in slices from WT2+ and A30P2+ mice to confirm that the underlying mechanisms of SPWs were similar in A30P2+ mice.

It was first important to establish a measure of how SPWs changed over time before any experiments with pharmacological compounds could be carried out. This chapter previously established an increase in the proportion of slices with SPWs after 45 minutes in the recording chamber. This 45 minute time-point is henceforth referred to as “baseline”, and SPW frequency and amplitude within CA3 *st. radiatum* were measured for a further hour by extracellular field recordings (Figure 3.10A). Only slices with SPWs present from baseline were included in pharmacological experiments.

There was no significant change over one hour from baseline in SPW frequency (Figure 3.10B) in slices from either WT2+ or A30P2+ mice (WT2+ *baseline* 0.36 Hz [IQR 0.22 – 0.60] to WT2+ *plus one hour* 0.30 Hz [IQR 0.12 – 0.80]; A30P2+ *baseline* 0.27 Hz [IQR 0.12 – 0.37] to A30P2+ *plus one hour* 0.22 Hz [IQR 0.08 – 0.32]; genotype  $p > 0.05$ , time  $p > 0.05$ , interaction  $p > 0.05$ , RM 2-way ANOVA on ranks).

Similarly, there was no change over one hour in SPW amplitude (Figure 3.10C) in slices from either WT2+ or A30P2+ mice (WT2+ *baseline* -69.26  $\mu\text{V} \pm 20.31$  to WT2+ *plus one hour* -80.25  $\mu\text{V} \pm 25.54$ ; A30P2+ *baseline* -123.53  $\mu\text{V} \pm 24.50$  to A30P2+ *plus one hour* -126.31  $\mu\text{V} \pm 34.48$ ; genotype  $p > 0.05$ , time  $p > 0.05$ , interaction  $p > 0.05$ ; RM 2-way ANOVA). This indicates that following 45 minutes in the recording chamber, SPWs reach a stable period over 1 hour with respect to SPW frequency and amplitude, allowing for reliable pharmacological manipulation.

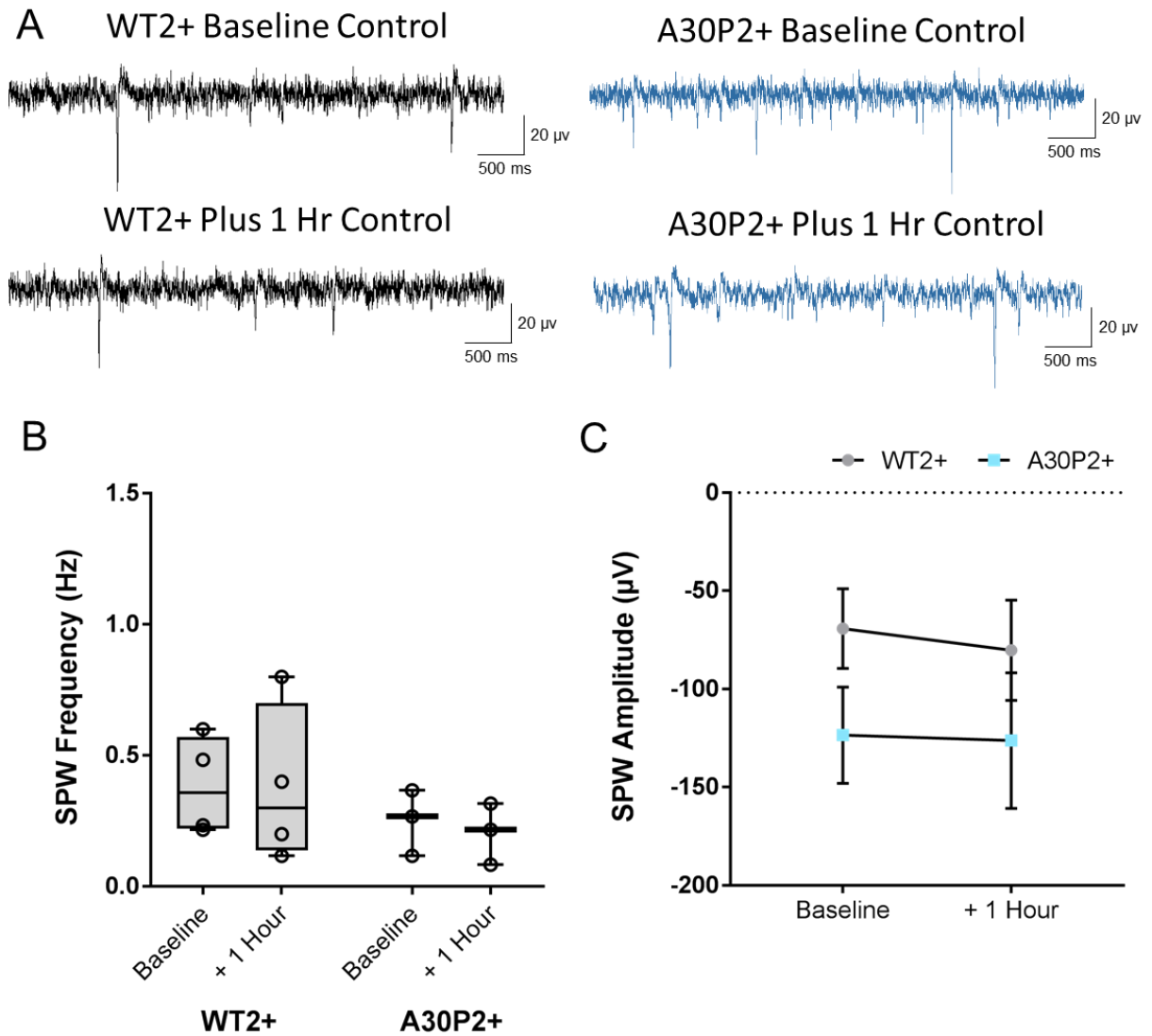


Figure 3.10 **SPWs remain stable for 1 hour in control conditions once established.** (A) Representative traces after 45 minutes in recording chamber (“baseline”) versus 1 hour later in slices from WT2+ (n = 4 slices from 1 mouse) and A30P2+ mice (n = 3 slices from 2 mice). Boxplot to show SPW frequency (B) at baseline and 1 hour later in WT2+ and A30P2+ mice. Line graph to show SPW amplitude (C) at baseline and 1 hour later in WT2+ and A30P2+ mice.

### 3.4.6.1 SPW amplitude is reduced by GABA<sub>A</sub> receptor antagonism

SPWs have previously been shown to be abolished by GABA<sub>A</sub> receptor antagonism (Wu *et al.*, 2006a) and I first wanted to examine this mechanism in slices from A30P2+ mice. At low concentrations, gabazine has been shown to effectively antagonise the GABA<sub>A</sub> receptor (Heaulme *et al.*, 1986; Wermuth *et al.*, 1987) before leading to increased excitability and interictal discharges at higher concentrations (Behrens *et al.*, 2007; Mann *et al.*, 2009; Kolbaev *et al.*, 2012). Therefore, a concentration of 100 nM was selected, and no interictal activity was observed at this concentration following extracellular field recordings for 1 hour in CA3 *st. radiatum*. The effect of GABA<sub>A</sub> receptor antagonism on SPW frequency and amplitude was therefore assessed in slices from WT2+ and A30P2+ mice (Figure 3.11A).

Application of gabazine for 1 hour led to no significant change in SPW frequency despite a trend towards a decrease (Figure 3.11B) in slices from WT2+ and A30P2+ mice (WT2+ *baseline* 0.13 Hz [IQR 0.03 – 0.37] to WT2+ *drug* 0.07 Hz [IQR 0 – 0.17]; A30P2+ *baseline* 0.16 Hz [IQR 0.05 – 0.52] to A30P2+ *drug* 0.03 Hz [IQR 0 – 0.45]; genotype  $p > 0.05$ , drug condition  $p > 0.05$ , interaction  $p > 0.05$ ; RM 2-way ANOVA on ranks). It should be noted that one slice in each group showed no SPWs after 1 hour of gabazine exposure, an effect that did not occur in control conditions.

On the other hand, SPW amplitude (Figure 3.11C) was significantly reduced following bath application of gabazine in slices from both WT2+ and A30P2+ mice (WT2+ *baseline* -106.77  $\mu\text{V} \pm 43.94$  to WT2+ *drug* -58.15  $\mu\text{V} \pm 32.52$ ; A30P2+ *baseline* -131.45  $\mu\text{V} \pm 24.56$  to A30P2+ *drug* -34.49  $\mu\text{V} \pm 12.69$ ; genotype  $p > 0.05$ , drug condition  $p < 0.05$ , interaction  $p > 0.05$ ; RM 2-way ANOVA; effect size = 4.61, power  $(1 - \beta) = 0.88$ ). Despite a reduction in amplitude, SPWs were not abolished at this concentration of gabazine.

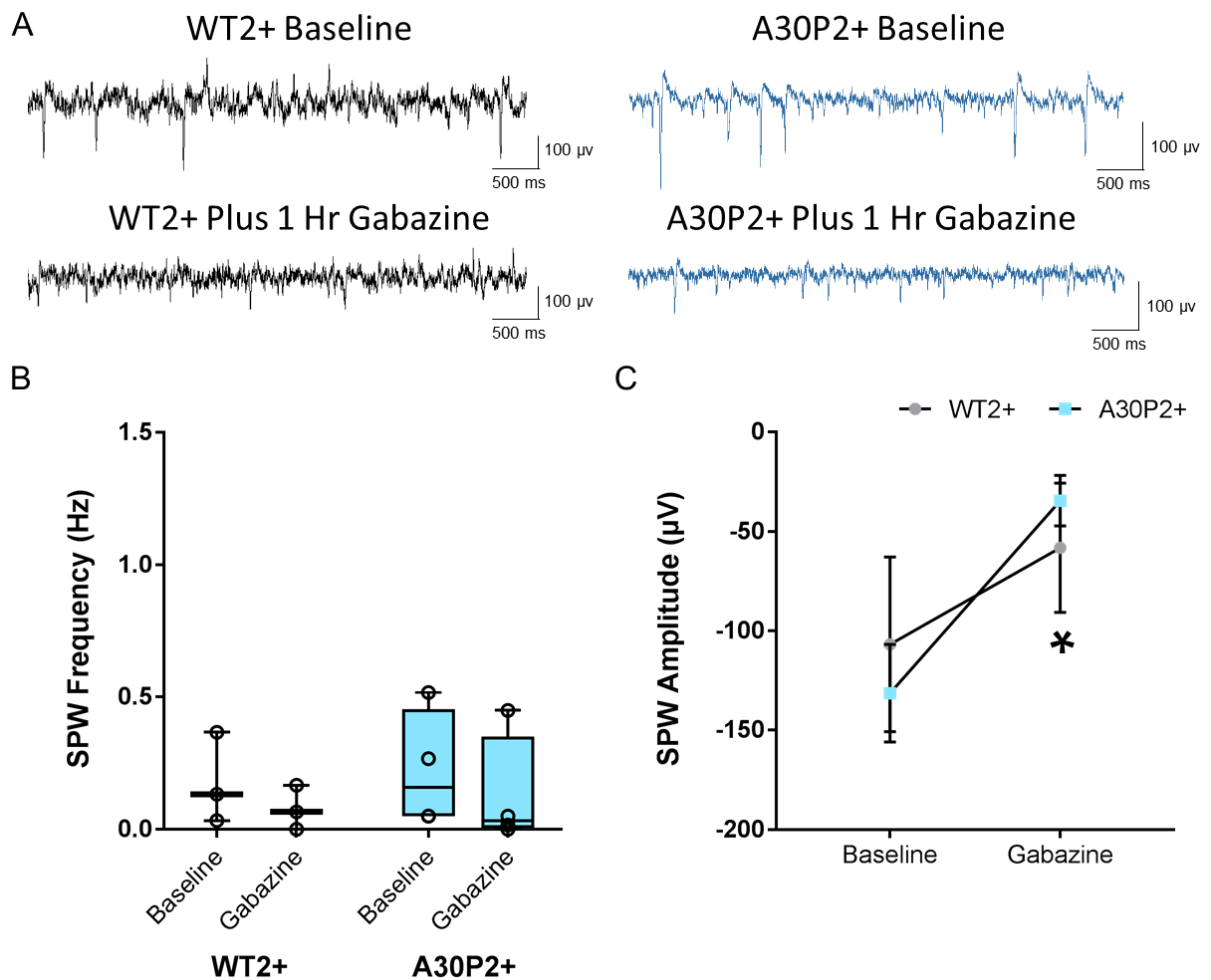


Figure 3.11 **GABA<sub>A</sub> receptor antagonism significantly decreases SPW amplitude.** (A) Representative traces before and after 1 hour of gabazine (100 nM) in slices from WT2+ (n = 3 slices from 2 mice) and A30P2+ mice (n = 4 slices from 2 mice). Boxplot to show SPW frequency (B) following gabazine application in WT2+ and A30P2+ mice. Line graph to show SPW amplitude (C) following gabazine application in WT2+ and A30P2+ mice. \* indicates significance at  $p < 0.05$ .

### 3.4.6.2 SPWs are not sensitive to NMDA receptor antagonism

SPW induction has previously been shown to be dependent on NMDA receptors (Behrens *et al.*, 2005). Once established, SPWs are not dependent on NMDA receptors (Behrens *et al.*, 2005; Wu *et al.*, 2006b) and NMDA receptor antagonists may even increase SPW amplitude in rat hippocampal slices (Colgin *et al.*, 2005). To investigate the role of NMDA receptors in SPW frequency and amplitude in slices from WT2+ and A30P2+ mice (Figure 3.12A), the NMDA receptor antagonist D-AP5 was applied at a concentration of 100  $\mu$ M (Morris, 1989; Davis *et al.*, 1992) for 1 hour.

Application of D-AP5 had no significant effect on SPW frequency in the CA3 *st. radiatum* (Figure 3.12B) in slices from WT2+ or A30P2+ mice (WT2+ *baseline* 0.18 Hz [IQR 0.07 – 0.58] to WT2+ *drug* 0.20 Hz, [IQR 0 – 1.28]; A30P2+ *baseline* 0.10 Hz [IQR 0.03 – 0.37] to A30P2+ *drug* 0.28 Hz, [IQR 0.03 – 0.53]; genotype  $p > 0.05$ , drug condition  $> 0.05$ , interaction  $p > 0.05$ ; RM 2-way ANOVA on ranks).

Despite a trend towards an increase in SPW amplitude (Figure 3.12C) following D-AP5 application, especially in slices from A30P2+ mice, no significant change in SPW amplitude was found in slices from WT2+ or A30P2+ mice likely due to variability between slices (WT2+ *baseline*  $-76.37 \mu\text{V} \pm 15.60$  to WT2+ *drug*  $-91.26 \mu\text{V} \pm 28.40$ ; A30P2+ *baseline*  $-101.85 \mu\text{V} \pm 20.81$  to A30P2+ *drug*  $-161.50 \mu\text{V} \pm 49.26$ ; genotype  $p > 0.05$ , drug condition  $> 0.05$ , interaction  $p > 0.05$ ; RM 2-way ANOVA). This confirms that SPWs are not sensitive to NMDA receptor antagonism in WT2+ or A30P2+ mice.

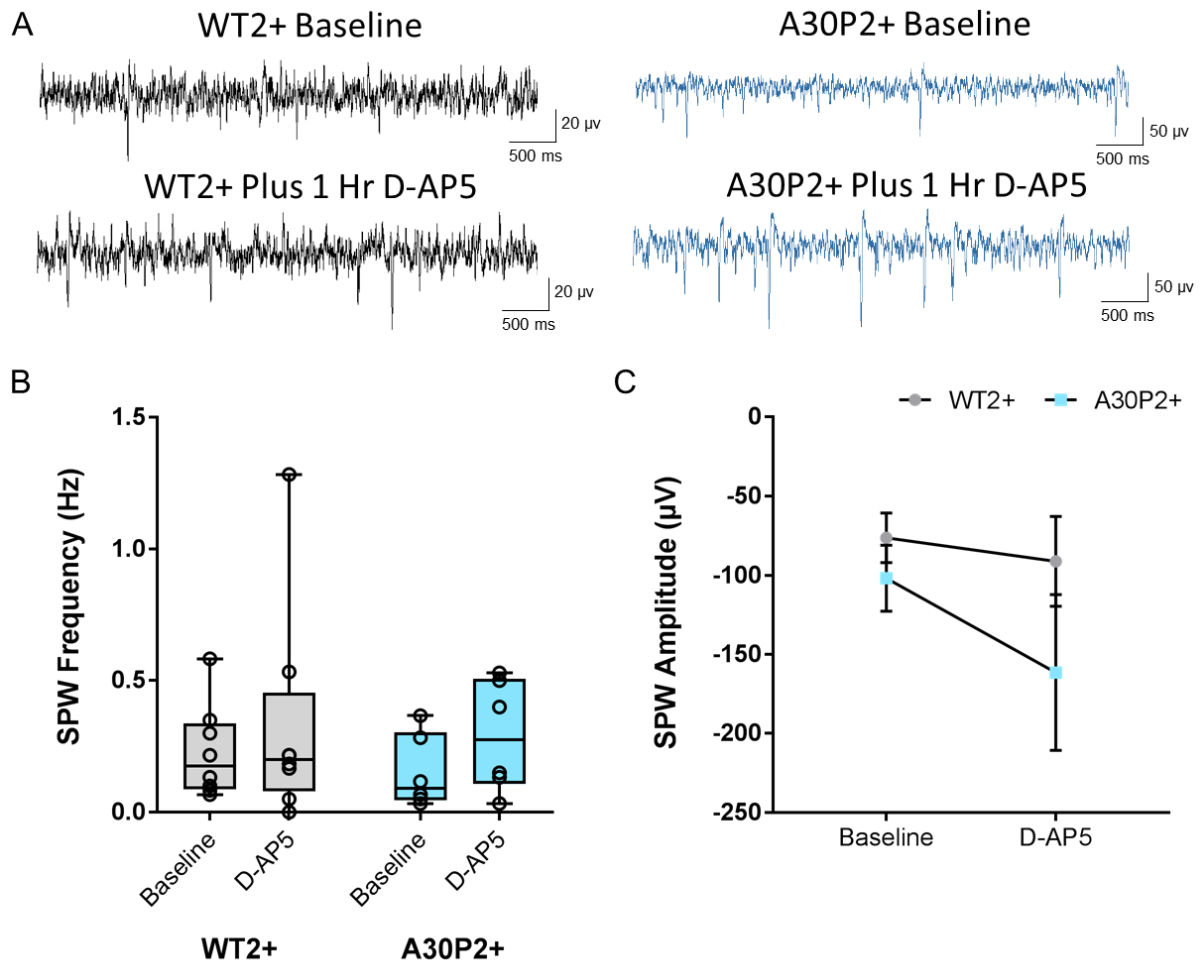


Figure 3.12 **No effect of NMDA receptor antagonism on SPWs.** (A) Representative traces before and after 1 hour of D-AP5 (100  $\mu\text{M}$ ) in slices from WT2+ ( $n = 8$  slices from 5 mice) and A30P2+ mice ( $n = 6$  slices from 6 mice). Boxplot to show SPW frequency (B) following D-AP5 application in WT2+ and A30P2+ mice. Line graph to show SPW amplitude (C) following D-AP5 application in WT2+ and A30P2+ mice.

### 3.4.6.3 Cholinergic receptor agonism

SPWs have previously been shown to be reduced and later abolished upon induction of fast network oscillations through cholinergic drive (Fischer *et al.*, 2014). The effect of the cholinergic agonist CCH (10  $\mu$ M) on CA3 *st. radiatum* SPW frequency and amplitude was therefore explored in slices from WT2+ and A30P2+ mice in the first 15 minutes of CCH bath application (Figure 3.13A).

SPW frequency decreased within the first 5 minutes of CCH exposure and SPWs were abolished by 15 minutes in slices from both WT2+ and A30P2+ mice (WT2+ *baseline* 0.07 Hz [IQR 0.02 – 0.25] to WT2+ *fifteen minutes* 0 Hz [IQR 0 – 0]; A30P2+ *baseline* 0.07 Hz [IQR 0.02 – 0.35] to A30P2+ *fifteen minutes* 0 Hz [IQR 0 – 0]; genotype  $p > 0.05$ , time  $p < 0.05$ , interaction  $p > 0.05$ , RM 2-way ANOVA on ranks; effect size = 1.57, power  $(1 - \beta) = 0.87$ ).

Equally, SPW amplitude decreased over 15 minutes until SPWs were abolished in slices from both WT2+ and A30P2+ mice (WT2+ *baseline* -78.42  $\mu$ V  $\pm$  17.01 to WT2+ *fifteen minutes* 0  $\mu$ V  $\pm$  0; A30P2+ *baseline* -89.80  $\mu$ V  $\pm$  27.45 to A30P2+ *fifteen minutes* 0  $\mu$ V  $\pm$  0; genotype  $p > 0.05$ , time  $p < 0.05$ , interaction  $p > 0.05$ , RM 2-way ANOVA; effect size = 2.26, power  $(1 - \beta) = 0.99$ ). By 15 minutes, no slices showed SPWs and instead gamma-frequency oscillations started to emerge as previously described (Traub *et al.*, 1992; Fisahn *et al.*, 1998). This suggests that the underlying circuitry required for the initial generation of CCH-induced gamma-frequency oscillations is intact in slices from A30P2+ mice.



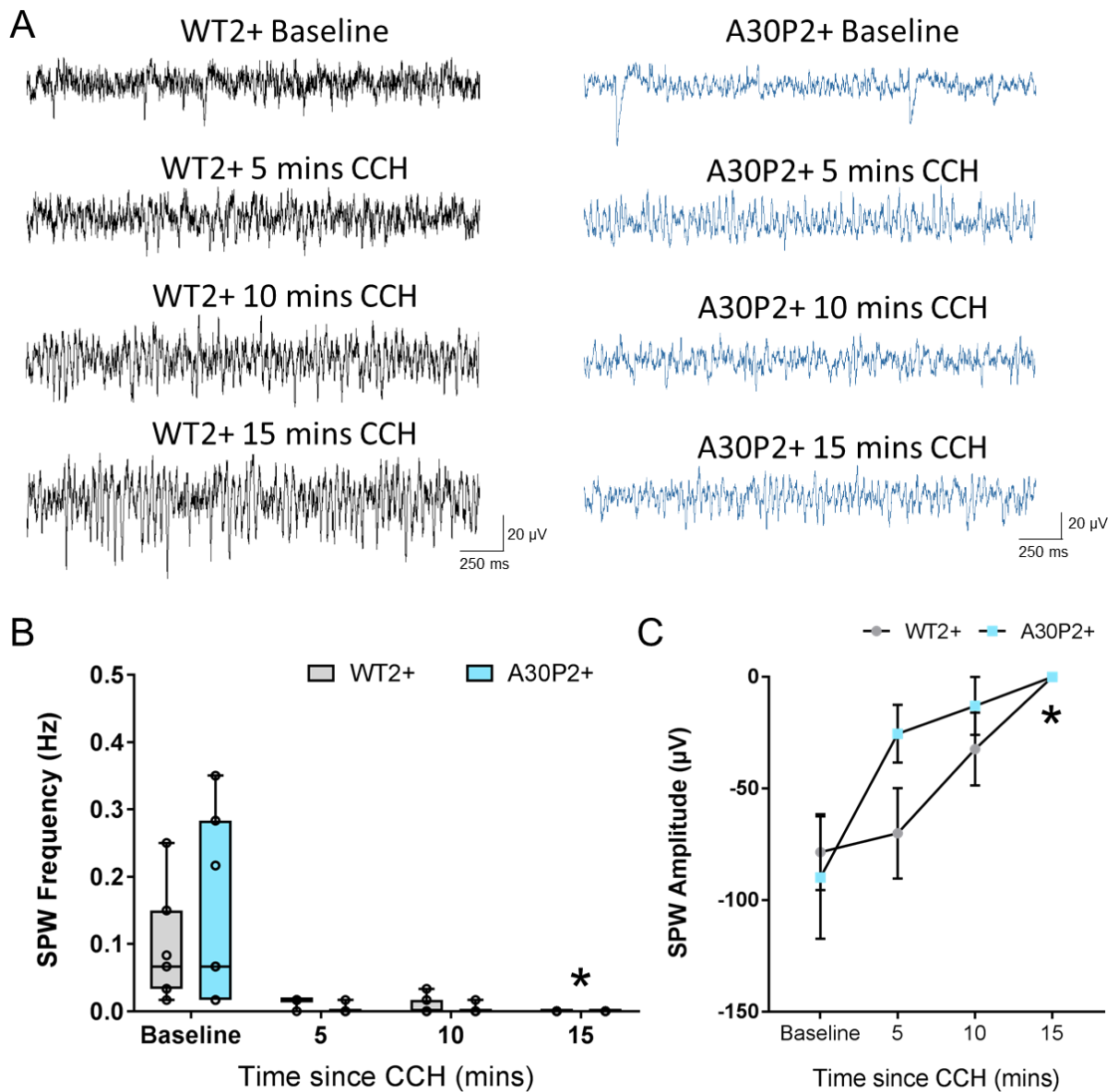


Figure 3.13 **Induction of fast network oscillations with CCH abolishes SPWs.** Representative traces of SPW activity over 15 minutes of CCH (A) in slices from WT2+ (n = 7 slices from 7 mice) and A30P2+ mice (n = 7 slices from 5 mice). Boxplot to show SPW frequency (B) over 15 minutes of CCH exposure in WT2+ and A30P2+ mice. Line graph to show SPW amplitude (C) over 15 minutes of CCH exposure in WT2+ and A30P2+ mice. \* indicates significance at  $p < 0.05$ .

### 3.4.7 Increase in PV+ interneurons in the CA3 region of A30P2+ mice

So far, this thesis has reported an increase in the frequency and amplitude of IPSPs arriving in CA3 pyramidal cells, and an increase in the amplitude of CA3 region GABA<sub>A</sub> receptor dependent SPWs in slices from A30P2+ mice. This chapter has also demonstrated the expression of human ASYN in PV+ interneurons within the CA3 and CA1 regions of the hippocampus. As the expression of PV in interneurons is plastic and can be modulated by activity (Donato *et al.*, 2013), I therefore decided to explore PV+ interneurons in the CA3 and CA1 regions in A30P mice (Figure 3.14A).

Interestingly, in region CA3 (Figure 3.14B) there was a significantly higher density of PV+ cells in slices from A30P2+ mice compared to WT2+ mice (33.5 cells/mm<sup>2</sup> ± 1.8 versus 26.8 cells/mm<sup>2</sup> ± 1.6 respectively,  $p < 0.05$ , unpaired  $t$  test; effect size = 1.59, power (1 -  $\beta$ ) = 0.82). Conversely, no difference was found between WT10+ and A30P10+ mice, indicating that PV+ cell density had decreased to similar levels as WT mice with ageing (28.2 cells/mm<sup>2</sup> ± 5.3 versus 24.4 cells/mm<sup>2</sup> ± 1.0 respectively,  $p > 0.05$ , unpaired  $t$  test).

No significant difference was found in PV+ cell density in region CA1 (Figure 3.14C) in slices from WT2+ and A30P2+ mice, despite a trend towards an increase (55.9 cells/mm<sup>2</sup> ± 15.0 versus 80.5 cells/mm<sup>2</sup> ± 8.5 respectively,  $p > 0.05$ , unpaired  $t$  test). Similarly, no difference was found between slices from WT10+ and A30P10+ mice in region CA1 (57.9 cells/mm<sup>2</sup> ± 14.3 versus 66.6 cells/mm<sup>2</sup> ± 4.3 respectively,  $p > 0.05$ , unpaired  $t$  test). This indicates that there is a higher density of PV+ interneurons in slices from A30P2+ mice in the CA3, but not the CA1, region.

Increased CA3 PV+ interneuron density in slices from A30P2+ mice was likely not dependent on dorsal/ventral hippocampal location (WT2+ *dorsal* 27.7 cells/mm<sup>2</sup> ± 4.9 [n = 3 slices]; WT2+ *ventral* 27.7 cells/mm<sup>2</sup> ± 1.5 [n = 7 slices]; A30P2+ *dorsal* 38.0 cells/mm<sup>2</sup> ± 2.8 [n = 4 slices]; A30P2+ *ventral* 31.6 cells/mm<sup>2</sup> ± 1.6, [n = 5 slices]; genotype  $p < 0.05$ , location  $p > 0.05$ , interaction  $p > 0.05$ , 2-way ANOVA; data not shown). Increased CA3 PV+ interneuron density in slices from A30P2+ mice was also likely not dependent on sex (WT2+ *male* 24.2 cells/mm<sup>2</sup> ± 2.4 [n = 3 slices]; WT2+ *female* 29.5 cells/mm<sup>2</sup> ± 2.4 [n = 3 slices]; A30P2+ *male* 33.4 cells/mm<sup>2</sup> ± 1.9 [n = 5 slices]; A30P2+ *female* 34.0 cells/mm<sup>2</sup> ± 4.1 [n = 2 slices]; genotype  $p < 0.05$ , sex  $p > 0.05$ , interaction  $p > 0.05$ ; 2-way ANOVA; data not shown).

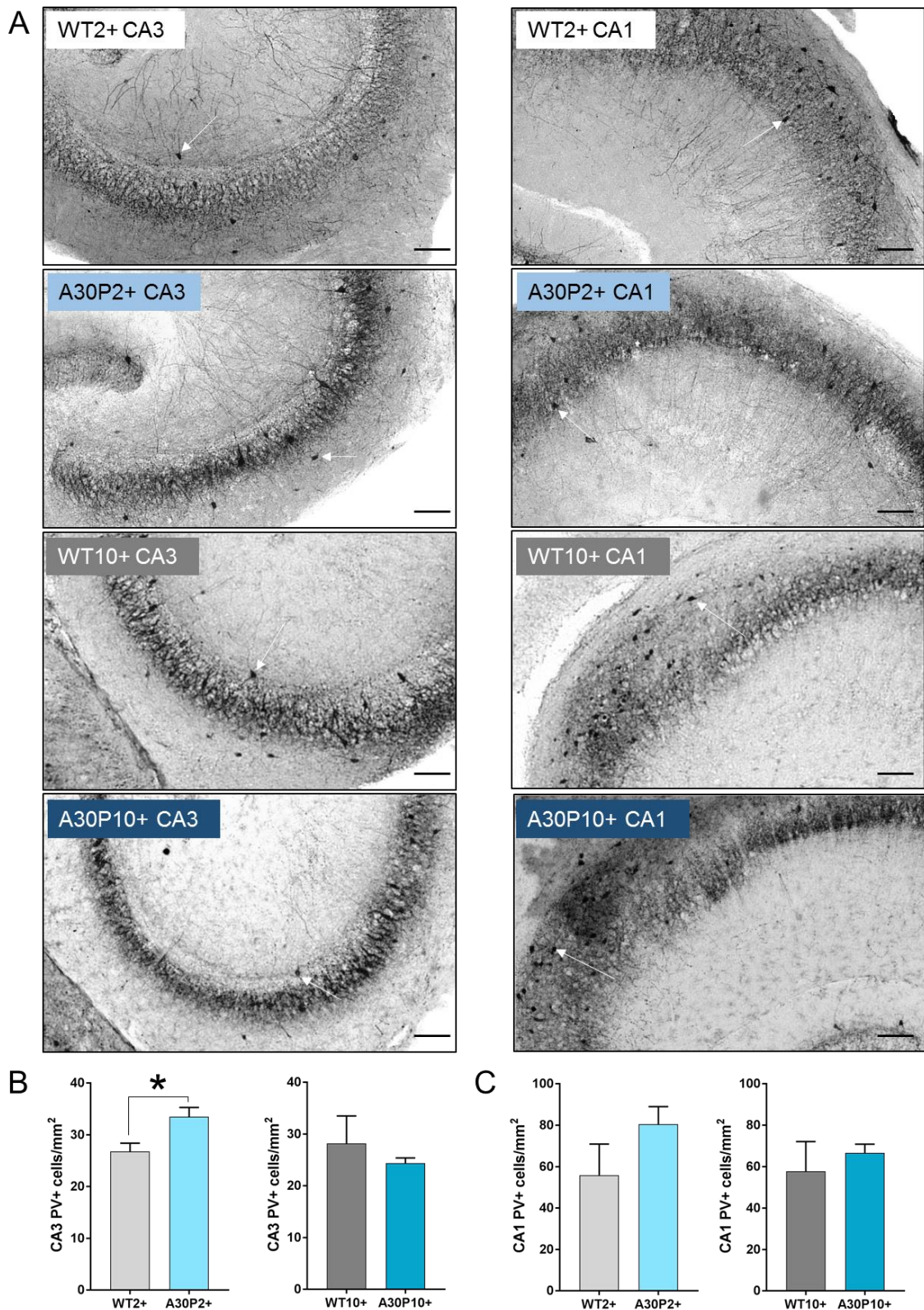


**Figure 3.14 Increase in PV+ cells in the A30P2+ mouse CA3 region.** Representative greyscale images at x4 magnification from WT and A30P mice in CA3/1 (A). White arrows indicate example PV+ cell. A plexus of PV+ axon terminals can be seen within *st. pyramidale*, with PV+ neurites extending through *st. radiatum*. Scale bar 100  $\mu$ m. Bar charts show PV+ cells/mm<sup>2</sup> in CA3 (B) and CA1 (C) in WT2+ (n = 10 slices from 6 mice), A30P2+ (n = 9 slices from 6 mice), WT10+ (n = 6 slices from 3 mice), and A30P10+ mice (n = 9 slices from 5 mice). \* represents significance at p < 0.05.

Another method to quantify immunohistochemistry previously used in the literature is a measure of optical density (OD) within a slice (Taylor and Levenson, 2006; van der Loos, 2008; Helps *et al.*, 2012; Bejnordi *et al.*, 2016). OD was measured by selecting a region incorporating both the cell bodies of PV+ interneurons within *st. pyramidale*, as well as PV+ neurites throughout *st. radiatum* and *st. lacunosum moleculare*. An area encompassing PV+ neurites was selected due to the observation that slices from young mice of both genotypes appeared to show more PV+ neurite immunoreactivity than ageing mice and it was expected that OD may reflect this.

Despite increased variance in the OD of slices from A30P2+ mice compared to WT2+ mice (Figure 3.15A), no significant difference was found in region CA3 or CA1 (WT2+ CA3 0.28 [IQR 0.18 – 0.38]; WT2+ CA1 0.28 [IQR 0.19 – 0.42]; A30P2+ CA3 0.17 [IQR 0.15 – 0.87]; A30P2+ CA1 0.17 [IQR 0.16 – 0.87]; mouse  $p > 0.05$ , region  $p > 0.05$ , interaction  $p > 0.05$ ; 2-way ANOVA on ranks). Similarly, no difference was found in slices from A30P10+ mice compared to WT10+ mice (Figure 3.15B) in regions CA3 or CA1 (WT10+ CA3 0.23 [IQR 0.19 – 0.36]; WT10+ CA1 0.25 [IQR 0.24 – 0.41]; A30P10+ CA3 0.22 [IQR 0.20 – 0.30]; A30P10+ CA1 0.23 [IQR 0.20 – 0.32]; mouse  $p > 0.05$ , region  $p > 0.05$ , interaction  $p > 0.05$ ; 2-way ANOVA on ranks).

The use of OD to quantify DAB peroxidase staining is controversial given that the amount of DAB product is not directly proportional to the amount of antigen present (van der Loos, 2008). As OD data were not normally distributed, and some slices were noted to stain notably darker than others within the same batch, I decided to measure density (cells/mm<sup>2</sup>) henceforth for DAB peroxidase staining within this thesis.

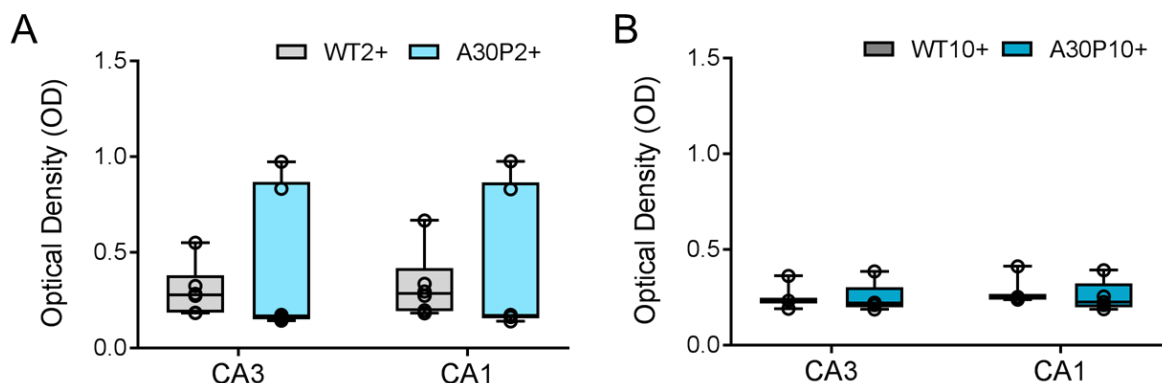


Figure 3.15 **No change in optical density of PV+ slices in A30P mice.** Boxplots to show optical density (OD) in regions CA3 and CA1 of (A) WT2+ (n = 10 slices from 6 mice) and A30P2+ mice (n = 9 slices from 6 mice), and in regions CA3 and CA1 of (B) WT10+ (n = 6 slices from 3 mice) and A30P10+ mice (n = 9 slices from 5 mice).

### 3.4.8 Increase in PNN+ cells in the CA3 region of A30P2+ mice

To further explore the increase in PV+ interneuron density in the A30P2+ mouse hippocampal CA3 region, the density of cells surrounded by a perineuronal net (PNN) was measured. As PNNs preferentially surround fast-spiking PV+ interneurons and afford them with protection against excitotoxicity (Morawski *et al.*, 2004; Cabungcal *et al.*, 2013a; Cabungcal *et al.*, 2013b), I expected to find an increase in CA3 region PNN+ cells to correlate with the increase in PV+ interneuron density.

Following immunohistochemistry for PNNs using lectin (Figure 3.16A), a mixture of CA3 region PNN+ cells with and without processes were observed as has been shown previously (Seeger *et al.*, 1994). Consistent with the increase in PV+ cells in the CA3 region, slices from A30P2+ mice showed an increase in CA3 region PNN+ cell density (Figure 3.16B) compared to WT2+ mice (53.4 cells/mm<sup>2</sup> ± 3.9 versus 41.6 cells/mm<sup>2</sup> ± 2.7 respectively;  $p < 0.05$ ; unpaired *t* test; effect size = 1.71, power (1 -  $\beta$ ) = 0.74). Post-hoc power analysis revealed that this experiment was slightly underpowered. This study could therefore benefit in future from an increased sample size as the change in PNN+ cell density was marginal. Conversely, the density of PNN+ cells in slices from A30P10+ mice was similar to slices from WT10+ mice (37.8 cells/mm<sup>2</sup> ± 4.5 versus 41.3 cells/mm<sup>2</sup> ± 3.3 respectively;  $p > 0.05$ , unpaired *t* test).

The increased density of CA3 region PNN+ cells in slices from A30P2+ mice was not dependent on dorsal/ventral hippocampal location (WT2+ *dorsal* 38.7 cells/mm<sup>2</sup> ± 6.0 [n = 3 slices]; WT2+ *ventral* 42.8 cells/mm<sup>2</sup> ± 4.0 [n = 7 slices]; A30P2+ *dorsal* 50.8 cells/mm<sup>2</sup> ± 4.3 [n = 6 slices]; A30P2+ *ventral* 54.2 cells/mm<sup>2</sup> ± 5.2 [n = 4 slices]; genotype  $p < 0.05$ , region  $p > 0.05$ , interaction  $p > 0.05$ ; 2-way ANOVA, data not shown). Furthermore, the increase in CA3 region PNN+ cell density in slices from A30P2+ mice was likely not dependent on sex (WT2+ *male* 42.3 cells/mm<sup>2</sup> ± 4.5 [n = 3 slices]; WT2+ *female* 40.4 cells/mm<sup>2</sup> ± 2.5 [n = 2 slices]; A30P2+ *male* 55.6 cells/mm<sup>2</sup> ± 4.6 [n = 3 slices]; A30P2+ *female* 47.6 cells/mm<sup>2</sup> ± 0.4 [n = 2 slices]; genotype  $p < 0.05$ , region  $p > 0.05$ , interaction  $p > 0.05$ ; 2-way ANOVA, data not shown).



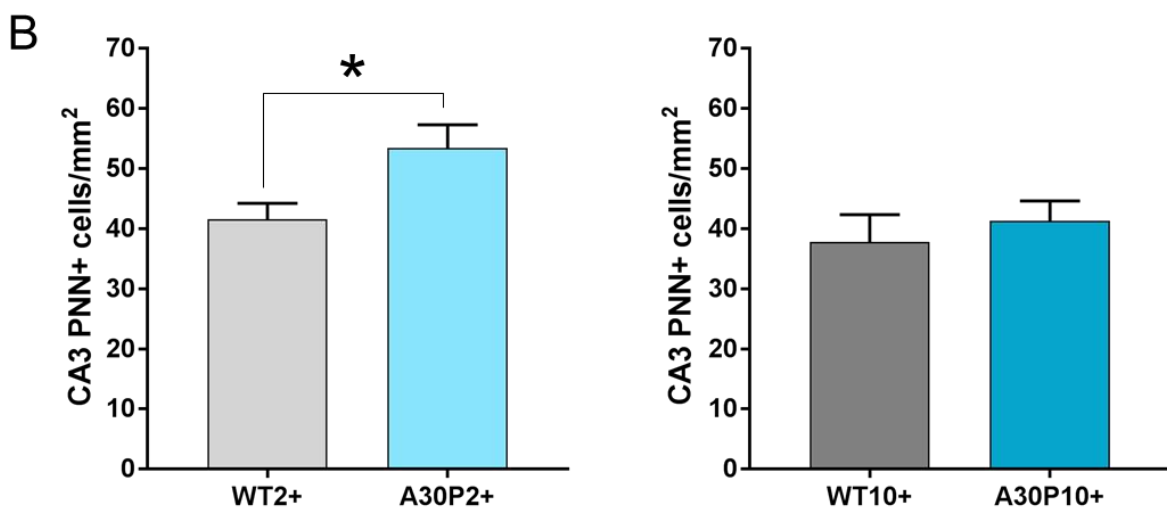
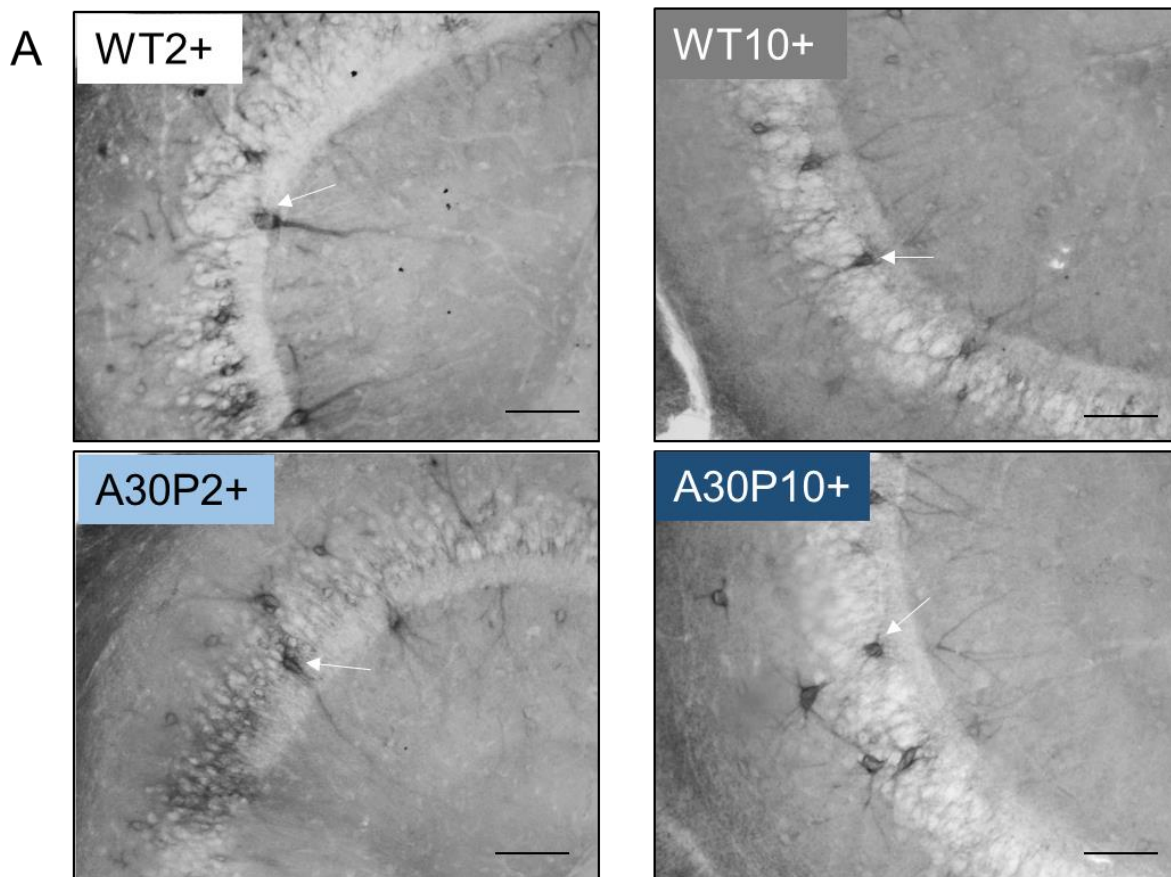


Figure 3.16 **Increased PNN+ cells in the A30P2+ mouse CA3 region.** (A) Representative greyscale images at x10 magnification of PNN expression in the CA3 region of the hippocampus in WT and A30P mice. (B) Bar charts showing PNN+ cells/mm<sup>2</sup> in the CA3 region of WT and A30P mice. WT2+ n = 10 slices from 5 mice, A30P2+ n = 10 slices from 4 mice, WT10+ n = 6 slices from 3 mice, A30P10+ n = 11 slices from 4 mice. \* indicates significance at p < 0.05.

### 3.4.9 Decrease in CB+ interneurons in the CA3 region of A30P2+ mice

Whilst the majority of PNN+ cells within the hippocampus have previously been reported to be fast-spiking PV+ interneurons, a small proportion of CB+ cells with a PNN have been reported within the mouse medial entorhinal cortex (Lensjo *et al.*, 2017) and dentate gyrus (Yamada *et al.*, 2015). A reduction of CB+ cells has been observed throughout the hippocampus in a rodent model of epilepsy (Carter *et al.*, 2008), and within the dentate gyrus of post-mortem DLB tissue and *Thy-1* WT ASYN mice (Morris *et al.*, 2015). As this chapter focuses on interneuron changes in A30P mice, I decided to explore changes in CB+ interneurons in region CA3 of A30P mice.

The density of CB+ interneurons was measured within the A30P mouse CA3 region (Figure 3.17A). This chapter has established that CB+ interneurons of region CA3 did not express human ASYN at detectable levels in A30P mice. It was surprising therefore that the density of CB+ interneurons in region CA3 (Figure 3.17B) was decreased in slices from A30P2+ mice compared to WT2+ mice (56.9 cells/mm<sup>2</sup> ± 9.1 versus 92.5 cells/mm<sup>2</sup> ± 7.1 respectively;  $p < 0.05$ , unpaired *t* test; effect size = 2.52, power (1 -  $\beta$ ) = 0.81). Despite a low sample size, this experiment was found to have an adequate observed power of 81% likely due to the magnitude of the effect size.

CB+ interneurons are not as vulnerable to stress as fast-spiking interneurons (Kann, 2016), and as no loss of PV+ cells was found in A30P10+ mice, I expected to find no change in CA3 CB+ cell density in A30P10+ mice. Indeed, CB+ cell density in slices from A30P10+ mice was similar to WT10+ mice (77.6 cells/mm<sup>2</sup> ± 3.4 versus 66.5 cells/mm<sup>2</sup> ± 10.6 respectively;  $p > 0.05$ ; unpaired *t* test). There appeared to be a decrease in CB+ cell density with physiological ageing in WT mice, a finding previously reported in the rodent hippocampus and correlated to age-related cognitive decline (Potier *et al.*, 1994; Soontornniyomkij *et al.*, 2012; Flores-Cuadrado *et al.*, 2016).

The decrease in CA3 CB+ interneuron density in slices from A30P2+ mice was not dependent on dorsal/ventral hippocampal location (WT2+ *dorsal* 80.1 cells/mm<sup>2</sup> ± 10.7 [n = 3 slices]; WT2+ *ventral* 99.9 cells/mm<sup>2</sup> ± 9.4 [n = 5 slices]; A30P2+ *dorsal* 49.3 cells/mm<sup>2</sup> ± 7.7 [n = 6 slices]; A30P2+ *ventral* 72.1 cells/mm<sup>2</sup> ± 14.1 [n = 3 slices]; genotype  $p < 0.05$ , region  $p > 0.05$ , interaction  $p > 0.05$ ; 2-way ANOVA, data not shown). Furthermore, the decrease in CA3 CB+ interneuron density in slices from A30P2+ mice was likely not dependent on sex (WT2+ *male* 92.6 cells/mm<sup>2</sup> ± 18.0 [n = 2 slices]; WT2+ *female* 92.5 cells/mm<sup>2</sup> ± 9.2 [n = 6 slices]; A30P2+ *male* 56.3 cells/mm<sup>2</sup>

$\pm 10.1$  [n = 6 slices]; A30P2+ *female* 58.0 cells/mm<sup>2</sup>  $\pm 12.7$  [n = 3 slices]; genotype p < 0.05, sex p > 0.05, interaction p > 0.05; 2-way ANOVA, data not shown).

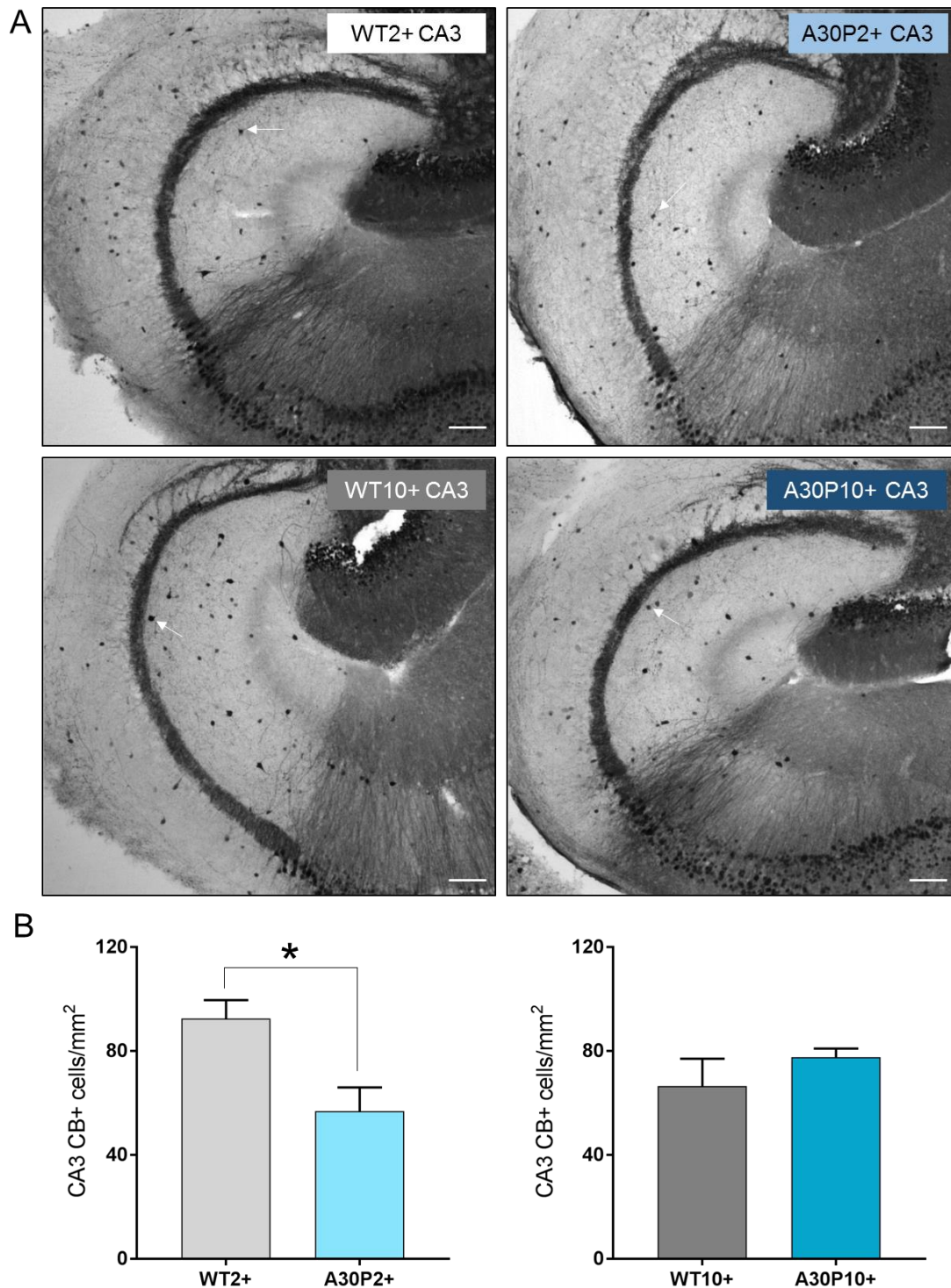


**Figure 3.17 Decreased CB+ cells in the A30P2+ mouse CA3 region.** (A) Representative greyscale images at x4 magnification from WT and A30P mice; CB+ interneurons of region CA3 and CB+ pyramidal cells of region CA1 can be seen. White arrows indicate example CA3 region CB+ interneuron. Scale bar 100  $\mu$ m. (B) Bar charts to show CB+ cells/mm<sup>2</sup> in the CA3 region in WT and A30P mice. WT2+ n = 8 slices from 3 mice, A30P2+ n = 9 slices from 3 mice, WT10+ n = 8 slices from 3 mice, A30P10+ n = 5 slices from 2 mice. \* represents significance at p < 0.05.



### 3.5 Discussion

A summary of the key findings from Chapter 3 is presented below:

- Expression of human ASYN in pyramidal cells and PV+ interneurons in A30P mice, but not in CB+ interneurons of the CA3 region. Overall density of human ASYN+ cells in A30P mice unchanged from 2-4 months to 10-13 months in both CA3 and CA1 regions.
- No change in CA3 *st. radiatum* spontaneous network oscillations in slices from A30P mice with respect to the proportion of slices showing spontaneous activity, area power, peak frequency, or rhythmicity.
- Increased amplitude of CA3 *st. radiatum* spontaneous SPWs in slices from A30P2+ mice but no change in SPW frequency or prevalence.
- Increased amplitude and frequency of spontaneous IPSPs in A30P2+ mouse CA3 region pyramidal cells under drug-free conditions.
- Increased density of CA3 region PV+ interneurons and PNN+ cells, and decreased density of CB+ interneurons in slices from A30P2+ mice.

#### 3.5.1 Differential vulnerability of CA3 region interneurons in A30P mice

Earlier reports have shown that human ASYN is expressed within the hippocampus of *Thy-1* A30P mice, though the cell types where expression occurs have not previously been explored (Rockenstein *et al.*, 2002). This thesis set out to explore the presence of human ASYN within the A30P mouse hippocampus and confirmed previous findings that human ASYN is expressed within CA3/1 pyramidal cells (Szego *et al.*, 2013). For the first time, however, this thesis has demonstrated evidence of the differential presence of human ASYN in PV+ and CB+ interneurons in A30P mice.

Previous optogenetic studies within the amygdala have found the *Thy-1* promoter to lead to expression of channelrhodopsins in glutamatergic neurons, but not PV+ or CB+ interneurons (Jasnow *et al.*, 2013). Expression of human ASYN under the *Thy-1* promoter in mice is entirely artificial rather than physiological. Murine ASYN has been shown to be present in glutamatergic, GABAergic, cholinergic, and catecholaminergic neurons (Vivacqua *et al.*, 2011) and so a more effective model to consider for future use may be to remove and replace expression of murine ASYN with human ASYN expression. It is important to note, however, that the same promoter may express in different cells and regions of the brain due to random insertion of the transcript (Feng *et al.*, 2000). This could result in different lines of the *Thy-1* A30P

mouse expressing human ASYN in different cell types, and ensuring that the same line of A30P mice is used in future experiments based on this thesis is therefore crucial.

Despite this, it is possible that human ASYN expression begins in glutamatergic pyramidal cells in the line of *Thy-1* A30P mice described in this thesis, and spreads through extracellular ASYN release (Diogenes *et al.*, 2012; Pacheco *et al.*, 2015; Yamada and Iwatsubo, 2018). The presence of human ASYN in PV+ interneurons but not CB+ interneurons could be a result of the fast-spiking property of PV+ interneurons increasing uptake of extracellular human ASYN, or a failure of PV+ interneurons to degrade internalised human ASYN. To fully confirm the time-course of *Thy-1* expression however, it would be important to examine mice in the immediate postnatal period or generate a line that also express green fluorescent protein under the *Thy-1* promoter to identify which cells initially express human ASYN.

Confirming the presence of human ASYN within neuronal subtypes based on immunohistochemistry alone is limited by the fact that human ASYN may be expressed in some cells below detectable levels. This may be improved by quantitative analysis of colocalisation using pixel intensity measures, as opposed to the qualitative analysis of colocalisation used in this thesis. Regardless, evidence of changes in human ASYN expression with ageing were demonstrated in this chapter by the changing pattern of ASYN expression in deep and superficial pyramidal cells. This somewhat anecdotal observation warrants further investigation, though such investigation would require the literature to advance considerably in reporting the physiological differences between deep and superficial pyramidal cells (Slomianka *et al.*, 2011).

This chapter has demonstrated that the presence of human ASYN within a certain neuronal population does not necessarily exclude changes from occurring in populations of neurons free from human ASYN. The surprising finding that young A30P mice exhibited a reduction in CA3 CB+ interneuron density despite the lack of human ASYN expression demonstrates this fact. It can be inferred that a reduction in cell density correlates with a decreased number of cells, though other possible explanations for this change exist including an increase in the size of cell bodies or a decrease in hippocampal size. However, it is proposed that changes in cell density throughout this chapter largely represent changes in cell number, rather than changes in hippocampal morphology, due to the altered density of PV+ interneurons, PNN+ cells and CB+ interneurons returning to levels comparable to WT mice with ageing.

Interpretation of cell density results presented in this chapter must be made with a degree of caution due to differences in cell density along the dorsal ventral hippocampal axis in mice (for review see Fanselow and Dong, 2010). Despite a similar number of sampled slices being taken from the dorsal and ventral hippocampus, the results do not necessarily represent changes throughout the entire hippocampal structure and may introduce bias in the form of pseudoreplication. Instead, stereology following serial sectioning of the entire hippocampal structure should be used in future to confirm the results obtained in this thesis (Golub *et al.*, 2015). In addition, examination of the enzymes involved in the synthesis of GABA (GAD65/67) would help to reveal whether changes in PV and CB cell density are related to changes in cell number, or changes in expression of the calcium binding proteins.

A transient decrease in CB expression within the dentate gyrus followed by normalisation has previously been reported in rats exposed to electroconvulsive shocks (Tonder *et al.*, 1994), and a decrease in CB expression in the dentate gyrus was recently reported as an epigenetic response to increased neuronal activity (You *et al.*, 2017). Despite both studies examining CB+ excitatory dentate gyrus granule cells, they demonstrate that CB is capable of adaptation and plasticity, particularly in response to neuronal activity. As this thesis has so far demonstrated increased GABAergic activity in young A30P mice, the decrease in CA3 region CB+ interneuron density in young A30P mice may be a compensatory response to increased GABAergic neuronal activity rather than a response to ASYN-induced cell death.

Previous studies have found a decrease in hippocampal CB+ interneurons with physiological ageing in rodents, but no change in PV+ interneurons (Potier *et al.*, 1994; Soontornniyomkij *et al.*, 2012; Flores-Cuadrado *et al.*, 2016). While a number of studies did not find physiological changes in CB+ interneurons until 24 – 26 months of age in rodents (Potier *et al.*, 1994; Soontornniyomkij *et al.*, 2012), one group monitored the change in CB+ interneurons at an earlier age and found a significant decrease by 11 months of age (Flores-Cuadrado *et al.*, 2016). This chapter therefore compliments existing literature in this respect though the literature does not explain the slight increase in CB+ interneuron density observed with ageing in A30P mice.

The decrease in CB+ interneurons with physiological ageing is associated with a decline in recognition memory (Soontornniyomkij *et al.*, 2012). Interestingly, the physiological decrease in CB+ interneurons does not occur in humans (Stefanits *et al.*, 2014), and as a result should be studied with some caution in mice. The fact that CA3

region CB+ interneuron density is significantly lower in slices from A30P2+ mice compared to slices from WT2+ mice may suggest an accelerated “ageing” process in A30P2+ mice where CB+ cell density is already reduced to the level of a 10-13 month old WT mouse. This is consistent with the lower density of CB+ cells found in a mouse over-expressing human A53T ASYN under the pan-neuronal prion protein promoter (Flores-Cuadrado *et al.*, 2016), though the authors did find expression of human ASYN in some CB+ interneurons within this mouse model unlike in our A30P mice.

It is interesting to note that both hippocampal PV+ and CB+ interneurons are reported to be mostly free from ASYN aggregates in DLB cases (Bernstein *et al.*, 2011; Rcom-H'cheo-Gauthier *et al.*, 2016) though both have also been found to be decreased in patients with DLB (Bernstein *et al.*, 2011; Morris *et al.*, 2015). It could therefore be proposed that the cells lost in DLB cases were those with ASYN aggregates, leaving only a surviving population of PV+ and CB+ cells with low ASYN expression or a lack of ASYN aggregates. ASYN was found to colocalise mainly within PV+ cells in the hippocampi of PD patients over other interneuron types (Flores-Cuadrado *et al.*, 2016), so evidence in this thesis of human ASYN colocalisation with PV+ interneurons compliments findings in patients with alpha-synucleinopathy.

Levels of total human ASYN+ cells in regions CA3 and CA1 were found to be unchanged between 2-4 months and 10-13 months of age in A30P mice. This compliments a previous finding in A30P mice in the brainstem and spinal cord (Ekmark-Lewen *et al.*, 2018), as well as the fact that *Thy-1* promoter expression remains stable from 3-4 weeks of age (Kollias *et al.*, 1987). The tendency for human ASYN expression to occur more in deep pyramidal cells than superficial pyramidal cells in A30P2+ mice was noted as an anecdotal finding to be explored in future work. This is particularly interesting given that deep pyramidal cells in region CA1 have lower CB expression compared to superficial pyramidal cells (Baimbridge and Miller, 1982). Young *Thy-1* A30P mice did, however, appear to show at least some co-localisation of human ASYN with CB+ pyramidal cells in region CA1.

The selective increase in CA3 PV+ interneuron density in young A30P mice may be explained, in part, by the presence of human ASYN within PV+ cells. As PV+ interneurons are fast-spiking, their high energy demands make them more vulnerable to the effects of excitotoxicity (Kann, 2016). However, the presence of the PNN preferentially surrounding fast-spiking PV+ interneurons provides some protection against excitotoxic cell death (Cabungcal *et al.*, 2013a). Whilst methods used in this

thesis did not differentiate between PV+ interneurons that were or were not fast-spiking, the associated increase in PNNs may infer that the increase in PV+ cell density specifically impacts fast-spiking interneurons. Future work should utilise Kv3.1 channel markers and patch clamping of interneurons to explore this further.

The proposal that fast-spiking PV+ interneurons are particularly vulnerable to changes in alpha-synucleinopathy is not entirely supported by the finding in this thesis that only CA3 PV+ interneuron density increased in A30P2+ mice, and not CA1 PV+ interneuron density. Whilst there was a trend towards a higher density of PV+ interneurons in this region in A30P2+ mice, this discrepancy can be reconciled by the fact that the CA3/2 region of the hippocampus is noted to be particularly vulnerable to the formation of Lewy bodies in human alpha-synucleinopathy (Churchyard and Lees, 1997), and so the rate at which pathology occurs in this region may be accelerated.

This chapter further found that slices from young A30P mice showed evidence of increased GABAergic interneuron activity in region CA3, but not region CA1, in the form of increased amplitude spontaneous SPWs and increased IPSP parameters. The observed increase in the density of PV+ interneurons within region CA3 in slices from A30P2+ mice correlated with the time-course of increased GABAergic activity. It can therefore be inferred that PV expression may either be causing the increase in GABAergic activity, or that excess GABAergic activity may be causing the increase in PV+ and PNN+ cell density. It has been reported that PV expression is upregulated in the substantia nigra of patients with PD post-mortem, compared to healthy controls and patients with AD (Soos *et al.*, 2004). While the authors did not examine CB+ or CR+ interneurons, a more recent study found a selective increase in the density of CA3 region PV+ interneurons, but not CB+ or CR+ interneurons, in post-mortem tissue from cases with autism (Lawrence *et al.*, 2010). The authors proposed that this may directly impact on information processing pathways within the hippocampus, as well as altering GABA receptor distribution (Lawrence *et al.*, 2010).

Beyond changes in GABAergic activity affecting SPWs and IPSP parameters, the consequences of increased PV+ interneuron activity may manifest as synaptic impairment with respect to LTP, for increased inhibition has been shown to impair LTP (Kleschevnikov *et al.*, 2004). In addition, a decrease in CB has also been shown to lead to LTP impairment (Molinari *et al.*, 1996) and this would be worth investigating in young and aged A30P mice especially given that human ASYN oligomers applied to hippocampal slices has been shown to oppose LTP (Diogenes *et al.*, 2012).

Both PV+ interneuron density and the increase in GABAergic interneuron activity “normalised” with ageing in A30P mice. This is not to assume that values obtained in 10-13 month old mice are “normal”, but that A30P10+ mouse values were now comparable to WT10+ mouse values. Notably, the increase in PV+ interneurons in A30P2+ mice appears to decrease with ageing to become comparable to WT10+ mice. As PV+ interneuron density did not decrease below WT levels, this likely does not explain the age-dependent impairment in CCH gamma-frequency oscillations in A30P mouse slices reported by our group (Robson *et al.*, 2018). However, this does not necessarily mean that PV+ interneurons are entirely functional.

Finally, it should be noted that the recognition of calcium binding proteins such as PV and CB by antibodies is dependent on the Ca<sup>2+</sup> binding status of the protein at the time of fixation (Winsky and Kuznicki, 1996; Zimmermann and Dours-Zimmermann, 2008). Whilst care was taken to ensure that all slices examined for immunohistochemistry experienced a similar length of time in the recording chamber and were exposed to the same drugs, the change in PV+ and CB+ interneuron density observed in this thesis should be confirmed using tissue prepared by PFA perfusion of mice without electrophysiology, or by analysis of mRNA expression levels.

### **3.5.2 Spontaneous network oscillations are intact in A30P mice**

Spontaneous gamma-frequency activity in acute hippocampal brain slice preparations possesses different pharmacological mechanisms to both KA and CCH-induced gamma-frequency rhythms, though all are dependent on the excitatory/inhibitory network and GABA<sub>A</sub> receptors (Fisahn *et al.*, 1998; Traub *et al.*, 2000; Pietersen *et al.*, 2009). It has been proposed that spontaneous activity is a more physiologically relevant representation of the excitatory/inhibitory network within an acute hippocampal brain slice than KA or CCH-induced oscillations (Skrobot, 2008; Pietersen *et al.*, 2009; Modebadze, 2014) and thus it was explored in the A30P model.

It has been shown in this thesis that spontaneous gamma-frequency oscillations did not differ between WT and A30P mice at any age tested. This would appear to suggest that the excitatory/inhibitory network in A30P mice is capable of generating spontaneous network activity, and the changes in PV+ and CB+ interneurons, or the increased frequency and amplitude of IPSPs arriving in pyramidal cells, do not result in changes to spontaneous oscillations. The increased density and activity of interneurons does not always equate to more efficient inhibition within a network,

however, given that the precise timing of spikes and synchrony between neurons is also required to generate fast network oscillations.

Fast-spiking PV+ interneurons play a critical role in the synchrony of fast network oscillations (Klausberger *et al.*, 2005), whilst the role of CB+ interneurons is less clear. It could be inferred that the increase in CA3 region PV+ interneuron density led to the increase in IPSP frequency and amplitude recorded from CA3 pyramidal cells. As each model of gamma-frequency oscillations discussed in this thesis is dependent on different receptors, it follows that different subpopulations of interneurons may be employed in each type of activity. Therefore, despite PV+ interneurons being important for spontaneous, CCH-induced and KA-induced gamma-frequency oscillations, further differentiation of PV+ interneurons by cell type (basket cell versus chandelier cell), expression of other markers such as neuropeptides, receptor subunit compositions, and electrophysiological properties could help to explore the consequence of increased PV+ interneuron density in young A30P mice.

The possibility that the increase in IPSP parameters is a result of intrinsic PV+ interneuron excitability, as opposed to an enhanced postsynaptic response to GABA in pyramidal cells or an increase in pyramidal cell drive of interneurons (Palop *et al.*, 2007), can only be explored fully through patch clamping of interneurons. Future work should also measure the density of cells expressing the calcium binding protein calretinin. Though there is less evidence of changes in CR+ cells in alpha-synucleinopathy, this thesis has proposed a spread of human ASYN throughout the hippocampal network and therefore all neuronal cell types should be explored.

### **3.5.3 Altered spontaneous hippocampal SPWs in young A30P mice**

The mouse hippocampus has long been studied for its ability to generate spontaneous SPW activity (Wu *et al.*, 2002). SPW incidence and frequency were found to be lower in this thesis compared to most studies on SPWs in the literature, and this is theorised to either be a result of the sucrose perfusion performed in this thesis or the fact that thicker slices are often employed in the literature to increase the appearance of SPWs through greater preservation of the network (Wu *et al.*, 2005b). Furthermore, SPWs were observed in both dorsal and ventral slices in this thesis, whereas in the literature they have largely been reported in the ventral hippocampus (Papatheodoropoulos and Kostopoulos, 2002a). It is possible that the equal distribution of SPWs in dorsal and ventral slices in this thesis is a result of sucrose perfusion maintaining sufficient inhibition throughout the hippocampus. It has previously been

established that it is difficult to evoke LTP in slices from sucrose-perfused animals due to the preservation of GABAergic inhibition (Kuenzi *et al.*, 2000) and that, interestingly, LTP is weak or absent in slices with SPWs (Colgin *et al.*, 2004). The increase in SPW amplitude in slices from A30P2+ mice may therefore have a detrimental effect on LTP.

The majority of the work in this thesis was carried out within the *st. radiatum* layer of the CA3 region and exploration into the fast ripple component of SPW ripples requires future recordings within *st. pyramidale* (Schonberger *et al.*, 2014). The increase in SPW amplitude in the *st. radiatum* of slices from A30P2+ mice is interesting given that in a rodent model of temporal lobe epilepsy, spontaneous GABAergic inhibition of pyramidal cells was increased in *st. pyramidale*, but not *st. radiatum* (Cossart *et al.*, 2001). This suggests that increased somatic inhibition of pyramidal cells is a compensatory response to prevent epileptiform activity from occurring. This is of particular interest to future work in classifying subtypes of PV+ interneurons in A30P2+ mice to deduce where the increase in PV+ interneuron activity is occurring specifically and what consequences this may have for excitability.

The increase in SPW amplitude observed in A30P2+ mice normalised with age in a similar way to the increase in PV+ interneuron density. An increase in the amplitude but not the frequency of SPWs is proposed to represent either increased GABA release from interneurons, increased synchrony between interneurons, or an increased sensitivity of GABA receptors on pyramidal cells. However, increased PV+ interneuron density in A30P2+ mice suggests that the mechanism likely involves changes in either GABA release or synchrony. Despite an increase in both IPSP amplitude and frequency in CA3 pyramidal cells, SPWs are population events that require the synchronous action of a number of cells to occur. This explains the inconsistency between increased IPSP frequency and no change in extracellular SPW frequency, and may provide further support to changes in the synchrony between interneurons being an underlying mechanism of dysfunction in A30P mice.

Spontaneous SPWs first appear from around postnatal day 10, stabilise after day 15, and persist into adulthood (Wong *et al.*, 2005). This initial period coincides with the sharp increase in expression of human ASYN from week 1 to weeks 3-4 under the *Thy-1* promoter in A30P mice. Human ASYN expression during postnatal development is therefore important to explore in future work. Furthermore, this time period also coincides with the development of the inhibitory network, particularly of PV+ interneurons (Schlosser *et al.*, 1999). Conversely, CB+ interneuron density is highest



during embryogenesis and then decreases postnatally (Davila *et al.*, 2005), also lending support to the decrease observed in CB+ interneurons in A30P2+ mice being an acceleration of the physiological decrease observed in WT mice with ageing.

Due to their role in memory consolidation, SPWs have been explored in recent years in the context of diseases such as dementia (Ego-Stengel and Wilson, 2010). SPWs are impaired in both physiologically aged rats (Gerrard *et al.*, 2008), and through reduced inhibitory control in a mouse model of tauopathy (Witton *et al.*, 2016). It has previously been shown in the literature that SPWs are GABA<sub>A</sub> receptor dependent, NMDA-receptor independent (Wu *et al.*, 2006a) and do not exist at the same time as network oscillations, which reflect a state of high IPSP synchrony (Fischer *et al.*, 2014; Vandecasteele *et al.*, 2014). This chapter confirmed this to be the case also in A30P2+ mice, indicating that the physiological mechanisms of SPWs are intact in A30P mice and the alteration comes only in the form of increased amplitude.

Whilst the GABA<sub>A</sub> receptor antagonist gabazine had no significant effect on SPW frequency, the reduction in SPW amplitude is consistent with previous reports in which a higher concentration of gabazine was used to eliminate stimulus-induced SPWs prior to transformation into interictal discharges (Behrens *et al.*, 2007). SPWs have been shown to be NMDA-receptor independent events once established (Colgin *et al.*, 2005; Wu *et al.*, 2006a), and this was confirmed in both WT and A30P mice. However, the increase in SPW amplitude due to NMDA receptor antagonism reported by Colgin *et al.* (2005) in rat hippocampal slices was not observed in this thesis. This may be the result of a higher density of neurons within the mouse brain (DeFelipe *et al.*, 2002) altering vulnerability of SPWs to NMDA-receptor antagonism.

While this chapter demonstrated evidence of an increase in SPW amplitude in slices from young A30P mice, no change was found in SPWs in slices from A30P10+ mice compared to WT10+ mice. This is interesting given that SPWs play a role in memory consolidation (Buzsaki, 1998; Siapas and Wilson, 1998) and yet previous evidence indicates an age-dependent hippocampal spatial memory impairment in A30P mice (Freichel *et al.*, 2007). It is possible that *in vivo* recordings may elicit a more reliable measure of SPW activity and its role in cognition.

#### **3.5.4 Perineuronal net changes may be a neuroprotective adaptation**

One final component of the inhibitory interneuron network explored in this chapter is the expression of perineuronal nets. PNN expression has been found to

correlate closely to cells expressing higher levels of PV (Yamada *et al.*, 2015). This could explain the increase in PNN+ cell density in young A30P mice if cells are upregulating PV expression. Interestingly, an increase in hippocampal PNN+ cells has been described previously in a mouse model of AD, though this was not accompanied by a change in the density of PV+ interneurons (Vegh *et al.*, 2014). It is important to note, however, that evidence in the literature of PNN changes are often not specific to the N-acetylgalactosamine sugar measured in this thesis. The use of WFA lectin in this thesis to bind to N-acetylgalactosamine sugars in PNNs leads to the conclusion that the number of PNN-surrounded cells expressing this particular sugar is increased in young A30P mice, but changes in other residues remain to be explored.

In this thesis, a higher density of PNN+ cells than PV+ interneurons was reported in region CA3. It was expected that the remaining PNN+ cells may have been compensated for by CB+ interneurons in region CA3, but I surprisingly found a lower density of CB+ interneurons in young A30P mice. It can therefore be inferred that the increased density of PNN+ cells may not reflect the number of cells, but rather an increase in the size of the PNN. This should be explored further in future work, though the age-dependent changes in PNN+ cell density and PV+ interneuron density appear to correlate by increasing, then decreasing, at the same ages in A30P mice.

Interestingly, expression of the protein aggrecan in PNNs increases during postnatal days 10-28 and reaches a plateau around postnatal day 42 (Ye and Miao, 2013). The PV+ interneuron network undergoes a vast amount of change during this postnatal period, and concurrent increases in human ASYN expression in the first 3-4 weeks of life in A30P mice could disrupt this (Freichel *et al.*, 2007). As a result, it is possible that the increase in PV+ and PNN+ cells could occur as a direct result of early ASYN disruption. However, the normalisation of SPW amplitude, PV+ interneuron density, and PNN+ cell density with age in A30P10+ mice appears to support that it may be a transient, compensatory response. Degradation of PNNs has been proposed to reduce fast-spiking interneuron excitability (Balmer, 2016). This indicates that the increase in PNN+ cells may increase the excitability of fast-spiking interneurons and lead to increased GABAergic activity, or that conversely, the increase in PNN+ cells could be a compensatory protective response to the increased GABAergic activity.

### 3.6 Conclusion

So far, this work has shown that there are early changes in the GABAergic network in A30P mice, notably with respect to increased GABAergic activity in region CA3. This activity normalises with age in A30P mice to similar levels seen in WT mice. The A30P2+ mouse hippocampal CA3 region exhibits excess spontaneous inhibition, though no evidence of excess excitation in the form of spontaneous interictal or ictal activity was observed likely due to the increase in PV+ interneurons and PNNs.

The increase in PV+ interneuron density and associated PNNs may be caused by the presence of human ASYN in PV+ interneurons. This, in turn, may be causing the increase in GABAergic activity. Alternatively, the increase in PV+ interneuron density may simply reflect the increased activity of fast-spiking interneurons rather than cause it. Conversely, a reduction in CA3 region CB+ interneurons was observed in A30P2+ mice compared to age-matched WT mice, which also normalised with ageing. It is proposed that this may be a compensatory change to increased fast-spiking interneuron activity, due to the lack of ASYN within CB+ interneurons.

Despite the interneuron changes highlighted in this chapter, young A30P mice were not found in previous reports to show a hippocampal spatial memory impairment (Freichel *et al.*, 2007), and this may be due to compensatory changes within the E/I network to maintain balance. The possibility of changes within the excitatory pyramidal cell network will therefore be explored in *Chapter 4*.



## **Chapter 4. Early Hippocampal Hyperexcitability in A30P mice**



## 4.1 Introduction

So far in this thesis, evidence has been found for altered CA3 region GABAergic activity in the CA3 region of young A30P mice in the form of increased PV+ interneuron density, increased PNN+ cell density, decreased CB+ interneuron density, increased IPSP frequency and amplitude, and increased amplitude of GABA<sub>A</sub> receptor dependent SPWs. All may impact on excitability within the hippocampus and/or be compensatory changes to excess neuronal activity. As no change in spontaneous network oscillations were reported in this thesis as a result of GABAergic changes, it follows that induced network oscillations should next be investigated.

Work from our group has previously shown an age-dependent reduction in CCH-induced gamma-frequency oscillations in A30P mice by 9+ months of age (Robson *et al.*, 2018), and so it follows that an alternate model of gamma-frequency oscillations acting through different mechanisms and induced with the kainate receptor agonist KA should be explored. KA is used to model seizure activity at high concentrations (Ben-Ari and Cossart, 2000), though at low concentrations KA induces fast network oscillations in acute brain slice preparations (Buhl *et al.*, 1998; Hajos *et al.*, 2000; Cunningham *et al.*, 2003). Interestingly, it has previously been shown that KA-induced, but not spontaneous, gamma-frequency oscillations are reduced with physiological ageing in mice by 22-25 months of age (Lu *et al.*, 2011).

Kainate receptor agonism is proposed to drive the excitatory/inhibitory network in a similar way to spontaneous and CCH-induced gamma-frequency oscillations though differences in receptor contribution and subpopulations of interneurons have been reported (Skrobot, 2008; Pietersen *et al.*, 2009; Modebadze, 2014). Whilst all three models of network oscillations are dependent on GABA<sub>A</sub> receptors, differences in response to pharmacological agonists and antagonists exist (Skrobot, 2008; Pietersen *et al.*, 2009; Modebadze, 2014). As a result, the selective decrease in power of CCH-induced gamma-frequency oscillations (Robson *et al.*, 2018) but no impairment in spontaneous oscillations as explored in *Chapter 3* may begin to reveal the intricacies of receptor and interneuron population differences in A30P mice.

As this thesis has reported an increase in PV+ interneurons in the CA3 region of slices from A30P2+ mice and a decrease in CB+ interneurons at the same age, I wanted to explore the consequence of altered GABAergic activity on KA-induced oscillations. KA-induced gamma-frequency oscillations have been shown to be reduced by disruption of fast-spiking PV+ interneurons and their synchrony (Fuchs *et*

*al.*, 2007; Huang *et al.*, 2016), however less is known about the role of CB+ interneurons in gamma-frequency oscillations.

Given evidence of inhibitory network changes in A30P2+ mice, it was also decided to explore the role of astrocytes within the A30P mouse hippocampus. Astrocytes are specialised glial cells which play a variety of roles within a network, including but not limited to removal of excess neurotransmitters and control of network excitability through release of GABA (Heja *et al.*, 2012), or conversely by converting inhibition to excitation (Perea *et al.*, 2016). It was therefore proposed that astrocytes may play a role in conserving network balance by reducing excess inhibition in A30P2+ mice, or that they may even be responsible for the increase in inhibition.

It has been shown that increased neuronal activity can alter astrocyte gene expression and function, leading to increased glucose metabolism by astrocytes, a process that is impaired in both physiological ageing and neurodegeneration (Hasel and Dando, 2017). Indeed, human WT ASYN has been shown to activate rodent astrocytes in culture (Lee *et al.*, 2010) and an increase in GFAP immunoreactivity in astrocytes has been found in regions with more human A30P ASYN immunoreactivity in 8-11 month A30P mice (Ekmark-Lewen *et al.*, 2018). As a result, evidence of astrocytic changes due to human ASYN expression will be explored in this chapter in the context of excitatory/inhibitory network disturbances in A30P mice.

Imbalance in the excitatory/inhibitory network may manifest as hyperexcitability and epileptiform interictal or ictal activity. Indeed, a mouse model overexpressing human WT ASYN under the *Thy-1* promoter recently showed evidence of *in vivo* EEG epileptiform activity associated with a loss of CB+ cells from the dentate gyrus (Morris *et al.*, 2015). It has previously been reported that 21.7% of DLB patients exhibit myoclonic jerks (Morris *et al.*, 2015), and the rates at which DLB patients experience myoclonus is greater than in AD with a recent estimate of a cumulative probability of 58.1% (Beagle *et al.*, 2017). More recently, a 14.7% cumulative probability of developing seizures after disease onset was reported in DLB patients, comparable to the probability of seizures in AD (Beagle *et al.*, 2017). Evidence of excitatory/inhibitory network imbalance will be explored in more detail in A30P mice within this chapter.



## 4.2 Aims

- Explore KA-induced gamma-frequency oscillations in the CA3 region of the hippocampus in A30P mice.
- To investigate changes in astrocyte GFAP immunoreactivity, as a possible mechanism by which excitatory/inhibitory network balance changes.

### 4.3 Methods

Once spontaneous baseline activity had been recorded, slices were left for 45 minutes in the recording chamber to fully acclimatise to the new conditions and allow consistent extracellular local field potential recordings over a long period of time. KA was bath applied at a concentration of 50 nM to induce gamma-frequency oscillations. As not all slices oscillated at this concentration in preliminary experiments, the concentration was increased to 100 nM and it was at this concentration that 15 – 45 Hz area power ( $\mu V^2$ ) and peak frequency (Hz) were compared in A30P mice.

At a higher concentration of 150 nM KA, oscillations were classified to occur with or without “spikes”. Oscillations were first classified visually and later confirmed using AxoGraph’s peak detect function to detect peaks greater than 5 \* standard deviation of baseline. The presence of interictal discharges (IIDs) were confirmed visually and analysed offline using peak detect functions in MATLAB to compute IID frequency (Hz) and IID peak-to-peak amplitude (mV): the difference between the maximum positive peak and the minimum negative peak.

In a separate set of slices, sharp intracellular recordings were made of CA3 pyramidal cells to explore changes in the intrinsic cell properties of resting membrane potential (mV), firing threshold (mV), spike frequency (Hz), and spike amplitude (mV). Spike parameters were computed by MATLAB as described in *Chapter 2.6*.

Locomotor activity was measured by open field test as described in *Chapter 2.8*. Mice were compared by distance travelled (cm) over time blocked in to 5 minute intervals, and average ambulatory time (sec) at each minute averaged over the entire 90 minute recording period. Mice using for locomotor testing were a separate cohort of mice from those used for *in vitro* experiments throughout this thesis.

Immunohistochemistry for GFAP+ astrocytes was performed by free-floating immunohistochemistry, as described in *Chapter 2.7*, and quantified in region CA3 of WT and A30P mouse slices by density of GFAP+ cells per  $mm^2$ . Slices used for immunohistochemistry did not exhibit interictal activity.

## 4.4 Results

### 4.4.1 Increased power of KA-induced network oscillations in A30P2+ mice

Whilst it has previously been shown by our group that CCH-induced gamma-frequency oscillations exhibit an age-dependent reduction in power (Robson *et al.*, 2018), this thesis has so far demonstrated no change in spontaneous gamma-frequency oscillations in slices from A30P mice. As each type of oscillation works through different mechanisms, I next set out to explore a third model of gamma-frequency oscillations using low concentrations of the kainate receptor agonist KA.

Following bath application of 50 nM KA, extracellular field recordings were performed in the *st. radiatum* of the CA3 region. The same proportion of slices exhibited gamma-frequency oscillations within 30 minutes from WT2+ mice (77.8%; 7/9 slices) and A30P2+ mice (77.8%; 7/9 slices). Likewise, a similar proportion of slices exhibited gamma oscillations at 50nM KA from WT10+ mice (92.3%; 12/13 slices) and A30P10+ mice (100%; 13/13 slices). To reliably evoke gamma-frequency activity in all slices, the concentration of KA was increased to 100 nM in the same set of slices and a comparison of area power and frequency were made after 30 minutes.

Slices from A30P2+ mice exhibited a significantly larger gamma-frequency area power at 100 nM KA (Figure 4.1A/B) compared to slices from WT2+ mice (5790  $\mu\text{V}^2$  [IQR 3220 – 29740] versus 1940  $\mu\text{V}^2$  [IQR 1310 – 3520] respectively;  $p < 0.05$ , Mann-Whitney rank sum test; effect size = 1.46, power  $(1 - \beta) = 0.75$ ). Post-hoc power analysis revealed that this experiment was slightly underpowered, likely due to the increased variance of values in slices from A30P2+ mice limiting the magnitude of the effect size. It is unlikely that increasing the sample size would be beneficial, and instead attention should be turned to the fact that the largest area power values seen in A30P2+ mice were never seen in slices from WT2+ mice.

Conversely, peak frequency at 100 nM KA (Figure 4.1C) was not significantly different between slices from A30P2+ and WT2+ mice (29.9 Hz  $\pm$  1.7 versus 30.0 Hz  $\pm$  0.8 respectively,  $p > 0.05$ ; unpaired *t* test). This indicates that slices from A30P2+ mice are more sensitive to the oscillogenic effects of KA.

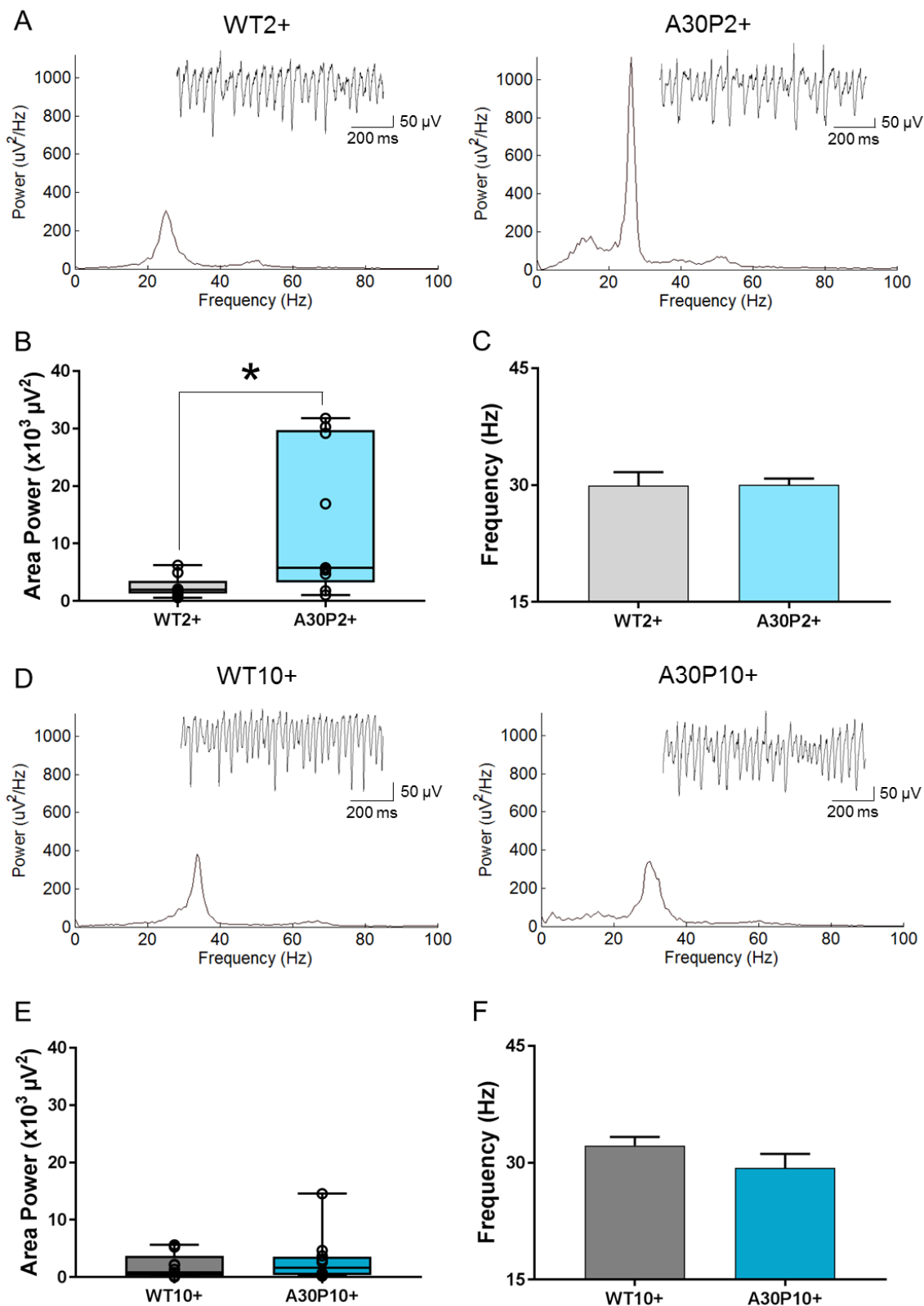


Figure 4.1 **Increased power of KA-induced oscillations in A30P2+ mice.** Representative power spectra and LFP traces (inset) with scale bars in (A) WT2+ (n = 9 slices from 5 mice) and A30P2+ mice (n = 9 slices from 7 mice). Boxplot to show area power (B) and bar chart to show peak frequency (C) in WT2+ and A30P2+ mice. Representative power spectra and LFP traces in (D) WT10+ (n = 13 slices from 4 mice) and A30P10+ mice (n = 10 slices from 3 mice). Boxplot to show area power (E) and bar chart to show peak frequency (F) in WT10+ and A30P10+ mice.

Upon comparing slices from A30P10+ and WT10+ mice at 100 nM KA (Figure 4.1D/E), the dramatic increase in the area power of KA-induced oscillations observed in A30P2+ mice had decreased and no significant difference was found between slices from A30P10+ and WT10+ mice ( $1650 \mu\text{V}^2$  [IQR 360 – 3540] versus  $830 \mu\text{V}^2$  [IQR 220 – 3730] respectively;  $p > 0.05$ ; Mann-Whitney rank sum test). Likewise, no difference was found in the peak frequency of oscillations (Figure 4.1F) between slices from A30P10+ and WT10+ mice ( $32.2 \text{ Hz} \pm 1.1$  versus  $29.3 \text{ Hz} \pm 6.3$  respectively,  $p > 0.05$ ; unpaired  $t$  test). This indicates that no gamma-frequency oscillation deficit occurs in A30P10+ mice when oscillations are induced with low concentrations of KA, unlike the deficits reported with CCH-induced oscillations (Robson *et al.*, 2018).

The increase in KA-induced gamma-frequency oscillation area power in slices from A30P2+ mice was confirmed not to be dependent on dorsal/ventral hippocampal slice location (WT2+ *dorsal*  $1760 \mu\text{V}^2$  [IQR 920 – 3070]  $n = 6$  slices; WT2+ *ventral*  $3520 \mu\text{V}^2$  [IQR 1930 – 5890]  $n = 4$  slices; A30P2+ *dorsal*  $5790 \mu\text{V}^2$  [IQR 520 – 29740]  $n = 5$  slices; A30P2+ *ventral*  $5020 \mu\text{V}^2$  [IQR 1600 – 20640]  $n = 6$  slices; genotype  $p < 0.05$ , location  $p > 0.05$ , interaction  $p > 0.05$ ; 2-way ANOVA on ranks; data not shown). Due to a small number of slices from WT2+ female mice, it was not possible to explore the effect of sex on the area power of KA-induced gamma-frequency oscillations.

The rhythmicity of an oscillation can give further indications as to how synchronous excitatory and inhibitory network components are, and this was also compared following 30 minutes of 100 nM KA (Figure 4.2). No significant difference was found between slices from WT2+ and A30P2+ mice ( $0.37 \pm 0.05$  versus  $0.44 \pm 0.05$  respectively;  $p > 0.05$ , unpaired  $t$  test) or between slices from WT10+ and A30P10+ mice ( $0.37 \pm 0.05$  versus  $0.33 \pm 0.05$  respectively;  $p > 0.05$ , unpaired  $t$  test). Therefore, despite an increase in KA-induced oscillation area power in slices from A30P2+ mice, the rhythmicity of the oscillation was unchanged. Furthermore, the rhythmicity of KA-induced oscillations was not impaired in A30P10+ mice.

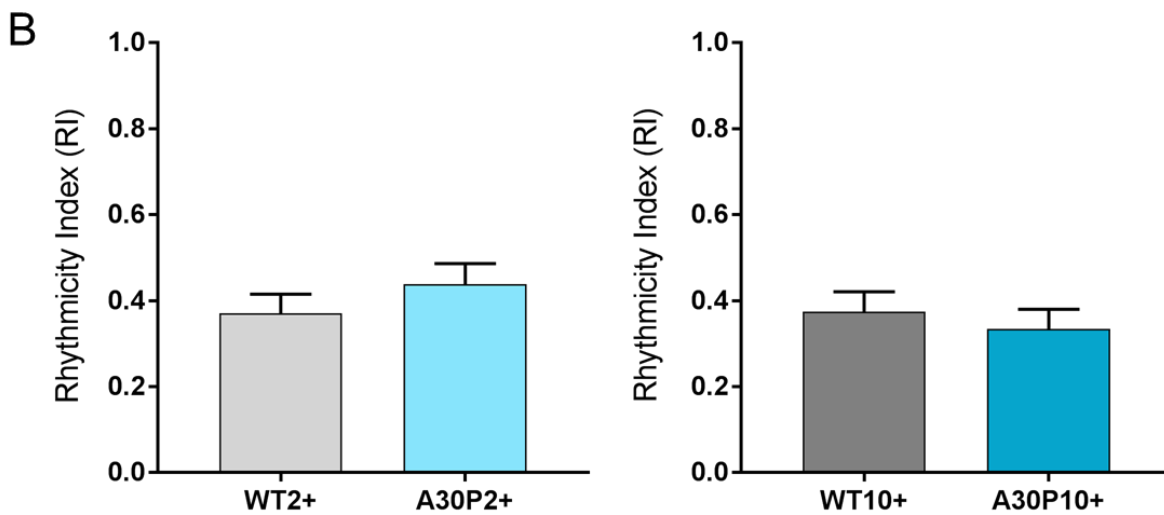
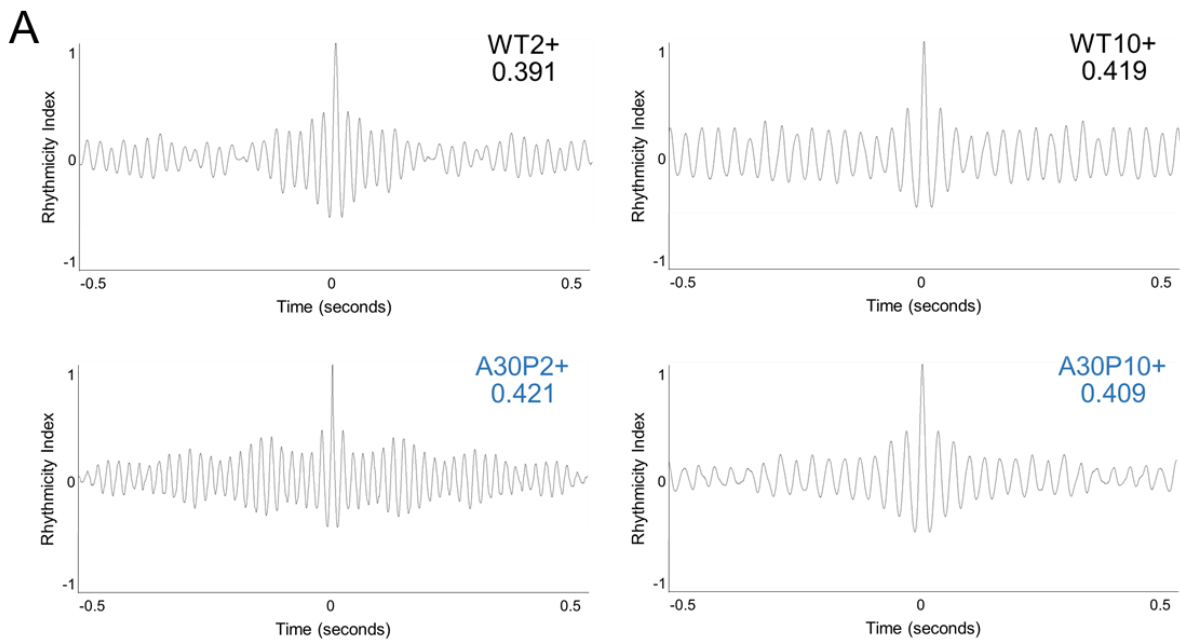


Figure 4.2 **No change in rhythmicity of KA-induced oscillations in A30P mice.** (A) Representative autocorrelations with associated rhythmicity index (RI) values in WT and A30P mice. (B) Bar charts to show computed RI values in slices from WT and A30P mice. WT2+ n = 9 slices from 5 mice, A30P2+ n = 9 slices from 7 mice, WT10+ n = 9 slices from 4 mice, A30P10+ n = 10 slices from 3 mice.

#### 4.4.2 Interictal discharges in A30P2+ mice at low concentrations of KA

To explore if 100 nM KA was the concentration that produced maximal gamma-frequency oscillation power, the concentration of KA was further increased by 50 nM to 150 nM KA. At this concentration, 92.9% of slices from WT2+ mice (13/14 slices) exhibited a gamma frequency oscillation. The remaining 7.1% of slices from WT2+ mice (1/14 slices) exhibited a gamma-frequency oscillation with spikes, representative of a network with excess excitation (Figure 4.3). In contrast, 20.0% of slices from A30P2+ mice (3/15 slices) exhibited oscillations with spikes and a further 40.0% of slices (6/15 slices) surprisingly exhibited interictal discharges (IIDs) at 150 nM KA.

As interictal activity was never seen in slices from WT2+ mice at 150 nM KA, I decided to examine network excitability in response to KA in another mouse model of alpha-synucleinopathy to explore if hyperexcitability is a common early occurrence. A cohort of mice over-expressing human WT ASYN under the *PDGF* promoter were included in this experiment at 2-6 months of age (henceforth referred to as PDGF2+ mice, see *Chapter 2.1*). Slices from PDGF2+ mice exhibited oscillations with spikes in 38.1% of slices (8/21 slices), and IIDs in a further 14.3% of slices (3/21 slices).

A comparison within the 2+ month age cohort confirmed a significant increase in the proportion of slices showing oscillations with spikes in PDGF2+ mice compared to both WT2+ and A30P2+ mice ( $\chi^2$  (df 2) = 12.37,  $p < 0.05$ ; chi-square test; effect size = 1.03, power ( $1 - \beta$ ) = 0.90), as well as a significant increase in the proportion of slices with IIDs in both A30P2+ and PDGF2+ mice compared to WT2+ mice ( $\chi^2$  (df 2) = 15.66,  $p < 0.05$ ; chi-square test; effect size = 1.01, power ( $1 - \beta$ ) = 0.89). This suggests that network excitability in response to KA may be a common early occurrence in mouse models of alpha-synucleinopathy.

Next, I wanted to explore the effect of ageing on A30P mouse network excitability in greater detail by examining a cohort of 6-8 month WT and A30P mice. Slices from WT6+ mice exhibited oscillations with spikes in 20.0% of slices (2/10 slices) but still did not exhibit IIDs. Conversely, slices from A30P6+ mice exhibited oscillations with spikes in 31.3% of slices (5/16 slices) and IIDs in a further 31.3% (5/16 slices). Whilst the number of slices exhibiting oscillations with spikes was not significantly different between WT6+ and A30P6+ mice ( $\chi^2$  (df 1) = 0.40,  $p > 0.05$ ; chi-square test), the proportion of slices exhibiting IIDs was significantly larger in A30P6+ mice compared to WT6+ mice, indicating that excitability persists to at least 6-8 months ( $\chi^2$  (df 1) = 3.87,  $p < 0.05$ ; chi-square test; effect size = 1.11, power ( $1 - \beta$ ) = 0.85).

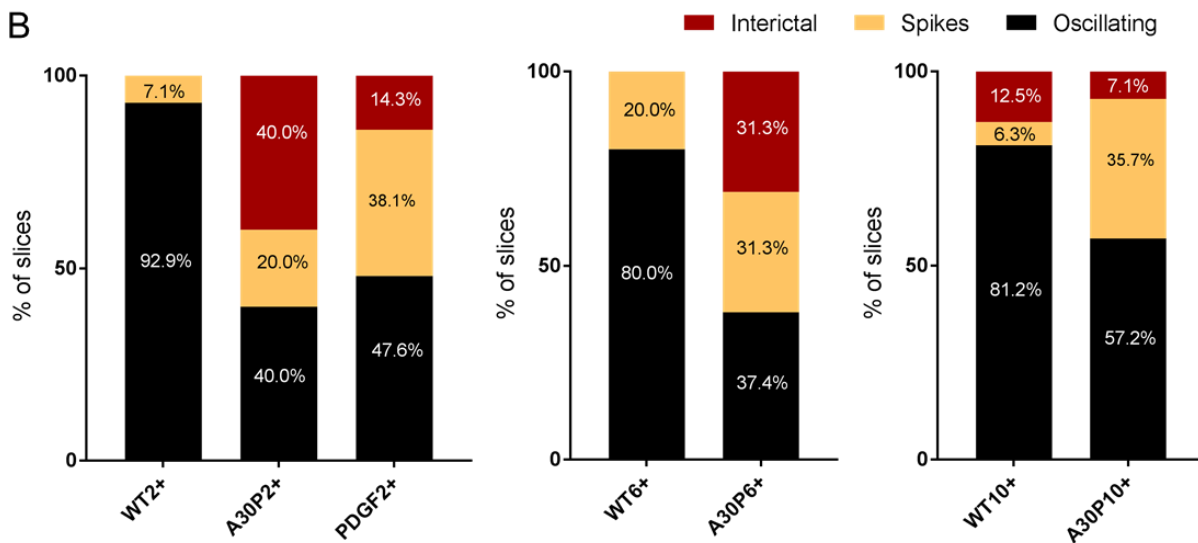
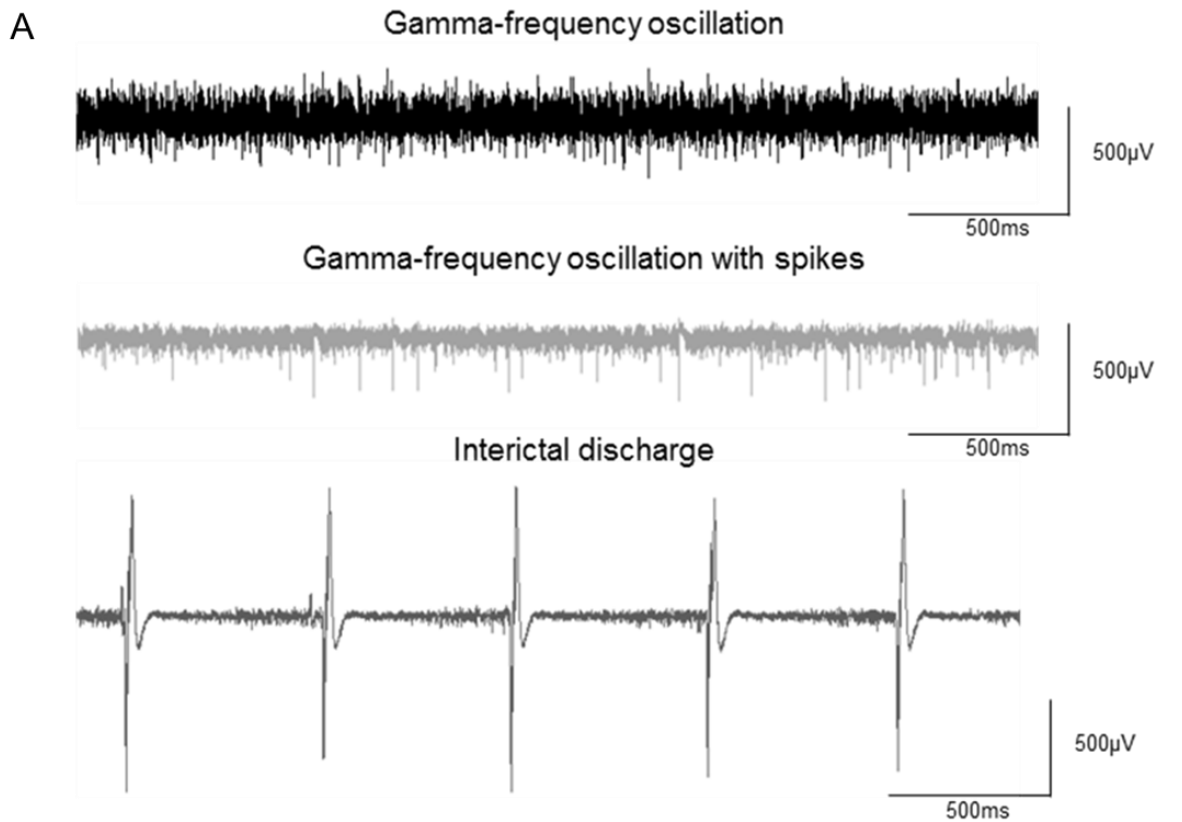


**Figure 4.3 A30P2+ mouse slices exhibit IIDs in low concentrations of KA.** Types of activity observed at 150 nM KA (A): gamma-frequency oscillations (red), gamma-frequency oscillations with spikes (yellow), and interictal discharges (black). Proportion of slices showing each type of activity at 150 nM KA (B) in WT2+ (n = 14 slices from 9 mice), A30P2+ (n = 15 slices from 10 mice), PDGF2+ (n = 21 slices from 12 mice), WT6+ (n = 10 slices from 6 mice), A30P6+ (n = 16 slices from 9 mice), WT10+ (n = 16 slices from 10 mice), and A30P10+ mice (n = 14 slices from 9 mice).



With physiological ageing, slices from WT10+ mice started to exhibit IIDs in response to 150 nM KA. IIDs were observed in 12.5% of slices from WT10+ mice (2/16 slices), and oscillations with spikes were observed in 6.3% of slices (1/16 slices). In contrast, slices from A30P10+ mice exhibited IIDs in 7.1% of slices (1/14 slices) and oscillations with spikes in 35.7% of slices (5/14 slices). This shows that the appearance of IIDs was now comparable to age-matched WT mice in slices from A30P10+ mice ( $\chi^2$  (df 1) = 0.24,  $p > 0.05$ ; chi-square test), but that a greater proportion of slices exhibited oscillations with spikes in A30P10+ mice compared to WT10+ mice ( $\chi^2$  (df 1) = 4.05,  $p < 0.05$ ; chi-square test; effect size = 0.74, power (1 -  $\beta$ ) = 0.63). Post-hoc power analysis revealed that this experiment was underpowered. This is likely due to the marginal difference in the proportion of slices showing oscillations with spikes. Increasing the sample size for future experiments could be beneficial to improve the observed power and confirm that the effect is indeed significant.

Interestingly, 100% of slices with IIDs from A30P2+ and A30P6+ mice were from the dorsal hippocampus (A30P2+ IIDs in 6/15 slices, A30P6+ IIDs in 5/16 slices; data not shown). In 10-13 month old mice, slices with IIDs appeared more often in the dorsal hippocampus in both WT and A30P mice, but due to a low number of slices in each group with IIDs this could not be statistically confirmed. Furthermore, there was a possible trend towards more slices with IIDs being from male mice (data not shown). However, as this is based on a low number of slices, only a tentative conclusion regarding a sex difference should be drawn from this data.

Sharp intracellular recordings were next performed in CA3 pyramidal cells whilst recording from the CA3 *st. radiatum* concurrently, to explore the intracellular correlate of IIDs. In 3 cells from A30P2+ mice, a large depolarising event was observed in CA3 pyramidal cells at the same time as IIDs in the local field potential (Figure 4.4). IIDs were preceded by gamma-frequency oscillations before oscillations were briefly silenced after the discharge and then gradually increased in amplitude until the next IID. Whilst enough cells were collected to observe the intracellular correlate of KA-induced IIDs, the sample size was not large enough to quantify activity beyond this.

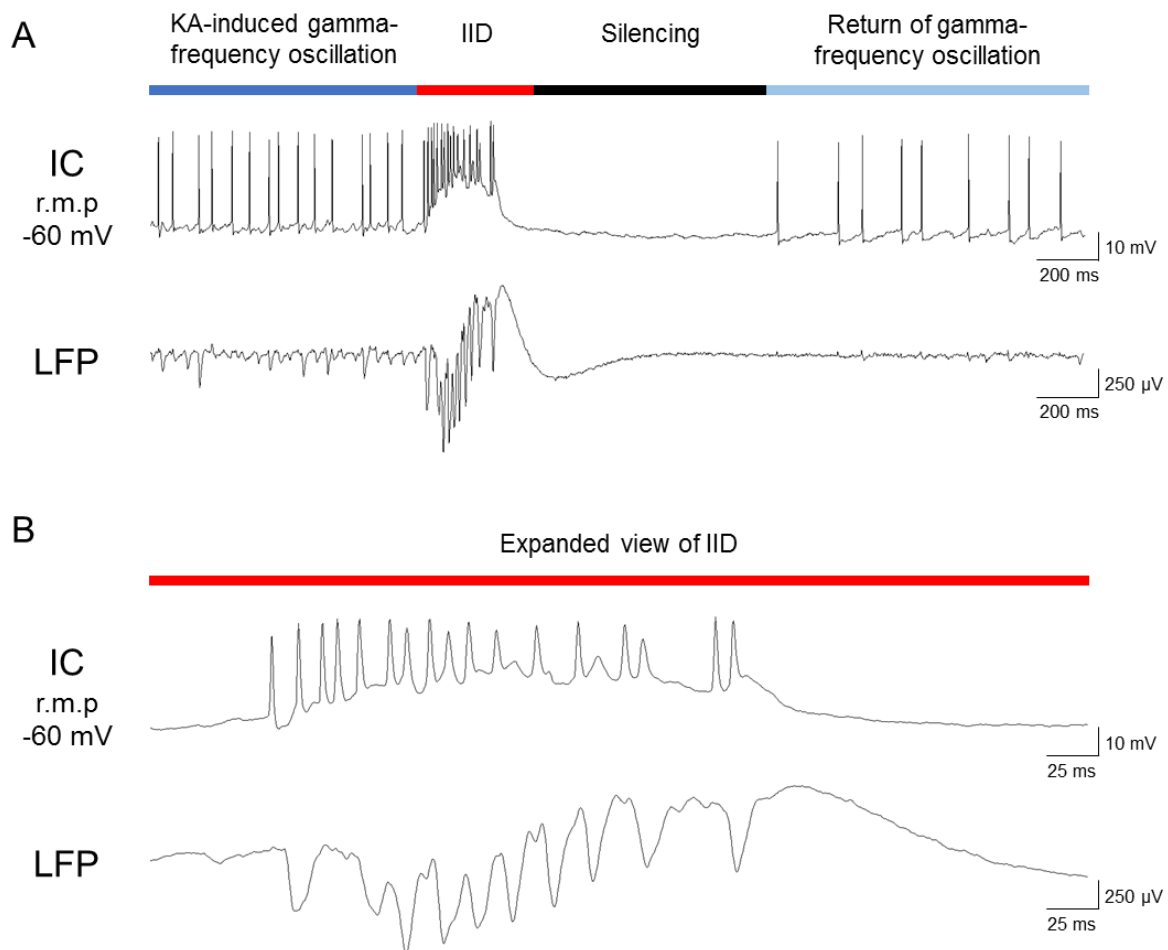


Figure 4.4 **KA-induced interictal discharges in A30P2+ mice.** Representative traces of intracellular recordings at resting membrane potential (IC), and LFP recordings with scale bars showing gamma-frequency oscillations interrupted by interictal discharges (IIDs, red) (A) and expanded view of IID event (B). A30P2+ n = 3 cells from 3 mice.

#### 4.4.3 Concentration-dependent changes in KA-induced gamma oscillations

This chapter has so far demonstrated that slices from A30P2+ mice are more sensitive to the oscillogenic and epileptogenic effects of low concentrations of KA. I therefore decided to perform a more detailed KA concentration response in a subset of slices without IIDs to explore differences in KA-induced network oscillations in A30P mice. The concentration of KA was increased by 50 nM every 30 minutes until 200 nM, at which point KA concentration was increased by 200 nM every 30 minutes. Gamma-frequency oscillations persisted through increasing concentrations of KA, until higher concentrations when oscillations began to collapse. In all slices from WT2+ (6/6 slices) and WT10+ mice (12/12 slices), oscillations had collapsed by 1000 nM KA. Surprisingly, a small peak of activity persisted at 1000 nM KA in 40.0% (2/5 slices) of slices from A30P2+ mice, and in 80.0% of slices (8/10 slices) from A30P10+ mice.

Consistent with the previous finding of an increased sensitivity to the oscillogenic effects of KA, the area power over increasing concentrations of KA (Figure 4.5A) was significantly larger overall in slices from A30P2+ mice compared to WT2+ mice (1420  $\mu\text{V}^2$  [IQR 470 – 11760] versus 730  $\mu\text{V}^2$  [IQR 140 – 1770] respectively; mouse  $p < 0.05$ , concentration  $p > 0.05$ , interaction  $p > 0.05$ ; RM 2-way ANOVA on ranks). No difference in area power was detected at any specific concentration.

Unexpectedly, slices from A30P10+ mice (Figure 5.4B) also exhibited a significantly larger power overall than WT10+ mice (2090  $\mu\text{V}^2$  [IQR 780 – 4830] versus 330  $\mu\text{V}^2$  [IQR 130 – 2660] respectively; mouse  $p < 0.05$ , concentration  $p < 0.05$ , interaction  $p > 0.05$ ; RM 2-way ANOVA on ranks; effect size = 0.78, power  $(1 - \beta) = 0.55$ ). This was surprising as no difference was detected previously in this chapter at 100 nM KA. Post-hoc power analysis revealed that this experiment was underpowered and so the significance of the effect should be considered. The effect may instead be due to a number of slices from A30P10+ mice oscillating up to 1000 nM KA rather than collapsing at a lower concentration of KA. Increasing the sample size to improve the observed power may be beneficial in future experiments to confirm this finding.

The peak frequency of KA-induced oscillations between 50 nM and 200 nM was analysed prior to oscillations collapsing (Figure 4.5C/D). Slices from A30P2+ mice oscillated at an overall faster frequency compared to slices from WT2+ mice (29.6 Hz  $\pm$  0.8 versus 27.4 Hz  $\pm$  0.4; mouse  $p < 0.05$ , concentration  $p > 0.05$ , interaction  $p > 0.05$ ; 2-way ANOVA; effect size = 1.89, power  $(1 - \beta) = 0.89$ ). Although the specific concentration this occurred at was not detected, the faster frequency appeared most

prominently at 50 nM KA. As this experiment was adequately powered at an observed power of 89%, it is possible that this finding may be due to inadequacy of the Holm-Sidak post-hoc test in detecting a difference at a specific concentration of KA.

No significant difference in frequency was found between slices from WT10+ mice and slices from A30P10+ mice across increasing concentrations of KA (32.0 Hz  $\pm$  1.0 versus 30.1 Hz  $\pm$  0.3; mouse  $p > 0.05$ , concentration  $p > 0.05$ , interaction  $p > 0.05$ ; 2-way ANOVA), though here there appeared to be a trend towards a slower peak frequency in slices from A30P10+ mice at 50 nM KA.

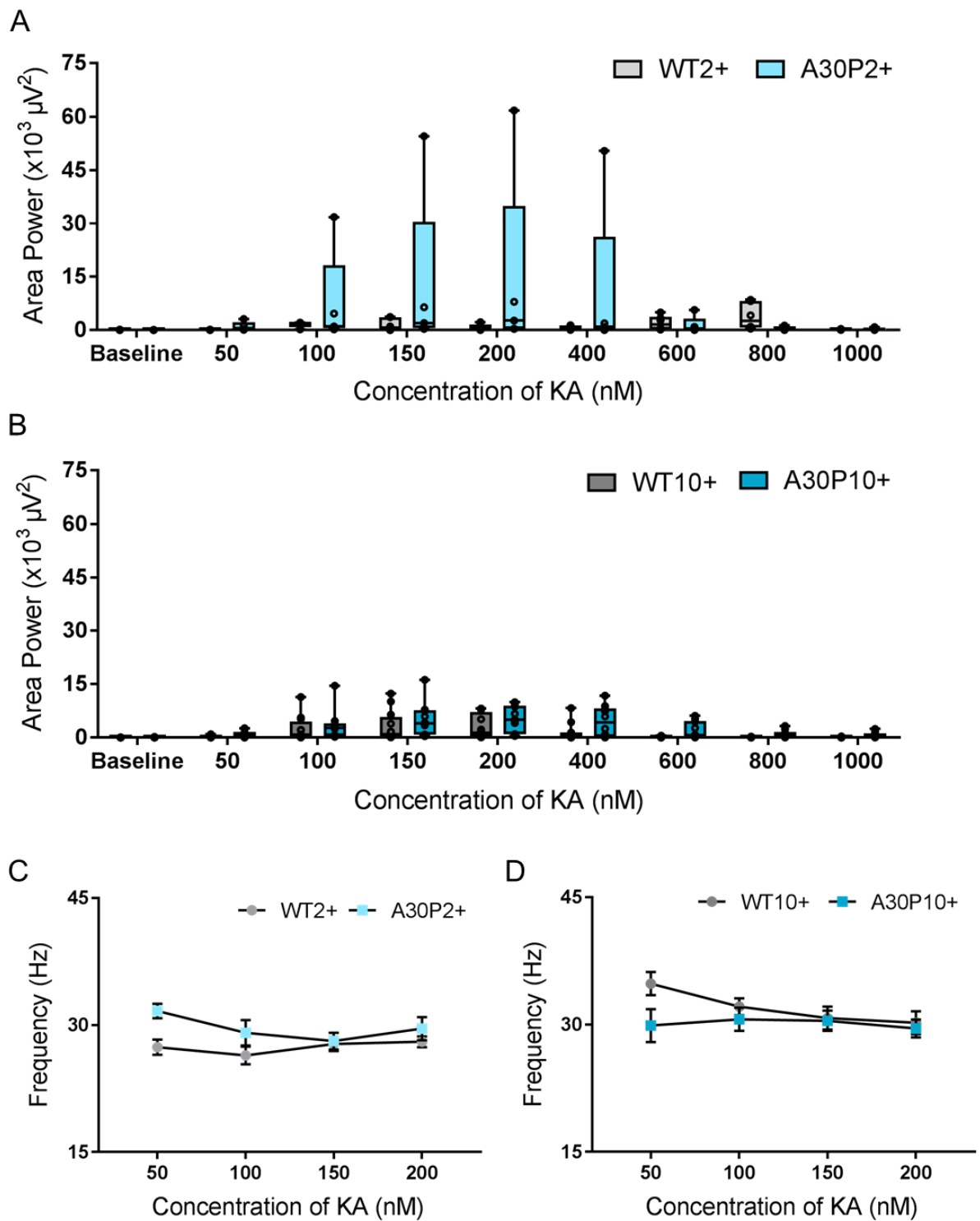


**Figure 4.5 Increased KA oscillation power over increasing concentrations in A30P mice.** Boxplots to show area power over increasing concentrations of KA in slices from A30P2+ (A) and A30P10+ (B) mice compared to age-matched WT control mice. Line graphs to show peak frequency over increasing concentrations of KA in slices from A30P2+ (C) and A30P10+ (D) mice compared to age-matched WT control mice. WT2+ n = 6 slices from 3 mice, A30P2+ n = 5 slices from 3 mice, WT10+ n = 12 slices from 4 mice, A30P10+ n = 10 slices from 3 mice.

#### 4.4.4 Increased sensitivity to GABA<sub>A</sub> receptor antagonism in A30P2+ mice

Having shown that low concentrations of KA causes IIDs in slices from A30P2+ mice, I next decided to investigate the inhibitory component of the network in more detail. GABA<sub>A</sub> receptor antagonism has been shown to induce IIDs and even seizure activity (Behrens *et al.*, 2007; Kilb *et al.*, 2007). An increased sensitivity to interictal and ictal activity in response to GABA<sub>A</sub> receptor antagonism has been reported in a mouse model of AD (Palop *et al.*, 2007), and so I wanted to explore this in A30P mice for the first time. Through exposure to increasing concentrations of GABA<sub>A</sub> receptor antagonist gabazine, I expected to find that the altered GABAergic activity explored in *Chapter 3* may impact gabazine-induced IID threshold in slices from A30P2+ mice.

A starting concentration of 50 nM gabazine was selected in order to elucidate subtle differences in A30P2+ mice. gabazine concentration was increased incrementally by 50 nM every 20 minutes, and no IIDs were seen in slices from WT2+ or A30P2+ mice until at least 250 nM (Figure 4.6A). At 250 nM gabazine, 16.7% of WT2+ and A30P2+ slices (1/6 slices) showed IIDs (Figure 4.6B), indicating that there was no difference in gabazine sensitivity regarding the lowest concentration at which interictal activity could occur ( $\chi^2$  (df 1) = 0,  $p > 0.05$ ; chi-square test).

When 500 nM gabazine was reached however, 83.3% of slices from A30P2+ mice (5/6 slices) exhibited IIDs compared to 33.3% of WT2+ slices (2/6 slices), which was a significantly greater proportion ( $\chi^2$  (df 1) = 3.88,  $p < 0.05$ ; chi-square test; effect size = 1.54, power (1 -  $\beta$ ) = 0.80). As the majority of slices from A30P2+ mice now exhibited IIDs, the concentration of gabazine was increased by 100 nM every 20 minutes to see if the proportion of WT2+ slices with IIDs would increase. By 1000 nM gabazine, the same 33.3% of WT2+ slices (2/6 slices) showed IIDs as at 500 nM. However, 100% of slices (6/6 slices) from A30P2+ mice now exhibited IIDs. Thus, slices from A30P2+ mice were more sensitive to the generation of IIDs in response to higher concentrations of GABA<sub>A</sub> receptor antagonism ( $\chi^2$  (df 1) = 6.0,  $p < 0.05$ ; chi-square test; effect size = 1.72, power (1 -  $\beta$ ) = 0.87).

It was noted that a large proportion of slices from WT2+ mice did not exhibit IIDs even at 1000 nM gabazine, so in 3 slices from WT2+ mice the concentration was increased to 10  $\mu$ M for 20 minutes. IIDs began to appear within 10 minutes of 10  $\mu$ M gabazine (data not shown). This indicates that some slices from WT2+ mice are simply resistant to interictal activity at lower concentrations of gabazine but that the slices remained viable and capable of such activity at high concentrations of gabazine.

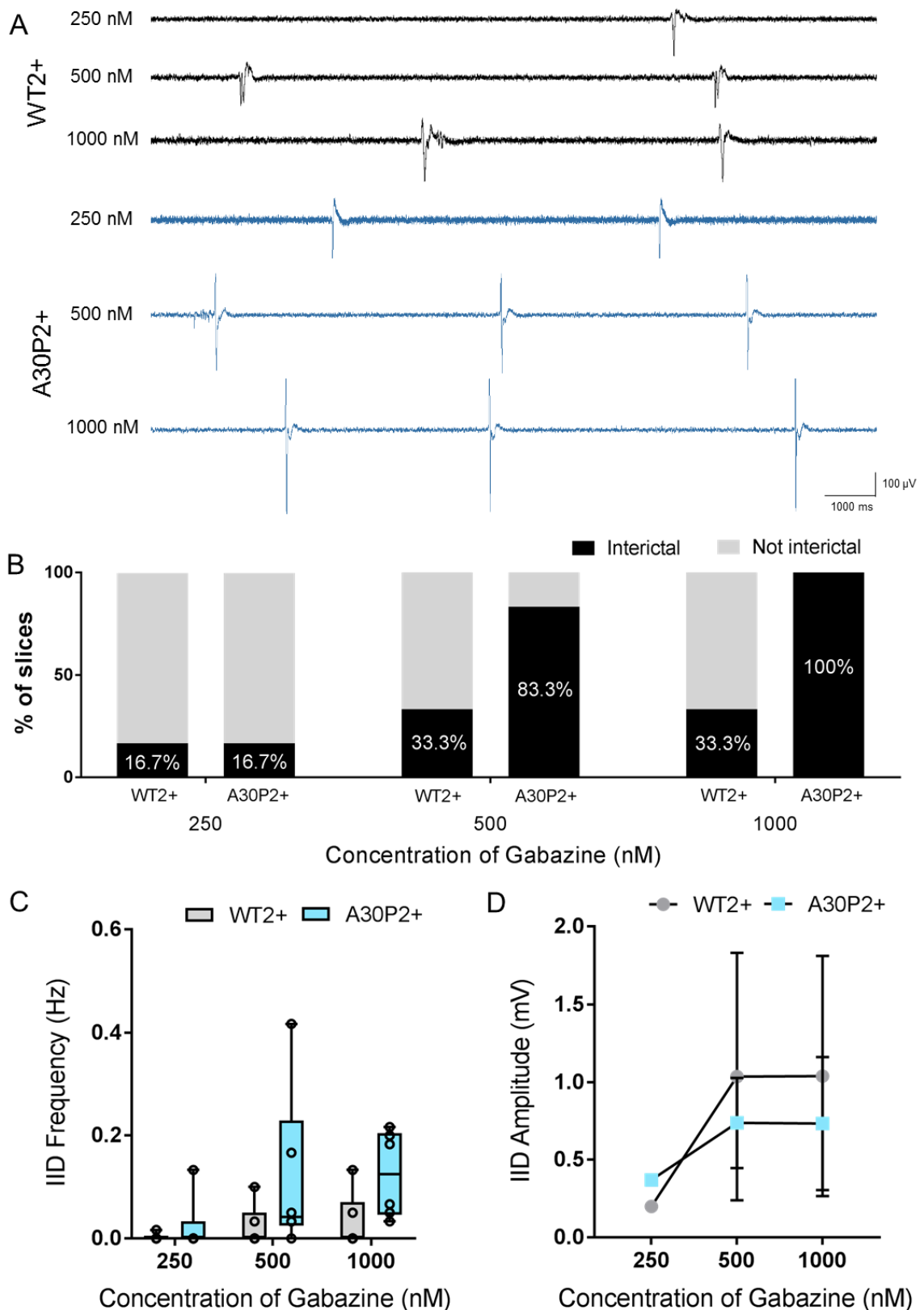


Figure 4.6 **A30P2+ mice more sensitive to GABA<sub>A</sub>-R antagonism.** (A) Representative traces of interictal discharges over increasing concentrations of gabazine in slices from WT2+ (n = 6 slices from 3 mice) and A30P2+ mice (n = 6 slices from 3 mice). Proportion of slices exhibiting interictal activity (B) at each concentration of gabazine. Boxplot to show IID frequency (C) at each gabazine concentration. Line graph to show IID amplitude (D) at each gabazine concentration.

Furthermore, there was a significantly higher IID frequency (Figure 4.6C) in slices from A30P2+ mice compared to WT2+ mice overall (0.12 Hz [IQR 0.02 – 0.13] versus 0.02 Hz [IQR 0.01 – 0.03] respectively; genotype  $p < 0.05$ , concentration  $p > 0.05$ , interaction  $p > 0.05$ ; RM 2-way ANOVA on ranks; effect size = 1.69, power ( $1 - \beta$ ) = 0.86). The increase in IID frequency could not be detected at any specific concentration despite this experiment achieving an adequate observed power of 86%. This indicates that, in addition to appearing in a greater proportion of slices from A30P2+ mice, IIDs also occurred at a greater frequency in A30P2+ mice across increasing concentrations of gabazine.

Conversely, the amplitude of IIDs (Figure 4.6D) was not significantly different overall between slices from WT2+ and A30P2+ mice at any concentration of gabazine, potentially due to the low sample size of slices from WT2+ mice exhibiting IIDs in this experiment ( $0.76 \mu\text{V} \pm 0.28$  versus  $0.61 \mu\text{V} \pm 0.12$  respectively; genotype  $p > 0.05$ , concentration  $p > 0.05$ , interaction  $p > 0.05$ ; RM 2-way ANOVA).

It was further confirmed that the increase in IID frequency in slices from A30P2+ mice was not dependent on dorsal/ventral hippocampal location by separating data at 1000 nM gabazine (WT2+ *dorsal* 0 Hz [IQR 0 – 0.05]  $n = 3$  slices; WT2+ *ventral* 0 Hz [IQR 0 – 0.13]  $n = 3$  slices; A30P2+ *dorsal* 0.07 Hz [IQR 0.05 – 0.20]  $n = 3$  slices; A30P2+ *ventral* 0.18 Hz [IQR 0.03 – 0.22]  $n = 3$  slices; genotype  $p < 0.05$ , location  $p > 0.05$ , interaction  $p > 0.05$ ; 2-way ANOVA on ranks, data not shown).

The effect of sex on IID frequency could not be explored due to a lack of slices from female mice within the A30P2+ mouse group.



#### 4.4.5 CA3 pyramidal cells intrinsically more excitable in A30P2+ mice

This thesis so far presents evidence of excitability in both inhibitory and excitatory networks in slices from A30P2+ mice that normalises with ageing. The intrinsic properties of CA3 pyramidal cells were therefore next assessed to determine whether excitability originates from changes to pyramidal cell excitability, or whether it arises indirectly through the excitatory/inhibitory hippocampal network.

Intracellular recordings revealed that the resting membrane potential (RMP) of CA3 pyramidal cells (Figure 4.7A) was more depolarised in A30P2+ mice compared to WT2+ mice ( $-48.4 \text{ mV} \pm 4.1$  versus  $-61.0 \text{ mV} \pm 2.3$  respectively,  $p < 0.05$ , unpaired  $t$  test; effect size = 1.77, power  $(1 - \beta) = 0.93$ ). No significant difference was found in the RMP of CA3 pyramidal cells in WT10+ and A30P10+ mice ( $-56.4 \text{ mV} \pm 5.0$  versus  $-50.3 \text{ mV} \pm 0.7$  respectively,  $p > 0.05$ , unpaired  $t$  test), despite a trend to cells from A30P10+ mice being more depolarised.

CA3 pyramidal cells were next depolarised to firing threshold (Figure 4.7B). There was no significant difference in the firing threshold of A30P2+ mouse CA3 pyramidal cells compared to WT2+ mice ( $-49.8 \text{ mV} \pm 5.3$  versus  $-50.0 \text{ mV} \pm 4.5$  respectively,  $p > 0.05$ , unpaired  $t$  test). This indicates that despite a more depolarised resting membrane potential, CA3 pyramidal cells from A30P2+ mice are almost at firing threshold so need little depolarisation to fire. Furthermore, no difference was found in the firing threshold of A30P10+ mouse CA3 pyramidal cells compared to WT10+ mice ( $-51.0 \text{ mV} \pm 3.2$  versus  $-48.0 \text{ mV} \pm 4.6$  respectively,  $p > 0.05$ , unpaired  $t$  test).

The average firing rate and spike amplitude at firing threshold were next compared (Figure 4.8A). Despite a strong trend to higher firing rates in A30P2+ mouse CA3 pyramidal cells compared to WT2+ mice (Figure 4.8B), no significant difference was found ( $8.0 \text{ Hz} \pm 2.9$  versus  $2.2 \text{ Hz} \pm 0.6$  respectively;  $p = 0.08$ , unpaired  $t$  test). This was likely due to variability between A30P2+ mouse cells. Furthermore, no significant difference was found between WT10+ and A30P10+ mice in pyramidal cell firing rate ( $1.1 \text{ Hz} \pm 0.4$  versus  $3.9 \text{ Hz} \pm 1.3$  respectively,  $p > 0.05$ , unpaired  $t$  test). With respect to spike amplitude (Figure 4.8C), no significant differences were found in A30P2+ mouse CA3 pyramidal cells compared to WT2+ mice ( $42.6 \text{ mV} \pm 2.8$  versus  $43.8 \text{ mV} \pm 4.5$  respectively,  $p > 0.05$ , unpaired  $t$  test), or in A30P10+ mice compared to WT10+ mice ( $51.1 \text{ mV} \pm 1.8$  versus  $57.7 \text{ mV} \pm 4.4$  respectively,  $p > 0.05$ , unpaired  $t$  test). Taken together, these results suggest an intrinsic A30P2+ pyramidal cell excitability with a significantly more depolarised resting membrane potential.

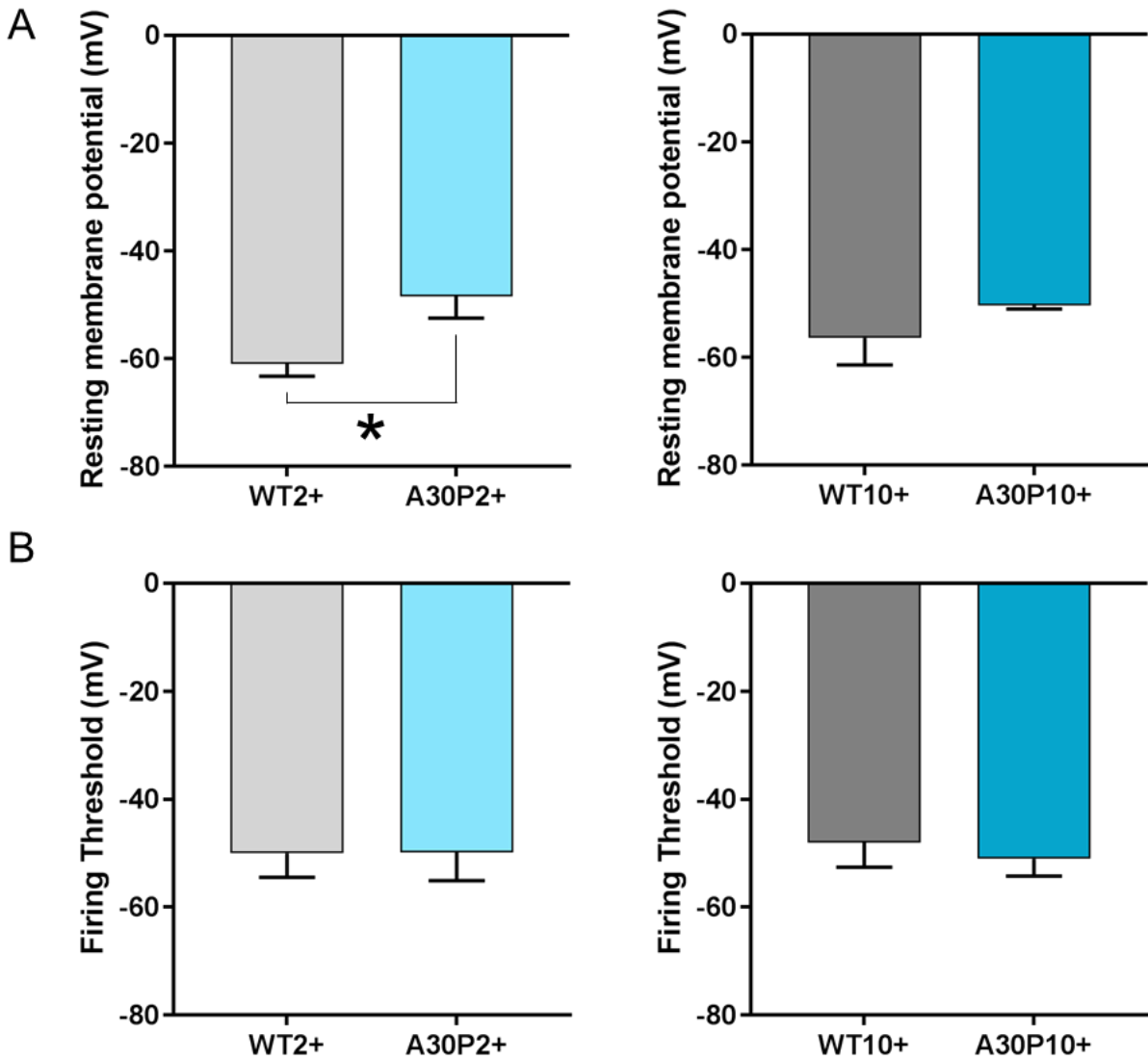


Figure 4.7 **More depolarised RMP of CA3 pyramidal cells of A30P2+ mice.** Bar charts showing (A) resting membrane potential (RMP) and (B) firing threshold in CA3 pyramidal cells measured by sharp intracellular recordings from WT2+ (n = 7 cells from 7 mice), A30P2+ (n = 7 cells from 7 mice), WT10+ (n = 4 cells from 4 mice) and A30P10+ mice (n = 3 cells from 2 mice). \* indicates significance at p < 0.05.

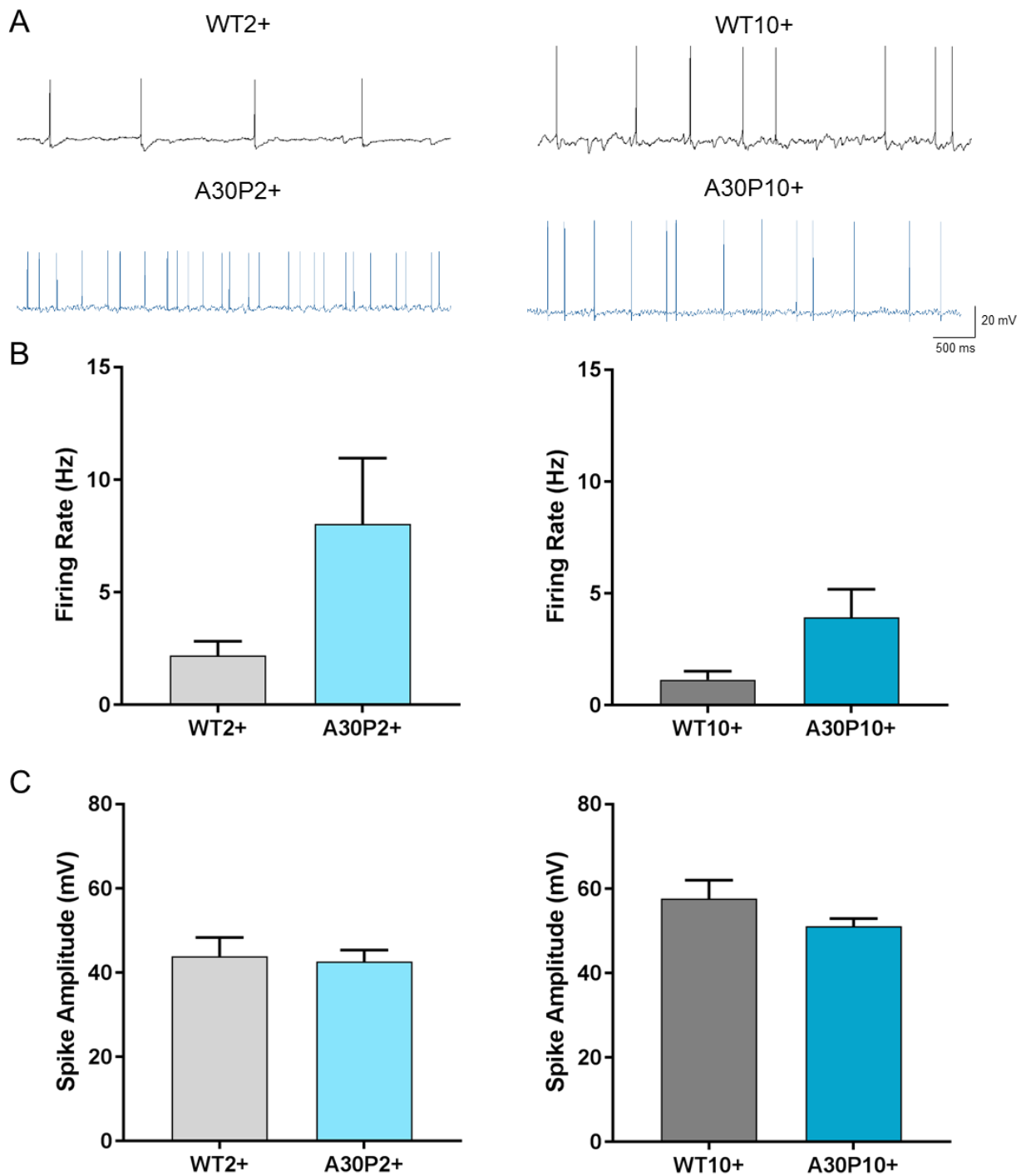


Figure 4.8 **No difference in spiking parameters at firing threshold in A30P mice.** (A) Representative traces of CA3 pyramidal cell firing measured by sharp intracellular recordings from WT2+ (n = 5 cells from 4 mice), A30P2+, (n = 5 cells from 5 mice), WT10+ (n = 5 cells from 4 mice), and A30P10+ mice (n = 5 cells from 5 mice). Bar charts to show firing rate (B) and spike amplitude (C) at firing threshold.

#### 4.4.6 Hyperlocomotion in A30P mice

It has been reported previously that excess activity within cortical networks can lead to hyperlocomotion in rodents (Procaccini *et al.*, 2013). Given evidence so far of both interneuron and pyramidal cell excitability in A30P2+ mice, I expected to find increased locomotor activity in young, but not ageing, A30P mice. WT and A30P mice were tested in an open field test over 90 minutes for evidence of hyperlocomotion.

Distance travelled was blocked into 5 minute intervals and then compared between WT2+ and A30P2+ mice (Figure 4.9A). A30P2+ mice were found to travel a greater distance overall compared to WT2+ mice (367.90 cm  $\pm$  18.52 versus 263.46 cm  $\pm$  20.05 respectively; mouse  $p < 0.05$ , time  $p < 0.05$ , interaction  $p > 0.05$ ; RM 2-way ANOVA; effect size = 1.29, power (1 -  $\beta$ ) = 0.92). Both WT2+ and A30P2+ mice decreased in distance travelled over time as a result of habituation to the novel environment. A further measure of average ambulatory time was made to confirm that increased locomotor activity was indeed occurring (Figure 4.9B). On average, A30P2+ mice spent more time ambulatory at each minute than WT2+ mice (16.47 sec  $\pm$  1.54 versus 12.30 sec  $\pm$  1.23 respectively,  $p < 0.05$ , unpaired  $t$  test; effect size = 2.99, power (1 -  $\beta$ ) = 0.99), thus confirming hyperlocomotion in A30P2+ mice.

A separate cohort of aged mice were tested and hyperlocomotion was found to persist in A30P10+ mice compared to WT10+ mice (Figure 4.9C) with a greater distance travelled overall (321.54 cm  $\pm$  15.08 versus 172.86 cm  $\pm$  10.24 respectively; mouse  $p < 0.05$ , time  $p < 0.05$ , interaction  $p > 0.05$ ; RM 2-way ANOVA; effect size = 2.71, power (1 -  $\beta$ ) = 0.99). A reduction in distance travelled over time occurred in both WT10+ and A30P10+ mice, once again confirming that habituation occurred. This is despite WT10+ and A30P10+ mice appearing to travel different distances within the first 5 minutes, unlike in WT2+ and A30P2+ mice. A comparison of average ambulatory time (Figure 4.9D) confirmed that A30P10+ mice showed increased locomotor activity compared to WT10+ mice (15.14 sec  $\pm$  1.43 versus 8.62 sec  $\pm$  1.08 respectively,  $p < 0.05$ , unpaired  $t$  test; effect size = 5.15, power (1 -  $\beta$ ) = 0.99).

As ambulatory time appears to provide a reliable yet simple comparison of locomotor activity, I decided to compare this value after separating data by sex. Young female mice spent a greater portion of time ambulatory compared to young male mice, regardless of mouse genotype (overall *male* 13.21 sec  $\pm$  0.52 [ $n = 8$  mice] versus overall *female* 17.10 sec  $\pm$  0.70 [ $n = 16$  mice]; mouse  $p < 0.05$  sex  $p < 0.05$ , interaction  $p > 0.05$ , 2-way ANOVA, data not shown). Though the increase in locomotor activity in

A30P2+ mice were present in both male and female A30P2+ mice, this highlights the importance of separating mice by sex in behavioural testing. Conversely, no significant difference was found between male and female mice at 10-13 months of age (overall *male* 10.74 sec  $\pm$  1.14 [n = 6 mice] versus overall *female* 13.40 sec  $\pm$  1.31 [n = 8 mice]; mouse p < 0.05, sex p > 0.05, interaction p > 0.05, 2-way ANOVA, data not shown). This indicates that in addition to the increased locomotor activity in A30P10+ mice, male and female mice displayed similar levels of locomotor activity overall.

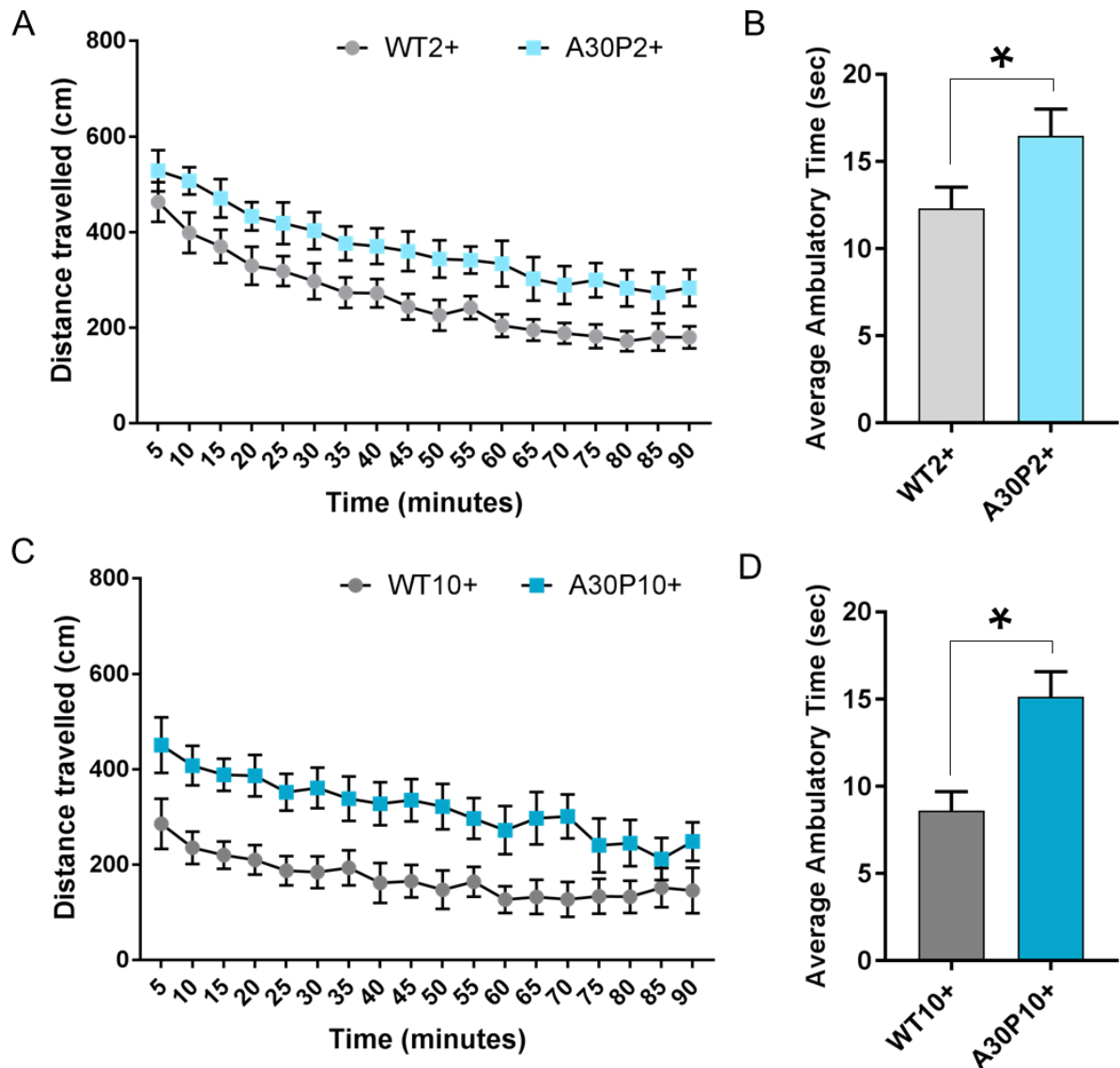


Figure 4.9 **Hyperlocomotion in A30P mice.** (A) Line graph to show distance travelled in WT2+ and A30P2+ mice over 90 minutes. (B) Bar chart to show average ambulatory time in seconds in WT2+ (n = 12 mice) and A30P2+ mice (n = 12 mice). (C) Line graph to show distance travelled in WT10+ and A30P10+ mice over 90 minutes. (D) Bar chart to show average ambulatory time in seconds in WT10+ (n = 7 mice) and A30P10+ mice (n = 7 mice). \* indicates significance at p < 0.05.

#### 4.4.7 Decrease in GFAP+ astrocytes in the A30P2+ mouse CA3 region

Given evidence of excitability in the A30P2+ mouse hippocampus, it was decided to next explore possible mechanisms of excitability. Astrocytes within the hippocampus play a role in regulating excitability (Heja *et al.*, 2012). It has also been shown that mouse astrocytes in culture take up ASYN released from neurons and this induces an inflammatory response in astrocytes (Rannikko *et al.*, 2015). As a result, astrocytic function may be affected by human ASYN overexpression and I therefore decided to explore GFAP immunoreactivity in astrocytes in A30P mice (Figure 4.10A).

GFAP expression is upregulated as astrocytes become reactive (Pekny and Pekna, 2004). It was noted by qualitative assessment that a number of slices from A30P2+ mice displayed little GFAP immunoreactivity in the CA3 region but were immunoreactive elsewhere in the slice. This was reflected through quantitative assessment of GFAP+ cells, where a significant reduction in GFAP+ cell density within region CA3 was found in slices from A30P2+ mice (Figure 4.10B) compared to WT2+ mice (106.3 cells/mm<sup>2</sup> ± 36.9 versus 205.9 cells/mm<sup>2</sup> ± 16.3 respectively,  $p < 0.05$ , unpaired  $t$  test; effect size = 3.22, power (1 -  $\beta$ ) = 0.99).

Conversely, no significant difference was found in GFAP+ cell density in slices from A30P10+ mice compared to WT10+ mice (154.4 cells/mm<sup>2</sup> ± 49.2 versus 164.5 cells/mm<sup>2</sup> ± 64.3 respectively,  $p > 0.05$ , unpaired  $t$  test). It was noted that GFAP+ astrocytes presented with dense somata and processes in ageing mice of both genotypes, though no scar formation was observed. While this may represent an ageing astrocyte phenotype, the change in morphology did not appear to affect quantification as the highest density of cells/mm<sup>2</sup> was in slices from WT2+ mice.

The decrease in GFAP+ cell density in A30P2+ mice was not dependent on dorsal/ventral slice location, however there were significantly more GFAP+ cells in the dorsal hippocampus of young mice compared to the ventral hippocampus, regardless of genotype (197.8 cells/mm<sup>2</sup> ± 18.0 [ $n = 6$  slices] versus 131.1 cells/mm<sup>2</sup> ± 13.9 [ $n = 10$  slices] respectively; mouse  $p < 0.05$ , region  $p < 0.05$ , interaction  $p > 0.05$ , 2-way ANOVA; data not shown). This suggests a physiological difference in GFAP+ astrocyte distribution along the hippocampal axis. Finally, the decrease in GFAP+ cells in A30P2+ mice was likely not dependent on sex (WT2+ *male* 205.5 cells/mm<sup>2</sup> ± 39.1 [ $n = 2$  mice]; WT2+ *female* 206.2 cells/mm<sup>2</sup> ± 8.1 [ $n = 2$  mice]; A30P2+ *male* 149.9 cells/mm<sup>2</sup> ± 32.8 [ $n = 2$  mice]; A30P2+ *female* 62.6 cells/mm<sup>2</sup> ± 57.3 [ $n = 2$  mice]; mouse  $p < 0.05$ , sex  $p > 0.05$ , interaction  $p > 0.05$ , 2-way ANOVA; data not shown).

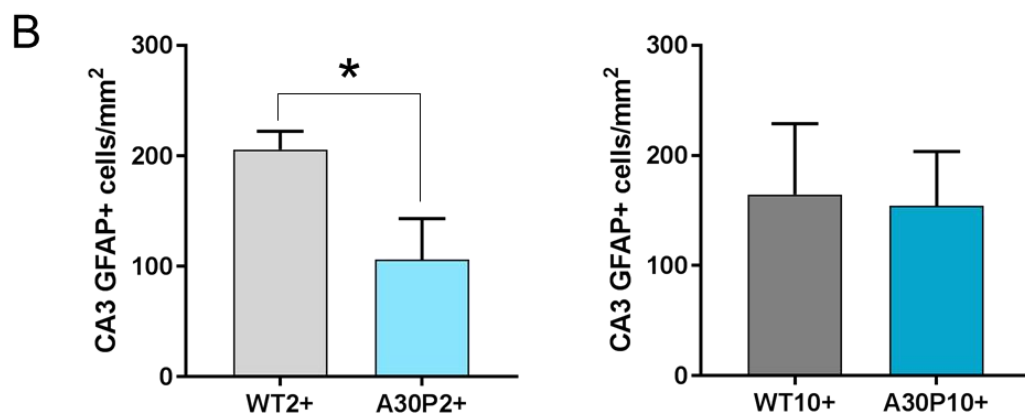
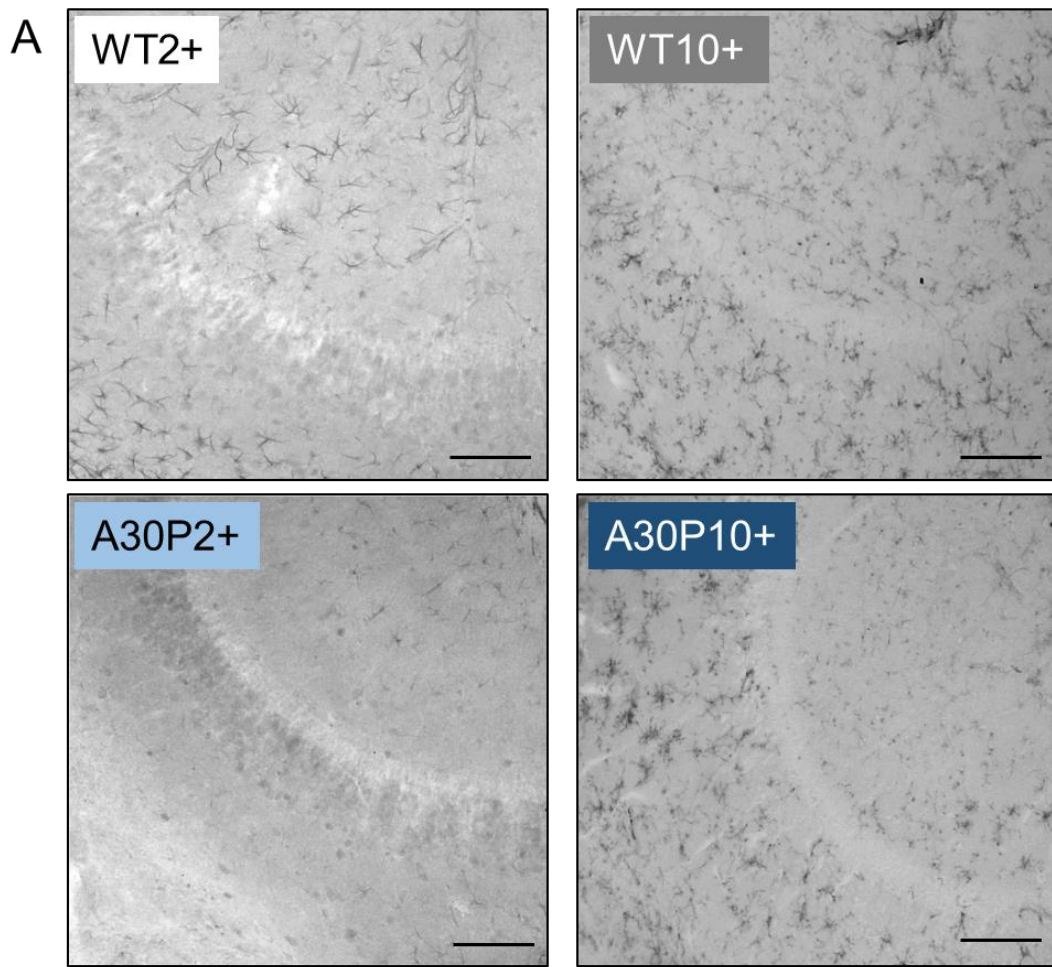


Figure 4.10 **Decreased GFAP+ astrocytes in the A30P2+ mouse CA3 region.** (A) Representative images of the CA3 region at x10 magnification. Scale bar 100  $\mu$ m. (B) Bar charts to show GFAP+ cells per mm<sup>2</sup> in the CA3 region of WT and A30P mice. WT2+ n = 8 slices from 4 mice, A30P2+ n = 8 slices from 4 mice. WT10+ n = 4 slices from 2 mice, A30P10+ n = 8 slices from 4 mice. \* indicates significance at p < 0.05.

## 4.5 Discussion

**A summary of key findings in Chapter 4 are as follows:**

- A30P2+ mouse slices show CA3 region gamma-frequency oscillations of a greater power, but not frequency, in response to kainate receptor agonism with KA across a range of concentrations.
- No impairment in CA3 region KA oscillations in A30P10+ mice, unlike previously reported with CCH oscillations (Robson *et al.*, 2018).
- A30P2+ mouse slices progress from oscillations to IIDs at low concentrations of KA, indicating a sensitivity to the epileptogenic effects of KA in young A30P mice that decreases with age.
- A30P2+ mouse slices are more sensitive to GABA<sub>A</sub> receptor antagonist-induced IIDs due to disinhibition. IIDs in A30P2+ mouse slices are also of a greater frequency.
- A30P2+ mouse CA3 pyramidal cells have a more depolarised resting membrane potential and trend towards a higher firing rate.
- Both A30P2+ and A30P10+ mice exhibit hyperlocomotion.
- A30P2+ mice present with decreased CA3 region GFAP+ astrocyte density in the hippocampus, but normalised levels with age.

### 4.5.1 Hyperexcitability in young A30P mice normalises with ageing

There have been reports for a number of years of increased network excitability in mouse models of AD (Palop *et al.*, 2007) and an increased incidence of seizures in patients with AD (Amatniek *et al.*, 2006). It is only recently emerging that hyperexcitability also exists in mouse models of alpha-synucleinopathy, with a recent study describing EEG epileptiform activity in mice over-expressing human WT ASYN under the *Thy-1* promoter (Morris *et al.*, 2015). Whilst there is evidence of myoclonus in a proportion of patients with DLB, clinical seizures were not thought to be common compared to in AD (Caviness *et al.*, 2003; Puschmann *et al.*, 2009; Morris *et al.*, 2015). However, more recent evidence has suggested a similar cumulative probability of seizures in DLB compared to AD following disease onset (Beagle *et al.*, 2017).

Despite this, evidence of subclinical seizures has not yet been investigated in LBD as they are not easily detectable non-invasively through EEG recordings. However, there is increasing evidence that hippocampal network excitability can lead to changes in molecular expression patterns of receptors, neuropeptides and even CB



(Marksteiner *et al.*, 1990; Tonder *et al.*, 1994; Vezzani *et al.*, 1999; You *et al.*, 2017). Therefore, even if a patient does not present with seizures clinically, increased neuronal activity still has extensive consequences in a network.

An increase in ASYN levels in patients with intractable epilepsy was observed in the serum and CSF (Rong *et al.*, 2015), potentially providing a link between the physiological function of ASYN and the regulation of excitability within a network. As ASYN interacts with vesicles (Jensen *et al.*, 1998), it follows that ASYN's role in neurotransmitter release could modulate excitability. Hyperexcitability in response to human ASYN has been reported previously in cell culture models, whereby hippocampal cells transfected with either WT or A53T ASYN expressed non-selective cation channels and increased in excitability (Mironov, 2015). Conversely, when oligomers but not monomers of human ASYN were injected into pyramidal cells, reduced excitability has been reported (Kaufmann *et al.*, 2016). This provides evidence that human ASYN can increase excitability in certain structural forms, and may explain why, with ageing in A30P mice as oligomer formation increases (Ekmark-Lewen *et al.*, 2018), excitability appears to reduce and normalise. This information is complicated, however, by the finding that the A30P mutation in ASYN may confer a loss of vesicle binding ability (Jensen *et al.*, 1998). The effect that this may have on neurotransmitter release and neuronal excitability is complex and should be explored further through patch clamping and calcium imaging techniques.

The mechanism by which over-expression of human A30P ASYN could lead to increased neuronal excitability was not elucidated in this thesis, though future work should examine such pathways. However, it is proposed that the intrinsic hyperexcitability of pyramidal cells in young A30P mice is likely to be a direct result of the presence of human ASYN in pyramidal cells. Hyperexcitable pyramidal cells could, in turn, drive interneuron hyperexcitability. As a result, the expression of human ASYN within interneurons is not necessarily essential for generating the GABAergic interneuron hyperexcitability reported in *Chapter 3*, though the extracellular spread of ASYN to interneurons may exacerbate aberrant network activity.

The question of whether the altered interneuron activity shown in *Chapter 3* is accompanied by evidence of general hyperexcitability was explored in this chapter. Slices from A30P2+ mice exhibit increased sensitivity to low concentrations of KA receptor agonism in the form of increased power gamma-frequency oscillations, and the appearance of interictal activity never seen in WT2+ mice.

Previous work using the KA model of epilepsy have reported that vulnerability to seizures increases with physiological ageing following KA injection in rats (Albala *et al.*, 1984; Dawson and Wallace, 1992; Sarkisian *et al.*, 1997). Despite our cohort of WT10+ mice only spanning 10 - 13 months of age, this may explain why low concentrations of KA induce IIDs in a small proportion of slices never seen in slices from WT2+ mice. Conversely, the A30P2+ mouse network is more vulnerable to KA-induced interictal activity, and this may be the result of A30P2+ CA3 pyramidal cells exhibiting a more depolarised resting membrane potential and as a result requiring less depolarisation to reach firing threshold.

In drug-free conditions, pyramidal cell hyperexcitability in A30P2+ mice is likely balanced by increased GABAergic activity, and as a result spontaneous interictal or ictal activity is not observed in slices. In turn, this may explain why spontaneous network oscillations were unchanged in A30P2+ mice in *Chapter 3*, despite evidence of increased IPSP parameters and PV+ interneuron density. Furthermore, despite both being GABA<sub>A</sub> receptor dependent, KA oscillations may depend more on PV+ interneurons than spontaneous oscillations as both PV+ interneuron density and the increase in KA oscillation power follow the same pattern of change in A30P mice; KA sensitivity normalises with ageing to a level of excitability similar to WT10+ mice, as pyramidal cell excitability and PV+ cell density normalise too.

The reason for an increase in oscillation power with KA but not with CCH in A30P2+ mice remains to be explored (Robson *et al.*, 2018). However, it is likely due to the populations of neurons targeted by KA and the receptors that these subtypes possess. It is of note that in addition to the increased power of KA-induced oscillations in A30P2+ mice, they also tended to oscillate at a faster frequency. Indeed, in different strains of laboratory mice different frequencies of oscillations have been found to occur, and differences in the subunits of GABA<sub>A</sub> receptors has been suggested to explain this (Heistek *et al.*, 2010). As A30P2+ mice have been shown in this thesis to exhibit a higher IPSP frequency recorded in CA3 pyramidal cells, it follows that GABA decay kinetics may be faster and as a result a faster frequency could occur (Otis and Mody, 1992; Heistek *et al.*, 2010; Lee and Jones, 2013).

Interestingly, in A30P2+ mice only slices from the dorsal hippocampus exhibited IIDs in response to KA, whereas in human epilepsy cases it is the anterior (ventral) hippocampus that is specifically more vulnerable to bursting and seizure initiation (Strange *et al.*, 2014). Whilst no differences in the dorsal/ventral hippocampus were

found elsewhere in this thesis, including in PV+ interneuron density, it is possible that KA receptors may differ along the hippocampal axis in mice. This is supported by the finding in this chapter that the GABA<sub>A</sub> receptor antagonist gabazine produced IIDs equally in dorsal and ventral hippocampal slices in A30P2+ mice.

It is noteworthy that not every slice exhibited IIDs in response to KA, even when originating from the same animal. Care was taken in this thesis to only perform immunohistochemistry on slices that did not exhibit IIDs. However, further immunohistochemical investigations into interneuron density and kainate receptor distributions in slices that exhibited IIDs in response to KA should be explored to elucidate what confers sensitivity or vulnerability to KA-induced excitability.

A small cohort of slices from young *PDGF* WT ASYN mice also exhibited IIDs, though in a lower proportion of slices than in A30P2+ mice. While this supports the finding that excitability may be common to models of alpha-synucleinopathy, the lower proportion of slices with IIDs in *PDGF* WT ASYN mice may be due to human WT ASYN over-expression often leading to a slower onset of symptoms and pathology than human mutant ASYN mice (Jensen *et al.*, 1998; Nielsen *et al.*, 2013; Sahay *et al.*, 2015; Flagmeier *et al.*, 2016). Whilst *PDGF* WT ASYN mice have previously been shown to express human ASYN in hippocampal pyramidal cells and a subset of unspecified GABAergic interneurons (Amschl *et al.*, 2013), the differential presence of human ASYN in different interneuron subtypes has not yet been explored. Furthermore, the extent to which human ASYN expression is a result of the extracellular spread of ASYN as opposed to what is expressed under the *PDGF* promoter can only be explored by further characterisation of the *PDGF* promoter.

#### **4.5.2 Increased sensitivity to GABA<sub>A</sub> receptor antagonism in A30P2+ mice**

It has long been reported that disinhibition leads to epileptiform events (Martin and Sloviter, 2001; Kanamori, 2015) and this thesis demonstrated evidence of underlying network hyperexcitability in slices from A30P2+ mice in response to GABA<sub>A</sub> receptor antagonist gabazine. While slices from A30P2+ mice showed IIDs at the same concentration as WT2+ mice for the first time, by the time the concentration of gabazine reached 500 nM it was clear that slices from A30P2+ mice were more sensitive to gabazine's effects. This was somewhat surprising, given that A30P2+ mice show increased GABAergic activity in *Chapter 3* of this thesis. Instead, it was expected that slices might be more resistant to the effects of gabazine if the increase in GABAergic activity was truly a compensatory network change to increase inhibition.

Whilst it was expected that the increased GABAergic inhibition would be sufficient to prevent IIDs in A30P2+ mice, it is possible that inhibition in A30P2+ mice is increased but dysfunctional. There is evidence that excess inhibition can also lead to excitability in absence epilepsy (Cope *et al.*, 2009), though the exact mechanisms by which this occurs are still unknown. A study exploring temporal lobe epilepsy in rats found that reduced dendritic inhibition of pyramidal cells may decrease seizure threshold, whereas increased somatic inhibition of pyramidal cells may prevent seizures (Cossart *et al.*, 2001). CB+ interneurons primarily target the dendrites of pyramidal cells, and as this thesis found evidence of decreased CB+ interneuron density in slices from young A30P mice this may be a mechanism by which seizure threshold is decreased. An increase in PV+ interneuron density may therefore be a compensatory attempt to increase somatic inhibition and prevent seizures.

Excess inhibition can be further modulated by astrocytes removing excess GABA and releasing glutamate (Perea *et al.*, 2016), thereby decreasing inhibition and increasing excitation. Interestingly, aggregates of ASYN are found in astrocytes in both patients and mouse models of alpha-synucleinopathy (Gu *et al.*, 2010). Dysregulation in the astrocytic regulation of excitability could therefore be a factor influencing hyperexcitability within the hippocampal network.

It was somewhat surprising to find that the density of CA3 region GFAP+ astrocytes was reduced in slices from young A30P mice compared to young WT mice. This finding is complicated by the fact that GFAP+ cell density appears to decrease with ageing in WT mice and to slightly increase with ageing in A30P mice. A deficiency in GFAP immunoreactivity is a phenotype not commonly reported, and this is certainly the first time it has been reported in A30P mice. There is evidence of reduced GFAP+ cell density in the anterior cingulate cortex of sheep following a high dose of lipopolysaccharide *in utero* (Gantert *et al.*, 2012). Lipopolysaccharide is used to activate an immune response and interestingly the authors also found a reduction in CB+ and PV+ cell density. This is proposed to model glutamatergic dysfunction in schizophrenia, including a reduction in GFAP reactivity (Gantert *et al.*, 2012).

GFAP+ astrocyte density normalised with ageing in A30P mice, and this could be a result of increased excitability in young A30P mice leading to activation of astrocytes through increased metabolic requirements, or the activity-dependent release of extracellular ASYN stimulating astrocyte reactivity (Paillusson *et al.*, 2013). The *Thy-1* promoter does not express in glial cells (Feng *et al.*, 2000; Porrero *et al.*,

2010), and therefore any future work exploring the presence of human ASYN in astrocytes in A30P mice must consider the mechanism by which ASYN appears there.

The finding of normalised GFAP+ astrocyte density in A30P10+ mice compliments a previous study which found no overall changes in GFAP+ cell density in A30P mice at 11 months of age, though the authors did observe an increase in GFAP immunoreactivity in regions with higher human A30P ASYN expression (Ekmark-Lewen *et al.*, 2018). The group that generated the *Thy-1* A30P mouse found an increase in GFAP+ astrocytes in A30P mice that survived to 20 months of age, and interestingly obesity caused by a high fat diet led to an accelerated increase in GFAP+ astrocytes by 16 months of age (Rotermund *et al.*, 2014). Importantly, it has previously been confirmed that the body weight of A30P mice was not different to age-matched WT control mice (Ekmark-Lewen *et al.*, 2018).

A change in GFAP immunoreactivity is suggested to represent a change in protein expression as opposed to changes in the number of astrocytes (Serrano-Pozo *et al.*, 2013). The fact that healthy human tissue is at times not immunoreactive for GFAP at all (Sofroniew and Vinters, 2010) emphasises the need for additional markers of astrocytic function in future studies to avoid the limitations of this study in determining what change is actually occurring with age. It is possible that a reduction in GFAP in slices from A30P2+ mice could therefore represent either a deficiency in the astrocytic response, or neuroprotection in response to early hyperexcitability.

#### **4.5.3 Functional output of cortical hyperexcitability *in vivo***

One functional consequence of hyperactivity and excess excitability within the hippocampus has been reported previously in the form of increased locomotor activity (Procaccini *et al.*, 2013). Evidence of increased hippocampal excitability presented so far in this thesis could explain why young A30P mice showed increased locomotor activity in the open field test compared to young WT mice. However, it was surprising to find that A30P mice exhibited increased locomotor activity with ageing, given evidence in this thesis of normalised excitability with age. Two possibilities exist for this: that hyperlocomotion is a result of hyperexcitability spreading beyond the hippocampus with ageing, or that the underlying cause of the hyperlocomotion differs from the cause in A30P2+ mice. This is supported by the finding that the distance travelled in the first 5 minutes of the open field test appeared to differ between WT10+ and A30P10+ mice. This was not seen in WT2+ and A30P2+ mice and may suggest that the nature of the hyperlocomotion differs in young and ageing A30P mice.

Increased neuronal activity in the hippocampus as measured by c-fos has been linked to hyperlocomotion in rodents (Procaccini *et al.*, 2013), though a number of other underlying causes have been reported and this thesis did not investigate the source of the hyperlocomotion in A30P mice. The possibility that hyperlocomotion is associated with changes in the basal ganglia should not be ignored, though may still be associated with a similar mechanism of hyperexcitability. NMDA-receptor antagonism (Ma *et al.*, 2012), hippocampal lesion and altered GABA transmission (Francois *et al.*, 2009), and dopamine receptor agonism (O'Neill and Shaw, 1999) have also been shown to increase locomotor activity in rodents. Indeed, in slices exposed to human WT ASYN oligomers, a reduction in LTP occurs through activation of NMDA receptors (Diogenes *et al.*, 2012), and a possible NMDA-receptor dysfunction should be explored further.

Whilst the results presented in this thesis complimented a previous study using A30P mice in which increased locomotor activity was observed at 12 months of age prior to severe motor dysfunction (Freichel *et al.*, 2007), the same study did not find increased locomotor activity at 4 months. A more recent study using a larger cohort of A30P mice described reduced locomotor activity at 8 months that was then similar to control mice by 11 months of age (Ekmark-Lewen *et al.*, 2018). Discrepancies in the literature can be reconciled by the fact that behavioural testing is subject to much variability (room conditions, experimenters present etc.) and it is therefore important to report all details of the experimental procedure. In this thesis, care was taken to ensure animals were left undisturbed during the testing process and that all experiments were carried out over the same 4 hour period in the morning over 2-3 days to control for the circadian effect on locomotor activity (Eckel-Mahan and Sassone-Corsi, 2015).

While Freichel *et al.* (2007) examined locomotor activity over a period of 120 minutes, Ekmark-Lewen *et al.* (2018) did so for only 20 minutes, though the study did benefit from the use of a larger cohort of mice. The period of time spent in the open field arena is important to consider. In this thesis, distance travelled decreases over time with habituation until a plateau is reached at around 60 minutes in the open field arena. Therefore, use of a shorter testing time of 20 minutes may instead represent the initial habituation period and the exploratory response to a novel environment in A30P mice. As aged A30P mice have been reported to exhibit reduced exploratory behaviour (Keane, 2013), comparison beyond the initial habituation period may be more appropriate than comparison during habituation. Discrepancies in the literature may further be explained by physiological differences in locomotion between different

strains of C57BL/6 mice. It is therefore important to consider for future experiments based on this thesis that the strain and source of control mice remains consistent.

Other studies do not mention the time of day that testing was carried out, and whether mice were alone in the room during this time, so even with a smaller sample size than Ekmark-Lewen *et al.* (2018), I am confident that confounding factors were controlled for in this thesis. Future investigations should employ a video tracking system to monitor anxiety and exploratory behaviour, given evidence of amygdala pathology, impairment in fear conditioning (Freichel *et al.*, 2007), and reduced exploratory behaviour in aged A30P mice (Keane, 2013).

## 4.6 Conclusion

This chapter has demonstrated an intrinsic pyramidal cell and hippocampal network excitability in slices from A30P2+ mice, which may lead to compensatory changes in inhibition or drive the increase in GABAergic activity reported in *Chapter 3*. Hyperexcitability of excitatory cells was revealed through KA-receptor agonism to drive excitation beyond what inhibition can control, and through GABA<sub>A</sub> receptor antagonism to remove inhibition and expose the more excitable excitatory network. It is proposed that changes in seizure threshold may be a result of CB+ interneuron loss in young A30P mice, with an attempt to compensate for this by the increase in PV+ interneurons. However, an increase in inhibition is not always effective inhibition.

Excitability may be underpinned by changes in GFAP+ astrocytes as a result of ASYN uptake in glial cells, with fewer activated astrocytes in the CA3 region of slices from A30P2+ mice compared to WT2+ mice. Furthermore, astrocytes have the ability to convert inhibition to excitation, or excitation to inhibition, and this regulation of excitability is crucial for network balance. It is proposed that astrocytes may either occupy a neuroprotective state in young A30P mice, or possess a deficient response, and their phenotype should be explored in future. In *Chapter 5*, changes in A30P10+ mice as a consequence of early excitability and excitotoxicity will be explored.



## **Chapter 5. Age-Dependent Network Deficits in A30P mice**



## 5.1 Introduction

Network hyperexcitability can lead to a number of consequences as a result of excitotoxicity, most notably cellular dysfunction or even cell death. Hippocampal rhythms relevant to cognition depend heavily on the function and interplay between pyramidal cells and interneurons and as a result, fast network oscillations will be explored in this chapter. While it has been shown so far in this thesis that no difference in spontaneous or KA-induced gamma-frequency oscillations exist in A30P10+ mice, a third model of carbachol (CCH)-induced network oscillations was previously shown to be impaired in 9+ month old A30P mice by our group (Robson *et al.*, 2018).

CCH drives oscillations through the cholinergic network and given that both AD and alpha-synucleinopathy present with cholinergic deficits underpinning cognitive dysfunction, this is perhaps the most interesting network oscillation inducer to consider in A30P10+ mice. Whilst A30P mice do not show a cholinergic deficit at 2-3 months of age, they have been shown to exhibit a loss of septal cholinergic neurons when treated with mitochondrial Complex I toxin MPTP (Szego *et al.*, 2013). Evidence of a cholinergic deficit in aged A30P mice has not been explored, though the association between mitochondrial function and neuronal survival is interesting to consider.

Hippocampal gamma-frequency oscillations have been reported to decrease in power as a result of physiological ageing in mice between 16 months (Driver *et al.*, 2007) and 22 months of age (Vreugdenhil and Toescu, 2005). As our group found an age-dependent reduction in gamma-frequency oscillation power in A30P mice, it was of interest to explore this deficit in greater detail using age-matched WT mice. Furthermore, this chapter will expand upon published findings by using a narrower 10-13 month age group, as well as a WT control bred directly from the A30P line.

It is apparent so far in this thesis that hyperexcitability has decreased in A30P mice by the time they are 10-13 months of age. Whilst no loss of PV+ or CB+ interneurons were found in A30P10+ mice in *Chapter 3*, it is possible that cellular dysfunction may instead occur with ageing in A30P mice. Notably, it is proposed that deficits may be underpinned by mitochondrial dysfunction, and indeed functional mitochondria have been shown to be essential for fast network oscillations (Kann *et al.*, 2011; Whittaker *et al.*, 2011; Robson *et al.*, 2018). Mitochondrial dysfunction can occur as the result of mutations within components of the ETC, and mitochondrial mutations have further been linked to increased ROS production in PD (Hwang, 2013).

Indeed, ASYN has been shown to accumulate in mitochondria under conditions of stress in dopaminergic neurons of both PD patients and A53T mutated ASYN mouse models (Devi *et al.*, 2008; Chinta *et al.*, 2010), suggesting that physiologically ASYN is protective to mitochondria. However, pathological accumulation of ASYN or aggregated ASYN has been reported to lead to mitochondrial Complex I inhibition (Devi *et al.*, 2008; Reeve *et al.*, 2015). Recently, I have shown an increase in mitochondrial dysfunction with ageing in A30P mice (Robson *et al.*, 2018) and this dysfunction will be explored in greater detail in this chapter.

One final factor to be explored is based on evidence of low-grade inflammation and microglial activation in post-mortem tissue in DLB (Mackenzie, 2000; Mackenzie, 2001). Furthermore, *Chapter 4* of this thesis described evidence of a decrease in GFAP+ astrocyte density in A30P2+ mice. A decrease in GFAP immunoreactivity has previously been described following lipopolysaccharide injection to sheep *in utero* (Gantert *et al.*, 2012). Exposure to lipopolysaccharide triggers an immune response, and this highlights the important association between astrocytes and inflammation.

As with astrocytes, microglia can occupy both pro-inflammatory and anti-inflammatory states, and occupying the correct inflammatory state is just as important as the timing at which it occurs. Pro-inflammatory microglia are essential for the clearance of misfolded and aggregated ASYN (Codolo *et al.*, 2013), and this would explain their increase in patient tissue at the end-stage of disease. However, microglial immunoreactivity at this stage would appear to be too little too late in the clearance of aggregated ASYN and prevention of network dysfunction. Therefore, the immunoreactivity of Iba1 in microglia will be examined in young and ageing A30P mice to establish the neuroprotective steps taken by microglia in alpha-synucleinopathy and at which stage this might fail.

## 5.2 Aims

- Explore age-related network deficits in A30P10+ mice compared to age-matched WT controls.
- Expand on the finding of an age-dependent impairment in CCH-induced gamma-frequency oscillation power and mitochondrial dysfunction published in (Robson *et al.*, 2018).

### 5.3 Methods

A proportion of slices were pre-incubated in the recording chamber with circulating D-AP5 (100  $\mu$ M) in aCSF for 1 hour. Control slices without D-AP5 were left for 1 hour in drug-free conditions. Following this, gamma-frequency oscillations were induced using 10  $\mu$ M Carbachol (CCH) with extracellular local field potential recordings made from region CA3 in the *st. radiatum*. The induction of oscillations occurred within the first 30 minutes of CCH application. As a result, 30 minutes was the first time point at which 15 – 45 Hz area power ( $\mu$ V<sup>2</sup>), peak frequency (Hz), and rhythmicity index (RI) were compared as if a slice were to oscillate it would be oscillating by this point.

The time-dependent build-up in the area power of CCH gamma-frequency oscillations was recorded only in CA3 *st. radiatum* and occurred over 2-4 hours following CCH application. The majority of slices reach a stable endpoint where the area power fluctuates < 10% over time. Recordings were continued to 4 hours as more than 80% of slices from WT mice stabilised within this time.

When data were normalised for build-up analysis, area power or peak frequency were normalised to the stable endpoint of 100%. Small fluctuations occur following stability up to 4 hours. Recordings were performed throughout the entire build-up period, but data were presented over a 1 minute epoch every 30 minutes in this thesis.

Following stability, a second electrode was moved to the CA1 *st. radiatum* to monitor the propagation of CCH-induced oscillations from region CA3 to CA1. A cross-correlation to measure the time delay (ms) of signal propagation between regions CA3 and CA1 was performed as described in *Chapter 2.6*.

Free-floating DAB peroxidase immunohistochemistry for the density of Iba1+ microglia was carried out as described in *Chapter 2.7* and measured by Iba1+ cells per mm<sup>2</sup>. Slices used for immunohistochemistry did not exhibit IIDs.

COX/SDH histochemistry as a measure of mitochondrial dysfunction was performed according to *Chapter 2.9*, based on previous work from the Mitochondrial Research Group at Newcastle University (Betts *et al.*, 2006; Robson *et al.*, 2018).

## 5.4 Results

### 5.4.1 Build-up of hippocampal CCH-induced oscillations

Following bath application of the cholinergic agonist CCH (10  $\mu$ M), extracellular field recordings were performed in the CA3 *st. radiatum*. The majority of slices presented with a discernible peak within the 15 – 45 Hz range within 30 minutes of CCH application (“induction”). Following this initial induction period, the area power of CCH-induced gamma-frequency oscillations increased over 2-4 hours (“build-up”) before reaching a plateau of “stability” (Figure 5.1A), as defined in *Chapter 5.3*.

A similar proportion (Figure 5.1B) of slices from WT2+ mice (86.6%; 13/15 slices) stabilised within 4 hours compared to slices from A30P2+ mice (94.1%; 16/17 slices) ( $\chi^2$  (df 1) = 0.52,  $p > 0.05$ , chi-square test). Conversely, significantly fewer slices from A30P10+ mice (60.0%; 12/20 slices) reached stability within 4 hours, compared to slices from WT10+ mice (80.0%; 12/15 slices) ( $\chi^2$  (df 1) = 3.86,  $p < 0.05$ , chi-square test; effect size = 0.63, power (1 –  $\beta$ ) = 0.56). Post-hoc power analysis revealed that this experiment was underpowered. Future experiments could incorporate a larger sample size, which would improve the observed power and detect small differences in the number of slices reaching stability with greater confidence.

Of the slices that did not reach stability, two patterns of activity emerged: oscillations that continued to increase in power, and oscillations that decreased in power and collapsed. A similar proportion of slices from WT2+ mice (6.7%; 1/15 slices) and A30P2+ mice (5.9%; 1/17 slices) exhibited oscillations that continued to rise in power ( $\chi^2$  (df 1) = 0.01,  $p > 0.05$ , chi-square test). In comparison, slices from A30P10+ mice never showed this pattern of activity (0/20 slices) whereas 6.7% of slices from WT10+ mice did (1/15 slices) ( $\chi^2$  (df 1) = 1.37,  $p > 0.05$ , chi-square test).

Instead, 40.0% of slices from A30P10+ mice (8/20 slices) exhibited a collapse in oscillation power, compared to just 13.3% of slices from WT10+ mice (2/15 slices). This was a statistically significant difference ( $\chi^2$  (df 1) = 3.90,  $p < 0.05$ , chi-square test; effect size = 0.83, power (1 –  $\beta$ ) = 0.77). Post-hoc power analysis revealed that this comparison was slightly underpowered, likely due to a marginal difference in the proportion of slices exhibiting a collapse in oscillations. Increasing the sample size in future experiments could increase confidence that the observed effect was significant.

Conversely, collapsing oscillations were never seen in slices from A30P2+ mice (0/17 slices) and in only 6.7% of slices from WT2+ mice (1/15 slices) ( $\chi^2$  (df 1) = 1.17,

$p > 0.05$ , chi-square test). It should be noted that though several collapsing oscillations reached a high area power value before collapsing as illustrated in Figure 5.1A, several oscillations were of a low power before collapse. It can therefore be inferred that collapse does not always follow an unsustainable increase in oscillation power.

To further explore the increased number of slices from A30P10+ mice that did not stabilise within 4 hours and instead collapsed in CCH, it was confirmed that this difference was not dependent on dorsal/ventral hippocampal slice location when data were separated ( $\chi^2$  (df 1) = 0.55,  $p > 0.05$ , data not shown, A30P10+ dorsal  $n = 14$  slices, A30P10+ ventral  $n = 11$  slices; chi-square test).

Interestingly, the difference in stability was potentially dependent on sex, as none of the 4 slices from male A30P10+ mice reached stability within 4 hours compared to 75.0% of slices from female A30P10+ mice (12/16 slices). This was confirmed as statistically significant ( $\chi^2$  (df 1) = 7.5,  $p < 0.05$ , data not shown, chi-square test), though a low sample size of male A30P10+ mice means this should be investigated further. Regardless, in this thesis all subsequent analysis of stable CCH-induced oscillations will only include slices from female A30P10+ mice.



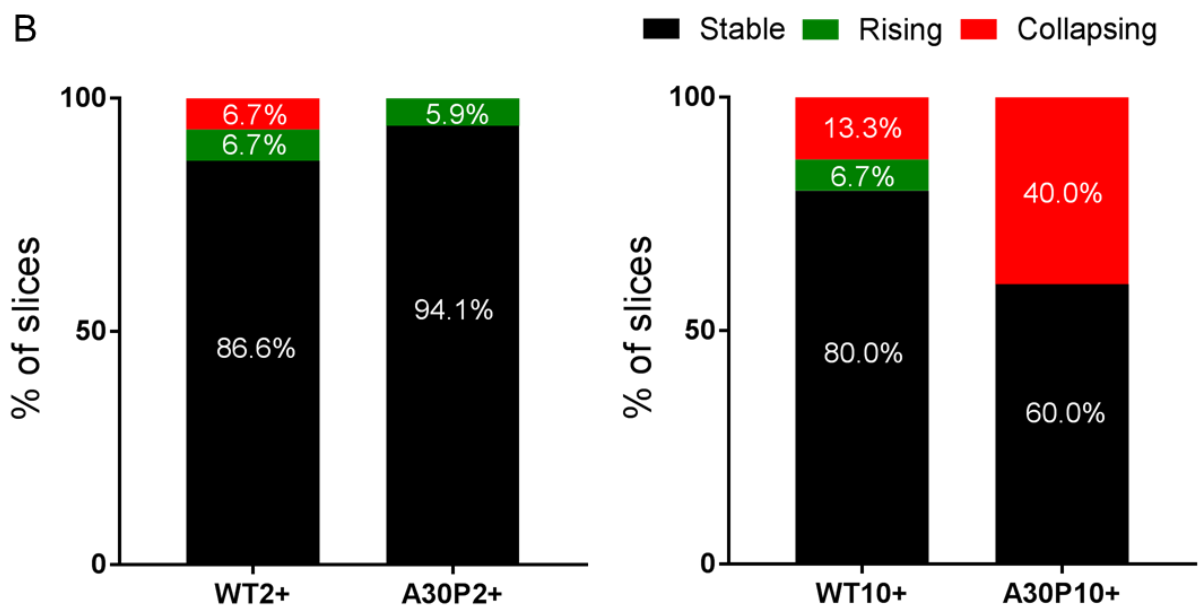
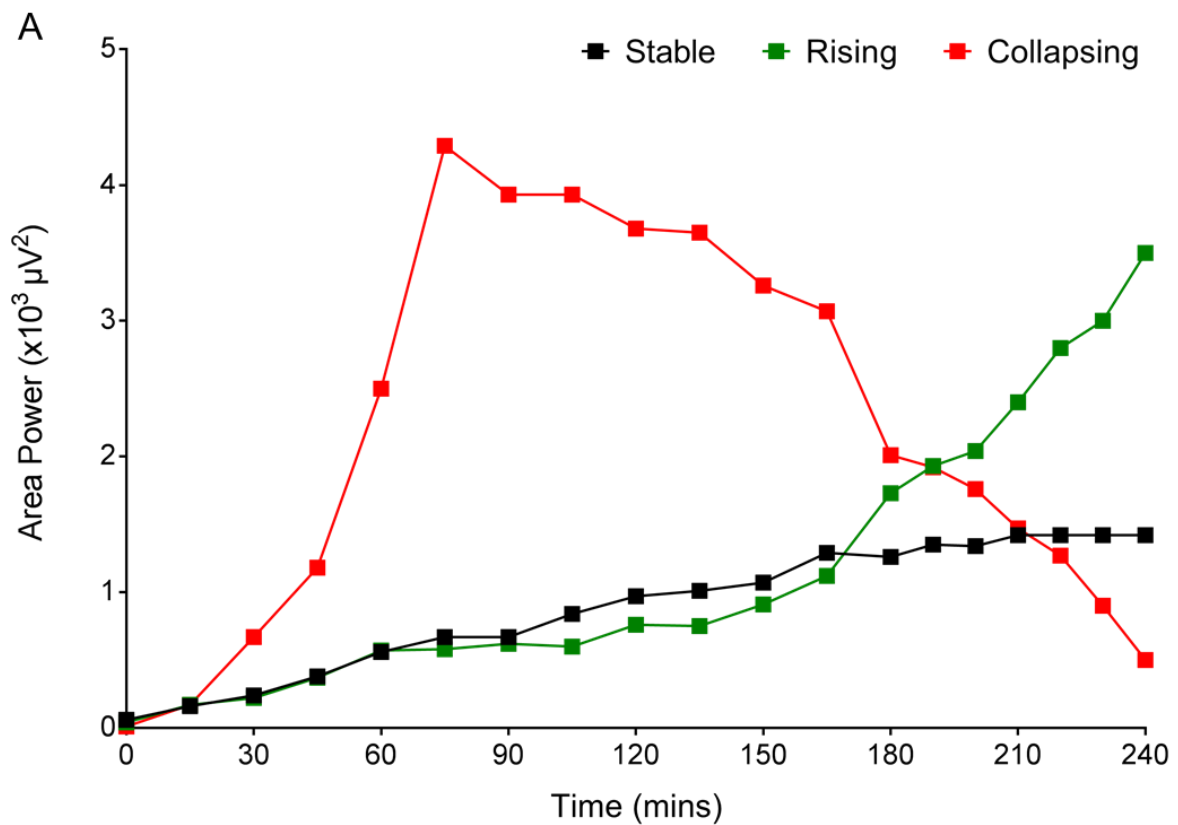


Figure 5.1 **Time-dependent changes in CCH-induced oscillations.** Representative examples from WT2+ mice (A) showing a gradual time-dependent build-up in area power that stabilises within 4 hours (black), a rising build-up (green), and a collapsing build-up (red). Proportion of slices exhibiting each type of build-up (B) in slices from WT2+ (n = 15 slices from 9 mice), A30P2+ (n = 17 slices from 9 mice), WT10+ (n = 15 slices from 9 mice), and A30P10+ mice (n = 20 slices from 7 mice).

#### 5.4.2 The time-dependent build-up of CCH-induced gamma-frequency oscillations is an NMDA-receptor dependent process

The mechanisms underlying the time-dependent build-up in power of persistent CCH gamma-frequency oscillations have not yet been elucidated in the literature. Given differences in the number of slices reaching stability in A30P mice, I decided to explore the mechanisms underlying the time-dependent build-up of CCH oscillations in WT mice. As CCH has been shown in the literature to induce LTD in acute hippocampal slices (Kumar, 2010), we theorised that the time-dependent build-up may encompass an NMDA-receptor mediated process of plasticity under physiological conditions. Once established, persistent CCH oscillations are not sensitive to application of the NMDA receptor antagonist D-AP5 (Fisahn *et al.*, 1998). I therefore decided to pre-incubate WT2+ mouse slices for 1 hour with D-AP5 (100  $\mu$ M) prior to the addition of 10  $\mu$ M CCH to explore the role of NMDA receptors in the build-up of CCH oscillations. Oscillations still emerged within 30 minutes of CCH application in the presence of D-AP5. Only slices that reached stability within 4 hours were analysed.

Interestingly, gamma-frequency oscillation area power was significantly larger in slices pre-incubated with D-AP5 (Figure 5.2A) over the entire recording period (pre-incubated 3140  $\mu$ V<sup>2</sup> [IQR 2690 – 3200] versus control 1350  $\mu$ V<sup>2</sup> [IQR 730 – 1690]; condition  $p < 0.05$ , time  $p < 0.05$ , interaction  $p > 0.05$ ; RM 2-way ANOVA on ranks; effect size = 2.03, power (1 –  $\beta$ ) = 0.99). Despite this, the area power of CCH-induced gamma-frequency oscillations still increased significantly over time. An accelerated build-up was confirmed by normalising all values to the stable endpoint (100%). Normalised data revealed a significantly accelerated build-up of CCH oscillations in D-AP5 pre-incubated slices, specifically between 30 and 90 minutes. By 90 minutes post-CCH, the D-AP5 pre-incubated slices appeared to have reached ~100% of the stable endpoint on average, while control slices did not reach this point until 180 minutes post-CCH (pre-incubated slices at 90 minutes 102.4% [IQR 25.1 – 264.3] versus control slices at 90 minutes 69.1% [IQR 37.3 – 100.6]; condition  $p < 0.05$ , time  $p < 0.05$ , interaction  $p < 0.05$ ; RM 2-way ANOVA on ranks).

The peak frequency of CCH oscillations (Figure 5.2B) was significantly slower in D-AP5 preincubated slices than control conditions overall (26.8 Hz  $\pm$  0.5 versus 28.3 Hz  $\pm$  0.2 respectively; condition  $p < 0.05$ , time  $p > 0.05$ , interaction  $p > 0.05$ ; 2-way ANOVA; effect size = 1.55, power (1 –  $\beta$ ) = 0.92). No specific time points were significantly different despite the experiment achieving an observed power of 92%.

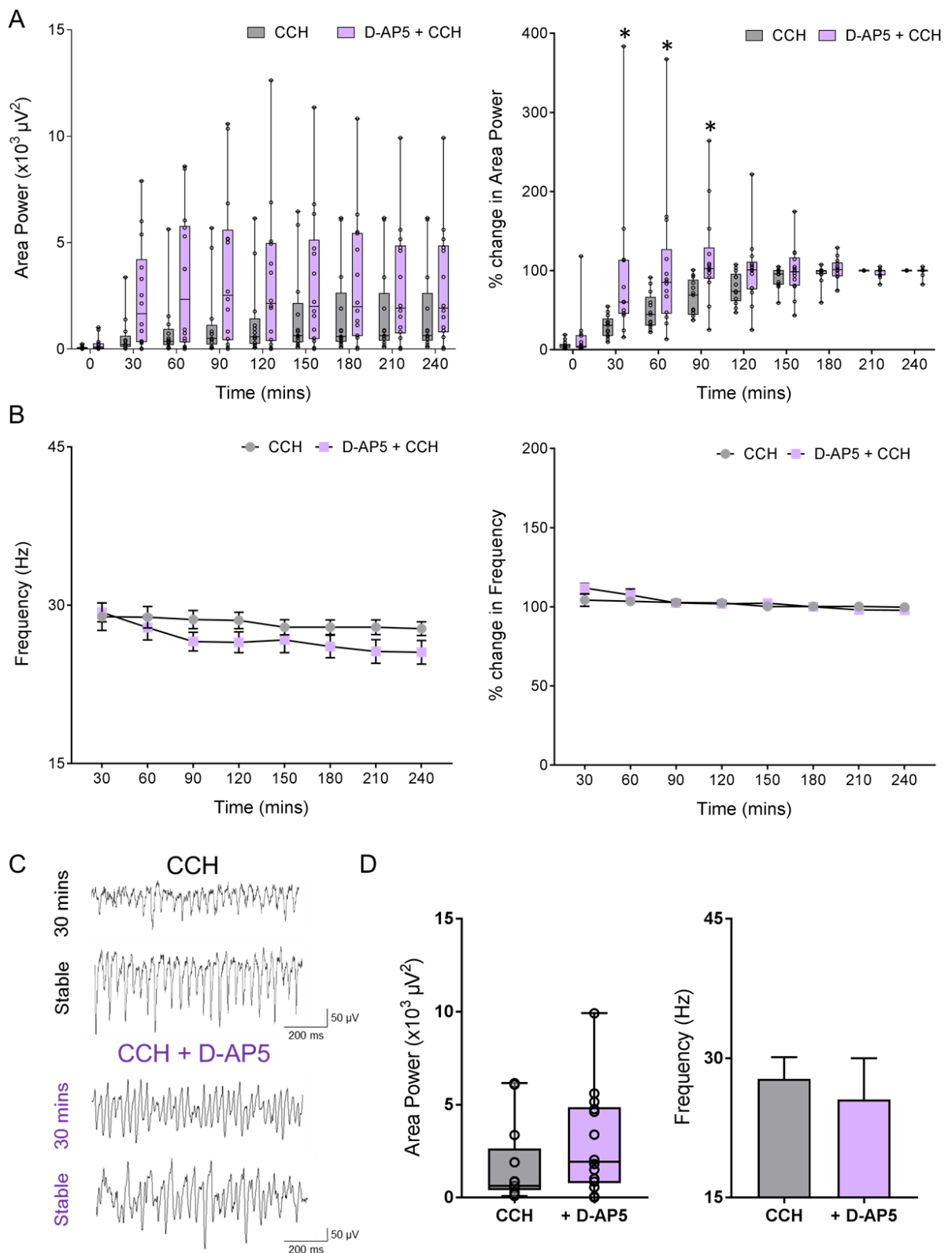


**Figure 5.2 NMDA-R antagonism accelerates CCH oscillation build-up in WT mice.** (A) Boxplots to show raw area power and % change normalised to stable endpoint with and without D-AP5 pre-incubation. (B) Line graphs to show raw peak frequency and normalised % change. (C) Representative LFP traces with scale bars inset at 30 mins post-CCH and stability. (D) Boxplot to show area power at stable endpoint. (E) Bar chart to show peak frequency at stable endpoint. WT2+ CCH control n = 13 slices from 9 mice; D-AP5 + CCH n = 14 slices from 8 mice. \* indicates significance at  $p < 0.05$ .

When data were normalised to the stable endpoint of 100%, the peak frequency was found to start at a higher frequency then decrease over time regardless of the presence of D-AP5 (control *30 minutes* 104.3%  $\pm$  3.9 to *240 minutes* 99.8%  $\pm$  0.2; pre-incubated *30 minutes* 111.9%  $\pm$  2.9 to *240 minutes* 97.8%  $\pm$  1.4; condition  $p > 0.05$ , time  $p < 0.05$ , interaction  $p > 0.05$ ; 2-way ANOVA). Frequency changes over time inversely correlate with area power changes over time; as area power values increase during the build-up period, the peak frequency of the oscillation decreases.

Within 4 hours of CCH application, 73.7% of WT2+ mouse slices pre-incubated with D-AP5 (14/19 slices) had reached stability, compared to 86.6% of slices exposed to CCH alone (13/15 slices). This was not found to be statistically significant ( $\chi^2$  (df 1) = 0.86,  $p > 0.05$ , data not shown; chi-square test). A comparison of area power at the stable endpoint (Figure 5.2D) confirmed that D-AP5 pre-incubation did not affect stable area power despite a trend towards larger values and more variability in D-AP5 pre-incubated slices (control 630  $\mu\text{V}^2$  [IQR 400 – 2640] versus pre-incubated 1920  $\mu\text{V}^2$  [IQR 780 – 4860];  $p > 0.05$ , Mann-Whitney rank sum test).

Furthermore, the peak frequency of stable oscillations was not significantly different between control and D-AP5 pre-incubated conditions despite a trend to slower oscillations in D-AP5 pre-incubated slices (control 27.6 Hz [IQR 26.6 – 29.6] versus pre-incubated 26.3 Hz [IQR 21.5 – 27.4];  $p > 0.05$ , unpaired  $t$  test). It can therefore be concluded that it is the time-dependent build-up of CCH oscillations that is NMDA receptor dependent and not the mechanisms leading to stability.

### 5.4.3 Reduced power stable CCH-induced gamma oscillations in A30P10+ mice

This chapter has so far shown that the time-dependent build-up in area power of CCH-induced oscillations is an NMDA-receptor dependent process. As a result, I decided to compare the build-up and stability of CCH-induced oscillations with respect to area power and peak frequency in the CA3 *st. radiatum* of A30P mice. Only slices that stabilised within 4 hours of CCH application were included in this section.

There was no significant difference in overall area power (Figure 5.3A) in slices from WT2+ and A30P2+ mice, though both increased in power over time during the build-up period (overall 1350  $\mu\text{V}^2$  [IQR 730 – 1690] versus 1360  $\mu\text{V}^2$  [IQR 870 – 1700] respectively; genotype  $p > 0.05$ , time  $p < 0.05$ , interaction  $p > 0.05$ ; RM 2-way ANOVA on ranks). To confirm that the time-dependent build-up was not altered in A30P2+ mice, a comparison was made with data normalised to the stable endpoint (100%), where there was a significant build-up over time irrespective of mouse genotype (WT2+ *baseline* 4.9% [IQR 1.0 – 18.8] to *240 minutes* 100% [IQR 99.8 – 100.5]; A30P2+ *baseline* 3.8% [IQR 0.5 – 33.8] to *240 minutes* 100% [IQR 100 – 104.1]; genotype  $p > 0.05$ , time  $p < 0.05$ , interaction  $p > 0.05$ ; RM 2-way ANOVA on ranks).

Following the initial induction period, the frequency of CCH oscillations in young mice decreased within the 15 – 45 Hz gamma-frequency range from 30 minutes until stability was reached (Figure 5.3B). This was a pattern seen regardless of mouse genotype (WT2+ *30 minutes* 29.5 Hz  $\pm$  0.9 to *240 minutes* 27.9 Hz  $\pm$  0.7; A30P2+ *30 minutes* 29.6 Hz  $\pm$  0.7 to *240 minutes* 27.3 Hz  $\pm$  0.5; genotype  $p > 0.05$ , time  $p < 0.05$ , interaction  $p > 0.05$ ; 2-way ANOVA). This pattern persisted when data were normalised to the stable endpoint of 100% (WT2+ *30 minutes* 104.4%  $\pm$  3.7 to *240 minutes* 100.4%  $\pm$  0.4; A30P2+ *30 minutes* 108.5%  $\pm$  1.9 to *240 minutes* 99.9%  $\pm$  0.4; genotype  $p > 0.05$ , time  $p < 0.05$ , interaction  $p > 0.05$ ; 2-way ANOVA).

Once slices had reached stability (Figure 5.3C), a further comparison was made of the stable area power and peak frequency (Figure 5.3D). There was no significant difference in stable area power between slices from WT2+ and A30P2+ mice (630  $\mu\text{V}^2$  [IQR 400 – 2640] versus 1100  $\mu\text{V}^2$  [IQR 730 – 2340] respectively;  $p > 0.05$ , Mann-Whitney rank sum test) nor was there a difference in frequency between slices from WT2+ and A30P2+ mice (27.9 Hz  $\pm$  0.7 versus 27.3 Hz  $\pm$  0.5 respectively,  $p > 0.05$ , unpaired *t* test). This data indicates that the NMDA-receptor dependent build-up in gamma-frequency oscillations is intact in slices from A30P2+ mice.

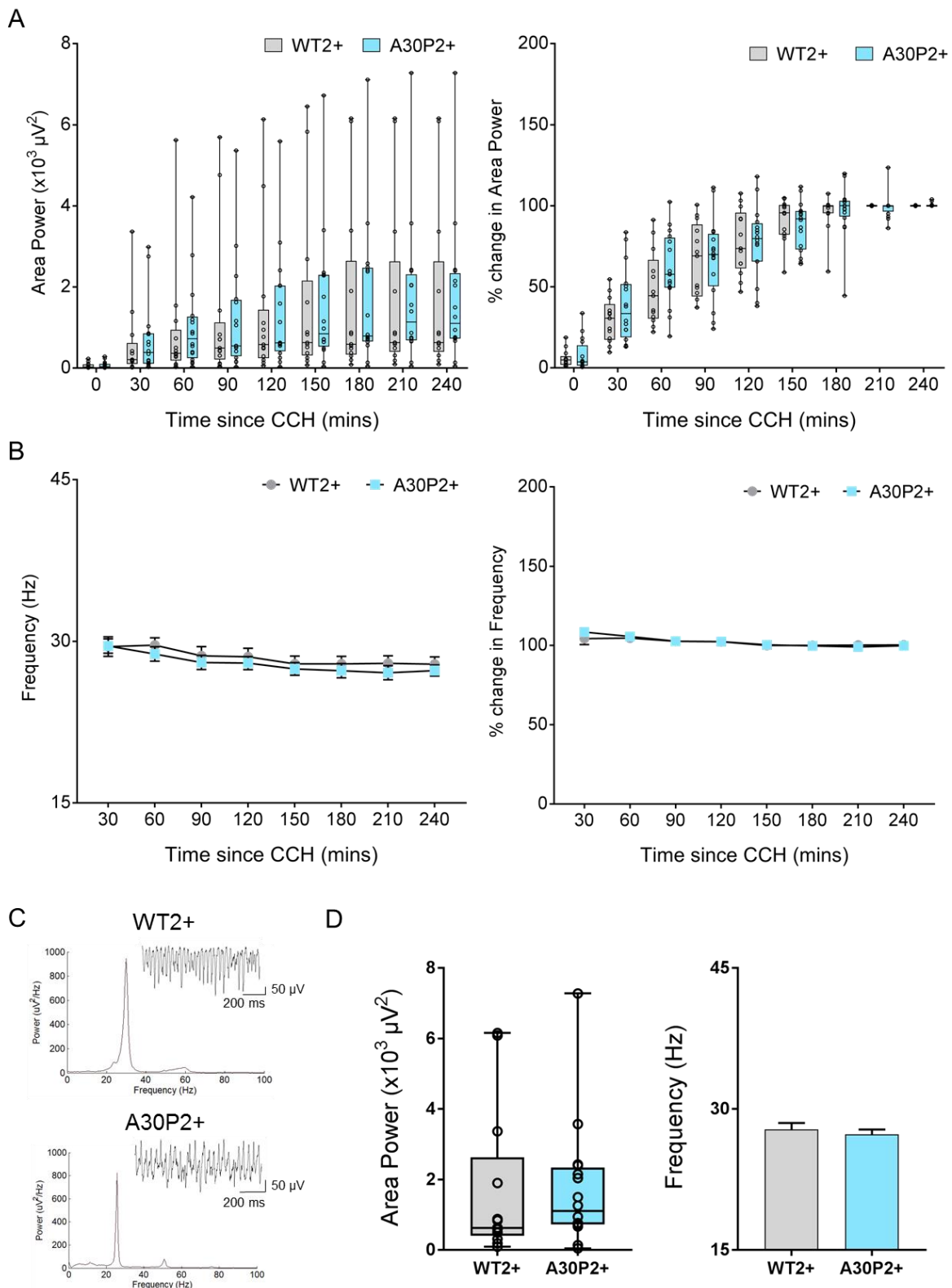


**Figure 5.3 No difference in CCH-induced oscillations in A30P2+ mice.** (A) Boxplots to show raw area power and normalised area power as % of stable endpoint in WT2+ and A30P2+ mice. (B) Line graphs to show raw frequency and normalised frequency as % of stable endpoint in WT2+ and A30P2+ mice. (C) Representative power spectra of stable endpoint with LFP inset with scale bar. (D) Boxplot to show stable area power and bar chart to show frequency of CCH-induced oscillations in WT2+ and A30P2+ mice. WT2+ n = 13 slices from 9 mice, A30P2+ n = 16 slices from 10 mice.

Work from our group has previously shown a reduction in CCH-induced gamma-frequency oscillation power in A30P mice at 9-16 months compared to 2-5 months (Robson *et al.*, 2018). For the purpose of this thesis, a narrower age group of 10-13 months was utilised and directly compared with age-matched WT controls, in addition to exploration of the time-dependent build-up of oscillation power. Once again, only slices reaching stability within 4 hours of CCH application were included in this section.

In slices from A30P10+ mice (Figure 5.4A), the area power of CCH induced oscillations was significantly smaller overall than in slices from WT10+ mice, though both increased in power over time during the build-up period (overall  $600 \mu\text{V}^2$  [IQR 310 – 690] versus  $1570 \mu\text{V}^2$  [IQR 1110 – 1860] respectively; genotype  $p < 0.05$ , time  $p < 0.05$ , interaction  $p > 0.05$ ; RM 2-way ANOVA on ranks; effect size = 1.67, power  $(1 - \beta) = 0.99$ ). No specific time-point was identified as significantly different, despite the experiment achieving an observed power of 99%. An unimpaired gamma-frequency oscillation build-up was confirmed through analysis of data normalised to the stable endpoint (100%), where a significant increase over time was observed regardless of mouse genotype (WT10+ *baseline* 6.0% [IQR 0.8 – 43.0] to *240 minutes* 100% [IQR 72.2 – 100]; A30P10+ *baseline* 11.5% [IQR 1.3 – 100] to *240 minutes* 100% [IQR 89.0 – 122.7]; genotype  $p > 0.05$ , time  $p < 0.05$ , interaction  $p > 0.05$ ; RM 2-way ANOVA on ranks. This indicates that the NMDA-receptor dependent build-up in power still occurs in slices from A30P10+ mice, despite oscillations being smaller.

Slices from A30P10+ mice were found to oscillate at a significantly faster frequency (Figure 5.4B) compared to slices from WT10+ mice overall ( $28.6 \text{ Hz} \pm 0.3$  versus  $26.7 \text{ Hz} \pm 0.3$  respectively; mouse  $p < 0.05$ , time  $p > 0.05$ , interaction  $p > 0.05$ ; 2-way ANOVA; effect size = 1.56, power  $(1 - \beta) = 0.98$ ). No specific time-point could be identified as significantly different, however, despite the experiment achieving an observed power of 98%. However, unlike in slices from A30P2+ and WT2+ mice, no change in frequency occurred during the build-up period and this was confirmed through analysis of data normalised to the stable endpoint (WT10+ *30 minutes*  $100.8\% \pm 4.9$  to *240 minutes*  $99.9 \pm 0.5$ ; A30P10+ *30 minutes*  $101.7\% \pm 4.7$  to *240 minutes*  $100\% \pm 0$ ; genotype  $p > 0.05$ , time  $p > 0.05$ , interaction  $p > 0.05$ ; 2-way ANOVA).

A comparison between stable endpoint values in slices from WT10+ and A30P10+ mice was next performed (Figure 5.4C) for stable area power and frequency (Figure 5.4D). There was a significant reduction in stable area power in slices from A30P10+ mice compared to WT10+ mice ( $300 \mu\text{V}^2$  [IQR 120 – 1190] versus  $1040 \mu\text{V}^2$

[IQR 700 – 2850] respectively;  $p < 0.05$ , Mann-Whitney rank sum test; effect size = 0.98, power  $(1 - \beta) = 0.75$ ). This indicates that in addition to smaller area power values throughout the CCH build-up period, slices from A30P10+ mice stabilise at a smaller power compared to WT10+ mice. Post-hoc power analysis revealed that this experiment was slightly underpowered. This is likely due to a small detected effect size, and increasing the sample size in future experiments could increase the observed power and as a result the certainty of obtaining a significant effect.

With respect to the peak frequency of stable CCH oscillations, no significant difference was found between slices from WT10+ and A30P10+ mice (26.7 Hz  $\pm$  0.6 versus 28.8 Hz  $\pm$  1.4 respectively,  $p > 0.05$ , unpaired  $t$  test), despite a trend to a faster frequency in slices from A30P10+ mice. It can be concluded that despite slices from A30P10+ mice oscillating at a significantly faster frequency throughout the build-up of CCH-induced gamma-frequency oscillations, when stability was reached only a trend to a faster peak frequency was observed in slices from A30P10+ mice.

It was finally confirmed that the observed reduction in A30P10+ gamma-frequency oscillation area power was not dependent on dorsal/ventral slice location by separating stable endpoint data (WT10+ *dorsal* 1120  $\mu\text{V}^2$  [IQR 710 – 2890]  $n = 7$  slices; WT10+ *ventral* 950  $\mu\text{V}^2$  [IQR 370 – 2780]  $n = 5$  slices; A30P10+ *dorsal* 320  $\mu\text{V}^2$  [IQR 100 – 1360]  $n = 7$  slices; A30P10+ *ventral* 280  $\mu\text{V}^2$  [IQR 90 – 1500]  $n = 5$  slices; mouse  $p < 0.05$ , location  $p > 0.05$ , interaction  $p > 0.05$ ; 2-way ANOVA on ranks).

The effect of sex on the age-dependent reduction in CCH-induced oscillation power could not be explored in this thesis as no slices from male A30P10+ mice reached stability within 4 hours. Previous work published by our group used a larger cohort of mice and as a result achieved similar amounts of data in male and female A30P10+ mice (Robson *et al.*, 2018). Our group concluded that the age-dependent reduction in CCH-induced oscillations was independent of sex, and as a result it is expected that data presented in this thesis might support a similar conclusion.



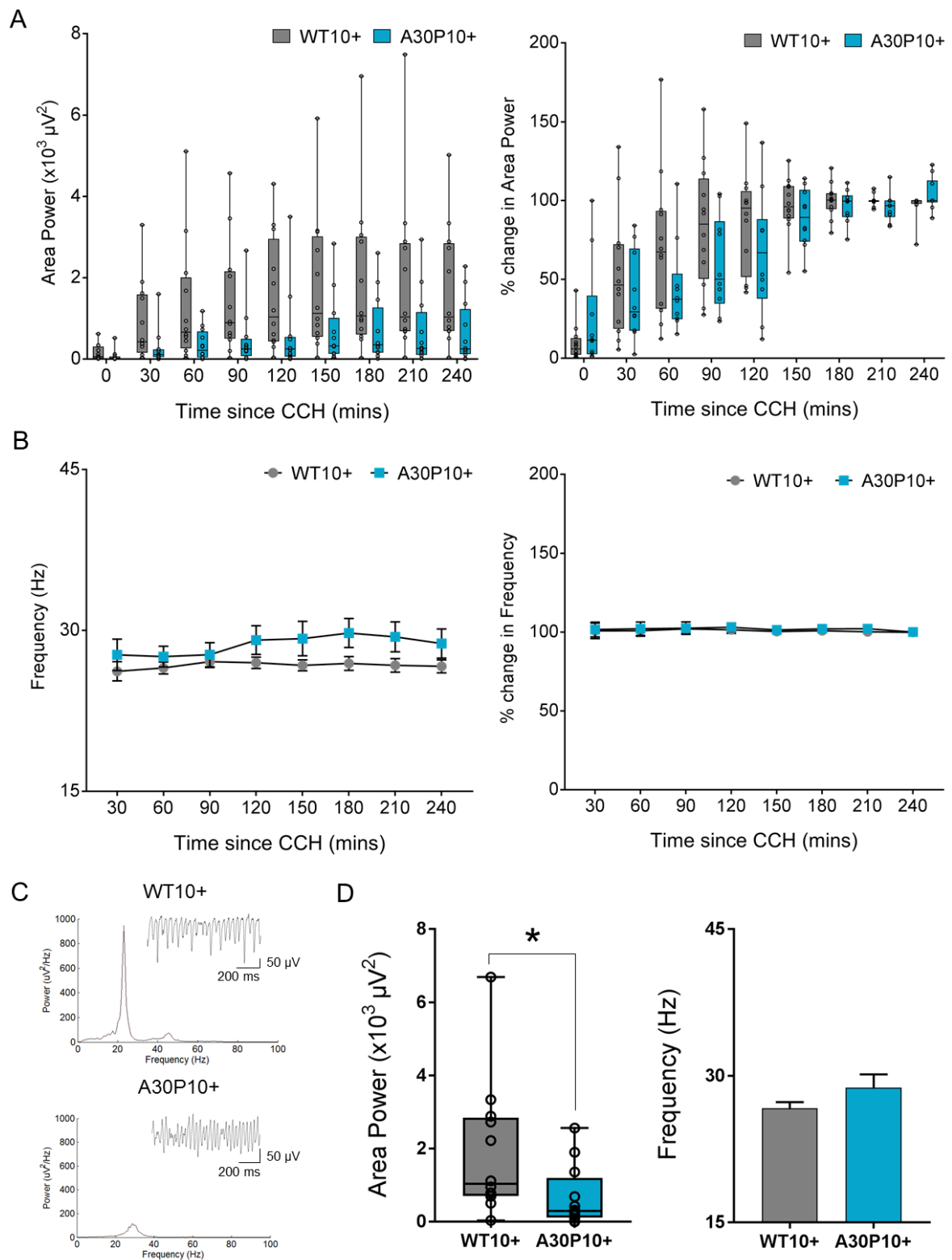


**Figure 5.4 Reduced power of CCH-induced oscillations in A30P10+ mice.** (A) Boxplots to show raw area power and normalised area power as % of stable endpoint in WT10+ and A30P10+ mice. (B) Line graphs to show raw frequency and normalised frequency as % of stable endpoint in WT10+ and A30P10+ mice. (C) Representative power spectra of stable endpoint with LFP inset with scale bar. (D) Boxplot to show stable area power and bar chart to show frequency of CCH-induced gamma oscillations in WT10+ and A30P10+ mice. WT10+ n = 12 slices from 9 mice, A30P10+ n = 12 slices from 5 mice. \* indicates significance at  $p < 0.05$ .

#### 5.4.4 No difference in CCH oscillation rhythmicity in A30P mice

The rhythmicity of an oscillation reflects the degree of synchrony within the excitatory/inhibitory network. Due to the reduction in the power of CCH-induced oscillations in slices from A30P10+ mice, I therefore went on to assess whether there were any differences in the rhythmicity of CCH-induced oscillations in slices from A30P mice. The induction of CCH-induced gamma-frequency oscillations generally occurred within the first 30 minutes following bath application, so a measure of rhythmicity index (RI) was taken at 30 minutes and compared to a measure when an oscillation was stable using AxoGraph's autocorrelation feature (Figure 5.5A-D).

Slices from WT2+ and A30P2+ mice (Figure 5.5E) showed a significant increase in rhythmicity from 30 minutes to the stable endpoint, regardless of mouse genotype. This indicates a time-dependent increase not only in the power of CCH-induced oscillations, but also in the rhythmicity of CCH oscillations. No difference was found in rhythmicity between slices from WT2+ and A30P2+ mice at either time-point examined (WT2+ 30 minutes  $0.33 \pm 0.06$  to stable  $0.57 \pm 0.06$ ; A30P2+ 30 minutes  $0.38 \pm 0.06$  to stable  $0.60 \pm 0.04$ ; genotype  $p > 0.05$ , time  $p < 0.05$ , interaction  $p > 0.05$ ; 2-way ANOVA). This was somewhat surprising given evidence so far in this thesis of changes in the excitatory/inhibitory network of young A30P mice.

The same pattern was found in slices from WT10+ and A30P10+ mice (Figure 5.5F), with an increase in rhythmicity as oscillations stabilise regardless of genotype. No difference was found between slices from WT10+ and A30P10+ mice in rhythmicity at either time-point (WT10+ 30 minutes  $0.28 \pm 0.07$  to stable  $0.44 \pm 0.06$ ; A30P10+ 30 minutes  $0.31 \pm 0.07$  to stable  $0.39 \pm 0.09$ ; genotype  $p > 0.05$ , time  $p < 0.05$ , interaction  $p > 0.05$ ; 2-way ANOVA). Interestingly, it was noted that RI tended to be smaller at stability in slices from 10-13 month old mice than in slices from 2-4 month old mice, regardless of genotype. As this appeared to be an effect of physiological ageing, this finding was not explored further in this thesis. It can be concluded that despite a reduction in the power of CCH oscillations in A30P10+ mouse slices, no change in the rhythmicity of CCH oscillations was found at either 30 minutes post-CCH, or at stability.

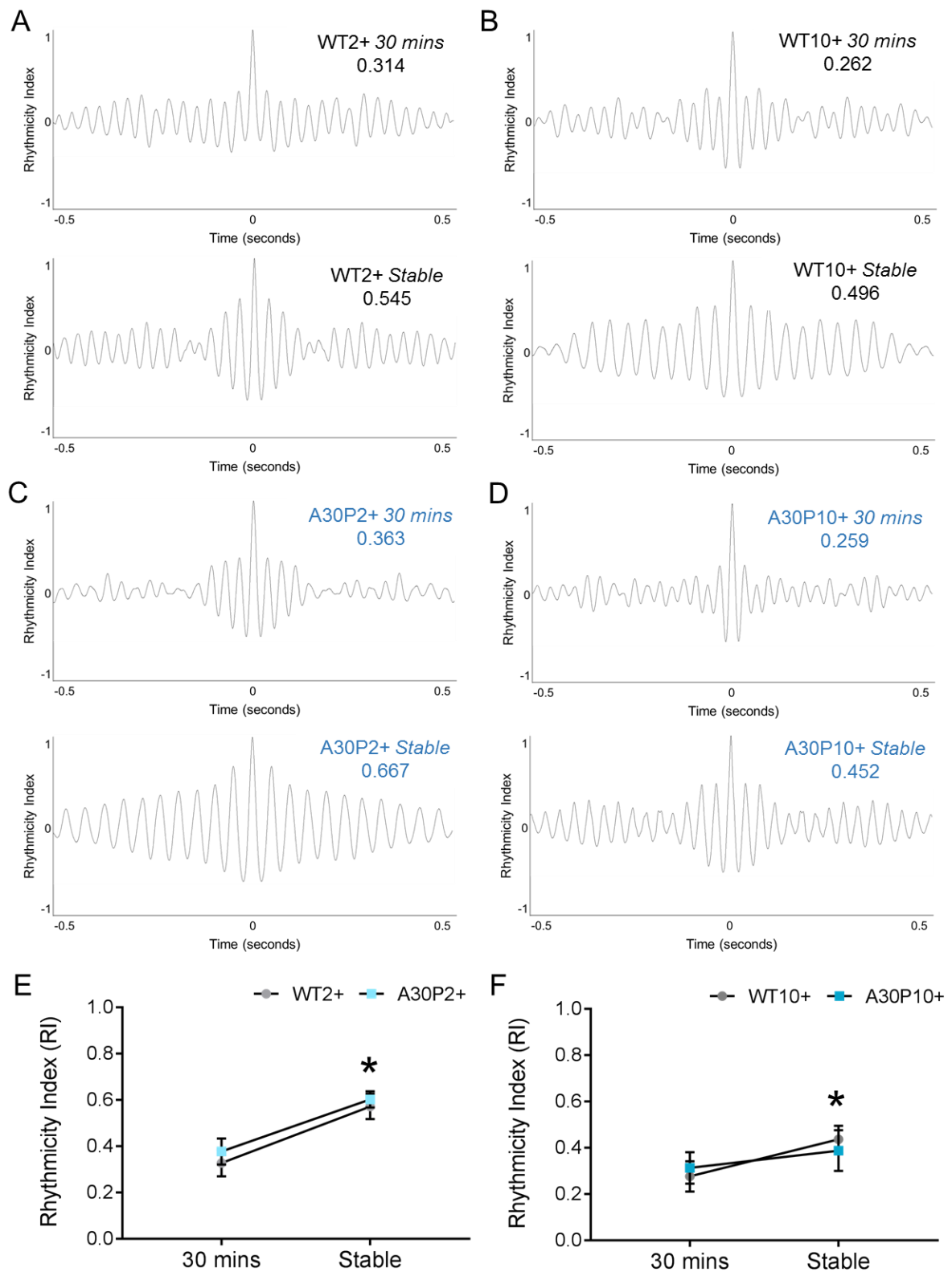


**Figure 5.5 No difference in rhythmicity of CCH-induced oscillations in A30P mice.** Representative autocorrelations with computed RI values at 30 minutes post-CCH and at the stable endpoint in slices from WT2+ mice (A), WT10+ mice (B), A30P2+ mice (C), and A30P10+ mice (D). Line graphs to show RI values in slices from WT2+ and A30P2+ mice (E), and in slices from WT10+ and A30P10+ mice (F) mice. WT2+ n = 13 slices from 9 mice, A30P2+ n = 16 slices from 9 mice, WT10+ n = 12 slices from 9 mice, A30P10+ n = 10 slices from 5 mice. \* indicates significance at  $p < 0.05$ .

#### 5.4.5 Propagation from CA3 to CA1 is intact in A30P mice

It has previously been shown that gamma-frequency oscillations are generated in the CA3 region *in vitro* and propagate to CA1 (Hajos and Paulsen, 2009). As this chapter has demonstrated evidence of a reduction in gamma-frequency oscillation power in A30P10+ mice, propagation to region CA1 may be affected. I was also interested to explore whether the deficit in region CA3 is also present in region CA1.

Recordings were made after an oscillation was stable in region CA3 by leaving one electrode in the CA3 *st. radiatum* and moving a second electrode to the CA1 *st. radiatum*. A cross-correlation was then performed (Figure 5.6A) between areas CA3 and CA1 to compute the time delay of propagation (Figure 5.6B). In slices from WT2+ and A30P2+ mice, no significant difference was found in CA3 to CA1 time delay ( $2.0 \text{ ms} \pm 0.5$  versus  $1.7 \text{ ms} \pm 0.5$  respectively,  $p > 0.05$ , unpaired *t* test). Likewise, slices from A30P10+ mice showed no significant difference in time delay compared to WT10+ mice ( $2.5 \text{ ms} \pm 0.9$  versus  $2.2 \text{ ms} \pm 0.6$  respectively,  $p > 0.05$ , unpaired *t* test), indicating that mechanisms of CA3 to CA1 propagation are intact.

I next compared the area power and peak frequency of CCH-induced oscillations in regions CA3 and CA1. Though the area power of CCH oscillations tended to be larger in the CA3 region of both WT2+ and A30P2+ mice (Figure 5.7A), no significant difference was found between regions nor between WT2+ and A30P2+ mice (WT2+ CA3  $780 \mu\text{V}^2$  [IQR 92 – 3530]; WT2+ CA1  $620 \mu\text{V}^2$  [IQR 200 – 1340]; A30P2+ CA3  $1490 \mu\text{V}^2$  [IQR 240 – 5380]; A30P2+ CA1  $540 \mu\text{V}^2$  [IQR 130 – 5070]; genotype  $p > 0.05$ , region  $p > 0.05$ , interaction  $p > 0.05$ , 2-way ANOVA on ranks).

In 10-13 month old mice, there once again appeared to be a trend to larger power values in the CA3 region compared to the CA1 region. Furthermore, the reduction in the power of CCH oscillations in slices from A30P10+ mice compared to WT10+ mice was found to occur in both the CA3 and CA1 region (WT10+ CA3  $1120 \mu\text{V}^2$  [IQR 190 – 3070]; WT10+ CA1  $650 \mu\text{V}^2$  [IQR 86 – 2540]; A30P10+ CA3  $280 \mu\text{V}^2$  [IQR 95 – 2510]; A30P10+ CA1  $270 \mu\text{V}^2$  [IQR 19 – 1250]; genotype  $p < 0.05$ , region  $p > 0.05$ , interaction  $p > 0.05$ ; 2-way ANOVA on ranks). This could indicate that the power deficit in the CA3 region of slices from A30P10+ mice also leads to a power deficit in the CA1 region due to the propagation of CCH-induced oscillations.

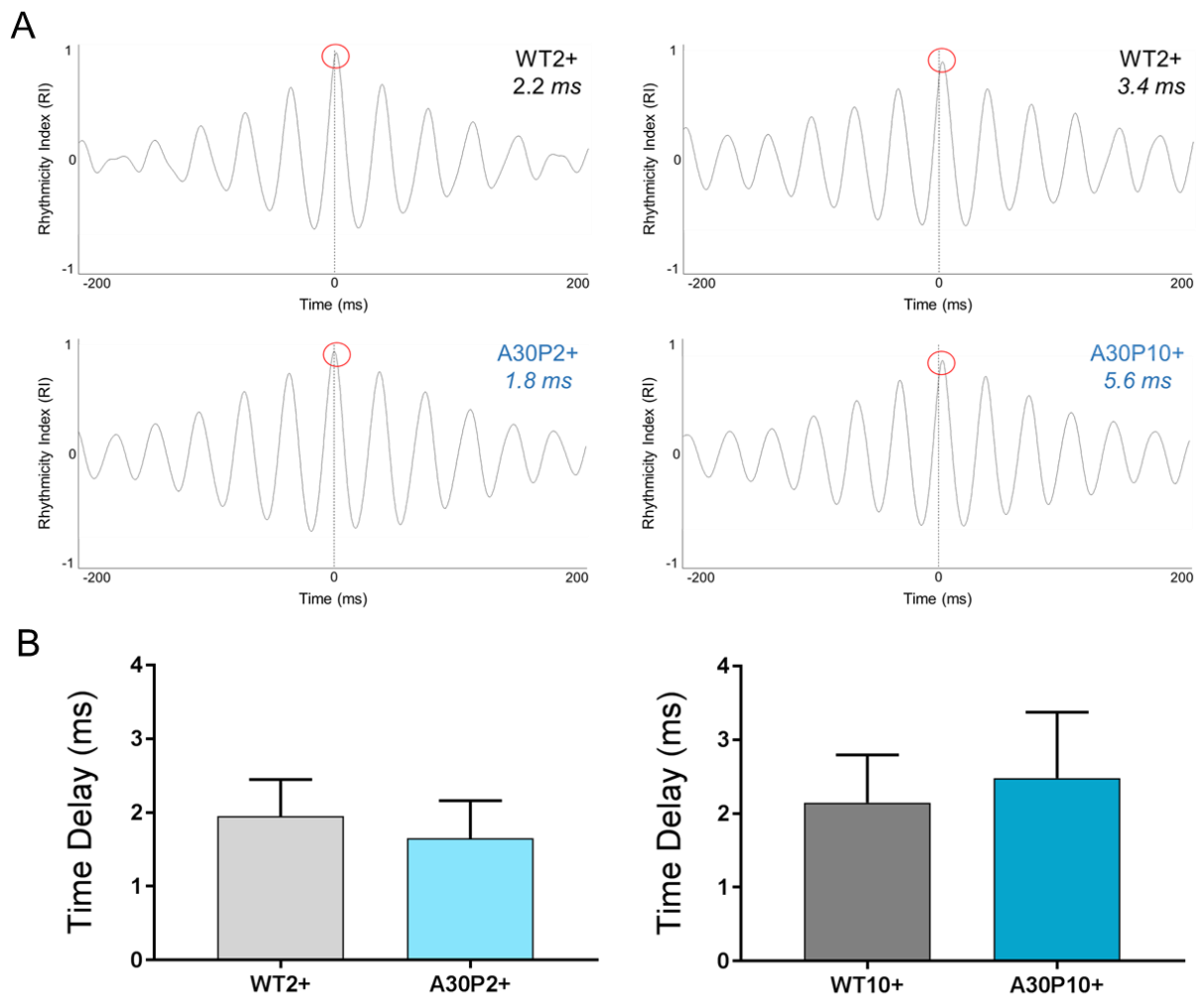
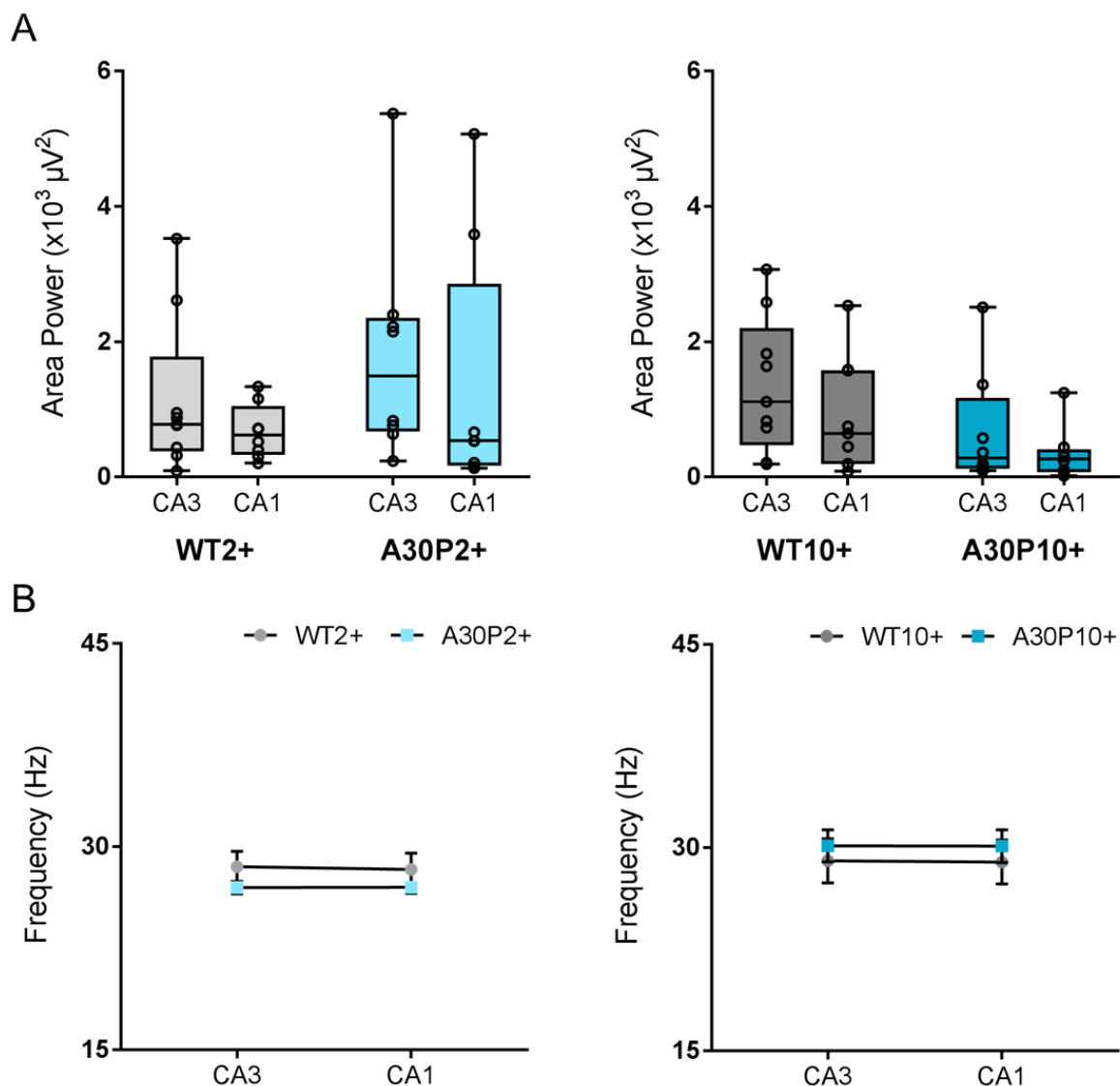


Figure 5.6 **CA3 to CA1 propagation time of CCH oscillations.** Representative time delay with values computed by cross-correlation of region CA3 to region CA1 in WT and A30P mice (A) with central peak highlighted in red and 0 ms as dotted line. Scale modified from 1000 ms to 400 ms to allow visualisation of central peak delay. (B) Bar charts to show average time delay from region CA3 to region CA1 in WT and A30P mice. WT2+ n = 4 slices from 4 mice, A30P2+ n = 4 slices from 4 mice, WT10+ n = 4 slices from 4 mice, A30P10+ n = 5 slices from 4 mice.

The peak frequency of CCH-induced oscillations within CA3 and CA1 (Figure 5.7B) was not significantly different compared to age-matched WT control mice in slices from A30P2+ mice (WT2+ CA3 28.5 Hz  $\pm$  1.1; WT2+ CA1 28.3 Hz  $\pm$  1.2; A30P2+ CA3 27.0 Hz  $\pm$  0.5; A30P2+ CA1 27.0 Hz  $\pm$  0.4; genotype  $p > 0.05$ , region  $p > 0.05$ , interaction  $p > 0.05$ ; 2-way ANOVA) or in slices from A30P10+ mice (WT10+ CA3 29.0 Hz  $\pm$  1.6; WT10+ CA1 28.9  $\pm$  1.6; A30P10+ CA3 30.1  $\pm$  1.2; A30P10+ CA1 30.1 Hz  $\pm$  1.2; genotype  $p > 0.05$ , region  $p > 0.05$ , interaction  $p > 0.05$ ; 2-way ANOVA). This indicates that despite the power deficit propagating from region CA3 to region CA1 in A30P10+ mice, the peak frequency of CCH oscillations remained similar.



**Figure 5.7 CCH-induced oscillations propagate from CA3 to CA1 in A30P mice.** (A) Boxplots to show 15- 45 Hz area power between regions CA3 and CA1 in WT and A30P mice. (B) Line graphs to show peak frequency between regions CA3 and CA1 in WT and A30P mice. WT2+  $n = 10$  slices from 7 mice, A30P2+  $n = 8$  slices from 5 mice, WT10+  $n = 9$  slices from 5 mice, A30P10+  $n = 8$  slices from 5 mice.

#### 5.4.6 Mitochondrial dysfunction in A30P15+ mice

As this chapter has so far demonstrated an age-dependent impairment in CCH-induced oscillation power and stability in A30P10+ mice, it was decided to next explore what may be causing such changes to occur. It can be hypothesised that although no loss of fast-spiking PV+ interneurons was found in *Chapter 3*, their function may still be impaired. One possible mechanism for fast-spiking interneuron dysfunction is mitochondrial dysfunction, and indeed I have previously shown a general increase in mitochondrial dysfunction between 2-5 and 9-16 months in A30P mice using COX/SDH histochemistry in work published by our group (Robson *et al.*, 2018).

I decided to explore mitochondrial function in the 10-13 month age group, in addition to a separate cohort of 15-17 month mice (A30P15+ mice), compared to age-matched WT mice (Figure 5.8A). COX/SDH histochemistry was selected as a simple technique to assess mitochondrial function, and a region including the CA3 pyramidal layer was analysed as this encompasses a large proportion of neuronal cell bodies. An increase in blue pixel density (Figure 5.8B) indicates mitochondrial dysfunction, as cells with dysfunctional Complex IV (COX) activity will stain blue rather than brown.

There was no significant difference in mitochondrial function throughout the CA3 pyramidal layer in slices from A30P2+ mice compared to WT2+ mice as measured by blue pixel density ( $45.4 \pm 1.5$  versus  $45.3 \pm 2.8$  respectively,  $p > 0.05$ , unpaired *t* test), nor in slices from A30P10+ mice compared to WT10+ mice ( $46.7 \pm 5.0$  versus  $46.5 \pm 1.6$  respectively,  $p > 0.05$ , unpaired *t* test). Interestingly, mitochondrial dysfunction in region CA3 was detected at 15-17 months of age, where A30P15+ mice exhibited a significantly higher mean blue count compared to WT15+ mice ( $57.3 \pm 2.1$  versus  $48.6 \pm 3.1$  respectively,  $p < 0.05$ , unpaired *t* test; effect size = 2.01, power  $(1 - \beta) = 0.73$ ). Post-hoc power analysis revealed that this experiment was slightly underpowered, likely due to the marginal change in blue pixel density. Increasing the sample size in future experiments could be beneficial to confirm the validity of the observed effect.

This data indicates that mitochondrial dysfunction is not yet detectable with our methods at 10-13 months in A30P mice but is detectable by 15-17 months. Conversely, WT mice do not exhibit an age-dependent change in mitochondrial function. This expands on the data published in Robson *et al.* (2018), where I compared a cohort of 2 month A30P mice to a cohort of 9+ month A30P mice and found a significant increase in mitochondrial dysfunction with age. In this thesis I have benefitted from narrower age groups to specifically detect a subtle mitochondrial dysfunction at 15-17 months.



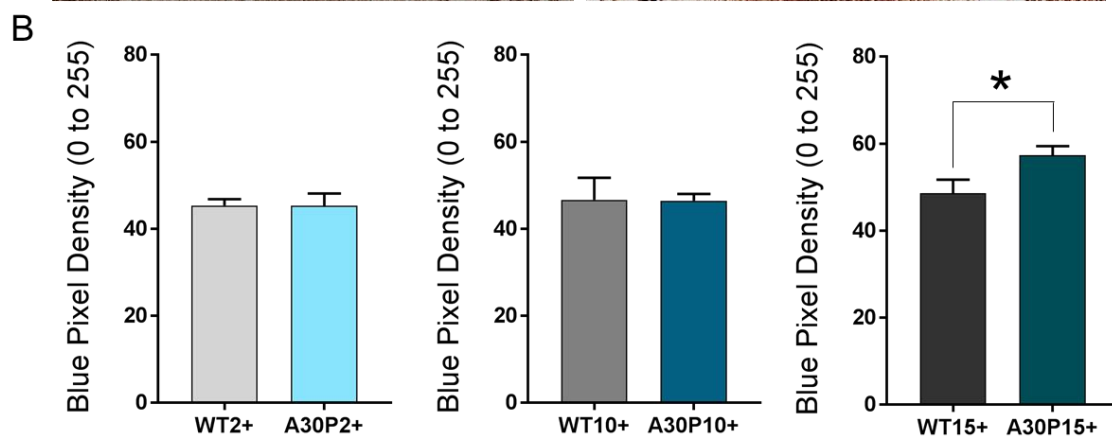
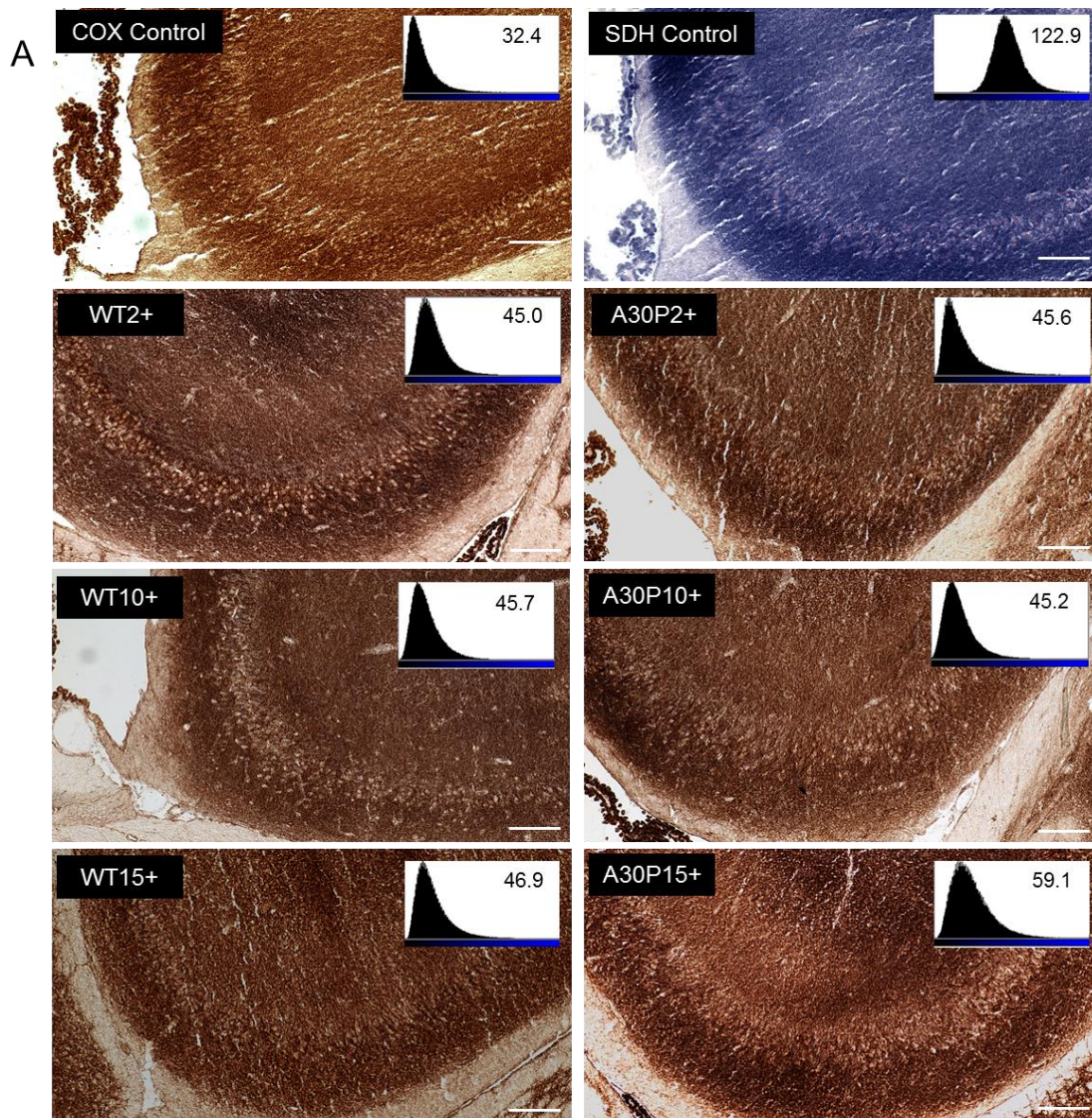


Figure 5.8 **Increased mitochondrial dysfunction in A30P15+ mice.** (A) Representative images of COX/SDH histochemistry at x10 magnification within the CA3 region, including COX and SDH only controls. Histogram from image inset with value indicating mean blue pixel count. Scalebars represent 100  $\mu$ m. (B) Bar charts to show mean blue values in the CA3 region in WT and A30P mice. WT2+ n = 20 slices from 5 mice; A30P2+ n = 23 slices from 5 mice; WT10+ n = 15 slices from 4 mice; A30P10+ n = 27 slices from 6 mice; WT15+ n = 9 slices from 3 mice; A30P15+ n = 11 slices from 4 mice; \* indicates significance at  $p < 0.05$ .



#### 5.4.7 Increase in Iba1+ microglia in A30P10+ mice

Microglia play a critical role in neuroinflammation and have also been shown to both influence, and be influenced by, excitability (Ferrini and De Koninck, 2013). Furthermore, microglia have been shown to be key regulators of the ASYN aggregation process by engulfing both extracellular ASYN and dysfunctional cells in humans (Sanchez-Guajardo *et al.*, 2013). Expression of the calcium-binding protein Iba1 is increased in activated microglia (Ito *et al.*, 1998), and therefore a measure of Iba1+ cell density may indicate levels of reactive microglia within the CA3 region .

Qualitative assessment of sections stained for Iba1 showed no clear regions of microgliosis (Streit *et al.*, 1999). Representative images from WT and A30P mouse slices (Figure 5.9A) indicate a similar shape of microglia, though slices from A30P10+ mice appeared to present with larger cell bodies. All Iba1+ cells were counted for the purpose of this thesis (Figure 5.9B). There was a significant decrease in Iba1+ cell density in slices from A30P2+ mice compared to WT2+ mice ( $91.6 \text{ cells/mm}^2 \pm 10.3$  versus  $138.3 \text{ cells/mm}^2 \pm 14.7$  respectively,  $p < 0.05$ , unpaired *t* test; effect size = 2.29, power  $(1 - \beta) = 0.82$ ), and a significant increase in Iba1+ cell density in slices from A30P10+ mice compared to WT10+ mice ( $201.6 \text{ cells/mm}^2 \pm 22.3$  versus  $133.3 \text{ cells/mm}^2 \pm 6.5$  respectively,  $p < 0.05$ , unpaired *t* test; effect size = 1.63, power  $(1 - \beta) = 0.85$ ). Notably, the density of Iba1+ cells in WT mice at both ages were comparable. Qualitative observation of Iba1+ microglia in slices from A30P10+ mice suggested larger cell bodies, which may increase the probability of cells being counted. This could explain the increased density of Iba1+ microglia in A30P10+ mice, though it should be noted that both Iba1 expression and increased cell size indicate microglial activation.

The decrease in Iba1+ cells in slices from A30P2+ mice was not dependent on dorsal/ventral hippocampal slice location (WT2+ *dorsal*  $149.4 \text{ cells/mm}^2 \pm 16.0$  [ $n = 7$  slices]; WT2+ *ventral*  $143.8 \text{ cells/mm}^2 \pm 16.0$  [ $n = 7$  slices]; A30P2+ *dorsal*  $100.7 \text{ cells/mm}^2 \pm 14.9$  [ $n = 8$  slices]; A30P2+ *ventral*  $87.91 \text{ cells/mm}^2 \pm 17.2$  [ $n = 6$  slices]; genotype  $p < 0.05$ , region  $p > 0.05$ , interaction  $p > 0.05$ ; 2-way ANOVA, data not shown). Likewise, the increase in Iba1+ cell density in slices from A30P10+ mice was not dependent on dorsal/ventral hippocampal slice location, though there was a significantly higher density of Iba1+ microglia in dorsal hippocampal slices regardless of mouse genotype (*dorsal overall*  $192.40 \text{ cells/mm}^2 \pm 12.74$  [ $n = 14$  slices] versus *ventral overall*  $136.42 \text{ cells/mm}^2 \pm 11.8$  [ $n = 16$  slices]; genotype  $p < 0.05$ , region  $p < 0.05$ , interaction  $p > 0.05$ ; 2-way ANOVA, data not shown).

Whilst the decrease in Iba1+ cell density in slices from A30P2+ mice was likely not dependent on sex (WT2+ *female* 113.8 cells/mm<sup>2</sup> ± 12.4 [n = 3 slices]; WT2+ *male* 156.7 cells/mm<sup>2</sup> ± 20.5 [n = 4 slices]; A30P2+ *female* 86.8 cells/mm<sup>2</sup> ± 7.7 [n = 2 slices]; A30P2+ *male* 93.5 cells/mm<sup>2</sup> ± 14.7 [n = 5 slices]; genotype p < 0.05, region p > 0.05, interaction p > 0.05; 2-way ANOVA, data not shown), the effect of sex on the increase in Iba1+ cell density in A30P10+ mice could not be explored due to a low sample size.

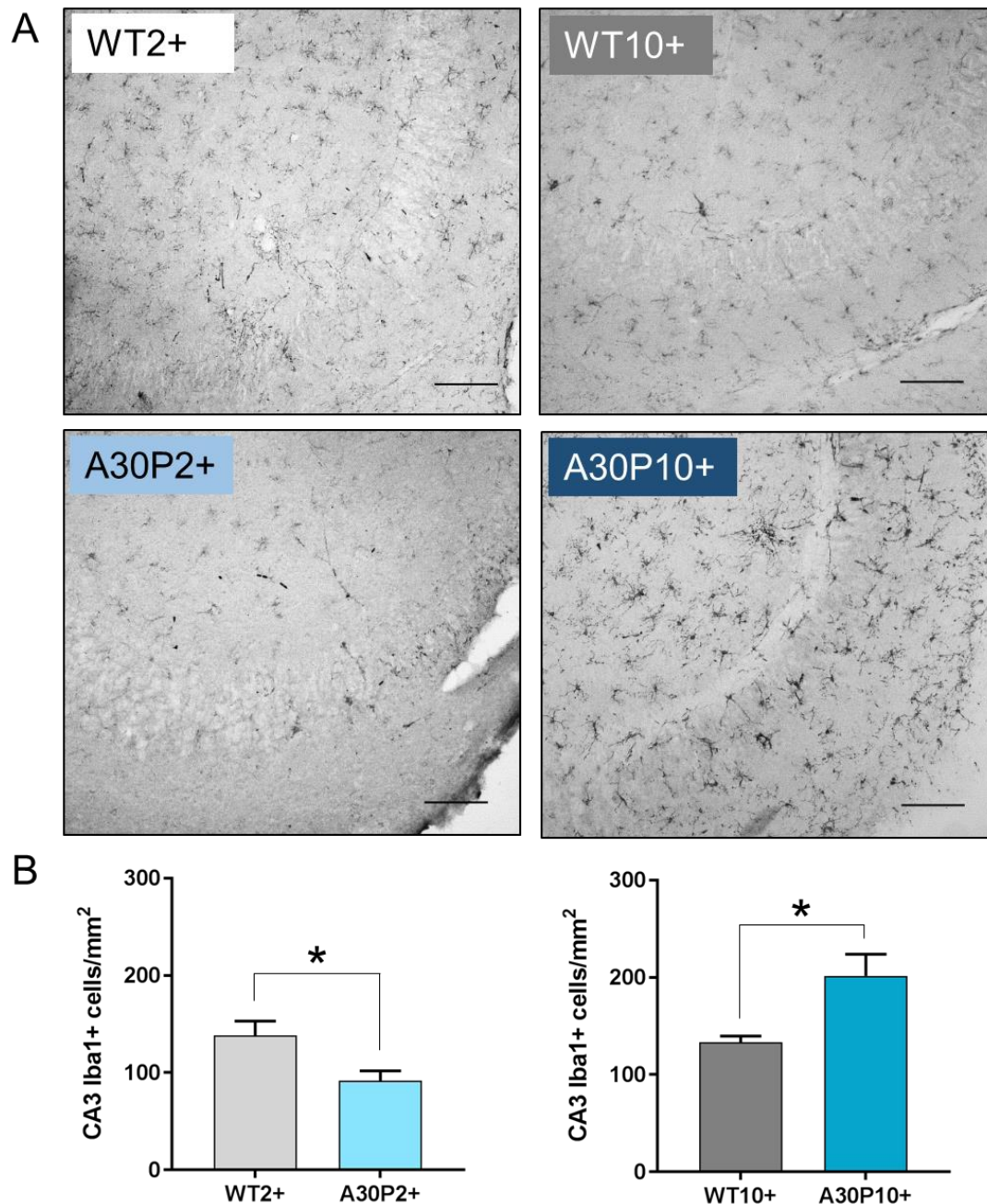


Figure 5.9 **Decreased Iba1+ cells in A30P2+ mice increased in A30P10+ mice.** (A) Representative greyscale images in region CA3 at x10 magnification. Scale bar 100  $\mu$ m. (B) Bar charts show Iba1+ cells/mm<sup>2</sup> in CA3 region of WT and A30P mice. WT2+ n = 7 slices from 4 mice, A30P2+ n = 7 slices from 3 mice. WT10+ n = 16 slices from 5 mice, A30P10+ n = 14 slices from 8 mice. \* indicates significance at p < 0.05.

## 5.5 Discussion

**A summary of key findings in Chapter 5 are as follows:**

- The gradual time-dependent build-up of CA3 CCH gamma-frequency oscillations in mice is an NMDA-receptor dependent process.
- A30P10+ mice show reduced power of CA3 CCH-induced gamma-frequency oscillations which propagate to CA1 and collapse more often. No differences in the NMDA-receptor dependent build-up, oscillation rhythmicity, stable frequency, or CA1 propagation time.
- A30P15+ mice exhibit mitochondrial dysfunction, not detectable with COX/SDH histochemistry at 10-13 months of age.
- A30P10+ mice show an increase in the density of Iba1+ microglia whilst A30P2+ mice show reduced Iba1+ immunoreactivity.

### 5.5.1 Cholinergic-induced network oscillation deficit in A30P10+ mice

Cognitive dysfunction may be underpinned by cholinergic deficits, which have been observed with some spatial and temporal differences in DLB (Perry *et al.*, 1990; Tiraboschi *et al.*, 2000) and in AD (Davies and Maloney, 1976). No septal cholinergic neuron loss was found in A30P mice when examined at 2-3 months of age (Szego *et al.*, 2013), but so far no studies have examined it with respect to the age-dependent decline in cognition. As cholinergic neurons innervate the hippocampus, it is proposed that changes in the cholinergic system may have an effect here.

Despite no change in spontaneous or KA-induced oscillations in slices from A30P10+ mice, this chapter found that slices from A30P10+ mice show a deficit in the power of CCH-induced oscillations. Interestingly, KA oscillations have been reported to be more susceptible to the effects of physiological ageing than CCH oscillations, showing a larger reduction in power in mice 22 months of age and older (Vreugdenhil and Toescu, 2005). This could indicate that physiological ageing leads to changes in different receptors and interneurons compared to the process of neurodegeneration. Indeed, a reduction in CCH oscillation power could indicate changes in the cholinergic receptors within the hippocampus, making them less capable of synchronising a network response required for high power network oscillations. The implications for hippocampal function as a result of the propagation of smaller power CCH-induced oscillations to region CA1 from region CA3 also remains to be explored.

The CCH oscillation deficit found in slices from A30P10+ mice could be specific to alterations in fast-spiking interneurons, for even though no loss of PV+ or CB+ interneurons were found in A30P10+ mice in *Chapter 3*, this does not mean that they are entirely functional. It is possible that CCH oscillation impairment may be in part explained by mitochondrial dysfunction in ageing A30P mice, particularly in the subset of neurons involved in CCH oscillations. Interestingly, MPTP is a Complex I antagonist and was shown to induce Parkinsonism in humans (Langston *et al.*, 1983). More recently, evidence has emerged in rodent models of PD that chronic MPTP treatment induces hyperlocomotion (Luchtman *et al.*, 2009; Moraes *et al.*, 2016). Therefore, hyperlocomotion in A30P10+ mice as discussed in *Chapter 4* could be the result of mitochondrial dysfunction as opposed to hyperexcitability.

COX/SDH histochemistry was used to elucidate mitochondrial function throughout the pyramidal layer of region CA3, a region which encompasses the cell bodies of both pyramidal cells and many interneurons. It would therefore be interesting to examine mitochondrial dysfunction within certain cell types using quadruple immunofluorescence. Different populations of inhibitory interneurons express different levels of mitochondrial ETC protein cytochrome C (Gulyas *et al.*, 2006), and so it is assumed that fast-spiking PV+ interneurons with their high level of cytochrome C expression may be selectively vulnerable to mitochondrial dysfunction.

Gamma-frequency oscillations are heavily dependent upon mitochondrial function (Kann *et al.*, 2011; Whittaker *et al.*, 2011; Robson *et al.*, 2018) and interestingly, mitochondrial blockade abolishes network oscillations through an effect on fast-spiking interneurons (Whittaker *et al.*, 2011). However, this thesis found no evidence of mitochondrial dysfunction at 10-13 months of age in A30P mice, despite this being the age at which oscillation power was reduced. Furthermore, WT mice begin to show a decrease in gamma oscillation power from as early as 15 months (Vreugdenhil and Toescu, 2005; Driver *et al.*, 2007), and yet no decrease in mitochondrial function was found in WT mice at 15-17 months in this thesis. It could be concluded that mitochondrial dysfunction is therefore not an underlying cause of the CCH oscillation deficit in A30P10+ mice, however COX/SDH histochemistry may not be the most sensitive method to detect changes given that it does not distinguish between different neuronal sub-types. More precise methods to detect mitochondrial dysfunction should be utilised in future, including measuring the mitochondrial membrane potential, and measuring respiratory rates of individual ETC complexes.

CCH-induced gamma-frequency oscillations in slices from A30P10+ mice were noted to collapse more frequently than any other group examined. Interestingly, all four slices from male A30P10+ mice collapsed in CCH. This effect was not explored in work published by our group previously, as a larger cohort of mice resulted in an equal number of stable oscillations from male and female mice (Robson *et al.*, 2018). CCH oscillations that collapsed were not always significantly larger than oscillations that did not, and so this does not entirely explain the collapse in A30P10+ mice. Instead, the collapse may be due to difficulty in slices from A30P10+ mice in sustaining the high energy demands of gamma-frequency oscillations, including the requirement of functional mitochondria (Kann *et al.*, 2011; Kann *et al.*, 2016).

The time-dependent build-up in power of network oscillations in slices has previously been reported in the literature with respect to KA-induced oscillations (Lu *et al.*, 2012a; Haggerty *et al.*, 2013), but has been explored in detail using CCH in mice during this thesis for the first time. We proposed that the time-dependent build-up of CCH oscillations may involve mechanisms of plasticity, given that CCH has been shown to induce LTD in rat hippocampal slices for at least 90 minutes through cholinergic receptors (Kumar, 2010). As CCH-induced oscillations take 2-4 hours on average to reach stability, this may reflect the time for CCH-induced depression to fade. Indeed, this thesis showed that preincubation with the NMDA receptor antagonist D-AP5 in WT2+ mouse slices caused an accelerated build-up and time to stability, though a similar number of slices reached stability. This was proposed to be the result of inhibition of NMDA receptor-dependent synaptic plasticity. Despite the reduction in CCH-induced oscillation power in A30P10+ mice, the NMDA-receptor dependent build-up was not altered in any age or genotype examined. This would suggest that A30P mice do not show any obvious changes in NMDA receptors, specifically NMDA receptor hypofunction, at either age examined, and that indeed mechanisms of long-term plasticity such as LTD may be intact (Kumar, 2010).

It should furthermore be noted that slices from A30P2+ mice did not show any difference in CCH oscillations, compared to the increased power observed upon induction of rhythms with KA. This would indicate that the increase in KA-induced oscillation power in slices from A30P2+ mice is not a direct result of intrinsic pyramidal cell hyperexcitability, but instead is dependent on the method of excitation through glutamatergic (KA and AMPA) receptors versus cholinergic receptors, and the various interneuron subtypes that possess differential levels of each receptor.

## 5.5.2 Changes in microglia in both young and ageing A30P mice

The effect of early hyperexcitability on later deficits in A30P mice was further explored with respect to changes in microglia in A30P mice, given their role in the clearance of ASYN and also in regulating excitability within the brain (Ferrini and De Koninck, 2013). A previous study found no change in expression of Mac-2, a marker of activated microglia, in 11 month A30P mice (Ekmark-Lewen *et al.*, 2018). It follows that the microglial phenotype with respect to the expression of various markers should be explored in greater detail in future. Regardless, this thesis has found evidence of an increase in the density of Iba1+ microglia in 10-13 month A30P mice compared to both 10-13 month WT mice, and also seemingly compared to 2-4 month A30P mice.

Interestingly, Iba1+ microglia cell density was unchanged between 2-4 and 10-13 months of age in WT mice. This could either reflect an increase in the number of microglia, an increase in Iba1 expression, or an increase in the size of microglial cell bodies with ageing in A30P mice. It was noted that slices from A30P10+ mice tended to present with microglia of a larger cell body. Regardless, both Iba1 expression and an increase in microglial cell body size are associated with reactive changes in microglia. Phagocytosis by microglia has been shown to be inhibited by aggregated ASYN but enhanced by monomeric ASYN (Park *et al.*, 2008). An increase in aggregated ASYN with ageing in A30P mice (Schell *et al.*, 2012) may therefore be associated with the increase in Iba1 microglial reactivity, though their effectiveness at clearing aggregated ASYN by phagocytosis may be impaired.

An increase in Iba1+ microglia density could have further devastating effects on the hippocampal network as astrocyte activation has been shown to occur as a result of microglia activation (Liddelow *et al.*, 2017). Indeed, *Thy-1* A30P mice have previously been reported to show an increase in GFAP+ astrocytes within the brainstem by 20 months of age (Rotermond *et al.*, 2014). It could be expected that if our cohort of A30P mice were examined at a later age, an increase in GFAP+ astrocytes might be found as a result of the increase in Iba1+ microglia reported in this chapter. Astrocytes play a role in network oscillations and recognition memory (Lee *et al.*, 2014b; Perea *et al.*, 2016), in addition to their role in excitability (Heja *et al.*, 2012), and so their importance to network function should not be understated.

Interestingly, the *PDGF* WT ASYN mouse model utilised in *Chapter 4* of this thesis has previously been investigated for changes in microglia (Amschl *et al.*, 2013). The authors found no human ASYN in microglia, which may suggest effective

clearance through phagocytosis (Amschl *et al.*, 2013). It would therefore be beneficial to examine the age-dependent change in human ASYN expression in glial cells of the A30P mouse hippocampus. Though the *Thy-1* promoter does not express in glial cells (Porrero *et al.*, 2010), the extracellular spread of ASYN and phagocytosis of ASYN by microglia means that accumulation of human ASYN may occur in glial cells.

The observed decrease in Iba1+ cell density in A30P2+ mice was unexpected but occurs at the same time as the decrease in GFAP+ astrocyte density explored in *Chapter 4*. A decrease in both Iba1+ and GFAP+ immunoreactivity at 2-4 months in A30P mice could represent an altered glial anti-inflammatory state as opposed to a pro-inflammatory state, but further investigation of microglial and astrocytic markers is required to draw any definitive conclusions. It possibly also remains that hippocampal slices from young A30P mice may exhibit a deficiency in basal microglial cell density and/or Iba1 reactivity, compared to the density of microglia and reactivity levels seen in young WT mice. It follows that any early intervention of treatment in A30P mice must be considered carefully with respect to the timing of microglia and astrocyte activation to prevent exacerbation of existing pathology.

## 5.6 Conclusion

In this chapter I have explored age-dependent deficits occurring in A30P10+ and A30P15+ mice, building on what has been published in Robson et al. (2018). A CCH-induced oscillation deficit was found in slices from A30P10+ mice with respect to a reduction in area power in region CA3. The power deficit was confirmed to propagate to region CA1. However, no explicit changes in CCH-induced oscillation frequency, rhythmicity, or propagation time to region CA1 were found. This would appear to indicate changes in the subpopulation of interneurons recruited by CCH, or changes in cholinergic receptors within the A30P10+ hippocampus, as no changes were found in either spontaneous network oscillations or in KA-induced oscillations at this age.

Secondly, mitochondrial dysfunction was explored further from work published in Robson et al. (2018) to show that this occurred in 15-17 month A30P mice and not in 10-13 month mice, though limitations exist as to how sensitive the technique used was. Finally, a decrease in Iba1+ microglia was reported in A30P2+ mice, in addition to an increase in A30P10+ mice. This could be a possible underlying mechanism to connect early hyperexcitability with later network dysfunction as a result of inflammation in response to the accumulation of human ASYN in A30P mice.

This chapter confirms that network dysfunction occurs in A30P mice at the same time that hippocampal spatial memory impairment was previously reported. Due to the nature of deficits being mitochondrial and potentially inflammatory by this point, it would be worthwhile to in future turn attention to the period of early hyperexcitability preceding this that may be causative of these later life deficits.



## **Chapter 6. General Discussion**



## 6.1 Summary of changes in A30P mice

A summary of findings reported in this thesis is presented in Table 6.1, organised by chapter and the age of A30P mice.

	2-4 months	10-13 months
<b>Chapter 3</b>		
Spontaneous CA3 gamma	Comparable to WT	Comparable to WT
Spontaneous CA3 SPWs	Amplitude ↑	Comparable to WT
CA3 pyramidal cell IPSPs	Amplitude/Freq ↑	N/A
CA3 SPW pharmacology	Comparable to WT	N/A
CA3 PV+ interneurons	Density ↑	Comparable to WT
CA3 PNN+ cells	Density ↑	Comparable to WT
CA3 CB+ interneurons	Density ↓	Comparable to WT
<b>Chapter 4</b>		
CA3 KA oscillation power	Area power ↑	Comparable to WT
CA3 KA oscillation freq.	Low conc. only ↑	Comparable to WT
IIDs at 150 nM KA	Present, never in WT	Present, comparable to WT
gabazine IID response	More common	N/A
gabazine IID frequency	Frequency ↑	N/A
CA3 pyramidal cell RMP	More depolarised	Comparable to WT
CA3 pyramidal cell firing	Comparable to WT	Comparable to WT
Locomotor activity	Locomotion ↑	Locomotion ↑
CA3 GFAP+ astrocytes	Density ↓	Comparable to WT
<b>Chapter 5</b>		
CA3 CCH collapse	Comparable to WT	More likely to collapse
CA3 CCH build-up	Comparable to WT	Comparable to WT
CA3 CCH stable power	Comparable to WT	Area power ↓
CA3 CCH stable frequency	Comparable to WT	Comparable to WT
CA3 mitochondrial function	Comparable to WT	Comparable to WT*
CA3 Iba1+ microglia	Density ↓	Density ↑

Table 6.1. **Summary of changes in A30P mice.** Comparison of A30P mice at 2-4 months (A30P2+) and 10-13 months (A30P10+) over three chapters. \*Mitochondrial dysfunction detected with COX/SDH histochemistry at 15-17 months in A30P mice.

## 6.2 Early hyperexcitability affects the E/I network in A30P mice

There is growing evidence in the literature that subclinical epileptic activity exists in patients with early AD (Vossel *et al.*, 2016; Lam *et al.*, 2017). As this has not been extensively explored in patients with alpha-synucleinopathy, it is entirely possible that a similar mechanism occurs in this disease. Seizure activity and excitability can cause lasting hippocampal damage (Lado *et al.*, 2002) as well as changes on a cellular level due to network remodelling (Swann *et al.*, 2001). It is proposed in this thesis that the expression of human A30P ASYN within the hippocampus itself leads to excitability of pyramidal cells and at least some populations of interneurons.

Overexpression of human WT ASYN in hippocampal glutamatergic cells in culture leads to impaired neurotransmitter release through inhibition of synaptic vesicle reclustering (Nemani *et al.*, 2010). It could therefore be inferred that due to A30P mutant ASYN showing reduced membrane interactions (for review see Snead and Eliezer, 2014) the release of glutamate in hippocampal pyramidal cells may either be unaffected by A30P ASYN overexpression, or increased. The impact that A30P ASYN has on neurotransmission in GABAergic neurons is also unknown.

While a number of studies have investigated the effect of the A30P mutation on the physiological function of ASYN, a significant majority of the work has been performed in cell culture models rather than in transgenic mouse models (for review see Snead and Eliezer, 2014). In young A30P mice, this thesis reported evidence of intrinsic pyramidal cell excitability in the form of a more depolarised resting membrane potential, and also of interneuron excitability in the form of increased IPSP frequency and amplitude. Whether excitability starts in pyramidal cells and drives interneurons, or is intrinsic to both pyramidal cells and interneurons as a result of intracellular human A30P ASYN, remains to be explored at an earlier time-point in A30P mice.

Despite normal hippocampal spatial memory performance previously reported on the Morris water maze at this age (Freichel *et al.*, 2007), this thesis found evidence of hyperexcitability within both excitatory and inhibitory networks in young A30P mice. A full battery of behavioural and cognitive tests would indicate whether this subtle change has an impact on *in vivo* performance. Furthermore, it would be interesting to perform awake behaving *in vivo* recordings in young A30P mice to explore the possibility of subclinical seizures within hyperexcitable cortical networks. Before this could be performed, however, it was important to explore the hippocampus and mechanisms of hyperexcitability in isolation through *in vitro* electrophysiology.

Hyperexcitability was further explored in mice overexpressing human WT ASYN under the *PDGF* promoter within this thesis. Human WT ASYN mice exhibited a less severe hyperexcitability than A30P mice. This is consistent with reports that human mutant ASYN produces a more severe phenotype in mice than WT ASYN (Chandra *et al.*, 2005). Regardless, this thesis proposes that hyperexcitability may be a common early occurrence in mouse models of alpha-synucleinopathy. Transgenic mouse models allow exploration of early synaptic changes preceding cognitive dysfunction, unlike the more acute effects of toxin treatment and viral expression of ASYN.

Overexpression of human WT ASYN in mice has been shown to lead to SNARE protein redistribution within the striatum leading to a reduction in dopaminergic neurotransmission (Garcia-Reitböck *et al.*, 2010). Conversely, an increase in hippocampal excitability has been reported in mice overexpressing human WT ASYN (Morris *et al.*, 2015), in addition to a reported increase in expression of the glutamatergic receptor mGluR5 within region CA3 (Price *et al.*, 2010; Overk *et al.*, 2014). The differential effect of WT ASYN to excitability levels in different brain regions and neurotransmitter systems highlights the complexity of animal model studies. The work described in this thesis compliments the existing literature relating to the mouse hippocampus following overexpression of human WT ASYN, though the effect that the A30P mutation may have on levels of excitability remain to be explored.

The use of *in vitro* slice electrophysiology is a powerful technique used for the first time in this thesis to explore early changes within the *Thy-1* A30P mouse network. Three models of network oscillations were studied in this thesis: spontaneous, CCH-induced, and KA-induced. Whilst much has been reported over the years on the mechanisms of oscillation generation in each model (Skrobot, 2008; Pietersen *et al.*, 2009; Modebadze, 2014), all rely on reciprocal communication between the excitatory and inhibitory networks, particularly PV+ fast-spiking interneurons (Klausberger *et al.*, 2005). Less is known about the contribution of CB+ cells to network oscillations, though given that CB is expressed in interneurons within CA3 and CA1, as well as excitatory CA1 pyramidal cells and granule cells of the dentate gyrus (Jouvenceau *et al.*, 1999), the role of CB+ cells is likely more complex than simply providing inhibition.

A comparison of the three oscillation types is difficult to make given the different experimental conditions that each recording was made in, though the data presented in this thesis does appear to follow the trend reported in the literature for spontaneous oscillations to be smaller in power and slower in frequency than hippocampal KA and

CCH oscillations (Pietersen *et al.*, 2009; Modebadze, 2014). The difference between KA and CCH-induced oscillation power and frequency is less well defined. Though KA oscillations appeared to be of a larger power and faster frequency than CCH and spontaneous oscillations in this thesis, other studies recorded in CA3 *st. radiatum* reported no difference within this region and layer (Vreugdenhil and Toescu, 2005).

The fact that increased gamma power in slices from A30P2+ mice is only observed in oscillations induced by KA suggests that the specific subpopulation of pyramidal cells and interneurons targeted by KA are driven more powerfully than with CCH, or perhaps are more vulnerable to changes caused by human A30P ASYN. It is proposed in this thesis that PV+ interneurons may be more involved in KA oscillations than in spontaneous or CCH oscillations, as the increased power of KA oscillations occurs at the same time as the increase in PV+ interneurons in A30P2+ mice.

One possible factor impacting on oscillation power could be the role of electrical gap junctions between inhibitory interneurons. Mice lacking connexin-36, a component of gap junctions, have previously shown a decrease in gamma-frequency oscillation power (Hormuzdi *et al.*, 2001; Buhl *et al.*, 2003), and it is possible that hypersynchrony between interneurons could be responsible for the increase in power observed after KA exposure. However, as gap junctions have been shown to increase synchrony of gamma oscillations (Traub *et al.*, 2001) and the rhythmicity of oscillations in A30P mice was unaffected, it is likely that the increased power of KA induced oscillations is more closely linked with the increase in PV+ interneurons in young A30P mice.

Previous optogenetic experiments *in vivo* demonstrated that depolarisation of cortical inhibitory cells increased gamma oscillation power, whilst hyperpolarisation decreased power (Sohal *et al.*, 2009). Furthermore, whilst a loss of PV has been explored in the context of schizophrenia, cells lacking PV also showed decreased excitation due to asynchronous GABA release, and as a result this led to a reduction in gamma-frequency activity (Volman *et al.*, 2011). The role of PV+ interneurons in network oscillations is complicated by the fact that a decrease in GABA synthesis in PV+ interneurons has been shown to lead to a compensatory increase in GABA transmission (Lewis *et al.*, 2005). Despite this, the authors still report impairment in working memory due to gamma-frequency oscillation disturbances (Lewis *et al.*, 2005).

The expression of PV has previously been proposed to be neuroprotective following excitotoxicity (Soos *et al.*, 2004), and injury (Dekkers *et al.*, 2004). This is

proposed to be due to the role of PV as a calcium buffer within the cell, which helps to prevent DNA damage and apoptosis (Soos *et al.*, 2004). However, ectopic PV expression in cells that do not express PV under physiological conditions has been shown to induce accelerated neurodegeneration, astrocyte immunoreactivity, and decreased mitochondrial volume in response to excitotoxic injury in mouse forebrain neurons (Maetzler *et al.*, 2004). Therefore, despite the increase of PV+ interneuron density potentially being to compensate for increased network activity, this mechanism may be more detrimental than beneficial and paradoxically lead to a vulnerability to excitotoxicity with ageing. Whether increased PV+ interneuron density is a cause or consequence of increased GABAergic activity also remains to be explored.

A consequence of increased PV+ interneuron density further manifests in the form of an increased amplitude of GABA<sub>A</sub> receptor-dependent SPWs, and increased PNN+ cell density in young A30P mice. Of particular interest was the increase in PNN+ cell density, given the neuroprotective role of PNNs to fast-spiking interneurons (Cabungcal *et al.*, 2013b). Neuroprotection by increased PNN+ cell density may be why, despite evidence of excitability in young A30P mice, mitochondrial dysfunction is not detectable by COX/SDH histochemistry at this age.

There is evidence that due to an increase in deltaFosB following neuronal activity, the density of CB+ granule cells within the dentate gyrus decreases and cognitive impairment occurs (You *et al.*, 2017). It is further suggested that downregulation of CB could be a homeostatic mechanism in CA1 pyramidal cells to protect against excitotoxicity (Klapstein *et al.*, 1998). The association of CB+ cell loss with network excitability was explored by Morris *et al.* (2015), with evidence of CB+ granule cell loss in the dentate gyrus of both DLB patients and mice overexpressing human WT ASYN. Furthermore, in a mouse model of AD a loss of CB+ expression in the dentate gyrus is associated with excitability and a compensatory increase in inhibition occurs (Palop *et al.*, 2007). While the literature typically explores CB in the context of excitatory cells of the dentate gyrus and CA1, this thesis set out to explore changes in CB+ interneurons within region CA3.

Evidence of the association between CB and excitability should not be ignored simply because it was collected from excitatory rather than inhibitory cells. The literature highlights that CB is capable of compensatory changes in response to excitation and alpha-synucleinopathy. This is complicated by the finding that human ASYN is not present in CA3 CB+ interneurons in A30P mice, and so it is proposed that

cells expressing human ASYN were either those already lost by 2 months, or that changes in CB+ interneurons occur as a result of compensatory mechanisms.

Upregulation of PV expression in rodents has previously been described following sensory deprivation in the first week of life (Watanabe *et al.*, 2012), and following periods of low intensity exercise (Arida *et al.*, 2004; Nguyen *et al.*, 2013). Indeed, in cultured cells from the rat visual cortex the expression of PV was shown to be activity dependent, with an increase in PV expression proposed to represent hyperactivity of PV cells (Patz *et al.*, 2004). It is therefore proposed that increased network excitability may lead to an increase in PV to buffer excess calcium within fast-spiking interneurons. This is possibly due to PV+ interneurons being surrounded by a PNN, which allows for plastic remodelling of the network and has been associated closely with the levels of PV within the cell (Yamada *et al.*, 2015; Favuzzi *et al.*, 2017).

A similar mechanism has been proposed to occur within the substantia nigra of patients with PD, but not in control subjects or patients with AD (Soos *et al.*, 2004). The authors propose that due to excitotoxicity and oxidative damage, levels of intracellular calcium were raised and an upregulation of PV occurred in response (Soos *et al.*, 2004). In cells that did not upregulate PV expression, upregulated components of the DNA damage response were reported instead (Soos *et al.*, 2004).

One final effect of network excitability discussed in this thesis is a decrease in the density of both Iba1+ microglia and GFAP+ astrocytes in young A30P mice. A reduction in the reactivity of microglia and astrocytes may have on the hippocampal network in the form of hyperexcitability. Microglia play a crucial role in synaptic pruning during development (Paolicelli *et al.*, 2011), and if this process is disturbed in A30P mice then the balance of the excitatory/inhibitory network may be impacted as a result. Furthermore, astrocytes function to maintain physiological levels of glutamate and GABA (Verkhratsky and Butt, 2007) and therefore dysfunction may also impact on the balance between excitation and inhibition.

To explore the mechanisms of altered glial reactivity in young A30P mice, it would be necessary to look at mice postnatally to determine if this phenotype is developmental. However, it is proposed that the increase in neuronal activity seen in young A30P mice leads to an increase in extracellular ASYN (Paillusson *et al.*, 2013), oxidative damage through increased ROS (Poon *et al.*, 2005) leading to mitochondrial dysfunction, and as a result an increase in human A30P ASYN aggregation and



oligomerisation with ageing (Ekmark-Lewen *et al.*, 2018). Microglia and astrocytes should function to mitigate damage caused by hyperexcitability, and it is possible that the lack of GFAP and Iba1 immunoreactivity is a result of a neuroprotective phenotype of glia that could be explored with the use of additional markers, or a deficiency in the glial response as a result of human ASYN over-expression.

This is interesting given that healthy human tissue is often not immunoreactive for GFAP (Sofroniew and Vinters, 2010). Following lipopolysaccharide injection to induce inflammation in mice, activation of microglia and astrocytes were detected through morphological changes despite a decrease in Iba1 mRNA (Silverman *et al.*, 2014). The authors of this study propose that this is an attempt to prevent further activation of microglia (Silverman *et al.*, 2014), and therefore careful examination into glial morphology, mRNA expression patterns, and postnatal phenotypes should be explored in A30P mice to elucidate the complex mechanism of glial reactivity.

### **6.3 Age-dependent network deficits in A30P mice**

In direct contrast to the young A30P hyperexcitable network, the ageing A30P mouse network instead presents with normalised levels of excitability but the appearance of deficits in the power of CCH gamma-frequency oscillations and the presence of mitochondrial dysfunction. It is proposed that early hyperexcitability in fact contributes to later age-dependent network deficits, though as a cohort of 6-8 month old A30P mice also show some evidence of excitability in response to kainate exposure, it is unclear at what age the switch between the two phenotypes occurs.

The exception to normal excitability with ageing in A30P mice was seen in the persistence of hyperlocomotion with age. However, it has been proposed in this thesis that this may be the result of either excitability spreading from the hippocampus to elsewhere in the brain, or else it may be the result of other mechanisms including NMDA receptor dysfunction (Ma *et al.*, 2012) or even disruptions in circadian rhythms (Arble *et al.*, 2010). One major limitation in this study is the inability to follow the same mouse longitudinally, and therefore future work should move towards awake behaving *in vivo* electrode implants where locomotor activity and excitability could be monitored over time and in response to pharmacological interventions.

Ageing A30P mice exhibited a specific reduction in the power, but not frequency or rhythmicity, of CCH-induced gamma oscillations, but not KA or spontaneous oscillations. The reason for this may be either due to changes in cholinergic receptors

within the hippocampus, or else due to dysfunction in the interneuron population specifically recruited during CCH oscillations. Connexin-36 gap junction knockout mice exhibit a reduction in the power, but not the frequency, of gamma oscillations (Buhl *et al.*, 2003) and this could indicate an impairment in synchrony between interneurons. However, no impairment in oscillation rhythmicity was found using our techniques.

Whilst it has previously been shown that exposure of slices to acute application of human WT ASYN oligomers impairs LTP through NMDA receptor activation (Diogenes *et al.*, 2012), the NMDA-receptor dependent build-up in power of CCH-induced oscillations was unimpaired in ageing A30P mice. It is possible that changes may be detected in an even older cohort of mice in the build-up of oscillations, but once again this implicates changes in the mechanisms specifically influencing oscillation power. As previously discussed, downregulation of PV+ interneurons leads to a reduction in gamma-frequency oscillation power (Sohal *et al.*, 2009; Volman *et al.*, 2011), though in this thesis no loss of PV+ interneuron density was found in slices from A30P10+ mice compared to age-matched WT mice.

Synaptic dysfunction in the absence of cell loss has been reported in both transgenic and non-transgenic rodent models of PD. Rats overexpressing human WT ASYN following viral injection to the midbrain develop synaptic dysfunction and early pathology despite no loss of cells (Phan *et al.*, 2017). Furthermore, a novel model of early PD generated by injection of the mitochondrial stressor aminochrome to the rat striatum led to dopaminergic cell dysfunction, mitochondrial dysfunction, and an increase in GABA release within the local area. As a result, attention turned in this thesis to neuronal dysfunction as opposed to neuronal cell loss.

Fast-spiking PV+ interneurons are incredibly energy demanding and are enriched in mitochondria as a result (Kann, 2016), with fast network oscillations heavily dependent on effective energy metabolism and functional mitochondria (Huchzermeyer *et al.*, 2008; Kann *et al.*, 2011). Whilst mitochondrial dysfunction was not yet detected in A30P mice until 15-17 months of age, it is possible that more sensitive measures of metabolic and mitochondrial function may reveal differences. Therefore, this thesis proposes that early hyperexcitability may lead to later mitochondrial dysfunction, and as a result neuronal dysfunction, through mechanisms of excitotoxicity following excessive neuronal activity.

It is entirely possible that the increase in human ASYN aggregates with ageing in A30P mice is exacerbated by early hyperexcitability. Neuronal activity exacerbates the release of extracellular ASYN, which contributes to the spread of pathology between cells and even between brain regions with age (Paillusson *et al.*, 2013). Furthermore, cell culture models highlight that oxidative stress accelerates the aggregation of WT ASYN (Hashimoto *et al.*, 1999; Paxinou *et al.*, 2001), and the very presence of either the A30P or A53T mutation in ASYN leads to an increased propensity to aggregate (Flagmeier *et al.*, 2016). This may account for the fact that the cohort of young *PDGF* WT ASYN mice described in *Chapter 4* also showed IIDs in response to low concentrations of KA but not to as great an extent as young *Thy-1* A30P mice did, due to the presence of WT rather than mutant ASYN.

Network excitability normalises with ageing in A30P mice and is accompanied by normalised GFAP+ astrocyte density and increased Iba1+ microglia density. The normalisation of GFAP+ astrocyte density in A30P mice with ageing may explain why hyperexcitability does not persist to this age, given the role of astrocytes in maintaining the balance of excitation and inhibition with the hippocampal network (Verkhatsky and Butt, 2007). The increase in GFAP and Iba1 reactivity with ageing in A30P mice may therefore be a response to the increase in human ASYN aggregates with ageing, and an attempt to clear misfolded human ASYN and dysfunctional cells. However, as mice die prematurely due to severe motor deficits from around 18 months, the microglial response is occurring too late in the disease process. Instead, the increase in Iba1+ cell density may play a role in the age-dependent reduction in gamma-frequency oscillation power observed in A30P mice. It is therefore important to consider the balance between glial cells attempting to reduce excitability and levels of misfolded and aggregated human ASYN, and the neuronal dysfunction that may occur due to excess or prolonged pro-inflammatory states.

## 6.4 Therapeutic implications

Overall, this thesis has presented evidence of an early hyperexcitability preceding cognitive dysfunction and network oscillation impairment in a mouse overexpressing human A30P ASYN. As hyperexcitability persists for some months after first detection, the potential to intervene and either delay or prevent later cognitive deficits is of therapeutic interest. Whilst no mouse model fully recapitulates the pathology and symptoms of the alpha-synucleinopathy, this thesis has demonstrated that similar mechanisms of hyperexcitability likely exist in mice expressing either A30P or WT human ASYN. It would be worthwhile to examine the pan-neuronal over-expression of human ASYN in comparison to mice only over-expressing human ASYN in certain neuronal subtypes. This could help to elucidate mechanisms of extracellular ASYN propagation, and the factors that may lead to differential disease progression.

Despite the differences in symptoms, regions affected, and time course of disease, a number of mechanistic similarities exist between AD and alpha-synucleinopathy. Whilst AD research is seemingly decades ahead of research into alpha-synucleinopathy, this thesis highlights the need to explore evidence of subclinical seizures in patients with alpha-synucleinopathy given the wealth of evidence of hyperexcitability in patients and rodent models of AD (Amatniek *et al.*, 2006; Minkeviciene *et al.*, 2009; Lam *et al.*, 2017).

Treating mice with chronic anti-inflammatory drugs has proven effective in some models of neurodegeneration (Eriksen *et al.*, 2003) but should be considered with caution given the reduced immunoreactivity of astrocytes and microglia in the early stages of disease in the *Thy-1* A30P mouse model. Instead, it is possible that a stimulus to trigger the pro-inflammatory response may instead prove useful to stimulate microglia to clear misfolded human ASYN before aggregates can form. Furthermore, the possibility of treatment with anti-epileptics and anti-oxidants as soon as hyperexcitability is detected is promising in this model, as this thesis has proposed that excitotoxicity and oxidative stress occurring through excess neuronal activity is likely a key pathological process leading to the later life deficits in A30P mice.

## 6.5 Future Work

This thesis presents evidence for the first time of early network hyperexcitability in the *Thy-1* A30P mouse model through electrophysiological and immunohistochemical techniques. The thesis benefits from the use of a range of techniques to examine network dysfunction, in addition to the inclusion of numerous age groups, examination in to the effect of sex, and the effect of dorsal/ventral hippocampal location to strengthen the findings presented in this thesis. The following areas have been identified as areas of future work to advance the findings of this thesis:

- Examination of A30P mice at 3-4 weeks of age as soon as animals are weaned. Mice would be explored for early changes in pyramidal cells and interneurons, as well as astrocytes and microglia, to confirm whether changes occur at this point or even earlier in development. Changes in human ASYN structure and phosphorylation states will also be monitored from an early age.
- Quadruple immunofluorescence for: Complex I of the ETC, Porin as a marker of mitochondrial mass, human ASYN, and either PV as a marker of interneurons or CaMKII as a marker of pyramidal cells. This would allow localisation of mitochondrial deficits to PV+ or CaMKII+ cells. Further exploration of mitochondrial function in A30P mice of all ages through recording of activity in each complex of the ETC, and measures such as mitochondrial membrane potential in different cell types.
- Dosing of A30P mice from 3-4 weeks of age as soon as animals are weaned with existing anti-epileptics or antioxidants. A functional output of hyperlocomotion could be measured by performing the open field test before and after treatment. Mice could be treated and then left till they reach 12 months of age at which point hippocampal spatial memory *in vivo* and CCH-induced network oscillations *in vitro* could be examined.
- Random transgene integration is used to produce the majority of transgenic mouse models, and an important limitation of this work is the possibility that this may impact other sections of the genome (Jacobsen *et al.*, 2017). Recent work has described elucidation of the site of genomic integration in mice using next-generation sequencing methods, and this would be important to confirm that the observed phenotype is due to the transgene itself.

## References

Aarsland, D., Ballard, C., Walker, Z., Bostrom, F., Alves, G., Kossakowski, K., Leroi, I., Pozo-Rodriguez, F., Minthon, L. and Londos, E. (2009) 'Memantine in patients with Parkinson's disease dementia or dementia with Lewy bodies: a double-blind, placebo-controlled, multicentre trial', *Lancet Neurol*, 8(7), pp. 613-8.

Adamczyk, A. and Strosznajder, J.B. (2006) 'Alpha-synuclein potentiates Ca<sup>2+</sup> influx through voltage-dependent Ca<sup>2+</sup> channels', *Neuroreport*, 17(18), pp. 1883-6.

Adamowicz, D.H., Roy, S., Salmon, D.P., Galasko, D.R., Hansen, L.A., Masliah, E. and Gage, F.H. (2017) 'Hippocampal  $\alpha$ -Synuclein in Dementia with Lewy Bodies Contributes to Memory Impairment and Is Consistent with Spread of Pathology', *J Neurosci*, 37(7), pp. 1675-84.

Aghajanian, G.K. and Rasmussen, K. (1989) 'Intracellular studies in the facial nucleus illustrating a simple new method for obtaining viable motoneurons in adult rat brain slices', *Synapse*, 3(4), pp. 331-8.

Albala, B.J., Moshe, S.L. and Okada, R. (1984) 'Kainic-acid-induced seizures: a developmental study', *Brain Res*, 315(1), pp. 139-48.

Amaral, D.G., Scharfman, H.E. and Lavenex, P. (2007) 'The dentate gyrus: fundamental neuroanatomical organization (dentate gyrus for dummies)', *Prog Brain Res*, 163, pp. 3-22.

Amatniek, J.C., Hauser, W.A., DelCastillo-Castaneda, C., Jacobs, D.M., Marder, K., Bell, K., Albert, M., Brandt, J. and Stern, Y. (2006) 'Incidence and predictors of seizures in patients with Alzheimer's disease', *Epilepsia*, 47(5), pp. 867-72.

Amschl, D., Neddens, J., Havas, D., Flunkert, S., Rabl, R., Römer, H., Rockenstein, E., Masliah, E., Windisch, M. and Hutter-Paier, B. (2013) 'Time course and progression of wild type  $\alpha$ -Synuclein accumulation in a transgenic mouse model', *BMC Neurosci*, 14, p. 6.

Anderson, M.A., Ao, Y. and Sofroniew, M.V. (2014) 'Heterogeneity of reactive astrocytes', *Neurosci Lett*, 565, pp. 23-9.

Andersson, M., Hansson, O., Minthon, L., Rosen, I. and Londos, E. (2008) 'Electroencephalogram variability in dementia with lewy bodies, Alzheimer's disease and controls', *Dement Geriatr Cogn Disord*, 26(3), pp. 284-90.

Andersson, R., Lindskog, M. and Fisahn, A. (2010) 'Histamine H3 receptor activation decreases kainate-induced hippocampal gamma oscillations in vitro by action potential desynchronization in pyramidal neurons', *J Physiol*, 588(Pt 8), pp. 1241-9.

Arble, D.M., Ramsey, K.M., Bass, J. and Turek, F.W. (2010) 'Circadian Disruption and Metabolic Disease: Findings from Animal Models', *Best Pract Res Clin Endocrinol Metab*, 24(5), pp. 785-800.

- Arida, R.M., Scorza, C.A., da Silva, A.V., Scorza, F.A. and Cavalheiro, E.A. (2004) 'Differential effects of spontaneous versus forced exercise in rats on the staining of parvalbumin-positive neurons in the hippocampal formation', *Neurosci Lett*, 364(3), pp. 135-8.
- Arnulf, I., Konofal, E., Gibson, K.M., Rabier, D., Beauvais, P., Derenne, J.P. and Philippe, A. (2005) 'Effect of genetically caused excess of brain gamma-hydroxybutyric acid and GABA on sleep', *Sleep*, 28(4), pp. 418-24.
- Augustinack, J.C., van der Kouwe, A.J., Salat, D.H., Benner, T., Stevens, A.A., Annese, J., Fischl, B., Frosch, M.P. and Corkin, S. (2014) 'H.M.'s contributions to neuroscience: a review and autopsy studies', *Hippocampus*, 24(11), pp. 1267-86.
- Avery, M.C. and Krichmar, J.L. (2017) 'Neuromodulatory Systems and Their Interactions: A Review of Models, Theories, and Experiments', *Front Neural Circuits*, 11.
- Baig, S., Wilcock, G.K. and Love, S. (2005) 'Loss of perineuronal net N-acetylgalactosamine in Alzheimer's disease', *Acta Neuropathol*, 110(4), pp. 393-401.
- Baimbridge, K.G. and Miller, J.J. (1982) 'Immunohistochemical localization of calcium-binding protein in the cerebellum, hippocampal formation and olfactory bulb of the rat', *Brain Res*, 245(2), pp. 223-9.
- Balmer, T.S. (2016) 'Perineuronal Nets Enhance the Excitability of Fast-Spiking Neurons', *eNeuro*, 3(4).
- Barker-Haliski, M. and White, H.S. (2015) 'Glutamatergic Mechanisms Associated with Seizures and Epilepsy', *Cold Spring Harb Perspect Med*, 5(8).
- Barnum, C.J. and Tansey, M.G. (2012) 'Neuroinflammation and non-motor symptoms: the dark passenger of Parkinson's disease?', *Curr Neurol Neurosci Rep*, 12(4), pp. 350-8.
- Bazelot, M., Telenczuk, M.T. and Miles, R. (2016) 'Single CA3 pyramidal cells trigger sharp waves in vitro by exciting interneurons', *J Physiol*, 594(10), pp. 2565-77.
- Beagle, A.J., Darwish, S.M., Ranasinghe, K.G., La, A.L., Karageorgiou, E. and Vossel, K.A. (2017) 'Relative Incidence of Seizures and Myoclonus in Alzheimer's Disease, Dementia with Lewy Bodies, and Frontotemporal Dementia', *Journal of Alzheimer's disease : JAD*, 60(1), pp. 211-223.
- Bear, M., Connors, B. and Paradiso, M. (2015) *Neuroscience: Exploring the Brain*. Lippincott Williams and Wilkins; Fourth, North American Edition (3 Feb. 2015).
- Behrens, C.J., van den Boom, L.P., de Hoz, L., Friedman, A. and Heinemann, U. (2005) 'Induction of sharp wave-ripple complexes in vitro and reorganization of hippocampal networks', *Nat Neurosci*, 8(11), pp. 1560-7.
- Behrens, C.J., van den Boom, L.P. and Heinemann, U. (2007) 'Effects of the GABA(A) receptor antagonists bicuculline and gabazine on stimulus-induced sharp wave-ripple complexes in adult rat hippocampus in vitro', *Eur J Neurosci*, 25(7), pp. 2170-81.

- Bejnordi, B.E., Litjens, G., Timofeeva, N., Otte-Holler, I., Homeyer, A., Karssemeijer, N. and van der Laak, J.A. (2016) 'Stain Specific Standardization of Whole-Slide Histopathological Images', *IEEE Trans Med Imaging*, 35(2), pp. 404-15.
- Ben-Ari, Y. and Cossart, R. (2000) 'Kainate, a double agent that generates seizures: two decades of progress', *Trends Neurosci*, 23(11), pp. 580-7.
- Bendor, J.T., Logan, T.P. and Edwards, R.H. (2013) 'The function of alpha-synuclein', *Neuron*, 79(6), pp. 1044-66.
- Bennett, M.V., Contreras, J.E., Bukauskas, F.F. and Saez, J.C. (2003) 'New roles for astrocytes: gap junction hemichannels have something to communicate', *Trends Neurosci*, 26(11), pp. 610-7.
- Berg, J., Tymoczko, J. and Stryer, L. (2002) *Biochemistry. 5th edition*. New York: W.H. Freeman.
- Bernstein, H.G., Johnson, M., Perry, R.H., LeBeau, F.E., Dobrowolny, H., Bogerts, B. and Perry, E.K. (2011) 'Partial loss of parvalbumin-containing hippocampal interneurons in dementia with Lewy bodies', *Neuropathology*, 31(1), pp. 1-10.
- Berridge, M.J., Lipp, P. and Bootman, M.D. (2000) 'The versatility and universality of calcium signalling', *Nat Rev Mol Cell Biol*, 1(1), pp. 11-21.
- Betts, J., Jaros, E., Perry, R.H., Schaefer, A.M., Taylor, R.W., Abdel-All, Z., Lightowlers, R.N. and Turnbull, D.M. (2006) 'Molecular neuropathology of MELAS: level of heteroplasmy in individual neurones and evidence of extensive vascular involvement', *Neuropathol Appl Neurobiol*, 32(4), pp. 359-73.
- Beyer, K. (2006) 'Alpha-synuclein structure, posttranslational modification and alternative splicing as aggregation enhancers', *Acta Neuropathol*, 112(3), pp. 237-51.
- Bignami, A., Eng, L.F., Dahl, D. and Uyeda, C.T. (1972) 'Localization of the glial fibrillary acidic protein in astrocytes by immunofluorescence', *Brain Res*, 43(2), pp. 429-35.
- Bitanhirwe, B.K., Lim, M.P., Kelley, J.F., Kaneko, T. and Woo, T.U. (2009) 'Glutamatergic deficits and parvalbumin-containing inhibitory neurons in the prefrontal cortex in schizophrenia', *BMC Psychiatry*, 9, p. 71.
- Bolos, M., Perea, J.R. and Avila, J. (2017) 'Alzheimer's disease as an inflammatory disease', *Biomol Concepts*, 8(1), pp. 37-43.
- Bonanni, E., Di Coscio, E., Maestri, M., Carnicelli, L., Tsekou, H., Economou, N.T., Paparrigopoulos, T., Bonakis, A., Papageorgiou, S.G., Vassilopoulos, D., Soldatos, C.R., Murri, L. and Ktonas, P.Y. (2012) 'Differences in EEG delta frequency characteristics and patterns in slow-wave sleep between dementia patients and controls: a pilot study', *J Clin Neurophysiol*, 29(1), pp. 50-4.
- Bonanni, L., Thomas, A., Tiraboschi, P., Perfetti, B., Varanese, S. and Onofri, M. (2008) 'EEG comparisons in early Alzheimer's disease, dementia with Lewy bodies



- and Parkinson's disease with dementia patients with a 2-year follow-up', *Brain*, 131(Pt 3), pp. 690-705.
- Borgers, C. and Kopell, N. (2005) 'Effects of noisy drive on rhythms in networks of excitatory and inhibitory neurons', *Neural Comput*, 17(3), pp. 557-608.
- Boyer, P.D. (1997) 'The ATP synthase--a splendid molecular machine', *Annu Rev Biochem*, 66, pp. 717-49.
- Braak, H., Del Tredici, K., Rub, U., de Vos, R.A., Jansen Steur, E.N. and Braak, E. (2003) 'Staging of brain pathology related to sporadic Parkinson's disease', *Neurobiol Aging*, 24(2), pp. 197-211.
- Brady, D.R. and Mufson, E.J. (1997) 'Parvalbumin-immunoreactive neurons in the hippocampal formation of Alzheimer's diseased brain', *Neuroscience*, 80(4), pp. 1113-25.
- Bragin, A., Engel, J., Jr., Wilson, C.L., Fried, I. and Mathern, G.W. (1999) 'Hippocampal and entorhinal cortex high-frequency oscillations (100--500 Hz) in human epileptic brain and in kainic acid--treated rats with chronic seizures', *Epilepsia*, 40(2), pp. 127-37.
- Bragin, A., Jando, G., Nadasdy, Z., Hetke, J., Wise, K. and Buzsaki, G. (1995) 'Gamma (40-100 Hz) oscillation in the hippocampus of the behaving rat', *J Neurosci*, 15(1 Pt 1), pp. 47-60.
- Braidy, N., Gai, W.P., Xu, Y.H., Sachdev, P., Guillemin, G.J., Jiang, X.M., Ballard, J.W., Horan, M.P., Fang, Z.M., Chong, B.H. and Chan, D.K. (2013) 'Uptake and mitochondrial dysfunction of alpha-synuclein in human astrocytes, cortical neurons and fibroblasts', *Transl Neurodegener*, 2(1), p. 20.
- Brightman, M.W. and Reese, T.S. (1969) 'Junctions between intimately apposed cell membranes in the vertebrate brain', *J Cell Biol*, 40(3), pp. 648-77.
- Bruckner, G., Brauer, K., Hartig, W., Wolff, J.R., Rickmann, M.J., Derouiche, A., Delpech, B., Girard, N., Oertel, W.H. and Reichenbach, A. (1993) 'Perineuronal nets provide a polyanionic, glia-associated form of microenvironment around certain neurons in many parts of the rat brain', *Glia*, 8(3), pp. 183-200.
- Bruckner, G., Grosche, J., Schmidt, S., Hartig, W., Margolis, R.U., Delpech, B., Seidenbecher, C.I., Czaniera, R. and Schachner, M. (2000) 'Postnatal development of perineuronal nets in wild-type mice and in a mutant deficient in tenascin-R', *J Comp Neurol*, 428(4), pp. 616-29.
- Buhl, D.L., Harris, K.D., Hormuzdi, S.G., Monyer, H. and Buzsaki, G. (2003) 'Selective impairment of hippocampal gamma oscillations in connexin-36 knock-out mouse in vivo', *J Neurosci*, 23(3), pp. 1013-8.
- Buhl, E.H., Tamas, G. and Fisahn, A. (1998) 'Cholinergic activation and tonic excitation induce persistent gamma oscillations in mouse somatosensory cortex in vitro', *J Physiol*, 513 ( Pt 1), pp. 117-26.

- Bukalo, O., Schachner, M. and Dityatev, A. (2001) 'Modification of extracellular matrix by enzymatic removal of chondroitin sulfate and by lack of tenascin-R differentially affects several forms of synaptic plasticity in the hippocampus', *Neuroscience*, 104(2), pp. 359-69.
- Butler, B., Sambo, D. and Khoshbouei, H. (2017) 'Alpha-synuclein modulates dopamine neurotransmission', *J Chem Neuroanat*, 83-84, pp. 41-49.
- Buzsaki, G. (1986) 'Hippocampal sharp waves: their origin and significance', *Brain Res*, 398(2), pp. 242-52.
- Buzsaki, G. (1998) 'Memory consolidation during sleep: a neurophysiological perspective', *J Sleep Res*, 7 Suppl 1, pp. 17-23.
- Buzsaki, G. (2005) 'Theta rhythm of navigation: link between path integration and landmark navigation, episodic and semantic memory', *Hippocampus*, 15(7), pp. 827-40.
- Buzsaki, G., Horvath, Z., Urioste, R., Hetke, J. and Wise, K. (1992) 'High-frequency network oscillation in the hippocampus', *Science*, 256(5059), pp. 1025-7.
- Buzsaki, G., Leung, L.W. and Vanderwolf, C.H. (1983) 'Cellular bases of hippocampal EEG in the behaving rat', *Brain Res*, 287(2), pp. 139-71.
- Cabungcal, J.H., Steullet, P., Kraftsik, R., Cuenod, M. and Do, K.Q. (2013a) 'Early-life insults impair parvalbumin interneurons via oxidative stress: reversal by N-acetylcysteine', *Biol Psychiatry*, 73(6), pp. 574-82.
- Cabungcal, J.H., Steullet, P., Morishita, H., Kraftsik, R., Cuenod, M., Hensch, T.K. and Do, K.Q. (2013b) 'Perineuronal nets protect fast-spiking interneurons against oxidative stress', *Proc Natl Acad Sci U S A*, 110(22), pp. 9130-5.
- Cadenas, E., Boveris, A., Ragan, C.I. and Stoppani, A.O. (1977) 'Production of superoxide radicals and hydrogen peroxide by NADH-ubiquinone reductase and ubiquinol-cytochrome c reductase from beef-heart mitochondria', *Arch Biochem Biophys*, 180(2), pp. 248-57.
- Canas, N., Valero, T., Villarroya, M., Montell, E., Verges, J., Garcia, A.G. and Lopez, M.G. (2007) 'Chondroitin sulfate protects SH-SY5Y cells from oxidative stress by inducing heme oxygenase-1 via phosphatidylinositol 3-kinase/Akt', *J Pharmacol Exp Ther*, 323(3), pp. 946-53.
- Carter, D.S., Harrison, A.J., Falenski, K.W., Blair, R.E. and DeLorenzo, R.J. (2008) 'Long-term decrease in calbindin-D28K expression in the hippocampus of epileptic rats following pilocarpine-induced status epilepticus', *Epilepsy Res*, 79(2-3), pp. 213-23.
- Caviness, J.N., Adler, C.H., Caselli, R.J. and Hernandez, J.L. (2003) 'Electrophysiology of the myoclonus in dementia with Lewy bodies', *Neurology*, 60(3), pp. 523-4.
- Celio, M.R. (1986) 'Parvalbumin in most gamma-aminobutyric acid-containing neurons of the rat cerebral cortex', *Science*, 231(4741), pp. 995-7.

- Ceriello, A. (2000) 'Oxidative stress and glycemic regulation', *Metabolism*, 49(2 Suppl 1), pp. 27-9.
- Chan, F. (2017) 'Modelling mitochondrial epilepsy in vitro: conceptualisation, mechanisms, and therapeutic implications', *PhD thesis, Newcastle University*.
- Chandra, S., Gallardo, G., Fernandez-Chacon, R., Schluter, O.M. and Sudhof, T.C. (2005) 'Alpha-synuclein cooperates with CSPalpha in preventing neurodegeneration', *Cell*, 123(3), pp. 383-96.
- Chinta, S.J., Mallajosyula, J.K., Rane, A. and Andersen, J.K. (2010) 'Mitochondrial alpha-synuclein accumulation impairs complex I function in dopaminergic neurons and results in increased mitophagy in vivo', *Neurosci Lett*, 486(3), pp. 235-9.
- Chow, A., Erisir, A., Farb, C., Nadal, M.S., Ozaita, A., Lau, D., Welker, E. and Rudy, B. (1999) 'K(+) channel expression distinguishes subpopulations of parvalbumin- and somatostatin-containing neocortical interneurons', *J Neurosci*, 19(21), pp. 9332-45.
- Churchyard, A. and Lees, A.J. (1997) 'The relationship between dementia and direct involvement of the hippocampus and amygdala in Parkinson's disease', *Neurology*, 49(6), pp. 1570-6.
- Clapham, D.E. (2007) 'Calcium signaling', *Cell*, 131(6), pp. 1047-58.
- Clarke, L.E., Liddelow, S.A., Chakraborty, C., Munch, A.E., Heiman, M. and Barres, B.A. (2018) 'Normal aging induces A1-like astrocyte reactivity', *Proc Natl Acad Sci U S A*, 115(8), pp. E1896-e1905.
- Clinton, L.K., Blurton-Jones, M., Myczek, K., Trojanowski, J.Q. and LaFerla, F.M. (2010) 'Synergistic Interactions between Abeta, tau, and alpha-synuclein: acceleration of neuropathology and cognitive decline', *J Neurosci*, 30(21), pp. 7281-9.
- Cobb, S.R., Halasy, K., Vida, I., Nyiri, G., Tamas, G., Buhl, E.H. and Somogyi, P. (1997) 'Synaptic effects of identified interneurons innervating both interneurons and pyramidal cells in the rat hippocampus', *Neuroscience*, 79(3), pp. 629-48.
- Codolo, G., Plotegher, N., Pozzobon, T., Brucale, M., Tessari, I., Bubacco, L. and de Bernard, M. (2013) 'Triggering of inflammasome by aggregated alpha-synuclein, an inflammatory response in synucleinopathies', *PLoS One*, 8(1), p. e55375.
- Colgin, L.L., Jia, Y., Sabatier, J.M. and Lynch, G. (2005) 'Blockade of NMDA receptors enhances spontaneous sharp waves in rat hippocampal slices', *Neurosci Lett*, 385(1), pp. 46-51.
- Colgin, L.L., Kubota, D., Jia, Y., Rex, C.S. and Lynch, G. (2004) 'Long-term potentiation is impaired in rat hippocampal slices that produce spontaneous sharp waves', *J Physiol*, 558(Pt 3), pp. 953-61.
- Cope, D.W., Di Giovanni, G., Fyson, S.J., Orban, G., Errington, A.C., Lorincz, M.L., Gould, T.M., Carter, D.A. and Crunelli, V. (2009) 'Enhanced tonic GABAA inhibition in typical absence epilepsy', *Nat Med*, 15(12), pp. 1392-8.

- Cossart, R., Dinocourt, C., Hirsch, J.C., Merchan-Perez, A., De Felipe, J., Ben-Ari, Y., Esclapez, M. and Bernard, C. (2001) 'Dendritic but not somatic GABAergic inhibition is decreased in experimental epilepsy', *Nat Neurosci*, 4(1), pp. 52-62.
- Coulin, C., Drakew, A., Frotscher, M. and Deller, T. (2001) 'Stereological estimates of total neuron numbers in the hippocampus of adult reeler mutant mice: Evidence for an increased survival of Cajal-Retzius cells', *J Comp Neurol*, 439(1), pp. 19-31.
- Crotti, A. and Ransohoff, R.M. (2016) 'Microglial Physiology and Pathophysiology: Insights from Genome-wide Transcriptional Profiling', *Immunity*, 44(3), pp. 505-515.
- Crystal, H.A., Dickson, D.W., Lizardi, J.E., Davies, P. and Wolfson, L.I. (1990) 'Antemortem diagnosis of diffuse Lewy body disease', *Neurology*, 40(10), pp. 1523-8.
- Cunningham, M.O., Davies, C.H., Buhl, E.H., Kopell, N. and Whittington, M.A. (2003) 'Gamma oscillations induced by kainate receptor activation in the entorhinal cortex in vitro', *J Neurosci*, 23(30), pp. 9761-9.
- Dalfo, E., Gomez-Isla, T., Rosa, J.L., Nieto Bodelon, M., Cuadrado Tejedor, M., Barrachina, M., Ambrosio, S. and Ferrer, I. (2004) 'Abnormal alpha-synuclein interactions with Rab proteins in alpha-synuclein A30P transgenic mice', *J Neuropathol Exp Neurol*, 63(4), pp. 302-13.
- Danzer, K.M., Schnack, C., Sutcliffe, A., Hengerer, B. and Gillardon, F. (2007) 'Functional protein kinase arrays reveal inhibition of p-21-activated kinase 4 by alpha-synuclein oligomers', *J Neurochem*, 103(6), pp. 2401-7.
- Davidson, W.S., Jonas, A., Clayton, D.F. and George, J.M. (1998) 'Stabilization of alpha-synuclein secondary structure upon binding to synthetic membranes', *J Biol Chem*, 273(16), pp. 9443-9.
- Davies, P. and Maloney, A.J. (1976) 'Selective loss of central cholinergic neurons in Alzheimer's disease', *Lancet*, 2(8000), p. 1403.
- Davila, J.C., Real, M.A., Olmos, L., Legaz, I., Medina, L. and Guirado, S. (2005) 'Embryonic and postnatal development of GABA, calbindin, calretinin, and parvalbumin in the mouse claustral complex', *J Comp Neurol*, 481(1), pp. 42-57.
- Davis, E.J., Foster, T.D. and Thomas, W.E. (1994) 'Cellular forms and functions of brain microglia', *Brain Res Bull*, 34(1), pp. 73-8.
- Davis, S., Butcher, S.P. and Morris, R.G. (1992) 'The NMDA receptor antagonist D-2-amino-5-phosphonopentanoate (D-AP5) impairs spatial learning and LTP in vivo at intracerebral concentrations comparable to those that block LTP in vitro', *J Neurosci*, 12(1), pp. 21-34.
- Dawson, R., Jr. and Wallace, D.R. (1992) 'Kainic acid-induced seizures in aged rats: neurochemical correlates', *Brain Res Bull*, 29(3-4), pp. 459-68.
- DeFelipe, J., Alonso-Nanclares, L. and Arellano, J.I. (2002) 'Microstructure of the neocortex: comparative aspects', *J Neurocytol*, 31(3-5), pp. 299-316.

- Dekkers, J., Bayley, P., Dick, J.R., Schwaller, B., Berchtold, M.W. and Greensmith, L. (2004) 'Over-expression of parvalbumin in transgenic mice rescues motoneurons from injury-induced cell death', *Neuroscience*, 123(2), pp. 459-66.
- Desai, V.G., Feuers, R.J., Hart, R.W. and Ali, S.F. (1996) 'MPP(+)-induced neurotoxicity in mouse is age-dependent: evidenced by the selective inhibition of complexes of electron transport', *Brain Res*, 715(1-2), pp. 1-8.
- Devi, L., Raghavendran, V., Prabhu, B.M., Avadhani, N.G. and Anandatheerthavarada, H.K. (2008) 'Mitochondrial import and accumulation of alpha-synuclein impair complex I in human dopaminergic neuronal cultures and Parkinson disease brain', *J Biol Chem*, 283(14), pp. 9089-100.
- Devinsky, O., Vezzani, A., Najjar, S., De Lanerolle, N.C. and Rogawski, M.A. (2013) 'Glia and epilepsy: excitability and inflammation', *Trends Neurosci*, 36(3), pp. 174-84.
- Dickinson, R., Awaiz, S., Whittington, M.A., Lieb, W.R. and Franks, N.P. (2003) 'The effects of general anaesthetics on carbachol-evoked gamma oscillations in the rat hippocampus in vitro', *Neuropharmacology*, 44(7), pp. 864-872.
- Diogenes, M.J., Dias, R.B., Rombo, D.M., Vicente Miranda, H., Maiolino, F., Guerreiro, P., Nasstrom, T., Franquelim, H.G., Oliveira, L.M., Castanho, M.A., Lannfelt, L., Bergstrom, J., Ingelsson, M., Quintas, A., Sebastiao, A.M., Lopes, L.V. and Outeiro, T.F. (2012) 'Extracellular alpha-synuclein oligomers modulate synaptic transmission and impair LTP via NMDA-receptor activation', *J Neurosci*, 32(34), pp. 11750-62.
- Distelmaier, F., Koopman, W.J., van den Heuvel, L.P., Rodenburg, R.J., Mayatepek, E., Willems, P.H. and Smeitink, J.A. (2009) 'Mitochondrial complex I deficiency: from organelle dysfunction to clinical disease', *Brain*, 132(Pt 4), pp. 833-42.
- Donato, F., Rompani, S.B. and Caroni, P. (2013) 'Parvalbumin-expressing basket-cell network plasticity induced by experience regulates adult learning', *Nature*, 504(7479), pp. 272-6.
- Dong, X., Wang, Y. and Qin, Z. (2009) 'Molecular mechanisms of excitotoxicity and their relevance to pathogenesis of neurodegenerative diseases', *Acta Pharmacol Sin*, 30(4), pp. 379-87.
- Driver, J.E., Racca, C., Cunningham, M.O., Towers, S.K., Davies, C.H., Whittington, M.A. and LeBeau, F.E. (2007) 'Impairment of hippocampal gamma-frequency oscillations in vitro in mice overexpressing human amyloid precursor protein (APP)', *Eur J Neurosci*, 26(5), pp. 1280-8.
- Du, J., Zhang, L., Weiser, M., Rudy, B. and McBain, C.J. (1996) 'Developmental expression and functional characterization of the potassium-channel subunit Kv3.1b in parvalbumin-containing interneurons of the rat hippocampus', *J Neurosci*, 16(2), pp. 506-18.
- Duda, J.E. (2004) 'Pathology and neurotransmitter abnormalities of dementia with Lewy bodies', *Dement Geriatr Cogn Disord*, 17 Suppl 1, pp. 3-14.

- Eckel-Mahan, K. and Sassone-Corsi, P. (2015) 'Phenotyping Circadian Rhythms in Mice', *Curr Protoc Mouse Biol*, 5(3), pp. 271-81.
- Ego-Stengel, V. and Wilson, M.A. (2010) 'Disruption of ripple-associated hippocampal activity during rest impairs spatial learning in the rat', *Hippocampus*, 20(1), pp. 1-10.
- Ekmark-Lewen, S., Lindstrom, V., Gumucio, A., Ihse, E., Behere, A. and Kahle, P.J. (2018) 'Early fine motor impairment and behavioral dysfunction in (Thy-1)-h[A30P] alpha-synuclein mice', 8(3), p. e00915.
- El-Agnaf, O.M., Jakes, R., Curran, M.D. and Wallace, A. (1998) 'Effects of the mutations Ala30 to Pro and Ala53 to Thr on the physical and morphological properties of alpha-synuclein protein implicated in Parkinson's disease', *FEBS Lett*, 440(1-2), pp. 67-70.
- Ellison, D.W., Beal, M.F., Mazurek, M.F., Bird, E.D. and Martin, J.B. (1986) 'A postmortem study of amino acid neurotransmitters in Alzheimer's disease', *Ann Neurol*, 20(5), pp. 616-21.
- Erecinska, M. and Silver, I.A. (2001) 'Tissue oxygen tension and brain sensitivity to hypoxia', *Respir Physiol*, 128(3), pp. 263-76.
- Eriksen, J.L., Sagi, S.A., Smith, T.E., Weggen, S., Das, P., McLendon, D.C., Ozols, V.V., Jessing, K.W., Zavitz, K.H., Koo, E.H. and Golde, T.E. (2003) 'NSAIDs and enantiomers of flurbiprofen target gamma-secretase and lower Abeta 42 in vivo', *J Clin Invest*, 112(3), pp. 440-9.
- Esposito, A., Dohm, C.P., Kermer, P., Bahr, M. and Wouters, F.S. (2007) 'alpha-Synuclein and its disease-related mutants interact differentially with the microtubule protein tau and associate with the actin cytoskeleton', *Neurobiol Dis*, 26(3), pp. 521-31.
- Fanselow, M.S. and Dong, H.W. (2010) 'Are The Dorsal and Ventral Hippocampus functionally distinct structures?', *Neuron*, 65(1), p. 7.
- Fares, M.B., Maco, B., Oueslati, A., Rockenstein, E., Ninkina, N., Buchman, V.L., Masliah, E. and Lashuel, H.A. (2016) 'Induction of de novo alpha-synuclein fibrillization in a neuronal model for Parkinson's disease', *Proc Natl Acad Sci U S A*, 113(7), pp. E912-21.
- Faul, F., Erdfelder, E., Lang, A.G. and Buchner, A. (2007) 'G\*Power 3: a flexible statistical power analysis program for the social, behavioral, and biomedical sciences', *Behav Res Methods*, 39(2), pp. 175-91.
- Favuzzi, E., Marques-Smith, A., Deogracias, R., Winterflood, C.M., Sanchez-Aguilera, A., Mantoan, L., Maeso, P., Fernandes, C., Ewers, H. and Rico, B. (2017) 'Activity-Dependent Gating of Parvalbumin Interneuron Function by the Perineuronal Net Protein Brevican', *Neuron*, 95(3), pp. 639-655.e10.
- Feng, G., Mellor, R.H., Bernstein, M., Keller-Peck, C., Nguyen, Q.T., Wallace, M., Nerbonne, J.M., Lichtman, J.W. and Sanes, J.R. (2000) 'Imaging neuronal subsets in

transgenic mice expressing multiple spectral variants of GFP', *Neuron*, 28(1), pp. 41-51.

Ferando, I. and Mody, I. (2015) 'In vitro gamma oscillations following partial and complete ablation of  $\delta$  subunit-containing GABA(A) receptors from parvalbumin interneurons', *Neuropharmacology*, 88, pp. 91-8.

Ferrini, F. and De Koninck, Y. (2013) 'Microglia control neuronal network excitability via BDNF signalling', *Neural Plast*, 2013, p. 429815.

Fisahn, A., Pike, F.G., Buhl, E.H. and Paulsen, O. (1998) 'Cholinergic induction of network oscillations at 40 Hz in the hippocampus in vitro', *Nature*, 394(6689), pp. 186-9.

Fischer, V., Both, M., Draguhn, A. and Egorov, A.V. (2014) 'Choline-mediated modulation of hippocampal sharp wave-ripple complexes in vitro', *J Neurochem*, 129(5), pp. 792-805.

Flagmeier, P., Meisl, G., Vendruscolo, M., Knowles, T.P.J., Dobson, C.M., Buell, A.K. and Galvagnion, C. (2016) 'Mutations associated with familial Parkinson's disease alter the initiation and amplification steps of  $\alpha$ -synuclein aggregation', *Proc Natl Acad Sci U S A*, 113(37), pp. 10328-33.

Flores-Cuadrado, A., Ubeda-Banon, I., Saiz-Sanchez, D., de la Rosa-Prieto, C. and Martinez-Marcos, A. (2016) 'Hippocampal alpha-synuclein and interneurons in Parkinson's disease: Data from human and mouse models', *Mov Disord*, 31(7), pp. 979-88.

Foulds, P.G., Diggle, P., Mitchell, J.D., Parker, A., Hasegawa, M., Masuda-Suzukake, M., Mann, D.M. and Allsop, D. (2013) 'A longitudinal study on alpha-synuclein in blood plasma as a biomarker for Parkinson's disease', *Sci Rep*, 3, p. 2540.

Francois, J., Ferrandon, A., Koning, E., Angst, M.J., Sandner, G. and Nehlig, A. (2009) 'Selective reorganization of GABAergic transmission in neonatal ventral hippocampal-lesioned rats', *Int J Neuropsychopharmacol*, 12(8), pp. 1097-110.

Freichel, C., Neumann, M., Ballard, T., Muller, V., Woolley, M., Ozmen, L., Borroni, E., Kretschmar, H.A., Haass, C., Spooren, W. and Kahle, P.J. (2007) 'Age-dependent cognitive decline and amygdala pathology in alpha-synuclein transgenic mice', *Neurobiol Aging*, 28(9), pp. 1421-35.

Freund, T.F. and Buzsaki, G. (1996) 'Interneurons of the hippocampus', *Hippocampus*, 6(4), pp. 347-470.

Friauf, E. (2000) 'Development of chondroitin sulfate proteoglycans in the central auditory system of rats correlates with acquisition of mature properties', *Audiol Neurootol*, 5(5), pp. 251-62.

Frisard, M. and Ravussin, E. (2006) 'Energy metabolism and oxidative stress: impact on the metabolic syndrome and the aging process', *Endocrine*, 29(1), pp. 27-32.

- Fuchs, E.C., Zivkovic, A.R., Cunningham, M.O., Middleton, S., Lebeau, F.E., Bannerman, D.M., Rozov, A., Whittington, M.A., Traub, R.D., Rawlins, J.N. and Monyer, H. (2007) 'Recruitment of parvalbumin-positive interneurons determines hippocampal function and associated behavior', *Neuron*, 53(4), pp. 591-604.
- Fukuda, A., Czurko, A., Hida, H., Muramatsu, K., Lenard, L. and Nishino, H. (1995) 'Appearance of deteriorated neurons on regionally different time tables in rat brain thin slices maintained in physiological condition', *Neurosci Lett*, 184(1), pp. 13-6.
- Furukawa, S., Fujita, T., Shimabukuro, M., Iwaki, M., Yamada, Y., Nakajima, Y., Nakayama, O., Makishima, M., Matsuda, M. and Shimomura, I. (2004) 'Increased oxidative stress in obesity and its impact on metabolic syndrome', *J Clin Invest*, 114(12), pp. 1752-61.
- Gantert, M., Kreczmanski, P., Kuypers, E., Jellema, R., Strackx, E., Bastian, N., Gavilanes, A.W., Zimmermann, L.J., Garnier, Y., Schmitz, C. and Kramer, B.W. (2012) 'Effects of in utero endotoxemia on the ovine fetal brain: a model for schizophrenia?', *Front Biosci (Elite Ed)*, 4, pp. 2745-53.
- Garcia-Reitböck, P., Anichtchik, O., Bellucci, A., Iovino, M., Ballini, C., Fineberg, E., Ghetti, B., Della Corte, L., Spano, P., Tofaris, G.K., Goedert, M. and Spillantini, M.G. (2010) 'SNARE protein redistribution and synaptic failure in a transgenic mouse model of Parkinson's disease', *Brain*, 133(Pt 7), pp. 2032-44.
- Gaugler, M.N., Genc, O., Bobela, W., Mohanna, S., Ardah, M.T., El-Agnaf, O.M., Cantoni, M., Bensadoun, J.C., Schneggenburger, R., Knott, G.W., Aebischer, P. and Schneider, B.L. (2012) 'Nigrostriatal overabundance of alpha-synuclein leads to decreased vesicle density and deficits in dopamine release that correlate with reduced motor activity', *Acta Neuropathol*, 123(5), pp. 653-69.
- Gehrmann, J., Matsumoto, Y. and Kreutzberg, G.W. (1995) 'Microglia: intrinsic immuneffector cell of the brain', *Brain Res Brain Res Rev*, 20(3), pp. 269-87.
- Gerrard, J.L., Burke, S.N., McNaughton, B.L. and Barnes, C.A. (2008) 'Sequence reactivation in the hippocampus is impaired in aged rats', *J Neurosci*, 28(31), pp. 7883-90.
- Gibson, J.R., Beierlein, M. and Connors, B.W. (1999) 'Two networks of electrically coupled inhibitory neurons in neocortex', *Nature*, 402(6757), pp. 75-9.
- Girardeau, G., Benchenane, K., Wiener, S.I., Buzsaki, G. and Zugaro, M.B. (2009) 'Selective suppression of hippocampal ripples impairs spatial memory', *Nat Neurosci*, 12(10), pp. 1222-3.
- Golan, D., Tashijan, A. and Armstrong, E. (2011) *Principles of Pharmacology: The Pathophysiologic Basis of Drug Therapy*. Lippincott Williams and Wilkins; 3rd ed. edition (1 April 2011).
- Golub, V.M., Brewer, J., Wu, X., Kuruba, R., Short, J., Manchi, M., Swonke, M., Younus, I. and Reddy, D.S. (2015) 'Neurostereology protocol for unbiased



- quantification of neuronal injury and neurodegeneration', *Front Aging Neurosci*, 7, p. 196.
- Gomez-Tortosa, E., Sanders, J.L., Newell, K. and Hyman, B.T. (2001) 'Cortical neurons expressing calcium binding proteins are spared in dementia with Lewy bodies', *Acta Neuropathol*, 101(1), pp. 36-42.
- Görlach, A., Bertram, K., Hudecova, S. and Krizanova, O. (2015) 'Calcium and ROS: A mutual interplay', *Redox Biol*, 6, pp. 260-71.
- Goutagny, R., Gu, N., Cavanagh, C., Jackson, J., Chabot, J.G., Quirion, R., Krantic, S. and Williams, S. (2013) 'Alterations in hippocampal network oscillations and theta-gamma coupling arise before Abeta overproduction in a mouse model of Alzheimer's disease', *Eur J Neurosci*, 37(12), pp. 1896-902.
- Green, D.R. (1998) 'Apoptotic pathways: the roads to ruin', *Cell*, 94(6), pp. 695-8.
- Grosmark, A.D., Mizuseki, K., Pastalkova, E., Diba, K. and Buzsaki, G. (2012) 'REM Sleep Reorganizes Hippocampal Excitability', 75(6), pp. 1001-7.
- Grozdanov, V. and Danzer, K.M. (2018) 'Release and uptake of pathologic alpha-synuclein', *Cell Tissue Res*, 373(1), pp. 175-182.
- Gu, X.L., Long, C.X., Sun, L., Xie, C., Lin, X. and Cai, H. (2010) 'Astrocytic expression of Parkinson's disease-related A53T alpha-synuclein causes neurodegeneration in mice', *Mol Brain*, 3, p. 12.
- Guardia-Laguarta, C., Area-Gomez, E., Rub, C., Liu, Y., Magrane, J., Becker, D., Voos, W., Schon, E.A. and Przedborski, S. (2014) 'alpha-Synuclein is localized to mitochondria-associated ER membranes', *J Neurosci*, 34(1), pp. 249-59.
- Gulyas, A.I., Buzsaki, G., Freund, T.F. and Hirase, H. (2006) 'Populations of hippocampal inhibitory neurons express different levels of cytochrome c', *Eur J Neurosci*, 23(10), pp. 2581-94.
- H. Benno, R., W. Tucker, L., H. Joh, T. and J. Reis, D. (1985) 'The Use of Quantitative Immunocytochemistry to Study the Regulation of Tyrosine Hydroxylase in Noradrenergic and Dopaminergic Neural Systems', in, pp. 269-286.
- Haggerty, D.C., Glykos, V., Adams, N.E. and Lebeau, F.E. (2013) 'Bidirectional modulation of hippocampal gamma (20-80 Hz) frequency activity in vitro via alpha(alpha)- and beta(beta)-adrenergic receptors (AR)', *Neuroscience*, 253, pp. 142-54.
- Hajos, N., Karlocai, M.R., Nemeth, B., Ulbert, I., Monyer, H., Szabo, G., Erdelyi, F., Freund, T.F. and Gulyas, A.I. (2013) 'Input-output features of anatomically identified CA3 neurons during hippocampal sharp wave/ripple oscillation in vitro', *J Neurosci*, 33(28), pp. 11677-91.
- Hajos, N., Katona, I., Naiem, S.S., MacKie, K., Ledent, C., Mody, I. and Freund, T.F. (2000) 'Cannabinoids inhibit hippocampal GABAergic transmission and network oscillations', *Eur J Neurosci*, 12(9), pp. 3239-49.

- Hajos, N. and Paulsen, O. (2009) 'Network mechanisms of gamma oscillations in the CA3 region of the hippocampus', *Neural Netw*, 22(8), pp. 1113-9.
- Harman, D. (1956) 'Aging: a theory based on free radical and radiation chemistry', *J Gerontol*, 11(3), pp. 298-300.
- Hartig, W., Brauer, K. and Bruckner, G. (1992) 'Wisteria floribunda agglutinin-labelled nets surround parvalbumin-containing neurons', *Neuroreport*, 3(10), pp. 869-72.
- Hartig, W., Derouiche, A., Welt, K., Brauer, K., Grosche, J., Mader, M., Reichenbach, A. and Bruckner, G. (1999) 'Cortical neurons immunoreactive for the potassium channel Kv3.1b subunit are predominantly surrounded by perineuronal nets presumed as a buffering system for cations', *Brain Res*, 842(1), pp. 15-29.
- Hasel, P. and Dando, O. (2017) 'Neurons and neuronal activity control gene expression in astrocytes to regulate their development and metabolism', 8, p. 15132.
- Hashimoto, M., Hsu, L.J., Xia, Y., Takeda, A., Sisk, A., Sundsmo, M. and Masliah, E. (1999) 'Oxidative stress induces amyloid-like aggregate formation of NACP/alpha-synuclein in vitro', *Neuroreport*, 10(4), pp. 717-21.
- Haydon, P.G. and Carmignoto, G. (2006) 'Astrocyte control of synaptic transmission and neurovascular coupling', *Physiol Rev*, 86(3), pp. 1009-31.
- Heaulme, M., Chambon, J.P., Leyris, R., Molimard, J.C., Wermuth, C.G. and Biziere, K. (1986) 'Biochemical characterization of the interaction of three pyridazinyl-GABA derivatives with the GABAA receptor site', *Brain Res*, 384(2), pp. 224-31.
- Heistek, T.S., Jaap Timmerman, A., Spijker, S., Brussaard, A.B. and Mansvelder, H.D. (2010) 'GABAergic synapse properties may explain genetic variation in hippocampal network oscillations in mice', *Front Cell Neurosci*, 4, p. 18.
- Heja, L., Nyitrai, G., Kekesi, O., Dobolyi, A., Szabo, P., Fiath, R., Ulbert, I., Pal-Szenthe, B., Palkovits, M. and Kardos, J. (2012) 'Astrocytes convert network excitation to tonic inhibition of neurons', *BMC Biol*, 10, p. 26.
- Helps, S.C., Thornton, E., Kleinig, T.J., Manavis, J. and Vink, R. (2012) 'Automatic nonsubjective estimation of antigen content visualized by immunohistochemistry using color deconvolution', *Appl Immunohistochem Mol Morphol*, 20(1), pp. 82-90.
- Hermann, D., Both, M., Ebert, U., Gross, G., Schoemaker, H., Draguhn, A., Wicke, K. and Nimrich, V. (2009) 'Synaptic transmission is impaired prior to plaque formation in amyloid precursor protein-overexpressing mice without altering behaviorally-correlated sharp wave-ripple complexes', *Neuroscience*, 162(4), pp. 1081-90.
- Hernandez-Pineda, R., Chow, A., Amarillo, Y., Moreno, H., Saganich, M., Vega-Saenz de Miera, E.C., Hernandez-Cruz, A. and Rudy, B. (1999) 'Kv3.1-Kv3.2 channels underlie a high-voltage-activating component of the delayed rectifier K<sup>+</sup> current in projecting neurons from the globus pallidus', *J Neurophysiol*, 82(3), pp. 1512-28.
- Hettiarachchi, N.T., Parker, A., Dallas, M.L., Pennington, K., Hung, C.C., Pearson, H.A., Boyle, J.P., Robinson, P. and Peers, C. (2009) 'alpha-Synuclein modulation of

Ca<sup>2+</sup> signaling in human neuroblastoma (SH-SY5Y) cells', *J Neurochem*, 111(5), pp. 1192-201.

Hoening, J. and Heisey, D.M. (2002) *The Abuse of Power: The Pervasive Fallacy of Power Calculations for Data Analysis*.

Hof, P., Nimchinsky, E., Kidd, G., Claudio, L. and Trapp, B. (2009) 'Cellular Components of Nervous Tissue', in Byrne JH, H.R., Waxham JH, Byrne JH, Roberts JL. (ed.) *From Molecules to Networks: 2nd Edition*. Academic Press.

Hofer, K.T., Kandrats, A., Ulbert, I., Pal, I., Szabo, C., Heja, L. and Wittner, L. (2015) 'The hippocampal CA3 region can generate two distinct types of sharp wave-ripple complexes, in vitro', *Hippocampus*, 25(2), pp. 169-86.

Hormuzdi, S.G., Pais, I., LeBeau, F.E., Towers, S.K., Rozov, A., Buhl, E.H., Whittington, M.A. and Monyer, H. (2001) 'Impaired electrical signaling disrupts gamma frequency oscillations in connexin 36-deficient mice', *Neuron*, 31(3), pp. 487-95.

Huang, Y., Yoon, K., Ko, H., Jiao, S., Ito, W., Wu, J.Y., Yung, W.H., Lu, B. and Morozov, A. (2016) '5-HT<sub>3a</sub> Receptors Modulate Hippocampal Gamma Oscillations by Regulating Synchrony of Parvalbumin-Positive Interneurons', *Cereb Cortex*, 26(2), pp. 576-85.

Huchzermeyer, C., Albus, K., Gabriel, H.J., Otahal, J., Taubenberger, N., Heinemann, U., Kovacs, R. and Kann, O. (2008) 'Gamma oscillations and spontaneous network activity in the hippocampus are highly sensitive to decreases in pO<sub>2</sub> and concomitant changes in mitochondrial redox state', *J Neurosci*, 28(5), pp. 1153-62.

Huls, S., Hogen, T., Vassallo, N., Danzer, K.M., Hengerer, B., Giese, A. and Herms, J. (2011) 'AMPA-receptor-mediated excitatory synaptic transmission is enhanced by iron-induced alpha-synuclein oligomers', *J Neurochem*, 117(5), pp. 868-78.

Hunt, D.L. and Castillo, P.E. (2012) 'Synaptic plasticity of NMDA receptors: mechanisms and functional implications', *Curr Opin Neurobiol*, 22(3), pp. 496-508.

Hwang, O. (2013) 'Role of oxidative stress in Parkinson's disease', *Exp Neurobiol*, 22(1), pp. 11-7.

Hynd, M.R., Scott, H.L. and Dodd, P.R. (2004) 'Glutamate-mediated excitotoxicity and neurodegeneration in Alzheimer's disease', *Neurochem Int*, 45(5), pp. 583-95.

Inan, M., Zhao, M., Manuszak, M., Karakaya, C., Rajadhyaksha, A.M., Pickel, V.M., Schwartz, T.H., Goldstein, P.A. and Manfredi, G. (2016) 'Energy deficit in parvalbumin neurons leads to circuit dysfunction, impaired sensory gating and social disability', *Neurobiol Dis*, 93, pp. 35-46.

Ito, D., Imai, Y., Ohsawa, K., Nakajima, K., Fukuuchi, Y. and Kohsaka, S. (1998) 'Microglia-specific localisation of a novel calcium binding protein, Iba1', *Brain Res Mol Brain Res*, 57(1), pp. 1-9.

Jacobsen, J.C., Erdin, S., Chiang, C., Hanscom, C., Handley, R.R., Barker, D.D., Stortchevoi, A., Blumenthal, I., Reid, S.J., Snell, R.G., MacDonald, M.E., Morton, A.J.,

Ernst, C., Gusella, J.F. and Talkowski, M.E. (2017) 'Potential molecular consequences of transgene integration: The R6/2 mouse example', *Sci Rep*, 7, p. 41120.

Jasnow, A.M., Ehrlich, D.E., Choi, D.C., Dabrowska, J., Bowers, M.E., McCullough, K.M., Rainnie, D.G. and Ressler, K.J. (2013) 'Thy1-Expressing Neurons in the Basolateral Amygdala May Mediate Fear Inhibition', *J Neurosci*, 33(25), pp. 10396-404.

Jenco, J.M., Rawlins, A., Daniels, B. and Morris, A.J. (1998) 'Regulation of phospholipase D2: selective inhibition of mammalian phospholipase D isoenzymes by alpha- and beta-synucleins', *Biochemistry*, 37(14), pp. 4901-9.

Jensen, P.H., Nielsen, M.S., Jakes, R., Dotti, C.G. and Goedert, M. (1998) 'Binding of alpha-synuclein to brain vesicles is abolished by familial Parkinson's disease mutation', *J Biol Chem*, 273(41), pp. 26292-4.

Jha, M.K., Lee, S., Park, D.H., Kook, H., Park, K.-G., Lee, I.-K. and Suk, K. (2015) 'Diverse functional roles of lipocalin-2 in the central nervous system', *Neuroscience & Biobehavioral Reviews*, 49, pp. 135-156.

Jinno, S. and Kosaka, T. (2010) 'Stereological estimation of numerical densities of glutamatergic principal neurons in the mouse hippocampus', *Hippocampus*, 20(7), pp. 829-40.

Jouveneau, A., Potier, B., Battini, R., Ferrari, S., Dutar, P. and Billard, J.M. (1999) 'Glutamatergic synaptic responses and long-term potentiation are impaired in the CA1 hippocampal area of calbindin D(28k)-deficient mice', *Synapse*, 33(3), pp. 172-80.

Kahle, P.J., Neumann, M., Ozmen, L., Muller, V., Jacobsen, H., Schindzielorz, A., Okochi, M., Leimer, U., van Der Putten, H., Probst, A., Kremmer, E., Kretschmar, H.A. and Haass, C. (2000) 'Subcellular localization of wild-type and Parkinson's disease-associated mutant alpha -synuclein in human and transgenic mouse brain', *J Neurosci*, 20(17), pp. 6365-73.

Kahle, P.J., Neumann, M., Ozmen, L., Muller, V., Odoj, S., Okamoto, N., Jacobsen, H., Iwatsubo, T., Trojanowski, J.Q., Takahashi, H., Wakabayashi, K., Bogdanovic, N., Riederer, P., Kretschmar, H.A. and Haass, C. (2001) 'Selective insolubility of alpha-synuclein in human Lewy body diseases is recapitulated in a transgenic mouse model', *Am J Pathol*, 159(6), pp. 2215-25.

Kamphuis, W., Middeldorp, J., Kooijman, L., Sluijs, J.A., Kooi, E.J., Moeton, M., Freriks, M., Mizee, M.R. and Hol, E.M. (2014) 'Glial fibrillary acidic protein isoform expression in plaque related astrogliosis in Alzheimer's disease', *Neurobiol Aging*, 35(3), pp. 492-510.

Kanamori, K. (2015) 'Disinhibition reduces extracellular glutamine and elevates extracellular glutamate in rat hippocampus in vivo', *Epilepsy Res*, 114, pp. 32-46.

Kann, O. (2016) 'The interneuron energy hypothesis: Implications for brain disease', *Neurobiol Dis*, 90, pp. 75-85.

- Kann, O., Hollnagel, J.O., Elzoheiry, S. and Schneider, J. (2016) 'Energy and Potassium Ion Homeostasis during Gamma Oscillations', *Front Mol Neurosci*, 9, p. 47.
- Kann, O., Huchzermeyer, C., Kovacs, R., Wirtz, S. and Schuelke, M. (2011) 'Gamma oscillations in the hippocampus require high complex I gene expression and strong functional performance of mitochondria', *Brain*, 134(Pt 2), pp. 345-58.
- Kaufmann, T.J., Harrison, P.M., Richardson, M.J., Pinheiro, T.J. and Wall, M.J. (2016) 'Intracellular soluble alpha-synuclein oligomers reduce pyramidal cell excitability', *J Physiol*, 594(10), pp. 2751-72.
- Keane, P. (2013) 'The mechanism of trichloroethylene neurotoxicity and its relation to Parkinsonism', *PhD thesis, Newcastle University*.
- Keener, A.M. and Bordelon, Y.M. (2016) 'Parkinsonism', *Semin Neurol*, 36(4), pp. 330-4.
- Kemshead, J.T., Ritter, M.A., Cotmore, S.F. and Greaves, M.F. (1982) 'Human Thy-1: expression on the cell surface of neuronal and glial cells', *Brain Res*, 236(2), pp. 451-61.
- Kilb, W., Sinning, A. and Luhmann, H.J. (2007) 'Model-specific effects of bumetanide on epileptiform activity in the in-vitro intact hippocampus of the newborn mouse', *Neuropharmacology*, 53(4), pp. 524-33.
- Klapstein, G.J., Vietla, S., Lieberman, D.N., Gray, P.A., Airaksinen, M.S., Thoenen, H., Meyer, M. and Mody, I. (1998) 'Calbindin-D28k fails to protect hippocampal neurons against ischemia in spite of its cytoplasmic calcium buffering properties: evidence from calbindin-D28k knockout mice', *Neuroscience*, 85(2), pp. 361-73.
- Klausberger, T., Marton, L.F., O'Neill, J., Huck, J.H., Dalezios, Y., Fuentealba, P., Suen, W.Y., Papp, E., Kaneko, T., Watanabe, M., Csicsvari, J. and Somogyi, P. (2005) 'Complementary roles of cholecystinin- and parvalbumin-expressing GABAergic neurons in hippocampal network oscillations', *J Neurosci*, 25(42), pp. 9782-93.
- Kleschevnikov, A.M., Belichenko, P.V., Villar, A.J., Epstein, C.J., Malenka, R.C. and Mobley, W.C. (2004) 'Hippocampal long-term potentiation suppressed by increased inhibition in the Ts65Dn mouse, a genetic model of Down syndrome', *J Neurosci*, 24(37), pp. 8153-60.
- Kolbaev, S.N., Sharopov, S., Dierkes, P.W., Luhmann, H.J. and Kilb, W. (2012) 'Phasic GABAA -receptor activation is required to suppress epileptiform activity in the CA3 region of the immature rat hippocampus', *Epilepsia*, 53(5), pp. 888-96.
- Kollias, G., Spanopoulou, E., Grosveld, F., Ritter, M., Beech, J. and Morris, R. (1987) 'Differential regulation of a Thy-1 gene in transgenic mice', *Proc Natl Acad Sci U S A*, 84(6), pp. 1492-6.
- Kosaka, T., Katsumaru, H., Hama, K., Wu, J.Y. and Heizmann, C.W. (1987) 'GABAergic neurons containing the Ca<sup>2+</sup>-binding protein parvalbumin in the rat hippocampus and dentate gyrus', *Brain Res*, 419(1-2), pp. 119-30.

- Krismer, F. and Wenning, G.K. (2017) 'Multiple system atrophy: insights into a rare and debilitating movement disorder', *Nature Reviews Neurology*, 13, p. 232.
- Kruger, R., Kuhn, W., Muller, T., Woitalla, D., Graeber, M., Kosel, S., Przuntek, H., Epplen, J.T., Schols, L. and Riess, O. (1998) 'Ala30Pro mutation in the gene encoding alpha-synuclein in Parkinson's disease', *Nat Genet*, 18(2), pp. 106-8.
- Kubota, D., Colgin, L.L., Casale, M., Brucher, F.A. and Lynch, G. (2003) 'Endogenous waves in hippocampal slices', *J Neurophysiol*, 89(1), pp. 81-9.
- Kuenzi, F.M., Fitzjohn, S.M., Morton, R.A., Collingridge, G.L. and Seabrook, G.R. (2000) 'Reduced long-term potentiation in hippocampal slices prepared using sucrose-based artificial cerebrospinal fluid', *J Neurosci Methods*, 100(1-2), pp. 117-22.
- Kumar, A. (2010) 'Carbachol-Induced Long-Term Synaptic Depression Is Enhanced During Senescence at Hippocampal CA3–CA1 Synapses', *J Neurophysiol*, 104(2), pp. 607-16.
- Lado, F.A., Laureta, E.C. and Moshe, S.L. (2002) 'Seizure-induced hippocampal damage in the mature and immature brain', *Epileptic Disord*, 4(2), pp. 83-97.
- Lam, A.D., Deck, G., Goldman, A., Eskandar, E.N., Noebels, J. and Cole, A.J. (2017) 'Silent hippocampal seizures and spikes identified by foramen ovale electrodes in Alzheimer's disease', *Nat Med*, 23(6), pp. 678-680.
- Langston, J.W., Ballard, P., Tetrud, J.W. and Irwin, I. (1983) 'Chronic Parkinsonism in humans due to a product of meperidine-analog synthesis', *Science*, 219(4587), pp. 979-80.
- Lau, L.W., Cua, R., Keough, M.B., Haylock-Jacobs, S. and Yong, V.W. (2013) 'Pathophysiology of the brain extracellular matrix: a new target for remyelination', *Nat Rev Neurosci*, 14(10), pp. 722-9.
- Lauri, S.E., Bortolotto, Z.A., Bleakman, D., Ornstein, P.L., Lodge, D., Isaac, J.T. and Collingridge, G.L. (2001) 'A critical role of a facilitatory presynaptic kainate receptor in mossy fiber LTP', *Neuron*, 32(4), pp. 697-709.
- Lawrence, Y.A., Kemper, T.L., Bauman, M.L. and Blatt, G.J. (2010) 'Parvalbumin-, calbindin-, and calretinin-immunoreactive hippocampal interneuron density in autism', *Acta Neurol Scand*, 121(2), pp. 99-108.
- Lawson, L.J., Perry, V.H. and Gordon, S. (1992) 'Turnover of resident microglia in the normal adult mouse brain', *Neuroscience*, 48(2), pp. 405-15.
- Lee, F.J., Liu, F., Pristupa, Z.B. and Niznik, H.B. (2001) 'Direct binding and functional coupling of alpha-synuclein to the dopamine transporters accelerate dopamine-induced apoptosis', *Faseb j*, 15(6), pp. 916-26.
- Lee, H.C. and Wei, Y.H. (2005) 'Mitochondrial biogenesis and mitochondrial DNA maintenance of mammalian cells under oxidative stress', *Int J Biochem Cell Biol*, 37(4), pp. 822-34.

- Lee, H.J., Bae, E.J. and Lee, S.J. (2014a) 'Extracellular alpha--synuclein-a novel and crucial factor in Lewy body diseases', *Nat Rev Neurol*, 10(2), pp. 92-8.
- Lee, H.J., Kim, C. and Lee, S.J. (2010) 'Alpha-synuclein stimulation of astrocytes: Potential role for neuroinflammation and neuroprotection', *Oxid Med Cell Longev*, 3(4), pp. 283-7.
- Lee, H.S., Ghetti, A., Pinto-Duarte, A., Wang, X., Dzievczapolski, G., Galimi, F., Huitron-Resendiz, S., Pina-Crespo, J.C., Roberts, A.J., Verma, I.M., Sejnowski, T.J. and Heinemann, S.F. (2014b) 'Astrocytes contribute to gamma oscillations and recognition memory', *Proc Natl Acad Sci U S A*, 111(32), pp. E3343-52.
- Lee, S. and Jones, S.R. (2013) 'Distinguishing mechanisms of gamma frequency oscillations in human current source signals using a computational model of a laminar neocortical network', *Front Hum Neurosci*, 7, p. 869.
- Lenaz, G., Bovina, C., Castelluccio, C., Fato, R., Formiggini, G., Genova, M.L., Marchetti, M., Pich, M.M., Pallotti, F., Parenti Castelli, G. and Biagini, G. (1997) 'Mitochondrial complex I defects in aging', *Mol Cell Biochem*, 174(1-2), pp. 329-33.
- Lensjo, K.K., Christensen, A.C., Tennoe, S., Fyhn, M. and Hafting, T. (2017) 'Differential Expression and Cell-Type Specificity of Perineuronal Nets in Hippocampus, Medial Entorhinal Cortex, and Visual Cortex Examined in the Rat and Mouse', 4(3).
- Lewis, D.A., Hashimoto, T. and Volk, D.W. (2005) 'Cortical inhibitory neurons and schizophrenia', *Nat Rev Neurosci*, 6(4), pp. 312-24.
- Li, W.W., Yang, R., Guo, J.C., Ren, H.M., Zha, X.L., Cheng, J.S. and Cai, D.F. (2007) 'Localization of alpha-synuclein to mitochondria within midbrain of mice', *Neuroreport*, 18(15), pp. 1543-6.
- Li, X.G., Somogyi, P., Tepper, J.M. and Buzsaki, G. (1992) 'Axonal and dendritic arborization of an intracellularly labeled chandelier cell in the CA1 region of rat hippocampus', *Exp Brain Res*, 90(3), pp. 519-25.
- Liddelw, S.A., Guttenplan, K.A., Clarke, L.E., Bennett, F.C., Bohlen, C.J., Schirmer, L., Bennett, M.L., Munch, A.E., Chung, W.S., Peterson, T.C., Wilton, D.K., Frouin, A., Napier, B.A., Panicker, N., Kumar, M., Buckwalter, M.S., Rowitch, D.H., Dawson, V.L., Dawson, T.M., Stevens, B. and Barres, B.A. (2017) 'Neurotoxic reactive astrocytes are induced by activated microglia', *Nature*, 541(7638), pp. 481-487.
- Lindstrom, V., Fagerqvist, T., Nordstrom, E., Eriksson, F., Lord, A., Tucker, S., Andersson, J., Johannesson, M., Schell, H., Kahle, P.J., Moller, C., Gellerfors, P., Bergstrom, J., Lannfelt, L. and Ingelsson, M. (2014) 'Immunotherapy targeting alpha-synuclein protofibrils reduced pathology in (Thy-1)-h[A30P] alpha-synuclein mice', *Neurobiol Dis*, 69, pp. 134-43.
- Liu, S., Ninan, I., Antonova, I., Battaglia, F., Trinchese, F., Narasanna, A., Kolodilov, N., Dauer, W., Hawkins, R.D. and Arancio, O. (2004) 'alpha-Synuclein produces a long-lasting increase in neurotransmitter release', *Embo j*, 23(22), pp. 4506-16.

- Lodish, H., Berk, A., Zipursky, S., Matsudaira, P., Baltimore, D. and Darnell, J. (2000) *Molecular Cell Biology, 4th Edition*. New York: W.H. Freeman.
- Lu, C., Wang, Z., Zhou, Y. and Vreugdenhil, M. (2012a) 'Temperature- and concentration-dependence of kainate-induced  $\gamma$  oscillation in rat hippocampal slices under submerged condition', *Acta Pharmacol Sin*, 33(2), pp. 214-20.
- Lu, C.B., Hamilton, J.B., Powell, A.D., Toescu, E.C. and Vreugdenhil, M. (2011) 'Effect of ageing on CA3 interneuron sAHP and gamma oscillations is activity-dependent', *Neurobiol Aging*, 32(5), pp. 956-65.
- Lu, C.B., Vreugdenhil, M. and Toescu, E.C. (2012b) 'The effect of aging-associated impaired mitochondrial status on kainate-evoked hippocampal gamma oscillations', *Neurobiol Aging*, 33(11), pp. 2692-703.
- Luchtman, D.W., Shao, D. and Song, C. (2009) 'Behavior, neurotransmitters and inflammation in three regimens of the MPTP mouse model of Parkinson's disease', *Physiol Behav*, 98(1-2), pp. 130-8.
- Ma, J., Tai, S.K. and Leung, L.S. (2012) 'Septohippocampal GABAergic neurons mediate the altered behaviors induced by n-methyl-D-aspartate receptor antagonists', *Hippocampus*, 22(12), pp. 2208-18.
- Mackenzie, I.R. (2000) 'Activated microglia in dementia with Lewy bodies', *Neurology*, 55(1), pp. 132-4.
- Mackenzie, I.R. (2001) 'Cortical inflammation in dementia with Lewy bodies', *Arch Neurol*, 58(3), pp. 519-20.
- Maetzler, W., Nitsch, C., Bendfeldt, K., Racay, P., Vollenweider, F. and Schwaller, B. (2004) 'Ectopic parvalbumin expression in mouse forebrain neurons increases excitotoxic injury provoked by ibotenic acid injection into the striatum', *Exp Neurol*, 186(1), pp. 78-88.
- Maier, N., Guldenagel, M., Sohl, G., Siegmund, H., Willecke, K. and Draguhn, A. (2002) 'Reduction of high-frequency network oscillations (ripples) and pathological network discharges in hippocampal slices from connexin 36-deficient mice', *J Physiol*, 541(Pt 2), pp. 521-8.
- Maier, N., Morris, G., Jochenning, F.W. and Schmitz, D. (2009) 'An approach for reliably investigating hippocampal sharp wave-ripples in vitro', *PLoS One*, 4(9), p. e6925.
- Maier, N., Nimmrich, V. and Draguhn, A. (2003) 'Cellular and network mechanisms underlying spontaneous sharp wave-ripple complexes in mouse hippocampal slices', *J Physiol*, 550(Pt 3), pp. 873-87.
- Manev, H., Favaron, M., Guidotti, A. and Costa, E. (1989) 'Delayed increase of  $Ca^{2+}$  influx elicited by glutamate: role in neuronal death', *Mol Pharmacol*, 36(1), pp. 106-12.
- Mann, E.O., Kohl, M.M. and Paulsen, O. (2009) 'Distinct roles of GABA(A) and GABA(B) receptors in balancing and terminating persistent cortical activity', *J Neurosci*, 29(23), pp. 7513-7518.



- Marksteiner, J., Lassmann, H., Saria, A., Humpel, C., Meyer, D.K. and Sperk, G. (1990) 'Neuropeptide Levels after Pentylentetrazol Kindling in the Rat', *Eur J Neurosci*, 2(1), pp. 98-103.
- Martin, J.L. and Sloviter, R.S. (2001) 'Focal inhibitory interneuron loss and principal cell hyperexcitability in the rat hippocampus after microinjection of a neurotoxic conjugate of saporin and a peptidase-resistant analog of Substance P', *J Comp Neurol*, 436(2), pp. 127-52.
- Marui, W., Iseki, E., Kato, M., Akatsu, H. and Kosaka, K. (2004) 'Pathological entity of dementia with Lewy bodies and its differentiation from Alzheimer's disease', *Acta Neuropathol*, 108(2), pp. 121-8.
- Marxreiter, F., Ettle, B., May, V.E.L., Esmer, H., Patrick, C., Kragh, C.L., Klucken, J., Winner, B., Riess, O., Winkler, J., Masliah, E. and Nuber, S. (2013) 'Glial A30P alpha-synuclein pathology segregates neurogenesis from anxiety-related behavior in conditional transgenic mice', *Neurobiology of Disease*, 59(0), pp. 38-51.
- Masliah, E., Rockenstein, E., Veinbergs, I., Mallory, M., Hashimoto, M., Takeda, A., Sagara, Y., Sisk, A. and Mucke, L. (2000) 'Dopaminergic loss and inclusion body formation in alpha-synuclein mice: implications for neurodegenerative disorders', *Science*, 287(5456), pp. 1265-9.
- Masuda-Suzukake, M., Nonaka, T., Hosokawa, M., Kubo, M., Shimozawa, A., Akiyama, H. and Hasegawa, M. (2014) 'Pathological alpha-synuclein propagates through neural networks', *Acta Neuropathol Commun*, 2, p. 88.
- Mauna, J.C., Miyamae, T., Pulli, B. and Thiels, E. (2011) 'Protein phosphatases 1 and 2A are both required for long-term depression and associated dephosphorylation of cAMP response element binding protein in hippocampal area CA1 in vivo', *Hippocampus*, 21(10), pp. 1093-104.
- McBride, H.M., Neuspiel, M. and Wasiak, S. (2006) 'Mitochondria: more than just a powerhouse', *Curr Biol*, 16(14), pp. R551-60.
- McDowell, K.A., Shin, D., Roos, K.P. and Chesselet, M.F. (2014) 'Sleep dysfunction and EEG alterations in mice overexpressing alpha-synuclein', *J Parkinsons Dis*, 4(3), pp. 531-539.
- McEwen, B.S. and Magarinos, A.M. (1997) 'Stress effects on morphology and function of the hippocampus', *Ann N Y Acad Sci*, 821, pp. 271-84.
- McKeith, I. (2004) 'Dementia with Lewy bodies', *Dialogues Clin Neurosci*, 6(3), pp. 333-41.
- McKeith, I.G., Boeve, B.F., Dickson, D.W., Halliday, G., Taylor, J.P., Weintraub, D., Aarsland, D., Galvin, J., Attems, J., Ballard, C.G., Bayston, A., Beach, T.G., Blanc, F., Bohnen, N., Bonanni, L., Bras, J., Brundin, P., Burn, D., Chen-Plotkin, A., Duda, J.E., El-Agnaf, O., Feldman, H., Ferman, T.J., Ffytche, D., Fujishiro, H., Galasko, D., Goldman, J.G., Gomperts, S.N., Graff-Radford, N.R., Honig, L.S., Iranzo, A., Kantarci, K., Kaufer, D., Kukull, W., Lee, V.M.Y., Leverenz, J.B., Lewis, S., Lippa, C., Lunde, A.,

Masellis, M., Masliah, E., McLean, P., Mollenhauer, B., Montine, T.J., Moreno, E., Mori, E., Murray, M., O'Brien, J.T., Orimo, S., Postuma, R.B., Ramaswamy, S., Ross, O.A., Salmon, D.P., Singleton, A., Taylor, A., Thomas, A., Tiraboschi, P., Toledo, J.B., Trojanowski, J.Q., Tsuang, D., Walker, Z., Yamada, M. and Kosaka, K. (2017) 'Diagnosis and management of dementia with Lewy bodies: Fourth consensus report of the DLB Consortium', *Neurology*, 89(1), pp. 88-100.

McMahon, L.L. and Kauer, J.A. (1997) 'Hippocampal interneurons express a novel form of synaptic plasticity', *Neuron*, 18(2), pp. 295-305.

McRae, P.A., Baranov, E., Rogers, S.L. and Porter, B.E. (2012) 'Persistent decrease in multiple components of the perineuronal net following status epilepticus', *Eur J Neurosci*, 36(11), pp. 3471-82.

McRae, P.A., Baranov, E., Sarode, S., Brooks-Kayal, A.R. and Porter, B.E. (2010) 'Aggrecan expression, a component of the inhibitory interneuron perineuronal net, is altered following an early-life seizure', *Neurobiol Dis*, 39(3), pp. 439-48.

Mecocci, P., MacGarvey, U. and Beal, M.F. (1994) 'Oxidative damage to mitochondrial DNA is increased in Alzheimer's disease', *Ann Neurol*, 36(5), pp. 747-51.

Megias, M., Emri, Z., Freund, T.F. and Gulyas, A.I. (2001) 'Total number and distribution of inhibitory and excitatory synapses on hippocampal CA1 pyramidal cells', *Neuroscience*, 102(3), pp. 527-40.

Meraz-Rios, M.A., Toral-Rios, D., Franco-Bocanegra, D., Villeda-Hernandez, J. and Campos-Pena, V. (2013) 'Inflammatory process in Alzheimer's Disease', *Front Integr Neurosci*, 7, p. 59.

Miles, R., Toth, K., Gulyas, A.I., Hajos, N. and Freund, T.F. (1996) 'Differences between somatic and dendritic inhibition in the hippocampus', *Neuron*, 16(4), pp. 815-23.

Milton, N.G. (2004) 'Role of hydrogen peroxide in the aetiology of Alzheimer's disease: implications for treatment', *Drugs Aging*, 21(2), pp. 81-100.

Minkeviciene, R., Rheims, S., Dobszay, M.B., Zilberter, M., Hartikainen, J., Fulop, L., Penke, B., Zilberter, Y., Harkany, T., Pitkanen, A. and Tanila, H. (2009) 'Amyloid beta-induced neuronal hyperexcitability triggers progressive epilepsy', *J Neurosci*, 29(11), pp. 3453-62.

Mironov, S.L. (2015) 'alpha-Synuclein forms non-selective cation channels and stimulates ATP-sensitive potassium channels in hippocampal neurons', *J Physiol*, 593(1), pp. 145-59.

Miyamoto, A., Wake, H., Moorhouse, A.J. and Nabekura, J. (2013) 'Microglia and synapse interactions: fine tuning neural circuits and candidate molecules', *Front Cell Neurosci*, 7, p. 70.

- Modebadze, T. (2014) 'Neuronal network dynamics during epileptogenesis in the medial temporal lobe', *PhD thesis, Aston University*, [http://publications.aston.ac.uk/24763/1/Modebadze\\_Tamara\\_2014.pdf](http://publications.aston.ac.uk/24763/1/Modebadze_Tamara_2014.pdf).
- Moehle, M.S. and West, A.B. (2015) 'M1 and M2 Immune Activation in Parkinson's Disease: Foe and Ally?', *Neuroscience*, 302, pp. 59-73.
- Molinari, S., Battini, R., Ferrari, S., Pozzi, L., Killcross, A.S., Robbins, T.W., Jouvenceau, A., Billard, J.M., Dutar, P., Lamour, Y., Baker, W.A., Cox, H. and Emson, P.C. (1996) 'Deficits in memory and hippocampal long-term potentiation in mice with reduced calbindin D28K expression', *Proc Natl Acad Sci U S A*, 93(15), pp. 8028-33.
- Moraes, L.S., Rohor, B.Z., Areal, L.B., Pereira, E.V., Santos, A.M., Facundo, V.A., Santos, A.R., Pires, R.G. and Martins-Silva, C. (2016) 'Medicinal plant *Combretum leprosum* mart ameliorates motor, biochemical and molecular alterations in a Parkinson's disease model induced by MPTP', *J Ethnopharmacol*, 185, pp. 68-76.
- Morawski, M., Bruckner, M.K., Riederer, P., Bruckner, G. and Arendt, T. (2004) 'Perineuronal nets potentially protect against oxidative stress', *Exp Neurol*, 188(2), pp. 309-15.
- Moreno, H., Burghardt, N.S., Vela-Duarte, D., Masciotti, J., Hua, F., Fenton, A.A., Schwaller, B. and Small, S.A. (2012) 'The absence of the calcium-buffering protein calbindin is associated with faster age-related decline in hippocampal metabolism', *Hippocampus*, 22(5), pp. 1107-20.
- Morris, M., Sanchez, P.E., Verret, L., Beagle, A.J., Guo, W., Dubal, D., Ranasinghe, K.G., Koyama, A., Ho, K., Yu, G.Q., Vossel, K.A. and Mucke, L. (2015) 'Network dysfunction in alpha-synuclein transgenic mice and human Lewy body dementia', *Ann Clin Transl Neurol*, 2(11), pp. 1012-28.
- Morris, R.G. (1989) 'Synaptic plasticity and learning: selective impairment of learning rats and blockade of long-term potentiation in vivo by the N-methyl-D-aspartate receptor antagonist AP5', *J Neurosci*, 9(9), pp. 3040-57.
- Morris, R.G., Anderson, E., Lynch, G.S. and Baudry, M. (1986) 'Selective impairment of learning and blockade of long-term potentiation by an N-methyl-D-aspartate receptor antagonist, AP5', *Nature*, 319(6056), pp. 774-6.
- Moser, M.B. and Moser, E.I. (1998) 'Functional differentiation in the hippocampus', *Hippocampus*, 8(6), pp. 608-19.
- Mrak, R.E. and Griffin, W.S. (2005) 'Glia and their cytokines in progression of neurodegeneration', *Neurobiol Aging*, 26(3), pp. 349-54.
- Nakazawa, K., Zsiros, V., Jiang, Z., Nakao, K., Kolata, S., Zhang, S. and Belforte, J.E. (2012) 'GABAergic interneuron origin of schizophrenia pathophysiology', *Neuropharmacology*, 62(3), pp. 1574-83.
- Nemani, V.M., Lu, W., Berge, V., Nakamura, K., Onoa, B., Lee, M.K., Chaudhry, F.A., Nicoll, R.A. and Edwards, R.H. (2010) 'Increased Expression of Alpha-Synuclein

Reduces Neurotransmitter Release by Inhibiting Synaptic Vesicle Reclustering After Endocytosis', *Neuron*, 65(1), pp. 66-79.

Neumann, M., Kahle, P.J., Giasson, B.I., Ozmen, L., Borroni, E., Spooen, W., Muller, V., Odooy, S., Fujiwara, H., Hasegawa, M., Iwatsubo, T., Trojanowski, J.Q., Kretzschmar, H.A. and Haass, C. (2002) 'Misfolded proteinase K-resistant hyperphosphorylated alpha-synuclein in aged transgenic mice with locomotor deterioration and in human alpha-synucleinopathies', *J Clin Invest*, 110(10), pp. 1429-39.

Nguyen, J.C., Killcross, A.S. and Jenkins, T.A. (2013) 'Effect of low-intensity treadmill exercise on behavioural measures and hippocampal parvalbumin immunoreactivity in the rat', *Behav Brain Res*, 256, pp. 598-601.

Niedermeyer, E. (1997) 'Alpha rhythms as physiological and abnormal phenomena', *Int J Psychophysiol*, 26(1-3), pp. 31-49.

Nielsen, S.B., Macchi, F., Raccosta, S., Langkilde, A.E., Giehm, L., Kyrsting, A., Svane, A.S., Manno, M., Christiansen, G., Nielsen, N.C., Oddershede, L., Vestergaard, B. and Otzen, D.E. (2013) 'Wildtype and A30P mutant alpha-synuclein form different fibril structures', *PLoS One*, 8(7), p. e67713.

Nieto, M., Gil-Bea, F.J., Dalfo, E., Cuadrado, M., Cabodevilla, F., Sanchez, B., Catena, S., Sesma, T., Ribe, E., Ferrer, I., Ramirez, M.J. and Gomez-Isla, T. (2006) 'Increased sensitivity to MPTP in human alpha-synuclein A30P transgenic mice', *Neurobiol Aging*, 27(6), pp. 848-56.

Nishioka, N. and Arnold, S.E. (2004) 'Evidence for oxidative DNA damage in the hippocampus of elderly patients with chronic schizophrenia', *Am J Geriatr Psychiatry*, 12(2), pp. 167-75.

Norris, E.H., Giasson, B.I. and Lee, V.M. (2004) 'Alpha-synuclein: normal function and role in neurodegenerative diseases', *Curr Top Dev Biol*, 60, pp. 17-54.

O'Keefe, J. and Dostrovsky, J. (1971) 'The hippocampus as a spatial map. Preliminary evidence from unit activity in the freely-moving rat', *Brain Res*, 34(1), pp. 171-5.

O'Neill, M.F. and Shaw, G. (1999) 'Comparison of dopamine receptor antagonists on hyperlocomotion induced by cocaine, amphetamine, MK-801 and the dopamine D1 agonist C-APB in mice', *Psychopharmacology (Berl)*, 145(3), pp. 237-50.

Olney, J.W., Newcomer, J.W. and Farber, N.B. (1999) 'NMDA receptor hypofunction model of schizophrenia', *J Psychiatr Res*, 33(6), pp. 523-33.

Orr, W.C. and Sohal, R.S. (1994) 'Extension of life-span by overexpression of superoxide dismutase and catalase in *Drosophila melanogaster*', *Science*, 263(5150), pp. 1128-30.

Otis, T.S. and Mody, I. (1992) 'Modulation of decay kinetics and frequency of GABA<sub>A</sub> receptor-mediated spontaneous inhibitory postsynaptic currents in hippocampal neurons', *Neuroscience*, 49(1), pp. 13-32.

- Overk, C.R., Cartier, A., Shaked, G., Rockenstein, E., Ubhi, K., Spencer, B., Price, D.L., Patrick, C., Desplats, P. and Masliah, E. (2014) 'Hippocampal neuronal cells that accumulate alpha-synuclein fragments are more vulnerable to Abeta oligomer toxicity via mGluR5--implications for dementia with Lewy bodies', *Mol Neurodegener*, 9, p. 18.
- Pacheco, C.R., Morales, C.N., Ramirez, A.E., Munoz, F.J., Gallegos, S.S., Caviedes, P.A., Aguayo, L.G. and Opazo, C.M. (2015) 'Extracellular alpha-synuclein alters synaptic transmission in brain neurons by perforating the neuronal plasma membrane', *J Neurochem*, 132(6), pp. 731-41.
- Paillusson, S., Clairembault, T., Biraud, M., Neunlist, M. and Derkinderen, P. (2013) 'Activity-dependent secretion of alpha-synuclein by enteric neurons', *J Neurochem*, 125(4), pp. 512-7.
- Palhalmi, J., Paulsen, O., Freund, T.F. and Hajos, N. (2004) 'Distinct properties of carbachol- and DHPG-induced network oscillations in hippocampal slices', *Neuropharmacology*, 47(3), pp. 381-9.
- Palop, J.J., Chin, J. and Mucke, L. (2006) 'A network dysfunction perspective on neurodegenerative diseases', *Nature*, 443(7113), pp. 768-73.
- Palop, J.J., Chin, J., Roberson, E.D., Wang, J., Thwin, M.T., Bien-Ly, N., Yoo, J., Ho, K.O., Yu, G.Q., Kreitzer, A., Finkbeiner, S., Noebels, J.L. and Mucke, L. (2007) 'Aberrant excitatory neuronal activity and compensatory remodeling of inhibitory hippocampal circuits in mouse models of Alzheimer's disease', *Neuron*, 55(5), pp. 697-711.
- Paolicelli, R.C., Bolasco, G., Pagani, F., Maggi, L., Scianni, M., Panzanelli, P., Giustetto, M., Ferreira, T.A., Guiducci, E., Dumas, L., Ragozzino, D. and Gross, C.T. (2011) 'Synaptic pruning by microglia is necessary for normal brain development', *Science*, 333(6048), pp. 1456-8.
- Papatheodoropoulos, C. and Kostopoulos, G. (2002a) 'Spontaneous GABA(A)-dependent synchronous periodic activity in adult rat ventral hippocampal slices', *Neurosci Lett*, 319(1), pp. 17-20.
- Papatheodoropoulos, C. and Kostopoulos, G. (2002b) 'Spontaneous, low frequency (approximately 2-3 Hz) field activity generated in rat ventral hippocampal slices perfused with normal medium', *Brain Res Bull*, 57(2), pp. 187-93.
- Park, J.Y., Paik, S.R., Jou, I. and Park, S.M. (2008) 'Microglial phagocytosis is enhanced by monomeric alpha-synuclein, not aggregated alpha-synuclein: implications for Parkinson's disease', *Glia*, 56(11), pp. 1215-23.
- Patz, S., Grabert, J., Gorba, T., Wirth, M.J. and Wahle, P. (2004) 'Parvalbumin expression in visual cortical interneurons depends on neuronal activity and TrkB ligands during an Early period of postnatal development', *Cereb Cortex*, 14(3), pp. 342-51.

Paxinou, E., Chen, Q., Weisse, M., Giasson, B.I., Norris, E.H., Rueter, S.M., Trojanowski, J.Q., Lee, V.M. and Ischiropoulos, H. (2001) 'Induction of alpha-synuclein aggregation by intracellular nitrate insult', *J Neurosci*, 21(20), pp. 8053-61.

Pekny, M. and Pekna, M. (2004) 'Astrocyte intermediate filaments in CNS pathologies and regeneration', *J Pathol*, 204(4), pp. 428-37.

Peng, C., Gathagan, R.J., Covell, D.J., Medellin, C., Stieber, A., Robinson, J.L., Zhang, B., Pitkin, R.M., Olufemi, M.F., Luk, K.C., Trojanowski, J.Q. and Lee, V.M. (2018) 'Cellular milieu imparts distinct pathological alpha-synuclein strains in alpha-synucleinopathies', *Nature*, 557(7706), pp. 558-563.

Peng, Z. and Houser, C.R. (2005) 'Temporal patterns of fos expression in the dentate gyrus after spontaneous seizures in a mouse model of temporal lobe epilepsy', *J Neurosci*, 25(31), pp. 7210-20.

Perea, G., Gomez, R., Mederos, S., Covelo, A., Ballesteros, J.J., Schlosser, L., Hernandez-Vivanco, A., Martin-Fernandez, M., Quintana, R., Rayan, A., Diez, A., Fuenzalida, M. and Agarwal, A. (2016) 'Activity-dependent switch of GABAergic inhibition into glutamatergic excitation in astrocyte-neuron networks', 5.

Perry, E.K., Marshall, E., Perry, R.H., Irving, D., Smith, C.J., Blessed, G. and Fairbairn, A.F. (1990) 'Cholinergic and dopaminergic activities in senile dementia of Lewy body type', *Alzheimer Dis Assoc Disord*, 4(2), pp. 87-95.

Petroff, O.A. (2002) 'GABA and glutamate in the human brain', *Neuroscientist*, 8(6), pp. 562-73.

Phan, J.A., Stokholm, K., Zareba-Paslawska, J., Jakobsen, S., Vang, K., Gjedde, A., Landau, A.M. and Romero-Ramos, M. (2017) 'Early synaptic dysfunction induced by alpha-synuclein in a rat model of Parkinson's disease', *Sci Rep*, 7(1), p. 6363.

Pietersen, A.N., Patel, N., Jefferys, J.G. and Vreugdenhil, M. (2009) 'Comparison between spontaneous and kainate-induced gamma oscillations in the mouse hippocampus in vitro', *Eur J Neurosci*, 29(11), pp. 2145-56.

Pitts, M.W., Raman, A.V., Hashimoto, A.C., Todorovic, C., Nichols, R.A. and Berry, M.J. (2012) 'Deletion of selenoprotein P results in impaired function of parvalbumin interneurons and alterations in fear learning and sensorimotor gating', *Neuroscience*, 208, pp. 58-68.

Poon, H.F., Frasier, M., Shreve, N., Calabrese, V., Wolozin, B. and Butterfield, D.A. (2005) 'Mitochondrial associated metabolic proteins are selectively oxidized in A30P alpha-synuclein transgenic mice--a model of familial Parkinson's disease', *Neurobiol Dis*, 18(3), pp. 492-8.

Porrero, C., Rubio-Garrido, P., Avendano, C. and Clasca, F. (2010) 'Mapping of fluorescent protein-expressing neurons and axon pathways in adult and developing Thy1-eYFP-H transgenic mice', *Brain Res*, 1345, pp. 59-72.

- Potier, B., Krzywkowski, P., Lamour, Y. and Dutar, P. (1994) 'Loss of calbindin-immunoreactivity in CA1 hippocampal stratum radiatum and stratum lacunosum-moleculare interneurons in the aged rat', *Brain Res*, 661(1-2), pp. 181-8.
- Povysheva, N.V., Zaitsev, A.V., Gonzalez-Burgos, G. and Lewis, D.A. (2013) 'Electrophysiological heterogeneity of fast-spiking interneurons: chandelier versus basket cells', *PLoS One*, 8(8), p. e70553.
- Pozzan, T., Rizzuto, R., Volpe, P. and Meldolesi, J. (1994) 'Molecular and cellular physiology of intracellular calcium stores', *Physiol Rev*, 74(3), pp. 595-636.
- Preston, A.R. and Eichenbaum, H. (2013) 'Interplay of hippocampus and prefrontal cortex in memory', *Curr Biol*, 23(17), pp. R764-73.
- Price, D.L., Rockenstein, E., Ubhi, K., Phung, V., MacLean-Lewis, N., Askay, D., Cartier, A., Spencer, B., Patrick, C., Desplats, P., Ellisman, M.H. and Masliah, E. (2010) 'Alterations in mGluR5 expression and signaling in Lewy body disease and in transgenic models of alpha-synucleinopathy--implications for excitotoxicity', *PLoS One*, 5(11), p. e14020.
- Procaccini, C., Maksimovic, M., Aitta-Aho, T., Korpi, E.R. and Linden, A.M. (2013) 'Reversal of novelty-induced hyperlocomotion and hippocampal c-Fos expression in GluA1 knockout male mice by the mGluR2/3 agonist LY354740', *Neuroscience*, 250, pp. 189-200.
- Puig, M.V., Ushimaru, M. and Kawaguchi, Y. (2008) 'Two distinct activity patterns of fast-spiking interneurons during neocortical UP states', *Proc Natl Acad Sci U S A*, 105(24), pp. 8428-33.
- Puschmann, A., Wszolek, Z.K., Farrer, M., Gustafson, L., Widner, H. and Nilsson, C. (2009) 'Alpha-synuclein multiplications with parkinsonism, dementia or progressive myoclonus?', *Parkinsonism Relat Disord*, 15(5), pp. 390-2.
- Quiroga, R.Q. (2013) 'Gnostic cells in the 21st century', *Acta Neurobiol Exp (Wars)*, 73(4), pp. 463-71.
- Rannikko, E.H., Weber, S.S. and Kahle, P.J. (2015) 'Exogenous alpha-synuclein induces toll-like receptor 4 dependent inflammatory responses in astrocytes', *BMC Neurosci*, 16, p. 57.
- Rcom-H'cheo-Gauthier, A.N., Davis, A., Meedeniya, A.C.B. and Pountney, D.L. (2016) 'Alpha-synuclein aggregates are excluded from calbindin-D28k-positive neurons in dementia with Lewy bodies and a unilateral rotenone mouse model', *Mol Cell Neurosci*, 77, pp. 65-75.
- Rees, M.D., Hawkins, C.L. and Davies, M.J. (2004) 'Hypochlorite and superoxide radicals can act synergistically to induce fragmentation of hyaluronan and chondroitin sulphates', *Biochem J*, 381(Pt 1), pp. 175-84.
- Reeve, A.K., Ludtmann, M.H., Angelova, P.R., Simcox, E.M., Horrocks, M.H., Klenerman, D., Gandhi, S., Turnbull, D.M. and Abramov, A.Y. (2015) 'Aggregated  $\alpha$ -

synuclein and complex I deficiency: exploration of their relationship in differentiated neurons', *Cell Death Dis*, 6(7), pp. e1820-.

Reyes-Marin, K.E. and Nunez, A. (2017) 'Seizure susceptibility in the APP/PS1 mouse model of Alzheimer's disease and relationship with amyloid beta plaques', *Brain Res*, 1677, pp. 93-100.

Ribak, C.E., Nitsch, R. and Seress, L. (1990) 'Proportion of parvalbumin-positive basket cells in the GABAergic innervation of pyramidal and granule cells of the rat hippocampal formation', *J Comp Neurol*, 300(4), pp. 449-61.

Rich, P.R. (2003) 'The molecular machinery of Keilin's respiratory chain', *Biochem Soc Trans*, 31(Pt 6), pp. 1095-105.

Roberts, E. and Frankel, S. (1950) 'gamma-Aminobutyric acid in brain: its formation from glutamic acid', *J Biol Chem*, 187(1), pp. 55-63.

Robson, E., Tweedy, C., Manzanza, N., Taylor, J.P., Atkinson, P., Randall, F., Reeve, A., Clowry, G.J. and LeBeau, F.E.N. (2018) 'Impaired Fast Network Oscillations and Mitochondrial Dysfunction in a Mouse Model of Alpha-synucleinopathy (A30P)', *Neuroscience*, 377, pp. 161-173.

Rockenstein, E., Mallory, M., Hashimoto, M., Song, D., Shults, C.W., Lang, I. and Masliah, E. (2002) 'Differential neuropathological alterations in transgenic mice expressing alpha-synuclein from the platelet-derived growth factor and Thy-1 promoters', *J Neurosci Res*, 68(5), pp. 568-78.

Rong, H., Jin, L., Wei, W., Wang, X. and Xi, Z. (2015) 'Alpha-synuclein is a potential biomarker in the serum and CSF of patients with intractable epilepsy', *Seizure*, 27, pp. 6-9.

Ross, J.M. (2011) 'Visualization of mitochondrial respiratory function using cytochrome c oxidase/succinate dehydrogenase (COX/SDH) double-labeling histochemistry', *J Vis Exp*, (57), p. e3266.

Rossor, M.N., Fox, N.C., Mummery, C.J., Schott, J.M. and Warren, J.D. (2010) 'The diagnosis of young-onset dementia', *Lancet Neurol*, 9(8), pp. 793-806.

Rossor, M.N., Iversen, L.L., Reynolds, G.P., Mountjoy, C.Q. and Roth, M. (1984) 'Neurochemical characteristics of early and late onset types of Alzheimer's disease', *Br Med J (Clin Res Ed)*, 288(6422), pp. 961-4.

Rotermund, C., Truckenmuller, F.M., Schell, H. and Kahle, P.J. (2014) 'Diet-induced obesity accelerates the onset of terminal phenotypes in alpha-synuclein transgenic mice', *J Neurochem*, 131(6), pp. 848-58.

Ruffmann, C., Calboli, F.C., Bravi, I., Gveric, D., Curry, L.K., de Smith, A., Pavlou, S., Buxton, J.L., Blakemore, A.I., Takousis, P., Molloy, S., Piccini, P., Dexter, D.T., Roncaroli, F. and Gentleman, S.M. (2016) 'Cortical Lewy bodies and Abeta burden are associated with prevalence and timing of dementia in Lewy body diseases', 42(5), pp. 436-50.



- Sahay, S., Ghosh, D., Dwivedi, S., Anoop, A., Mohite, G.M., Kombrabail, M., Krishnamoorthy, G. and Maji, S.K. (2015) 'Familial Parkinson disease-associated mutations alter the site-specific microenvironment and dynamics of alpha-synuclein', *J Biol Chem*, 290(12), pp. 7804-22.
- Samuel, F., Flavin, W.P., Iqbal, S., Pacelli, C., Sri Renganathan, S.D., Trudeau, L.E., Campbell, E.M., Fraser, P.E. and Tandon, A. (2016) 'Effects of Serine 129 Phosphorylation on alpha-Synuclein Aggregation, Membrane Association, and Internalization', *J Biol Chem*, 291(9), pp. 4374-85.
- Sanchez-Guajardo, V., Barnum, C.J., Tansey, M.G. and Romero-Ramos, M. (2013) 'Neuroimmunological processes in Parkinson's disease and their relation to alpha-synuclein: microglia as the referee between neuronal processes and peripheral immunity', *ASN Neuro*, 5(2), pp. 113-39.
- Sarkisian, M.R., Tandon, P., Liu, Z., Yang, Y., Hori, A., Holmes, G.L. and Stafstrom, C.E. (1997) 'Multiple kainic acid seizures in the immature and adult brain: ictal manifestations and long-term effects on learning and memory', *Epilepsia*, 38(11), pp. 1157-66.
- Savica, R., Bradley, B.F. and Mielke, M.M. (2018) 'When Do alpha-Synucleinopathies Start? An Epidemiological Timeline: A Review', *JAMA Neurol*, 75(4), pp. 503-509.
- Savica, R., Grossardt, B.R., Bower, J.H., Boeve, B.F., Ahlskog, J.E. and Rocca, W.A. (2013) 'Incidence of dementia with Lewy bodies and Parkinson disease dementia', *JAMA Neurol*, 70(11), pp. 1396-402.
- Schapira, A.H., Cooper, J.M., Dexter, D., Clark, J.B., Jenner, P. and Marsden, C.D. (1990) 'Mitochondrial complex I deficiency in Parkinson's disease', *J Neurochem*, 54(3), pp. 823-7.
- Schell, H., Boden, C., Chagas, A.M. and Kahle, P.J. (2012) 'Impaired c-Fos and polo-like kinase 2 induction in the limbic system of fear-conditioned alpha-synuclein transgenic mice', *PLoS One*, 7(11), p. e50245.
- Schell, H., Hasegawa, T., Neumann, M. and Kahle, P.J. (2009) 'Nuclear and neuritic distribution of serine-129 phosphorylated alpha-synuclein in transgenic mice', *Neuroscience*, 160(4), pp. 796-804.
- Schlingloff, D. and Kali, S. (2014) 'Mechanisms of sharp wave initiation and ripple generation', *34(34)*, pp. 11385-98.
- Schlosser, B., Klaus, G., Prime, G. and Ten Bruggencate, G. (1999) 'Postnatal development of calretinin- and parvalbumin-positive interneurons in the rat neostriatum: an immunohistochemical study', *J Comp Neurol*, 405(2), pp. 185-98.
- Schneiderman, J.H. (1986) 'Low concentrations of penicillin reveal rhythmic, synchronous synaptic potentials in hippocampal slice', *Brain Res*, 398(2), pp. 231-41.

- Schonberger, J., Draguhn, A. and Both, M. (2014) 'Lamina-specific contribution of glutamatergic and GABAergic potentials to hippocampal sharp wave-ripple complexes', *J Neurosci*, 8, p. 103.
- Schwartzkroin, P.A. and Haglund, M.M. (1986) 'Spontaneous rhythmic synchronous activity in epileptic human and normal monkey temporal lobe', *Epilepsia*, 27(5), pp. 523-33.
- Seaman, M.A., Levin, J.R. and Serlin, R.C. (1991) 'New developments in pairwise multiple comparisons: Some powerful and practicable procedures', *Psychological Bulletin*, 110(3), pp. 577-586.
- Seeger, G., Brauer, K., Hartig, W. and Bruckner, G. (1994) 'Mapping of perineuronal nets in the rat brain stained by colloidal iron hydroxide histochemistry and lectin cytochemistry', *Neuroscience*, 58(2), pp. 371-88.
- Serrano-Pozo, A., Gómez-Isla, T., Growdon, J.H., Frosch, M.P. and Hyman, B.T. (2013) 'A Phenotypic Change But Not Proliferation Underlies Glial Responses in Alzheimer Disease', *Am J Pathol*, 182(6), pp. 2332-44.
- Siapas, A.G. and Wilson, M.A. (1998) 'Coordinated interactions between hippocampal ripples and cortical spindles during slow-wave sleep', *Neuron*, 21(5), pp. 1123-8.
- Sigurdsson, T. and Duvarci, S. (2015) 'Hippocampal-Prefrontal Interactions in Cognition, Behavior and Psychiatric Disease', *Front Syst Neurosci*, 9.
- Silverman, H.A., Dancho, M., Regnier-Golanov, A., Nasim, M., Ochani, M., Olofsson, P.S., Ahmed, M., Miller, E.J., Chavan, S.S., Golanov, E., Metz, C.N., Tracey, K.J. and Pavlov, V.A. (2014) 'Brain Region-Specific Alterations in the Gene Expression of Cytokines, Immune Cell Markers and Cholinergic System Components during Peripheral Endotoxin-Induced Inflammation', *Mol Med*, 20(1), pp. 601-11.
- Skrobot, O.A. (2008) 'Mechanisms underlying spontaneous oscillations in the hippocampus in vitro', *PhD thesis, Newcastle University*.
- Slomianka, L., Amrein, I., Knuesel, I., Sørensen, J.C. and Wolfer, D.P. (2011) 'Hippocampal pyramidal cells: the reemergence of cortical lamination', *Brain Struct Funct*, 216(4), pp. 301-17.
- Sloviter, R.S., Sollas, A.L., Barbaro, N.M. and Laxer, K.D. (1991) 'Calcium-binding protein (calbindin-D28K) and parvalbumin immunocytochemistry in the normal and epileptic human hippocampus', *J Comp Neurol*, 308(3), pp. 381-96.
- Smith, W.W., Jiang, H., Pei, Z., Tanaka, Y., Morita, H., Sawa, A., Dawson, V.L., Dawson, T.M. and Ross, C.A. (2005) 'Endoplasmic reticulum stress and mitochondrial cell death pathways mediate A53T mutant alpha-synuclein-induced toxicity', *Hum Mol Genet*, 14(24), pp. 3801-11.
- Snead, D. and Eliezer, D. (2014) 'Alpha-synuclein function and dysfunction on cellular membranes', *Exp Neurobiol*, 23(4), pp. 292-313.

- Sofroniew, M.V. and Vinters, H.V. (2010) 'Astrocytes: biology and pathology', *Acta Neuropathol*, 119(1), pp. 7-35.
- Sohal, V.S., Zhang, F., Yizhar, O. and Deisseroth, K. (2009) 'Parvalbumin neurons and gamma rhythms enhance cortical circuit performance', *Nature*, 459(7247), pp. 698-702.
- Sommer, B., Barbieri, S., Hofele, K., Wiederhold, K., Probst, A., Mistl, C., Danner, S., Kauffmann, S., Spooren, W., Tolnay, M., Bilbe, G., van der Putten, H., Kafmann, S., Caromi, P. and Ruegg, M.A. (2000) 'Mouse models of alpha-synucleinopathy and Lewy pathology', *Exp Gerontol*, 35(9-10), pp. 1389-403.
- Somogyi, P. and Klausberger, T. (2005) 'Defined types of cortical interneurone structure space and spike timing in the hippocampus', *J Physiol*, 562(Pt 1), pp. 9-26.
- Song, W., Patel, A., Qureshi, H.Y., Han, D., Schipper, H.M. and Paudel, H.K. (2009) 'The Parkinson disease-associated A30P mutation stabilizes alpha-synuclein against proteasomal degradation triggered by heme oxygenase-1 over-expression in human neuroblastoma cells', *J Neurochem*, 110(2), pp. 719-33.
- Soontornniyomkij, V., Risbrough, V.B., Young, J.W., Soontornniyomkij, B., Jeste, D.V. and Achim, C.L. (2012) 'Hippocampal calbindin-1 immunoreactivity correlate of recognition memory performance in aged mice', *Neurosci Lett*, 516(1), pp. 161-5.
- Soos, J., Engelhardt, J.I., Siklos, L., Havas, L. and Majtenyi, K. (2004) 'The expression of PARP, NF-kappa B and parvalbumin is increased in Parkinson disease', *Neuroreport*, 15(11), pp. 1715-8.
- Sousa, V.L., Bellani, S., Giannandrea, M., Yousuf, M., Valtorta, F., Meldolesi, J. and Chieregatti, E. (2009) '{alpha}-synuclein and its A30P mutant affect actin cytoskeletal structure and dynamics', *Mol Biol Cell*, 20(16), pp. 3725-39.
- Spillantini, M.G., Schmidt, M.L., Lee, V.M., Trojanowski, J.Q., Jakes, R. and Goedert, M. (1997) 'Alpha-synuclein in Lewy bodies', *Nature*, 388(6645), pp. 839-40.
- Stefanits, H., Wesseling, C. and Kovacs, G.G. (2014) 'Loss of Calbindin immunoreactivity in the dentate gyrus distinguishes Alzheimer's disease from other neurodegenerative dementias', *Neurosci Lett*, 566, pp. 137-41.
- Steullet, P., Cabungcal, J.H., Kulak, A., Kraftsik, R., Chen, Y., Dalton, T.P., Cuenod, M. and Do, K.Q. (2010) 'Redox dysregulation affects the ventral but not dorsal hippocampus: impairment of parvalbumin neurons, gamma oscillations, and related behaviors', *J Neurosci*, 30(7), pp. 2547-58.
- Steward, O., Torre, E.R., Tomasulo, R. and Lothman, E. (1992) 'Seizures and the regulation of astroglial gene expression', *Epilepsy Res Suppl*, 7, pp. 197-209.
- Stinton, C., McKeith, I., Taylor, J.P., Lafortune, L., Mioshi, E., Mak, E., Cambridge, V., Mason, J., Thomas, A. and O'Brien, J.T. (2015) 'Pharmacological Management of Lewy Body Dementia: A Systematic Review and Meta-Analysis', *Am J Psychiatry*, 172(8), pp. 731-42.

- Strange, B.A., Witter, M.P., Lein, E.S. and Moser, E.I. (2014) 'Functional organization of the hippocampal longitudinal axis', *Nat Rev Neurosci*, 15(10), pp. 655-69.
- Streit, W.J., Walter, S.A. and Pennell, N.A. (1999) 'Reactive microgliosis', *Prog Neurobiol*, 57(6), pp. 563-81.
- Stylianou, M., Murphy, N., Peraza, L.R., Graziadio, S., Cromarty, R., Killen, A., JT, O.B., Thomas, A.J., LeBeau, F.E.N. and Taylor, J.P. (2018) 'Quantitative electroencephalography as a marker of cognitive fluctuations in dementia with Lewy bodies and an aid to differential diagnosis', *Clin Neurophysiol*, 129(6), pp. 1209-1220.
- Suttkus, A., Rohn, S., Jager, C., Arendt, T. and Morawski, M. (2012) 'Neuroprotection against iron-induced cell death by perineuronal nets - an in vivo analysis of oxidative stress', *Am J Neurodegener Dis*, 1(2), pp. 122-9.
- Suzuki, W.A. and Eichenbaum, H. (2000) 'The neurophysiology of memory', *Ann N Y Acad Sci*, 911, pp. 175-91.
- Swann, J.W., Smith, K.L. and Lee, C.L. (2001) 'Neuronal activity and the establishment of normal and epileptic circuits during brain development', *Int Rev Neurobiol*, 45, pp. 89-118.
- Szego, E.M., Outeiro, T.F., Kermer, P. and Schulz, J.B. (2013) 'Impairment of the septal cholinergic neurons in MPTP-treated A30P alpha-synuclein mice', *Neurobiol Aging*, 34(2), pp. 589-601.
- Taguchi, K., Watanabe, Y., Tsujimura, A., Tatebe, H., Miyata, S., Tokuda, T., Mizuno, T. and Tanaka, M. (2014) 'Differential expression of alpha-synuclein in hippocampal neurons', *PLoS One*, 9(2), p. e89327.
- Tang, Y. and Le, W. (2016) 'Differential Roles of M1 and M2 Microglia in Neurodegenerative Diseases', *Mol Neurobiol*, 53(2), pp. 1181-94.
- Taube, J.S. and Schwartzkroin, P.A. (1988) 'Mechanisms of long-term potentiation: a current-source density analysis', *J Neurosci*, 8(5), pp. 1645-55.
- Taylor, C.R. and Levenson, R.M. (2006) 'Quantification of immunohistochemistry--issues concerning methods, utility and semiquantitative assessment II', *Histopathology*, 49(4), pp. 411-24.
- Tiraboschi, P., Hansen, L.A., Alford, M., Sabbagh, M.N., Schoos, B., Masliah, E., Thal, L.J. and Corey-Bloom, J. (2000) 'Cholinergic dysfunction in diseases with Lewy bodies', *Neurology*, 54(2), pp. 407-11.
- Tonder, N., Kragh, J., Bolwig, T. and Zimmer, J. (1994) 'Transient decrease in calbindin immunoreactivity of the rat fascia dentata granule cells after repeated electroconvulsive shocks', *Hippocampus*, 4(1), pp. 79-83.
- Toth, K. and Freund, T.F. (1992) 'Calbindin D28k-containing nonpyramidal cells in the rat hippocampus: their immunoreactivity for GABA and projection to the medial septum', *Neuroscience*, 49(4), pp. 793-805.

- Traub, R.D., Bibbig, A., Fisahn, A., LeBeau, F.E., Whittington, M.A. and Buhl, E.H. (2000) 'A model of gamma-frequency network oscillations induced in the rat CA3 region by carbachol in vitro', *Eur J Neurosci*, 12(11), pp. 4093-106.
- Traub, R.D., Kopell, N., Bibbig, A., Buhl, E.H., LeBeau, F.E. and Whittington, M.A. (2001) 'Gap junctions between interneuron dendrites can enhance synchrony of gamma oscillations in distributed networks', *J Neurosci*, 21(23), pp. 9478-86.
- Traub, R.D., Miles, R. and Buzsaki, G. (1992) 'Computer simulation of carbachol-driven rhythmic population oscillations in the CA3 region of the in vitro rat hippocampus', *J Physiol*, 451, pp. 653-72.
- Traub, R.D., Whittington, M.A., Buhl, E.H., Jefferys, J.G. and Faulkner, H.J. (1999) 'On the mechanism of the gamma --> beta frequency shift in neuronal oscillations induced in rat hippocampal slices by tetanic stimulation', *J Neurosci*, 19(3), pp. 1088-105.
- Turrens, J.F. and Boveris, A. (1980) 'Generation of superoxide anion by the NADH dehydrogenase of bovine heart mitochondria', *Biochem J*, 191(2), pp. 421-7.
- Uhlhaas, P.J. and Singer, W. (2006) 'Neural synchrony in brain disorders: relevance for cognitive dysfunctions and pathophysiology', *Neuron*, 52(1), pp. 155-68.
- Unal-Cevik, I., Gursoy-Ozdemir, Y., Yemisci, M., Lule, S., Gurer, G., Can, A., Müller, V., Kahle, P.J. and Dalkara, T. (2011) 'Alpha-synuclein aggregation induced by brief ischemia negatively impacts neuronal survival in vivo: a study in [A30P]alpha-synuclein transgenic mouse', *J Cereb Blood Flow Metab*, 31(3), pp. 913-23.
- Urban, Z., Magloczky, Z. and Freund, T.F. (2002) 'Calretinin-containing interneurons innervate both principal cells and interneurons in the CA1 region of the human hippocampus', *Acta Biol Hung*, 53(1-2), pp. 205-20.
- van der Loos, C.M. (2008) 'Multiple immunoenzyme staining: methods and visualizations for the observation with spectral imaging', *J Histochem Cytochem*, 56(4), pp. 313-28.
- Vandecasteele, M., Varga, V., Berenyi, A., Papp, E., Bartho, P., Venance, L., Freund, T.F. and Buzsaki, G. (2014) 'Optogenetic activation of septal cholinergic neurons suppresses sharp wave ripples and enhances theta oscillations in the hippocampus', *Proc Natl Acad Sci U S A*, 111(37), pp. 13535-40.
- Vegh, M.J., Heldring, C.M., Kamphuis, W., Hijazi, S., Timmerman, A.J., Li, K.W., van Nierop, P., Mansvelter, H.D., Hol, E.M., Smit, A.B. and van Kesteren, R.E. (2014) 'Reducing hippocampal extracellular matrix reverses early memory deficits in a mouse model of Alzheimer's disease', *Acta Neuropathol Commun*, 2, p. 76.
- Verkhratsky, A. and Butt, A. (2007) *Glial Neurobiology: A Textbook*. John Wiley & Sons, Ltd.
- Vesce, S., Bezzi, P. and Volterra, A. (1999) 'The active role of astrocytes in synaptic transmission', *Cell Mol Life Sci*, 56(11-12), pp. 991-1000.

- Vezzani, A., Sperk, G. and Colmers, W.F. (1999) 'Neuropeptide Y: emerging evidence for a functional role in seizure modulation', *Trends Neurosci*, 22(1), pp. 25-30.
- Vila, M., Vukosavic, S., Jackson-Lewis, V., Neystat, M., Jakowec, M. and Przedborski, S. (2000) 'Alpha-synuclein up-regulation in substantia nigra dopaminergic neurons following administration of the parkinsonian toxin MPTP', *J Neurochem*, 74(2), pp. 721-9.
- Viswanathan, A. and Freeman, R.D. (2007) 'Neurometabolic coupling in cerebral cortex reflects synaptic more than spiking activity', *Nat Neurosci*, 10(10), pp. 1308-12.
- Vivacqua, G., Casini, A., Vaccaro, R., Fornai, F., Yu, S. and D'Este, L. (2011) 'Different sub-cellular localization of alpha-synuclein in the C57BL/6J mouse's central nervous system by two novel monoclonal antibodies', *J Chem Neuroanat*, 41(2), pp. 97-110.
- Volman, V., Behrens, M.M. and Sejnowski, T.J. (2011) 'Downregulation of parvalbumin at cortical GABA synapses reduces network gamma oscillatory activity', *J Neurosci*, 31(49), pp. 18137-48.
- Vossel, K.A., Ranasinghe, K.G., Beagle, A.J., Mizuiri, D., Honma, S.M., Dowling, A.F., Darwish, S.M., Van Berlo, V., Barnes, D.E., Mantle, M., Karydas, A.M., Coppola, G., Roberson, E.D., Miller, B.L., Garcia, P.A., Kirsch, H.E., Mucke, L. and Nagarajan, S.S. (2016) 'Incidence and impact of subclinical epileptiform activity in Alzheimer's disease', *Ann Neurol*, 80(6), pp. 858-870.
- Vreugdenhil, M. and Toescu, E.C. (2005) 'Age-dependent reduction of gamma oscillations in the mouse hippocampus in vitro', *Neuroscience*, 132(4), pp. 1151-7.
- Wallraff, A., Kohling, R., Heinemann, U., Theis, M., Willecke, K. and Steinhauser, C. (2006) 'The impact of astrocytic gap junctional coupling on potassium buffering in the hippocampus', *J Neurosci*, 26(20), pp. 5438-47.
- Wan, O.W. and Chung, K.K. (2012) 'The role of alpha-synuclein oligomerization and aggregation in cellular and animal models of Parkinson's disease', *PLoS One*, 7(6), p. e38545.
- Wang, Y., Rowan, M.J. and Anwyl, R. (1997) 'LTP induction dependent on activation of Ni<sup>2+</sup>-sensitive voltage-gated calcium channels, but not NMDA receptors, in the rat dentate gyrus in vitro', *J Neurophysiol*, 78(5), pp. 2574-81.
- Watanabe, M., Ueno, H., Suemitsu, S., Yokobayashi, E., Matsumoto, Y., Usui, S., Sujiura, H. and Okamoto, M. (2012) 'Attenuated sensory deprivation-induced changes of parvalbumin neuron density in the barrel cortex of FcγRIIB-deficient mice', *Acta Med Okayama*, 66(2), pp. 143-54.
- Wenning, G.K., Tison, F., Ben Shlomo, Y., Daniel, S.E. and Quinn, N.P. (1997) 'Multiple system atrophy: a review of 203 pathologically proven cases', *Mov Disord*, 12(2), pp. 133-47.
- Wermuth, C.G., Bourguignon, J.J., Schlewer, G., Gies, J.P., Schoenfelder, A., Melikian, A., Bouchet, M.J., Chantreux, D., Molimard, J.C., Heulme, M. and et al.

- (1987) 'Synthesis and structure-activity relationships of a series of aminopyridazine derivatives of gamma-aminobutyric acid acting as selective GABA-A antagonists', *J Med Chem*, 30(2), pp. 239-49.
- Wersinger, C., Jeannotte, A. and Sidhu, A. (2006a) 'Attenuation of the norepinephrine transporter activity and trafficking via interactions with alpha-synuclein', *Eur J Neurosci*, 24(11), pp. 3141-52.
- Wersinger, C., Rusnak, M. and Sidhu, A. (2006b) 'Modulation of the trafficking of the human serotonin transporter by human alpha-synuclein', *Eur J Neurosci*, 24(1), pp. 55-64.
- Whitlock, J.R., Heynen, A.J., Shuler, M.G. and Bear, M.F. (2006) 'Learning induces long-term potentiation in the hippocampus', *Science*, 313(5790), pp. 1093-7.
- Whittaker, R.G., Turnbull, D.M., Whittington, M.A. and Cunningham, M.O. (2011) 'Impaired mitochondrial function abolishes gamma oscillations in the hippocampus through an effect on fast-spiking interneurons', *Brain*, 134(Pt 7), p. e180; author reply e181.
- Whittington, M.A., Traub, R.D. and Jefferys, J.G. (1995) 'Synchronized oscillations in interneuron networks driven by metabotropic glutamate receptor activation', *Nature*, 373(6515), pp. 612-5.
- Willard, S.S. and Koochekpour, S. (2013) 'Glutamate, Glutamate Receptors, and Downstream Signaling Pathways', *Int J Biol Sci*, 9(9), pp. 948-59.
- Winsky, L. and Kuznicki, J. (1996) 'Antibody recognition of calcium-binding proteins depends on their calcium-binding status', *J Neurochem*, 66(2), pp. 764-71.
- Witter, M.P., Naber, P.A., van Haeften, T., Machielsen, W.C., Rombouts, S.A., Barkhof, F., Scheltens, P. and Lopes da Silva, F.H. (2000) 'Cortico-hippocampal communication by way of parallel parahippocampal-subicular pathways', *Hippocampus*, 10(4), pp. 398-410.
- Witton, J., Staniaszek, L.E., Bartsch, U., Randall, A.D., Jones, M.W. and Brown, J.T. (2016) 'Disrupted hippocampal sharp-wave ripple-associated spike dynamics in a transgenic mouse model of dementia', *J Physiol*, 594(16), pp. 4615-30.
- Wong, C.G., Bottiglieri, T. and Snead, O.C., 3rd (2003) 'GABA, gamma-hydroxybutyric acid, and neurological disease', *Ann Neurol*, 54 Suppl 6, pp. S3-12.
- Wong, T., Zhang, X.L., Asl, M.N., Wu, C.P., Carlen, P.L. and Zhang, L. (2005) 'Postnatal development of intrinsic GABAergic rhythms in mouse hippocampus', *Neuroscience*, 134(1), pp. 107-20.
- Wu, C., Asl, M.N., Gillis, J., Skinner, F.K. and Zhang, L. (2005a) 'An in vitro model of hippocampal sharp waves: regional initiation and intracellular correlates', *J Neurophysiol*, 94(1), pp. 741-53.

- Wu, C., Luk, W.P., Gillis, J., Skinner, F. and Zhang, L. (2005b) 'Size does matter: generation of intrinsic network rhythms in thick mouse hippocampal slices', *J Neurophysiol*, 93(4), pp. 2302-17.
- Wu, C., Shen, H., Luk, W.P. and Zhang, L. (2002) 'A fundamental oscillatory state of isolated rodent hippocampus', *J Physiol*, 540(Pt 2), pp. 509-27.
- Wu, C.P., Huang, H.L., Asl, M.N., He, J.W., Gillis, J., Skinner, F.K. and Zhang, L. (2006a) 'Spontaneous rhythmic field potentials of isolated mouse hippocampal-subicular-entorhinal cortices in vitro', *J Physiol*, 576(Pt 2), pp. 457-76.
- Wu, C.P., Huang, H.L., Nassiri Asl, M., He, J.W., Gillis, J., Skinner, F.K. and Zhang, L. (2006b) 'Spontaneous rhythmic field potentials of isolated mouse hippocampal-subicular-entorhinal cortices in vitro', *J Physiol*, 576(Pt 2), pp. 457-76.
- Yamada, J. and Jinno, S. (2015) 'Subclass-specific formation of perineuronal nets around parvalbumin-expressing GABAergic neurons in Ammon's horn of the mouse hippocampus', *J Comp Neurol*, 523(5), pp. 790-804.
- Yamada, J., Ohgomori, T. and Jinno, S. (2015) 'Perineuronal nets affect parvalbumin expression in GABAergic neurons of the mouse hippocampus', *Eur J Neurosci*, 41(3), pp. 368-78.
- Yamada, K. and Iwatsubo, T. (2018) 'Extracellular alpha-synuclein levels are regulated by neuronal activity', *Mol Neurodegener*, 13(1), p. 9.
- Yamaguchi, T., Winsky, L. and Jacobowitz, D.M. (1991) 'Calretinin, a neuronal calcium binding protein, inhibits phosphorylation of a 39 kDa synaptic membrane protein from rat brain cerebral cortex', *Neurosci Lett*, 131(1), pp. 79-82.
- Yamamoto, C. and McIlwain, H. (1966) 'Electrical activities in thin sections from the mammalian brain maintained in chemically-defined media in vitro', *J Neurochem*, 13(12), pp. 1333-43.
- Yavich, L., Tanila, H., Vepsäläinen, S. and Jakala, P. (2004) 'Role of alpha-synuclein in presynaptic dopamine recruitment', *J Neurosci*, 24(49), pp. 11165-70.
- Ye, Q. and Miao, Q.L. (2013) 'Experience-dependent development of perineuronal nets and chondroitin sulfate proteoglycan receptors in mouse visual cortex', *Matrix Biol*, 32(6), pp. 352-63.
- Ying, Z., Lin, F., Gu, W., Su, Y., Arshad, A., Qing, H. and Deng, Y. (2011) 'alpha-Synuclein increases U251 cells vulnerability to hydrogen peroxide by disrupting calcium homeostasis', *J Neural Transm*, 118(8), pp. 1165-72.
- Ylinen, A., Bragin, A., Nadasdy, Z., Jando, G., Szabo, I., Sik, A. and Buzsáki, G. (1995) 'Sharp wave-associated high-frequency oscillation (200 Hz) in the intact hippocampus: network and intracellular mechanisms', *J Neurosci*, 15(1 Pt 1), pp. 30-46.
- You, J.C., Muralidharan, K., Park, J.W., Petrof, I., Pyfer, M.S., Corbett, B.F., LaFrancois, J.J., Zheng, Y., Zhang, X., Mohila, C.A., Yoshor, D., Rissman, R.A., Nestler, E.J., Scharfman, H.E. and Chin, J. (2017) 'Epigenetic suppression of



hippocampal calbindin-D28k by DeltaFosB drives seizure-related cognitive deficits', *Nat Med*, 23(11), pp. 1377-1383.

Zhang, W., Wang, T., Pei, Z., Miller, D.S., Wu, X., Block, M.L., Wilson, B., Zhang, W., Zhou, Y., Hong, J.S. and Zhang, J. (2005) 'Aggregated alpha-synuclein activates microglia: a process leading to disease progression in Parkinson's disease', *Faseb j*, 19(6), pp. 533-42.

Zhang, Y., Chen, Y., Bressler, S.L. and Ding, M. (2008) 'Response preparation and inhibition: the role of the cortical sensorimotor beta rhythm', *Neuroscience*, 156(1), pp. 238-46.

Zimmermann, D.R. and Dours-Zimmermann, M.T. (2008) 'Extracellular matrix of the central nervous system: from neglect to challenge', *Histochem Cell Biol*, 130(4), pp. 635-53.

Zorec, R., Horvat, A., Vardjan, N. and Verkhatsky, A. (2015) 'Memory Formation Shaped by Astroglia', *Front Integr Neurosci*, 9.